Institute of Physics
Polish Academy of Sciences

Matrix isolation studies of structure and UV-induced transformations of selected N-heterocyclic molecules

Ganna Gerega

Dissertation submitted to the Institute of Physics
of the Polish Academy of Sciences
in partial fulfillment of the requirements for the degree of Doctor in Physics

Thesis adviser: Doc. dr hab. Maciej J. Nowak

Warsaw 2008

Abstract

The results of photochemical transformations occurring in isolated molecules exposed to the UV radiation are presented for the range of heterocyclic compounds. This work contains examples of unimolecular photochemical processes leading to the change of a structure of irradiated molecule. Several cases of phototautomeric oxo → hydroxy reaction were described and one example of formation of a new chemical compound, which formally is an isomer of the substrate molecule.

Particular emphasis is placed on the estimation of tautomeric equilibrium for the studied compounds. The change of a relative amount of tautomers in a matrix after irradiation, allowed experimental determination of a ratio of tautomers frozen during formation of a matrix. These tautomeric ratios measured for the bicyclic compounds which consist of a benzene ring fused with the heterocyclic ring in different positions (2-quinoxalinone, 2-quinolinone, 1-isoquinoline, 4-quinazolinone) strongly suggest that direct attachment of the benzene ring at one of the double bonds in the structure of the parent compounds (2-pyridinone, 2-pyrazinone and 4-pyrimidinone) leads to a significant increase of stability of the oxo tautomers, with respect to the corresponding hydroxy forms.

In this work, it was demonstrated that upon UV irradiation the reaction of intramolecular proton transfer occurred in all studied compounds (with except of 3-hydroxyisoquinoline). This photoreaction underwent in compounds with N-H and C=O groups in α-position attached to heterocyclic ring. The proton was transferred from nitrogen to oxygen atom. In the case of allopurinol, 9-methylhypoxanthine and hypoxanthine, along with oxo → hydroxy photoreaction, the accompanying process was observed leading to formation of open-ring species (conjugated ketenes).

The studies of photochemical transformations of *N*-hydroxypyridine-2(1*H*)-thione described in the last part of this work allowed a conclusion that the product of the photoreaction is thioperoxy derivative of pyridine. The photochemical formation of this new compound – 2-hydroxysulfanyl-pyridine - occurred in the matrix environment. Isolation of a substrate molecule in a matrix cage prevented fast detachment of photochemically formed ·OH radical, and allowed formation of the product.

In this work, the assignment of obtained IR spectra of almost all tautomeric forms of the studied compounds was carried out. This was performed as for tautomers initially present in low-temperature matrices, as for the spectra of photoproducts populated in the matrix upon UV irradiation. In this purpose, the experimental spectra were compared with the spectra simulated by DFT(B3LYP) quantum-mechanical calculations. The good agreement allowed assignment of experimentally observed absorption bands to the normal modes calculated for theoretically predicted spectra. Theoretical analysis of the normal modes was carried out for each compound. The forms of vibrations corresponding to absorption bands were described with calculated elements of PED (potential energy distribution) matrix.

The results of theoretical calculations with QCISD method showed that this method predicts well not only the shifts of tautomeric equilibria for the studied compounds, but provides also reliable values for calculated energy differences (ΔE) between tautomers of a given compound. This was demonstrated by comparing theoretically and experimentally estimated values of ΔE.

I would like to express my deepest respect and most sincere gratitude to my supervisor, doc. dr. hab. Maciej J. Nowak, to thank for valuable help in accomplishing this thesis as well as for all kinds of support provided during my studentship in Warsaw.

I want to thank also my colleges from the research group: dr. hab. Leszek Łapiński and dr. Hanna Rostkowska for the science discussions and for valuable remarks and advice.

My thanks and gratitude addressed to all my friends and colleagues who helped and supported me at the all stages of the realization of this project.

Ganna Gerega

List of publication

List of publications containing the results of the dissertation

1. A. Gerega, L. Lapinski, I. Reva, H. Rostkowska, and M. J. Nowak
"UV induced generation of rare tautomers of allopurinol and 9-methylhypoxanthine – a matrix isolation FTIR study",
Biophysical Chemistry, **122** (2006) 123.

2. A. Gerega, L. Lapinski, M. J. Nowak and H. Rostkowska
"UV-induced oxo → hydroxy unimolecular proton-transfer reactions in hypoxanthine",
Journal of Physical Chemistry A, **110** (2006) 10236.

3. A. Gerega, L. Lapinski, M. J. Nowak, A. Furmanchuk, and J. Leszczynski
"Systematic Effect of Benzo-Annelation on Oxo-Hydroxy Tautomerism of Heterocyclic Compounds. Experimental Matrix-Isolation and Theoretical Study"
Journal of Physical Chemistry A, **111** (2007) 4934.

4. L. Lapinski, A. Gerega, A.L. Sobolewski and M.J. Nowak „Thioperoxy derivative generated by UV-induced transformation of *N*-hydroxypyridine-2(1*H*)-thione isolated in low-temperature matrixes"
Journal of Physical Chemistry A, **112** (2008) 238.

Contents

1. Introduction

Investigation of isolated molecules is the first step in understanding of the properties of molecular systems. Recently much attention has been paid to experimental and theoretical studies [1-11] of isolated nucleic acid bases and their derivatives. The majority of these studies concerned determination of the structure of non-interacting molecules and photochemical effects occuring after exposure of this class of molecules to UV radiation. The low-temperature matrix isolation technique is one of the most effective methods used for such investigations. The current work presents new results in this area of research. Since it is known that exposure to solar light, among a number of biological effects, may cause mutations, the investigations of the photochemical transformations occurring in molecules present in DNA (or their derivatives) are of crucial importance. UV light generates DNA damage by several different mechanisms [12]. Most commonnly known damages are cyclobutane pyrimidine dimers and 6-4 lesions [13]. The photoprocesses occuring in single molecules which may affect biological material are still almost neglected in research.

1.1. Biological importance of pyrimidines and purines

The nucleic acids play a central role in the storage and expression of genetic information. They are divided into two major classes: (i) deoxyribonucleic acids (DNAs) - their function is storage of information, and (ii) ribonucleic acids (RNAs) which are involved in most steps of gene expression and protein biosynthesis. DNA is a long polymer of simple units called nucleotides, with a backbone made of sugar and phosphate moieties joined by ester bounds. One of four types of molecules, called bases, is attached to each sugar. The sequence of these four bases along the backbone encodes genetic information.

The bases that occur in nucleic acids are heterocyclic compounds - the derivatives of pyrimidine or purine. Pyrimidines consist of six-membered ring, purines have two condensed rings: five- and six-membered. The genetic code in the DNA is stored in the form of the sequence of hydrogen bonded purine and pyrimidine bases, and this specific sequence is unique for each individual. Alteration in DNA structure may lead to mutation by producing a permanent change in the genetic code [14].

The unproper pairing of the bases in polynucleotide chains leads to mutations. One of the possible causes of a mutation, proposed by Watson and Crick [15, 16] is creating a non-canonical complementary base-pair, with one of the bases adopting a rare tautomeric form.

In water environment each of the bases exist predominantly as one preferred tautomer, but at any moment a very small fraction adopts less stable tautomeric form (see Figure 1.1). Thus, rare tautomer B (imino-form of adenine) would not be able to pair with thymine, its proper pairing partner, but could pair with cytosine (Figure 1.2).

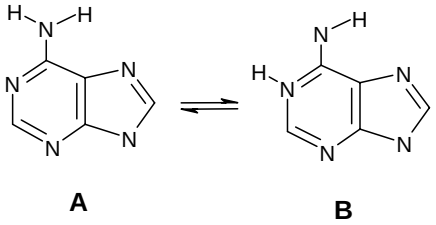

Figure 1.1. *Tautomerism of adenine*

If this event occurred to an AT pair during gene replication, an incorrect copy of the gene, differing in a single "code letter", would be formed. However, because the tautomerism is affected very strongly by the environment, the extent to which it may cause mispairing during enzymatic replication act is uncertain [17].

Genetic mutations may be caused by several factors, among them UV radiation. It is well known that nucleic acid bases absorb ultraviolet radiation efficiently; nevertheless, a case of mutation is a rare event. This implies that nucleic acid bases should be highly photostable. The high photostability was associated with observed low quantum yield of fluorescence (of the order of 10^{-4}), which indicates the presence of photophysical processes leading to fast nonradiative dissipation of energy gained by a molecule upon absorption of UV quantum [6]. It was even suggested that high photostability of nucleic acid bases is a reason for their selection as genetic species by nature. However, it does not need to be true, because it was observed that monomeric, isolated in Ar matrix, 1-methylcytosine (compound modeling cytidine) was subjected to photochemical modification. Upon UV ($\lambda > 295$ nm) irradiation, 1-methylcytosine transformed to open-ring isocyanate [18].

As it is known, in nucleic acids the complementary bases are connected by two or three hydrogen bonds. According to the recent theoretical models of the dissipation of electronic excitation in hydrogen-bonded base pairs, the presence of hydrogen bonds is the real origin of high photostability of DNA [19, 20].

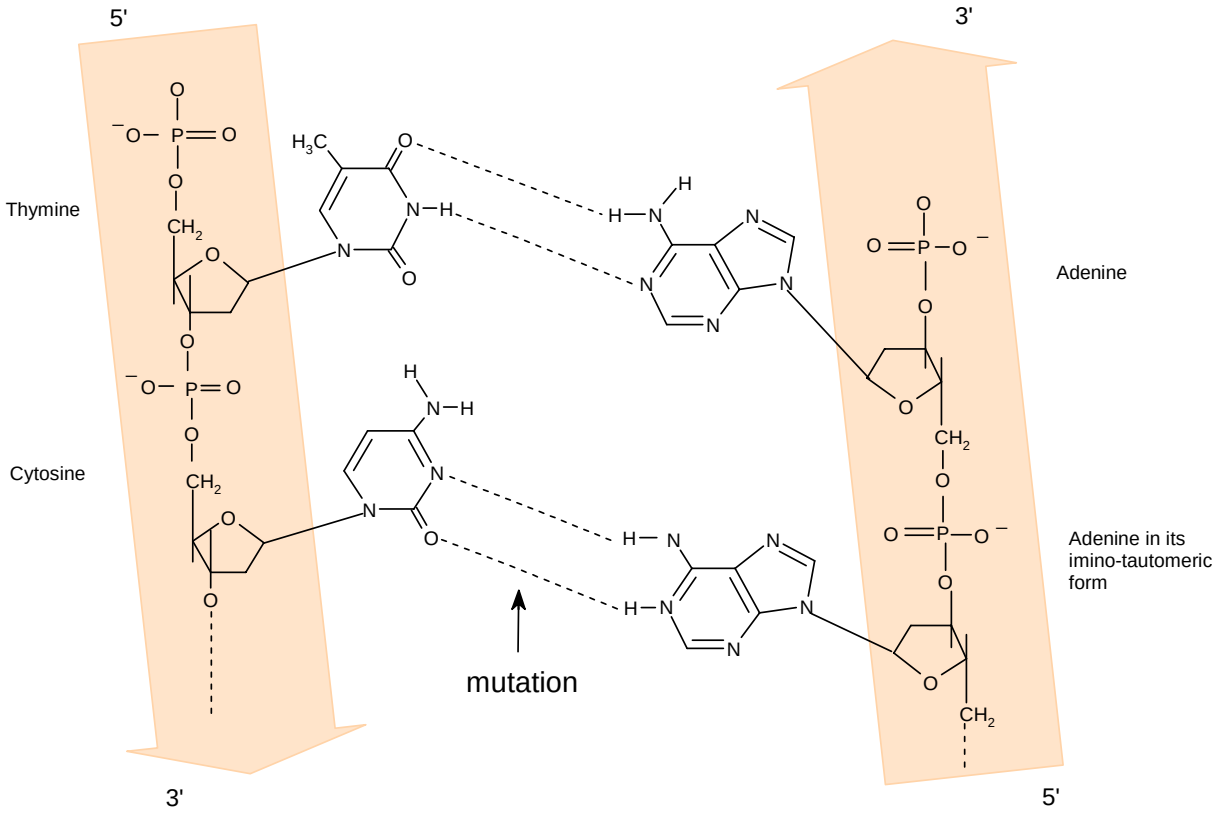

Figure 1.2. *The double helix of DNA has an invariable width because purines are always located opposite pyrimidines, forming specific base pair G-C and A-T. In this scheme, the imino tautomeric form of adenine forms a wrong complementary pair with the cytosine (instead of thymine) and thus causes the point mutation.*

Proton transfer represents one of the most fundamental processes involved in chemical reactions as well as in living systems. Vast number of research have been published regarding various types of proton transfer occurring in the ground state as well as in the excited states, since proton transfer leading to formation of rare tautomer may play a role in creation of point mutations.

The commonly known photochemical process of the proton-transfer occurring in the molecule after its excitation is known under acronym ESIPT (Excited-State Intramolecular Proton Transfer). ESIPT type of phototautomerization undergoes in the excited state where proton transfers through a low barrier or even without barrier [21, 22]. This is because the proton-transfer proceeds along an intramolecular hydrogen bond existing in S_0 and S_1 electronic state of the molecule. However, in monomeric nucleic acid bases there are no intramolecular hydrogen bonds. Computational studies of adenine, guanine and hypoxanthine have suggested that in the excited state the barrier for proton transfer is significantly large and, therefore, electronic excitation may not facilitate ESIPT processes for these species [23-25]. However, there is known

other type of proton (hydrogen atom) transfer, occurring after excitation of a molecule without intramolecular hydrogen bond. It was found in molecules with N-H group placed in α position with respect to C=O or C=S group [26-39]. This photoreaction was reported for cytosine where their rare hydroxy tautomeric form was obtained after UV irradiation of isolated molecule [40-42].

The investigation of this type of proton-transfer in the molecules described in the next paragraph is one of the main points of the current work.

1.2.Biological function of the studied compounds

tRNAs contain a number of unusual bases that are not normally found in DNA or other RNAs. These modified bases influence on the tRNA − mRNA base pairing and play a role in degeneracy of the genetic code [43-45]. Among these bases is hypoxanthine - a base of the rare, naturally-occuring nucleoside inosine (Figure 1.3).

Inosine nucleoside appears quite frequently in the anticodon region of natural tRNAs [48]. In bacteria, inosine can form wobble pairs with uridine, cytidine, and adenosine, and in eukaryotes only with uridine and cytidine. Inosine has been detected first in tRNA [46] and recently has been found in double-stranded RNAs, mRNAs, and virial RNAs [47].

In eukaryotic and prokaryotic messenger-RNA, inosine is formed during post-transcriptional editing by adenosine-to-inosine enzymatic conversion. Inosine monophosphate plays a key role in both biosynthesis and catabolism of purine nucleosides [49]. Hypoxanthine is present in muscles and other tissues, where it is formed during purine catabolism by deamination of adenine. This compound derives from adenine by replacement of its $–NH_2$ group with –OH and tautomerization to the oxo form.

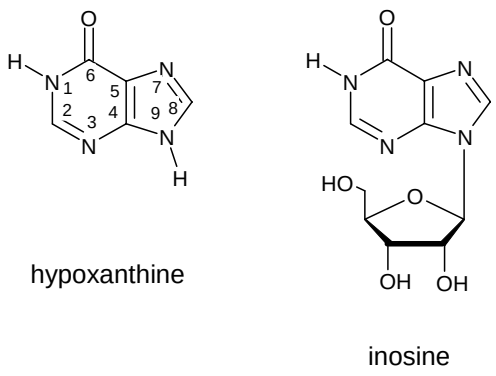

Figure 1.3. *Structures of hypoxanthine and inosine. Inosine is a nucleoside that is formed when hypoxanthine is attached to a ribose ring.*

Hypoxanthine and inosine found application in medicine. The first compound stimulates enzyme activity in both cardiac and skeletal muscle cells for improved regeneration of ATP (adenosine 5'-triphosphate). Inosine is widely available as a nutritional supplement in health food stores [50-52]. This compound has been used sporadically in clinical practice for various cardiovascular disorders, including some ischemic events [54]. Furthermore, inosine has been used recently, in small patient populations, for the therapy of multiple sclerosis [53]. Recent observations indicated that it might be possible to exploit inosine for the treatment of tissue damage caused by inflammation and ischemia [55]. Inosine ameliorates skeletal muscle ischemia - reperfusion injury, which makes it a potential candidate for therapeutic modulation of skeletal muscle reperfusion injury in the clinical setting [56].

Allopurinol is a heterocyclic molecule, closely related to hypoxanthine, in which N and C atoms in position 7 and 8 are interchanged (Figure 1.4).

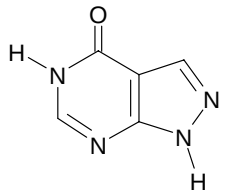

allopurinol

Figure 1.4. *Structure of allopurinol*

This compound is an inhibitor of xanthine oxidase, which catalyses the conversion of hypoxanthine to xanthine, thus reducing high level of uric acid in blood and serum, in such way preventing gout attacks and it is used to treat hyperuricemia [57-62]. Allopurinol is also used as chemoprotector during anticancer cytotoxic therapies [63, 64]. Moreover, this compound is known to effectively protect the heart against damage caused by oxygen free radicals in patients undergoing cardiac bypass surgery and coronary angioplasty [65-68]. Preliminary results of treatment of bipolar mania and schizophrenia suggest that allopurinol may be an effective adjuvant agent in the treatment of patients with these diseases [69, 70].

Quinoline (Figure 1.5) is present in many classes of biologically active compound, and its derivatives are known to exhibit a variety of biological effects.

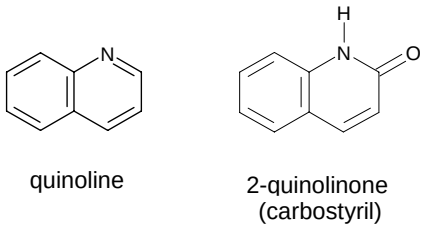

Figure 1.5. *Structure of quinoline and 2-quinolinone (carbostyril)*

A number of quinolines have been used as antifungal, antibacterial, and antiprotozoic drugs as well as antinoeplastics [71]. Styrylquinoline derivatives have gained strong attention recently due to their activity as perspective HIV integrase inhibitors [72-75]. Carbostyrils (2(1H)-quinolinones) can be considered as aza-analogues of coumarines which in turn have found application as photosensitizers [76], laser dyes [77-81] or pH-indicators in biochemistry and medicine [82, 83].

It is known also that substituted carbostyrils are good candidates for wave-shifting fluorophors in high energy particle detection [84]. Substituted carbostyrils (e.g. carbostyril 124 (7-amino-4-methyl-2(1H)-quinolinone)) are used as antenna molecules in luminescent lanthanide complexes. Such complexes consist of a lanthanide-binding chelate and organic-based chromophore, the latter acting as an antenna or sensitizer to absorb the excitation light and increase the weak absorbance of the lanthanides [85, 86].

The luminescent lanthanide complexes mentioned above find another application as probes in biological systems. In clinical using, luminescent lanthanide complexes applied as an immunological technique (solid-phase immunoassay) and used to quantify lipoprotein, which is a risk factor for coronary heart disease and ischemic cerebrovascular disease, in human serum [88]. Sensitized lanthanide fluorescence proves also to be attractive alternative to UV detection and other luminescence techniques in the chromatographic separation of drugs and xenobiotics [87]. Fluorescent heterocycles are also valuable enzyme substrates [89, 90], e.g. for proteases. Here carbostyril 124 was found to allow a more sensitive determination of enzyme activity than other fluorophors [89].

UV-induced damage to DNA has profound biological consequences, including photocarcinogenesis, a growing human health problem. It may be caused indirectly by photoproduction of hydroxyl radicals (·OH) in DNA environment. DNA damage induced by ·OH is an occurrence recognized in numerous experimental investigations [3, 91, 92]. Interaction with hydroxyl radicals was demonstrated to generate single-strand breaks in polynucleotide chains as well as modifications of nucleic acid bases. Recently, it was suggested that ·OH radicals can play a key role in oxidation of guanine to 8-oxo-7,8-dihydroguanine [93]. Hence, hydroxyl radicals give rise to oxidative modifications and mutations which can initiate carcinogenesis or/and a series of age-correlated degenerative diseases.

For the sake of experimental investigation of interactions of hydroxyl radicals with nucleic acids constituents, the method of *in situ* generation of ·OH radicals is of crucial importance. The photochemical methods based on light-induced decomposition of precursors (photo-Fenton reagents) have many advantages in comparison with chemical formation of such radicals (through the Fenton reaction [94]). These precursors allow photogeneration of ·OH radicals without inducing other photoreactions accompanying production of hydroxyl radicals.

N-Hydroxypyridine-2(1*H*)-thione (called also 2-mercaptopyridine *N*-oxide, omadine or pyrithione, Figure 1.6), is known to release a hydroxyl radical under ultraviolet irradiation. This photochemical source of ·OH radicals has been used in a number of studies on oxidative damage of DNA [95-98]. It was observed that UV excitation of *N*-hydroxypyridine-2(1*H*)-thione causes hemolytic N-O bond cleavage, which leads to the formation of the 2-pyridylthiyl and hydroxyl radicals [99-101]. However, unlike to its analogue *N*-hydroxy-2(1*H*)-pyridone, *N*-hydroxypyridine-2(1*H*)-thione undergoes other primary photoprocesses, which are pH-dependent [102-104].

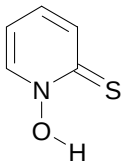

N-hydroxypyridine-2(1H)-thione

Figure 1.6. *Structure of N-hydroxypyridine-2(1H)-thione.*

N-hydroxypyridine-2(1H)-thione is a commercial substance known for its antibacterial, anticancer, antifungal and antidandruff activities [105-108]. The pyridine N-oxide derivatives represent a peculiar class of antiviral compounds that qualify as promising novel drugs for

exploration as potential anti-HIV agents. They have an entirely new mechanism of antiviral action and the capacity to retain antiviral activity against virus strains that have gained resistance to clinically used drugs [109].

Proceeding from all aforesaid, it must be confessed that interaction of radiation with organic compounds is responsible for many biological processes. Tautomerism, which may be a result of a photochemical reaction, plays an important role in modern organic chemistry, biochemistry, medicinal chemistry, pharmacology, molecular biology, and life itself. An intramolecular proton transfer may lead to a conversion of the molecule into another tautomeric form. Interconversion between thermodynamically stable tautomers is possible in solutions and in the gas phase for an isolated molecule. It may occur under the action of various factors, in particular, of light. Information about photochemistry of the studied in the current work compounds of biological importance may be very helpful for investigations of mechanisms of damages of living cells induced by UV light.

1.3. The aim of the thesis

In this work, the observations of UV-induced transformations in selected N-heterocyclic molecules isolated in low-temperature matrices are reported. Heterocylic compounds may exist in different tautomeric forms; hence, the tautomerism of the studied molecules was also one of the main aims of the investigations. The FT IR spectroscopy of matrix-isolated species was the experimental method used in this study.

Unimolecular photoprocesses were studied for:

- heterocyclic compounds with amide H-N-C=O group in a six-membered ring: 2-pyridinone (**2PD**), 4-pyrimidinone (**4PM**) and 2-pyrazinone (**2PZ**);
- compounds with fused hererocyclic and benzene rings, the analogs of **2PD**, **4PM** and **2PZ**: 2-quinoxalinone (**2QX**), 2-quinolinone (**2QL**), 1-isoquinolinone (**IQ**) 4-quinazolinone (**4QZ**) and 3-hydroxyisoquinolinone (**3IQ**);
- heterocyclic compounds with two, six- and five-membered, fused heterocyclic rings: allopurinol (**A**), 9-methylhypoxanthine (**mHx**) and hypoxanthine (**Hx**);
- heterocyclic compound with thione group attached to a six-membered ring – N-hydroxypyridine-2(1H)-thione (**Np**).

The investigations were aimed at:

- Experimental determination of the most stable tautomeric form of the studied molecules isolated in low temperature matrices.
- Investigations of an effect of UV irradiation of isolated molecules. Photoisomerization (or phototautomerization) processes were the main point of interest; therefore, irradiations were performed using filtered UV light to avoid photolysis of the molecules.
- Interpretation of IR spectra of observed tautomers and assignment of the absorption bands in experimental spectra to the normal modes predicted by theoretical calculations. Phototautomeric reactions allowed separation of the spectra due to different tautomers.
- Experimental determination of free energy difference ΔF between tautomers coexisting in a matrix. It was possible after the IR spectra had been separated and interpreted.
- Comparison between experimentally and theoretically determined relative stabilities of tautomers. This comparison allowed assessment of the accuracy of current (available on PC computer) methods of calculation of electronic energy of a molecule.
- Assessment of an effect of benzo-annelation on oxo-hydroxy tautomerism of hetrocyclic compounds.
- The study on the possibilty of the photogeneration of ·OH radicals after irradiation of N-hydroxypyridine-2(1H)-thione isolated in inert gas matrices, similarly, as it was in solutions.

The results presented in the thesis have been published (list of publication presented on page vii).

2. Matrix isolation and matrix-isolation photochemistry

2.1. Matrix isolation

The origin of matrix isolation spectroscopy can be traced to the early experiments of Vegard in the early 1920s [110, 111]. Vegard bombarded condensed rare gases or nitrogen with electrons and observed the resulting luminescence. He noted the similarity between a persistent green ≈5577 Å luminescence emanating from the cryogenic solids, and the prominent line detected in aurora borealis, and saw in the low-temperature spectroscopy a convenient method to study auroral glow and other atmospheric phenomena. The term "matrix isolation" was coined some 30 years later in 1954 by Pimentel [112] and co-workers, who used the technique for systematic studies of free radicals and other unstable or transient species.

In principle, studies of the particles which do not react with each other, have to be carried in the gaseous faze. Such a method is the best to determine the thermodynamic values which are characteristic of the particle in study. However, the studies of some compounds, for instance, of pyrimidine and purine derivatives, are difficult, often even impossible, because of high temperature of sublimation, low vapor pressure, and ability to thermal decomposition in the temperatures necessary to achieve sufficient vapor pressure (≈ 500K). Moreover, broad bands with traces of rotational branches are typical of the IR spectra of gaseous samples gained in high temperatures. The broadening is due to overlapping of the rotational lines. It complicates the identification of absorption bands and restricts the sensitivity of spectral method applied to recognition of small rate of species present in a gaseous sample, e.g. rare tautomers. In contrast, the spectra of molecules in matrix consist of narrow bands well separated from each other. In solid noble gases (or solid nitrogen) at low temperature the rotation of molecules is strongly prevented. Only small molecules as water or methane rotate, but they occupy only the lowest rotation levels. This leads to significant simplification of infrared spectra of matrix-isolated molecules.

Furthermore, investigation of pyrimidines and purines in weak-interacting solvent is impossible because of low solubility of the compounds. The inconveniences listed above do not take place if the low-temperature matrix isolation technique is applied. The matrix isolation method has been used for many years to study isolated pyrimidines and purines.

The matrix isolation technique is based on co-deposition of noble gas (or nitrogen) together with vapors of a studied compound onto a cold (4-20 K) window placed on a cold finger of

a liquid-helium-cooled cryostat. Good isolation of monomers is assured by a large (700-1000 fold) excess of matrix gas with respect to the number of the dopant molecules.

The interactions between the studied molecules and the atoms or molecules of the host matrix material are very weak. Hence, the energy states of molecules isolated in low-temperature inert gas matrices are only slightly perturbed in comparison with the states of monomers in the gas phase. On the other hand, in the experimental spectra of species trapped in a matrix, often multiplets are observed instead of a single bands corresponding to a given vibration. Such multiplets reflect the interactions with the matrix environment, which may be different in each of the trapping sites. It can lead to the splitting of the band in the spectrum. The magnitude of this splitting is from several up to about twenty cm^{-1}. More often, this interaction is expressed in the shift of the position of spectral lines – *matrix shift*, and can reflect the influence of the matrix environment on the energy states which participate in optical transitions.

Studies of nonradiative processes occurring in the matrix have shown that electronic relaxation often proceeds via two or more electronic states [113]. In a matrix, it is easier to understand the relaxation pathways and mechanisms. In such environment, the forbidden states could be populated by exciting of high-lying levels, and thus they could be studied spectroscopically.

Due to low temperature and absence of collisions, the reactive species can be stabilized under matrix-isolation conditions. The following species could be investigated: radicals, diradicals, high-energy isomers and products of fragmentation. Matrix isolation allows trapping primary products of photochemical transformations. Two types of photochemical changes can be observed following *in situ* irradiation of matrix-isolated species: photoisomerizations and photoinduced dissociations. In the second case, the fragments generated in a photoprocess are usually confined in the same cage of the matrix. Only very small fragments, such as the hydrogen atom or the fluorine atom, can diffuse out of the original cage. Products of photoisomerization or photofragmentation once generated and stabilized in a matrix cage, can then be studied at leisure using standard, stationary spectroscopic methods. The spectra of the species in the matrix can be accumulated over a long period and then can be studied. Absorption spectroscopy can be applied in a wide spectral range, because solid layers obtained from noble gases (or nitrogen) are transparent from far infrared to vacuum ultraviolet. The most information on the structure of the molecules can be drawn from IR spectra in 4000-200 cm^{-1} range.

2.2. Infrared spectroscopy and matrix isolation

Among other spectroscopic methods, the infrared (IR) spectroscopy is the most effective technique to determine the structure of the molecules isolated in low-temperature matrices. The IR spectra provide information about the vibronic states of the molecule. The spectra consist of the bands, which can be associated with the vibrations of the different groups of atoms in the molecule. One of the applications of IR spectroscopy is identification of the structure of molecules which may exist in different tautomeric forms. The groups, such as OH, NH, C=O, NH_2 are specific to tautomeric forms, and the strong absorption bands placed in well defined spectral range are characteristic of their vibrations. Therefore, the presence of these groups in the molecule can be easily identified during the analysis of obtained IR spectra, and hence, the tautomeric form can be determined.

Assignment of all observed absorption bands in the IR spectrum to the normal mode vibrations of a molecule is not an easy task. Fortunately, current quantum-chemical methods allow predicting IR spectra with quite good accuracy. The spectra obtained in calculations fit relatively well the spectral pattern obtained in matrix-isolation experiments. The good agreement between positions and intensities of the bands of the observed and calculated spectra usually allows interpretation of the majority of absorption bands.

There are several effects observed in the spectra of molecules in the matrix environment, which should be taken into account when spectra are interpreted.

(i) Matrix shift. Even weekly interacting matrix environment disturbs vibrational levels of a molecule. It can be easily seen, when the spectra obtained in Ar and N_2 matrices are compared. Molecular nitrogen matrix interacts stronger with isolated molecule than Ar environment. If an argon matrix is replaced by a nitrogen matrix, positions and shape of the bands will change. Usually, in N_2 matrix the frequencies of the stretching vibrations of the external groups of atoms in the molecule are lower while frequencies of deformation vibrations are higher than in an Ar matrix. The bands of skeleton vibrations are much less disturbed [26, 28]. Observation of this effect often helps in identification of the bands originated from deformation in-plane (as well as out-off-plane) vibrations of OH or NH groups in the absorption spectrum.

(ii) Matrix splitting. The bands in the matrix spectrum are often split. It can be due to different trapping sites in which the molecules are hold in the matrix. It is due to slightly different matrix-guest interactions in the matrix cages. This effect may interfere with the splitting due to coexistence of different conformers of isolated molecule. The change of the matrix gas modifies the splitting pattern due to the matrix, while the components of the split bands which originate from different conformers are subjected only to the matrix shift.

(iii) Structure of the bands due to self-association. If the concentration of the molecules in the matrix is not sufficiently low, then dimers (or even higher aggregates) of the studied compound also can be trapped. In such a case, except of the bands due to monomers, the bands originating from dimers and higher associates appear in the spectrum. The intensities of the bands due to associates depend on the matrix/guest ratio, the ability of the compound to aggregate (e.g. it depends on the possibility of formation of intermolecular hydrogen bonds), the temperature in which the matrix was formed, and the quality of the matrix.

(iv) Appearance of the bands due to impurities. The traces of water or other atmospheric components are difficult to eliminate because of the leaks in the vacuum elements and cryostat. In addition, the impurities from vacuum pumps may contaminate the matrix. The presence of such impurities may be observed in the matrix spectrum in the form of additional bands.

2.3. Tautomerism and phototautomerism

The first publication on prototropic tautomerism of the heterocyclic compounds appeared at the beginning of the 20^{th} century. The most of this works was dedicated to the researches of tautomeric equilibrium in the solvents and in the solid state. It was found out that tautomeric equilibrium constant depends on the solvent polarity [114, 115]. But first research of 2-pyridinone system in the gas phase [116] showed that the tautomeric equilibrium changes significantly in the case when the molecule does not interact with the environment.

The comparison of available data on tautomeric equilibria of the same systems in the gas phase and in the matrix has shown that relative participation of the tautomers of the isolated in the low-temperature matrix molecule corresponds to the equilibrium existing in the gas, from which the matrix was formed. One can say that tautomeric equilibrium state that exists in the gas is “frozen” in the matrix. That is why in all thermodynamic considerations, carried out using the data obtained from the spectra of matrices, not the temperature of the matrix itself, but the temperature of vapor during deposition of the matrix was applied as the temperature in which the tautomeric equilibrium was achieved.

Phototautomerism

The proton transfer (or hydrogen atom transfer) from one functional group to another is one of the most important reaction which play a fundamental role in chemistry and biochemistry [117]. This reaction is the base of many chemical and biochemical processes, including mechanisms regulating acid-base equilibrium in the cell [118] and enzymatic reaction [119]. Depending on the system, reaction can be intra- or intermolecular. Two types of intramolecular proton transfer processes induced by excitation to electronic states higher than S_0 are commonly known. One of them is the excited state intramolecular proton transfer (ESIPT) [120-123], and the second is Norish II type reaction [124, 125].

The proton transfer can be activated thermally or by excitation of the system with radiation. We have deal with the case when the activation energy allows proton to transit above the barrier dividing the substratum and the product. But many cases are known when the proton is tunneling through the barrier (proton tunneling) [126].

In this work, much less known process of intramolecular proton (hydrogen atom) transfer simulated by UV-Vis radiation was studied. The effect of this photoreaction is the change of tautomeric form of irradiated molecule. The nature of this photoreaction is different from those well known mechanisms like ESIPT and Norrish type II reaction. The difference between these reactions is that in above mentioned photoreactions, the proton transfer occurs along the intramolecular hydrogen bridge. However, in the molecules, which undergo the phototautomeric reaction of the type studied in this work, there are no intramolecular hydrogen bonds. Intermolecular hydrogen bonds are excluded by isolation in low-temperature matrix.

Excited S_1 state of the photoproduced tautomers (hydroxy, thiol or selenol) is energetically higher than the S_1 state of the initial tautomers (oxo, thione or selenone) [127-129] (Figure 2.1). In the ground electronic state, the photoproduced tautomers are separated by a high-energy barrier from the initial form. Hence, the photogenerated tautomers are stable (at least for several hours) under low-temperature conditions. In the case when the molecule is in other environment than matrix, i.e. when the molecule is not isolated, the barrier between tautomers is significantly lowered due to intermolecular interactions, and the process of tautomerism is much faster.

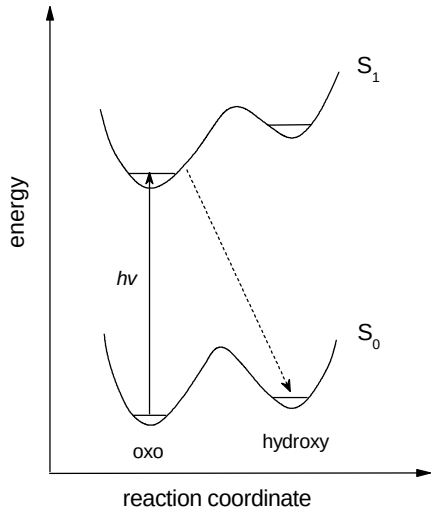

Figure 2.1. *Scheme of the phototautomeric reaction in the molecules with N-H and C=O groups.*

The proton transfer phenomenon which leads to the change of the tautomeric form from oxo to hydroxy due to irradiation of the matrix by the UV-light, was observed for the first time by M.J. Nowak et al. during studies of isolated 4-pyrimidinone [26]. Next, the same type of the reactions of phototautomerism was observed for the several other molecules, where the oxo-hydroxy, imino-amino, tion-tiol tautomerism is possible [26-39, 130-132] (Figure 2.2).

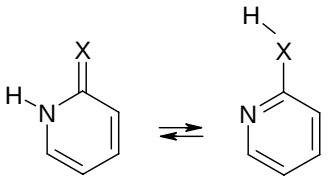

X=O – oxo-hydroxy tautomerism
X=NH – imino-amino tautomerism
X=S – tion-tiol tautomerism

Figure 2.2. *Types of prototropic tautomerism*

The experiments show, that photoreaction (the proton transfer from N-H group to O, S or Se atom due to the irradiation of the UV-light) is typical of the whole class of simple or heterocyclic molecules, and this is not an accidental occurrence characteristic of one or two species [26, 31, 34-37, 133].

The mechanism of the photoinduced proton transfer processes described here is still not well-elucidated. The most promising theoretical explanation of the phototautomeric phenomena may be drawn from the theoretical model provided by Sobolewski and co-workers [134-136]. On the basis of the advanced CASPT2 calculations authors postulate a key role of the exited $^1\pi\sigma^*$

states in hydrogen-atom-detachment and proton-transfer processes occurring in a variety of molecular systems. For the molecules with N-H groups, the excited $^1\pi\sigma^*$ states have a repulsive character with respect to the N-H stretching coordinate (Figure 2.3).

For a simple heterocyclic molecule, such as pyrrole, the optically dark $^1\pi\sigma^*$ state is energetically the lowest of all excited states. In more complex heterocycles, containing more heteroatoms (that lowers the energy of the $n\pi^*$ excited state) or/and more extended π-electron system (that lowers the energy of the $\pi\pi^*$ excited state), $^1\pi\sigma^*$ excited state is usually not the lowest, but it can be accessed upon crossing a low-energy barrier (Figure 2.3). Detachment of hydrogen atom from UV-excited pyrrole was recently experimentally demonstrated by Wei et. al. [138].

It can easily be imagined that in systems with either the C=O, C=S or the C=Se group in a direct vicinity of the N-H moiety, the proton which looses its attractive connection with the nitrogen atom can be trapped and form a new O-H, S-H or Se-H bond, instead of a complete detachment from a molecule. This mechanism seems to be the most promising way for rationalizing the experimental observations of the proton transfer processes described in this work.

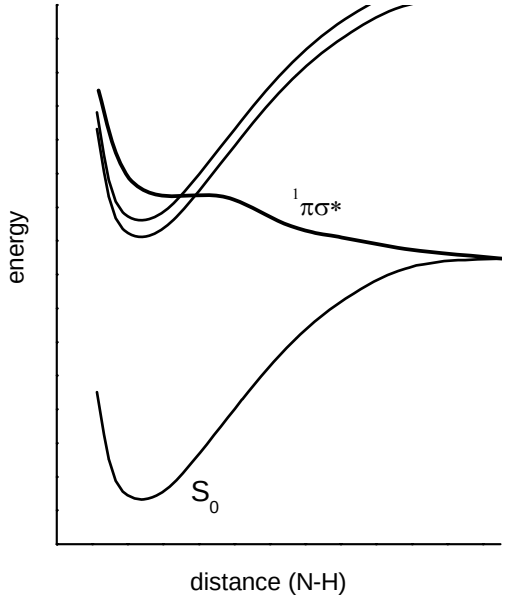

Figure 2.3. *Schematic representation of the excited $^1\pi\sigma^*$ state in a heterocyclic molecule (after [134, 137]).*

In this work we will deal with the type of tautomerism which is connected with intramolecular proton transfer between nitrogen atom of the heterocyclic ring and the C=O group in α-position with respect to each other, or with proton transfer between different nitrogen atoms in the heterocyclic ring (tautomerism N(7)-N(9) in purines). The studied compounds can exist in several tautomeric forms. Experimentally, the structures of the lowest free energy are observed. Relative energy of the tautomers depends of the properties of the molecule, and of the conditions in which the molecule exists.

It is observed that phototautomeric reaction proceeds independently on the ratio between tautomers existing in the matrix. As a result of the irradiation by the UV (UV-Vis) light, the relative intensities of the bands corresponding to the different tautomers have been changed. The increase of the intensity of the bands corresponding to one tautomer (hydroxy) and simultaneously, decrease of the bands from another tautomer (oxo) are observed. This effect gives an opportunity to assign absorption bands, which intensities change simultaneously, to different tautomeric forms appearing in the matrix. For the first time this method was applied to separate the spectra of tautomers of 4-pyrimidinone [26, 28]. At present, the results of separation of the spectra, obtained employing this method, are usually confirmed by comparison with spectra theoretically predicted for the tautomers of studied molecule.

3. Experimental

3.1. Experimental setup

Low-temperature matrices were prepared in the continuous-flow liquid helium cryostat designed by M.J. Nowak (Figure 3.1; **k** in Figure 3.2). The cold finger of the cryostat was cooled by liquid helium which was continuously transferred from the Dewar vessel (8 in Figure 3.2). The flow of the liquid helium was regulated by the needle valve placed in the helium transfer line. The rotary pump (9 in Figure 3.2) pumped gaseous helium from the cryostat to the gas line leading to the helium liquefier. The cryostat was equipped with an internal shield cooled with liquid nitrogen. This shield allowed better thermal isolation and acted as liquid nitrogen trap in the cryostat. Rests of water vapor and other gaseous impurites, which were not removed during the pumping before cooling the cryostat, were frozen on it.

The matrix was deposited on the window from caesium iodide monocrystal (CsI). The cold spectroscopic window was placed on the copper block, which was attached to the cold finger of the cryostat. Temperature of the copper block was measured with the silicon diode DT-471 of Lake Shore Cryonics (which is especially designed for measurements of the helium temperatures, 3 in Figure 3.2). The temperature of the CsI window was usually maintained at 10 K.

The matrix gas introduced to the cryostat passed trough a coil in the liquid-N_2-cooled jacket of the cryostat before deposition. The matrix-gas flow was controlled by the precise needle valve. The rate of matrix gas deposition on the CsI window was determined by controlling the pressure inside the cryostat during the matrix deposition.

During deposition of the matrix, the solid sample of the studied compound sublimated from a small electric oven located near the cold window. Temperature of this oven was regulated by changing electric current. The power supplier EL 302D of the Thurby-Thandar Instruments (4 in Figure 3.2) allowed precise regulation of the current.

In the case when at room temperature the saturated vapor pressure over the solid sample of the compound was high, the compound was placed in a glass tube connected to the vacuum chamber of the cryostat through a regulating valve.

The vapors of the studied compound were deposited with a large excess of inert gas on the cold window. The matrix gases (used in this work) are: argon (Ar) and nitrogen (N_2). Argon matrix gas of spectral purity 6.0 was supplied by Linde AG. Nitrogen of spectral purity was obtained from Technische Gase, Leipzig.

The matrix deposition lasted usually about two hours. The art of preparation of a good matrix consists in achieving a proper balance between concentration of the studied molecules and the thickness of a matrix, because the matrix should contain sufficient number of molecules of the studied compound in the path of the infrared spectrometer beam. The concentration of molecules introduced into a matrix should be as low as possible to avoid their association. The thickness of a matrix layer cannot be too large to avoid scattering of the spectral beam.

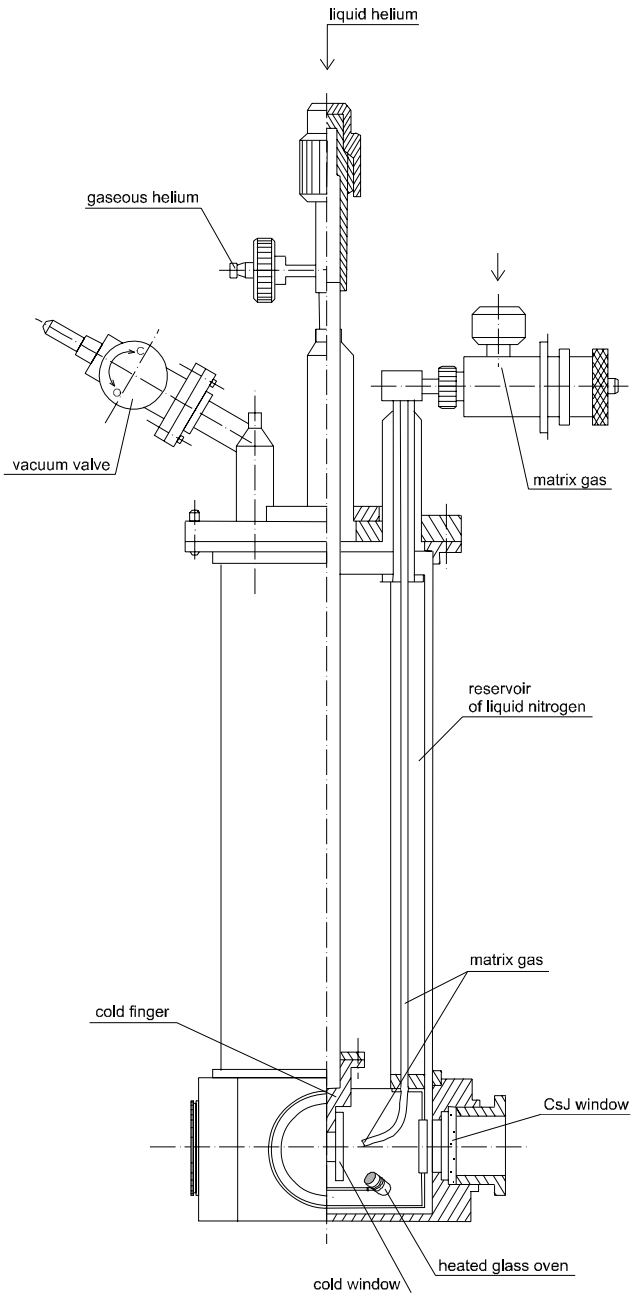

Figure 3.1. *Scheme of the continuous flow cryostat.*

The vacuum system with two stage mechanical vacuum pump and oil diffusion pump ensured the high vacuum inside the cryostat necessary for preservation of low temperatures and to create conditions for deposition of a matrix. The system allowed achieving vacuum of about 10^{-3} Torr in the area of forevacuum obtained by the two stage mechanical pump (14 in Figure 3.2) and 10^{-5} Torr in the area of high vacuum obtained by diffusion pump (11 in Figure 3.2). This vacuum system was equipped additionally with two liquid nitrogen traps to remove the rests of oil getting out from the pumps. The pressure in the vacuum system was measured with the resistance gauge PWN100 (TEPRO) (13 in Figure 3.2). The pressure inside the cryostat was controlled by Penning's gauge VPG1 (LP Praga) (2 in Figure 3.2). It allowed registration of the pressure inside the cryostat during the matrix deposition when the vacuum line was disconnected from the cryostat. The pressure inside cooled cryostat (at 10 K) was of the order of 10^{-7} Torr, during deposition of the matrix the pressure was about 3×10^{-4} Torr.

The spectra were recorded using Fourier transform infrared spectrometer Thermo Nicolet Nexus 670 (1 in Figure 3.2). The infrared beam from the spectrometer passed through the center of the optical window of the cryostat. The spectra were recorded in the range of 4000 – 400 cm^{-1} using KBr beam-splitter and a DTGS detector. The spectra in the low-frequency range up to 200 cm^{-1}, the limit of the spectral transmission of CsI, were obtained using solid-substrate beam-splitter and DTGS detector equipped with polyethylene window. The IR spectra were recorded with 0.5 cm^{-1} resolution. The spectrum was obtained after cumulating interferograms from 200 scans. The interferograms were collected and Fourier transformation was made by PC computer connected on-line to the spectrometer. The computer software OMNIC was used in this purpose. The same program was used in further processing of the collected spectra.

The space inside the spectrometer should be free of gases such as water vapor and carbon dioxide, which absorb in the infrared spectral range. For this purpose the spectrometer was connected to the air dryer. It consisted of the Parker Balston Purge Gas Generator Model 75-52 (6 in Figure 3.2) and compressor Atlas-Copco SF2 (5 in Figure 3.2).

Matrices were irradiated with the light from HBO200 high-pressure mercury lamp, which emitted ultraviolet irradiation. This lamp was fitted with a water filter (of 7 cm optical path length) which cut-off the infrared radiation from the lamp. The high energy part of the UV radiation was filtered from the mercury lamp light using different cut-off filters.

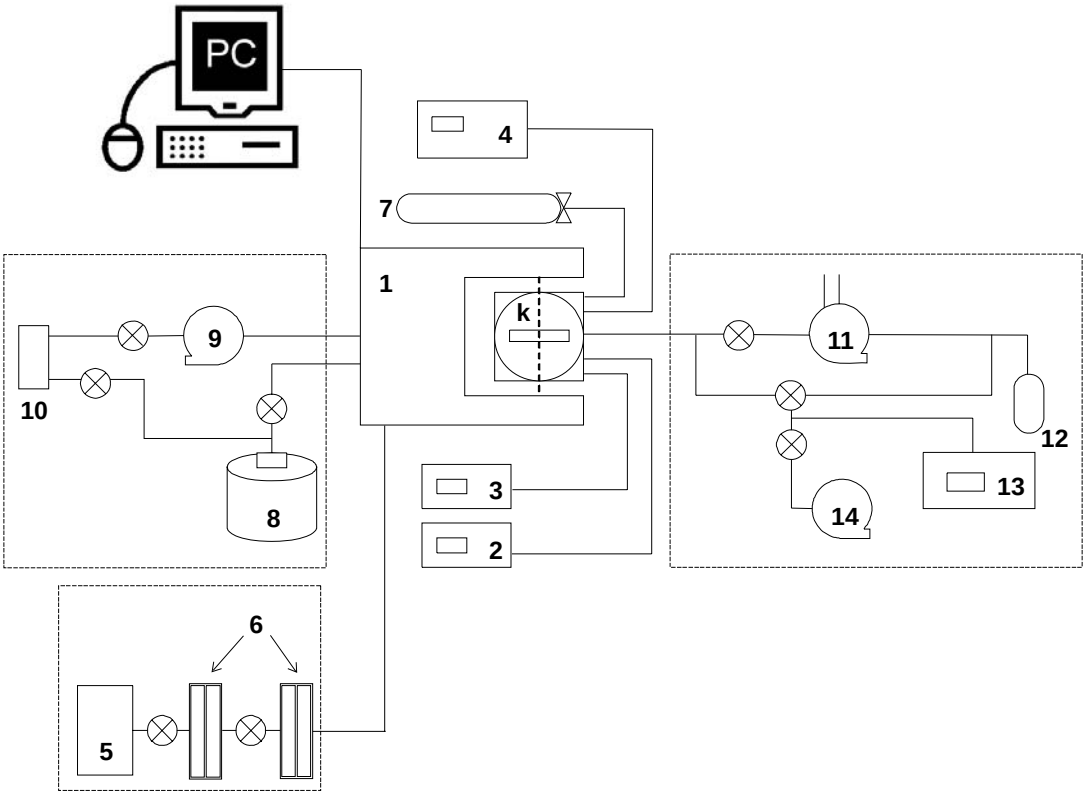

Fig. 3.2. *Scheme of the system used in the experiments.*

1. FT-IR Spectrometer (Thermo Nicolet Nexus 670), **k** –continuous-flow helium cryostat with cool (10 K) CsI window.
2. Vacuometer with the gauge inside the cryostat.
3. Controller of the CsI window temperature; temperature detector was a silicon diode.
4. The power supplier for the electric oven inside the cryostat.
5. Air compressor.
6. Columns with desiccant of the air purge generator.
7. Glass reservoir with the matrix gas.
8. Dewar vessel with liquid helium.
9. Rotary pump pumping helium to the helium liquefier system.
10. System transferring gaseous helium to the helium liquefier.
11. Diffusion oil pump.
12. Forevacuum chamber in the vacuum line.
13. Vacuum gauge in the vacuum system.
14. Two stage mechanical pump in the vacuum system.

The following cutoff filters from Advanced Optics SCHOTT AG were used: UG5 transmitting light with $\lambda > 240$ nm, UG11 transmitting light with $\lambda > 270$ nm, WG 345 transmitting light with $\lambda > 345$ nm, WG 335 transmitting light with $\lambda > 335$ nm, WG 320 transmitting light with $\lambda > 320$ nm and WG 295 transmitting light with $\lambda > 295$ nm. The ΦC-7 filter which transmitted light in the range of the near ultraviolet (275-375 nm), was used to cut-of the visible part of the emission spectra of the Hg lamp (which heated the matrix). The time of the irradiation of the matrix and the combination of the filters depended on the type of the studied substance and on the experiment. The time of irradiation of the matrices was usually in the limits from several minutes (in the case of the fast photochemical reaction) to several hours (when the photochemical reaction was slow).

3.2. The studied compounds

Allopurinol (mp >300 °C) used in the present study was a commercial product supplied by Aldrich. A sample of **9-methylhypoxanthine** was kindly made available by Professor Bernhard Lippert from Fachbereich Chemie, Universitat Dortmund, Germany.

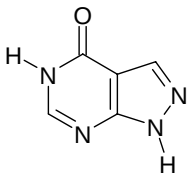

allopurinol

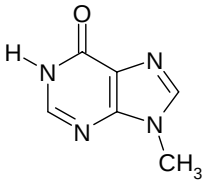

9-methylhypoxanthine

The sample of **hypoxanthine** (mp > 300 °C) used in the present study was supplied by Aldrich.

hypoxanthine 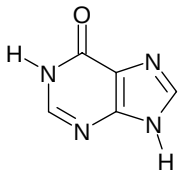

2-Pyridinone (mp = 280-281 °C), **4-pyrimidinone** (mp = 163-165 °C), **2-quinolinone** (mp = 198-199 °C), **1-isoquinolinone** (mp = 211-214 °C), **3-hydroxyisoquinoline** (mp = 192-194 °C), **2-quinoxalinone** (mp = 271-272 °C) and **4-quinazolinone** (mp = 216-219 °C) used in the present study were commercial products supplied by Sigma-Aldrich. The sample of **2-pyrazinone** (mp = 188 °C) was synthesized using the procedure described in Refs [139-141].

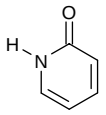

2-pyridinone

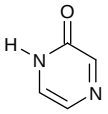

2-pyrazinone

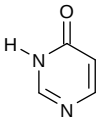

4-pyrimidinone

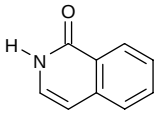

1-isoquinolinone

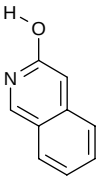

3-hydroxyisoquinoline

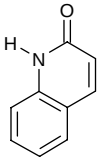

2-quinolinone

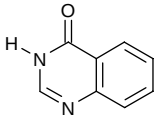

4-quinazolinone

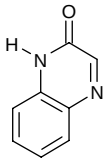

2-quinoxalinone

The sample of ***N*-hydroxypyridine-2(1*H*)-thione** used in the present study was supplied by Aldrich (as 2-thiopyridine-N-oxide) Its isotope analogue with the labile hydrogen atom replaced by deuterium was prepared by two cycles of dissolving in deuterated methanol (99% D, Aldrich) or deuterated ethanol (99.5% D, Aldrich) followed by drying in a stream of clean, gaseous nitrogen coming from above liquid N_2. Even at room temperature (typically 24 ºC) the saturated vapor pressure over the solid compound was sufficiently high for deposition of the matrixes.

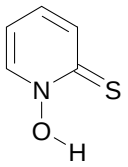

N-hydroxypyridine-2(1H)-thione

The nomenclature used above refers to the compounds neverless of their tautomeric form. If the further text will concern specified tautomer of a molecule then it will be explicitly indicated.

4. Theoretical background

4.1. Ab initio methods of quantum chemistry

The effects of interaction of molecules with electromagnetic radiation, studied experimentally, cannot be interpreted without theoretical background of quantum chemistry. The quantum chemistry has risen in the first half of 20th century, when the quantum mechanics has been applied to analyze the properties of the molecular systems. The present methods of quantum chemistry allowed determining many properties of the molecules:

- molecular energies and structures,
- energies and structures of transition states,
- bond and reaction energies,
- molecular orbitals,
- multipole moments,
- atomic charges and electrostatic potentials,
- vibrational frequencies in IR and Raman spectra,
- UV/VIS spectra,
- NMR properties,
- polarizabilities and hyperpolarizabilities,
- thermochemical properties,
- reaction pathways.

Spectroscopic methods, (such as microwave, infrared and ultraviolet/visible and NMR spectroscopy) are widely applied for verification of theoretically predicted molecular properties.

In order to resolve the physical or chemical problem for microscopic systems it is necessary to solve the Schrödinger equation for the whole system. In consequence there is a necessity of handling the second-order differential equations with singular potentials for thousands of variables. Because of its complexity, the exact solution of the Schrödinger equation is not possible for molecular systems. However, a number of simplifying assumptions allow obtaining an approximate solution for a range of systems. If the solution was generated without reference to the experimental data, the methods are usually called *ab initio*, in contrast to semi-empirical models. The latter methods are almost entirely substituted nowadays by *ab initio* methods in studies of molecular systems of small and medium size.

A molecular system consists of relatively heavy nuclei and much lighter electrons. Because of heavy masses of the nuclei, the electron motion occurs on a comparatively faster time scale.

Therefore, instantaneous changes in electronic structure (e.g. electronic excitation) occur with essentially stationary positions of the nuclei. The movements of the nuclei and the electrons can be approximately considered as independent. This leads to a commonly known Born-Oppenheimer approximation.

The simplest method of determination of electronic structure of a quantum mechanical system by solving the Schrödinger equation (within the Born-Oppenheimer approximation) is the Hartree-Fock (HF) or self-consistent field approximation. One of the limitations of HF calculations is that they do not include electron correlation. This means that HF takes into account the average effect of electron repulsion, but not the explicit electron-electron interaction. Within HF theory the probability of finding an electron at some location around an atom is determined by the distance from the nucleus but not the distance to the other electrons as shown in Figure 4.1. This is not physically true, but it is the consequence of the central field approximation, which defines the HF method.

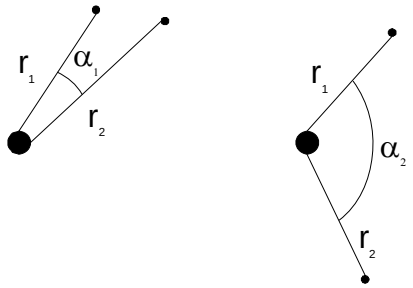

Figure 4.1. *Two arrangement of electrons around the nucleus of an atom having the same probability within HF theory, but not in correlated calculations.*

A number of types of calculation begin with a HF calculation and then correct for correlation. Some of these methods are Møller-Plesset perturbation theory (MPn, where n is the order of correction), coupled cluster theory (CC), configuration interaction (CI) method.

4.1.1. Møller-Plesset theory MP2

Correlation can be added as a perturbation from the Hartree-Fock wave function. This is called **Møller-Plesset perturbation theory**. In mapping the HF wave function onto a perturbation theory formulation, HF becomes a first-order perturbation. Thus, a minimal amount of correlation is added by using the second-order MP2 method [142]. Third-order (MP3) and fourth-order (MP4) calculations are also common. The accuracy of an MP4 calculation is roughly equivalent to the accuracy of a CISD (Configuration Interaction Single and Double excitations, see

Section *4.1.2*) calculation. MP5 and higher calculations are seldom done due to the high computational cost.

In the Møller-Plesset method, the zero-order Hamiltonian is defined as the sum of all the N one-electron Hartree-Fock operators, $\hat{F}(i)$:

$$\hat{H}^{(0)} = \sum_{i=1}^{N} \hat{F}(i) \tag{1}$$

The first-order perturbation is the difference between the zero-order Hamiltonian (1) and the electronic Hamiltonian:

$$\hat{H}^{(1)} = \hat{H} - \hat{H}^{(0)} \tag{2}$$

The Hartree-Fock ground-state wavefunction ψ_{HF} is an eigenfunction of the Hartree-Fock Hamiltonian $\hat{H}^{(0)}$, with an eigenvalue of $E^{(0)}$ (the sum of the orbital energies of all occupied spin-orbitals):

$$\hat{H}^{(0)}\psi_{HF} = E^{(0)}\psi_{HF} \tag{3}$$

$$E^{(0)} = \sum_{i}^{n} \varepsilon_i \tag{4}$$

The Hartree-Fock energy is associated with the normalized ground-state HF wavefunction:

$$E_{HF} = \langle \psi_{HF} | \hat{H} | \psi_{HF} \rangle = \langle \psi_{HF} | \hat{H}^{(0)} | \psi_{HF} \rangle + \langle \psi_{HF} | \hat{H}^{(1)} | \psi_{HF} \rangle = E^{(0)} + E^{(1)} \tag{5}$$

Hence, the HF energy is the sum of the zero and first-order energy.

Using the formalism of perturbation calculation of Rayleigh-Schrödinger, the energy of the system can be obtained:

$$E_{MP2} = E_{HF} + \sum_{k} \frac{\left| \langle \psi_k^{(0)} | \hat{H} \psi_{HF} \rangle \right|^2}{E^{(0)} - E_0^{(k)}} \tag{6}$$

The second item is a second-order correction, where as a wavefunctions $\psi_k^{(0)}$ the Slater determinants are used, corresponding to the energies $E_k^{(0)}$ and fulfilling the condition $\langle \psi_k^{(0)} | \psi_{HF} \rangle = 0$. This correction takes into account the dynamic correlation of the electrons.

The explicit formula for second-order Møller-Plesset correction is

$$E_{correct} = \sum_{i<j} \sum_{a<b} \frac{| \langle ij \mid ab \rangle - \langle ij \mid ba \rangle |^2}{\varepsilon_i + \varepsilon_j - \varepsilon_a - \varepsilon_b} \tag{7}$$

Symbols *i*, *j*, *k* are used for the occupied and *a*, *b*, *c* for virtual spin-orbitals, ε is the eigenvalue of one-electron Fock operator.

The MP2 method gives less accurate results of the calculation of the frequencies of the vibrations than DFT method. The error of obtained frequencies of out-of-plane vibrations in the molecule reaches up to 100 cm^{-1}.

4.1.2. Configuration interaction (CI), Quadratic configuration interaction with single and double excitation (QCISD) and Quadratic configuration interaction with single, double excitation and perturbative corrections for triple excitations (QCISD(T))

A **configuration interaction** wave function is a multiple-determinant wave function. This is constructed by starting with the HF wave function and making new determinants by promoting electrons from the occupied to unoccupied orbitals.

Hartree-Fock single-determinant wave function:

$$\psi_0 = \frac{1}{\sqrt{n!}} \det\{\phi_1 ... \phi_n\}, \tag{8}$$

where ϕ_i (i = 1,…n) are occupied spin orbitals.

Configuration interaction calculations [143] are classified by the number of excitations used to make each determinant. If only one electron has been moved for each determinant, it is called a configuration interaction single-excitation (CIS) calculation. CIS calculations give an approximation to the excited states of the molecule, but do not change the ground-state energy. Single and double excitation (CISD) calculations yield a ground-state energy that has been corrected for correlation. Triple excitation (CISDT) and quadruple excitation (CISDTQ) calculations are done only when very-high-accuracy results are desired.

The CI wave function: $\psi_{CI} = f(T_1, T_2, ...)\psi_0$.

The substitution operators:

$T_1 = \sum_{ia} a_i^a \hat{t}_i^a$ - single substitution operator,

$T_2 = \frac{1}{4} \sum_{ijab} a_{ij}^{ab} \hat{t}_{ij}^{ab}$ - double substitution operator,

$T_3 = \frac{1}{16} \sum_{ijkabc} a_{ijk}^{abc} \hat{t}_{ijk}^{abc}$ - triple substitution operator,

where a arrays involve coefficients to be determined; $\hat{t}_{ij}^{ab}$ are elementary substitution operators. Symbols i, j, k are used for the occupied and a, b, c for virtual spin orbitals.

The expansion coefficients are then varied using a variational approach until a minimum energy is achieved.

Quadratic configuration interaction calculations (QCI) use an algorithm that is a combination of the CI [143] and CC (Coupled Cluster) [144, 145] algorithms. This method might be described as configuration interaction with quadratic terms added to restore size-consistency. Thus, a QCISD method is an approximation to a CCSD calculation. These calculations are popular since they often give an optimal amount of correlation for high-accuracy calculations on organic molecules. Most popular is the single- and double-excitation calculation, QCISD. Sometimes, triple excitations are included as well, QCISD(T). The T in parentheses indicates that the triple excitations are included perturbatively.

If we define $E(total) = E_{HF} + E_{correlation}$, $\overline{H} = H(total) - E_{HF}$, the proposed equations leading to expression of the energy QCISD would be:

$$\langle \psi_0 \mid H \mid T_2 \psi_0 \rangle = E_{correlation} \tag{9}$$

$$\langle \psi_i^a \mid \overline{H} \mid (T_1 + T_2 + T_1 T_2)\psi_0 \rangle = a_i^a E_{correlation} \tag{10}$$

$$\langle \psi_{ij}^{ab} \mid \overline{H} \mid (T_1 + T_2 + \frac{1}{2}T_2^2)\psi_0 \rangle = a_{ij}^{ab} E_{correlation}, \tag{11}$$

where ψ_i^a is the singly substituted determinant $\hat{t}_i^a \psi_0$, ψ_{ij}^{ab} is a double substituted determinant $\hat{t}_{ij}^{ab} \psi_0$.

The final form of the equation can be written:

$$E_{correlation} = \frac{1}{4}\sum_{ijab}(ij \parallel ab)a_{ij}^{ab}\ , \tag{12}$$

$$a_i^a = -(\Delta_i^a)^{-1}[u_i^a + \upsilon_i^a], \tag{13}$$

$$a_{ij}^{ab} = -(\Delta_{ij}^{ab})^{-1}[(ab \parallel ij) + u_{ij}^{ab} + \upsilon_{ij}^{ab}], \tag{14}$$

where $(ab||ij)$ are the usual antisymmetrized two-electron integrals, $\Delta_i^a = \varepsilon_a - \varepsilon_i$, $\Delta_{ij}^{ab} = \varepsilon_a + \varepsilon_b - \varepsilon_i - \varepsilon_j$ (ε is the eigenvalue of one-electron Fock operator), u_i^a and u_{ij}^{ab} are the linear arrays used in CISD theory, υ_i^a and υ_{ij}^{ab} are the quadratic arrays.

The general concept of quadratic configuration interaction can also be applied to higher levels of substitution. But implementation of QCISDT for large system is impractical because of handling the large number of triple-triple Hamiltonian matrix elements. The useful approximation is the method in which the triple corrections ΔE_T is added to the QCISD energy, and it is denoted QCISD(T), as it represents a compromise in which triples are only treated in a partial manner. The formula for the triples correction ΔE_T:

$$\Delta E_T = -\frac{1}{36}\sum_{ijk}\sum_{abc}(\Delta_{ijk}^{abc})^{-1}(2\overline{u}_{ijk}^{abc} + \overline{\overline{u}}_{ijk}^{abc})\overline{\overline{u}}_{ijk}^{abc}\ . \tag{15}$$

4.1.3. Density Functional Theory (DFT)

All *ab initio* methods start with a Hartree-Fock (HF) approximation that results in the spin-orbitals, and then electron correlation is taken into account. Though the results of such calculations are reliable, the major disadvantage is that they are computationally intensive and cannot be readily applied to large molecules of interest. Density functional (DF) methods provide an alternative route that, in general, provides results comparable to CI and MP2 computational results; however, the difference is that DF computations can be done on molecules with 100 or more heavy atoms. Therefore, **Density functional theory** (DFT) has become very popular in recent years.

The basis for Density Functional Theory (DFT) is the theorem of Hohenberg and Kohn that ground-state energy of the molecule can be determined completely by the electron density ρ instead of a wave function. The goal of DFT methods is to design functionals connecting the electron density with the energy.

The electron density is expressed as a linear combination of basis functions:

$$\rho(r) = N \sum_{\sigma=-1/2}^{1/2} \int d\tau_2 d\tau_3 ... d\tau_N \mid \psi(r_1, \sigma_1, r_2, \sigma_2, ..., r_N, \sigma_N) \mid^2 \tag{16}$$

By contrast with HF method, DF models start with a Hamiltonian corresponding to an "idealized" many-electron system for which an exact wavefunction is known. The solution is obtained by optimizing the "ideal" system closer and closer to the real system. So, general DFT energy can be written as

$$E_{DFT} = T_0 + E_{nc}[\rho] + J[\rho] + E_{xc}[\rho], \tag{17}$$

where T_0 is the kinetic energy of non-interacting electron system,

E_{nc} is the potential energy of the nuclei-electron interaction,

and $$J[\rho] = \frac{1}{2} \int\int \frac{\rho(r_1)\rho(r_2)}{\mid r_1 - r_2 \mid} dr_1 dr_2 \tag{18}$$

is the expression for the classical Coulomb interaction electron-electron,

E_{xc} term is the exchange-correlation energy.

The equations for energy of a system using the electron density approach are expressed as [146]:

$$\left(V_{eff}(r_1) - \frac{1}{2} \nabla^2 \right) \phi_i = \varepsilon_i \phi_i, \tag{19}$$

where ∇^2 is the Laplace operator, ϕ_i are the Kohn-Sham orbitals, ε_i - the Kohn-Sham orbital energy, $V_{eff}(r)$ is the Kohn-Sham operator:

$$V_{eff}(r_1) = \int \frac{\rho(r_2)}{|r_1 - r_2|} dr_2 - \sum_A^M \frac{Z_A}{|r_1 - R_A|} + V_{xc}(r_1) \quad (20)$$

The first term represents the electron-electron interactions (characterized by the electron density $\rho(r_2)$ and distance between the electrons $|r_1-r_2|$). The second term contains nuclei-electron interactions (Z_A is the charge of nucleus A and $|r_1-R_A|$ is the distance from nucleus A to electron). The last term, exchange-correlation potential

$$V_{xc}(r_1) = \frac{\delta E_{xc}[\rho]}{\delta \rho(r_1)} \quad (21)$$

is a derivative of the exchange-correlation energy E_{xc} with respect to the density.

This approach does not contain any approximation and is in principle exact. The approximation emerges when the unknown functional V_{xc} is to be calculated. The estimation of unknown V_{xc} gives rise to several approximations in density functional theory, known as different functionals.

The simplest approximation to the complete problem is one based only on the electron density, called a Local Density Approximation (LDA). For high-spin systems, this is called a Local Spin Density Approximation (LSDA). A more complex set of functionals utilizes the electron density and gradient. These are called gradient-corrected methods. There are also hybrid methods that combine functionals from other methods with pieces of a Hartree-Fock calculation, usually the exchange integrals.

The hybrid B3LYP functionals were the most widely used for molecular calculations. This is due to the accuracy of the B3LYP results obtained for a large range of compounds, particularly organic molecules. The exchange term was proposed by Becke [147], and the correlation functional by Lee, Yang and Parr (the abbreviation is LYP) [148]. This approximation gives also good results for vibrational spectra.

In general, *ab initio* calculations give very good qualitative results and can yield increasingly accurate quantitative results as the molecules in question become smaller. The advantage of *ab initio* methods is that they converge to the exact solution once all the approximations are made sufficiently small in magnitude.

Sometimes, the calculation with smallest basis set gives a very accurate result for a given property. There are four sources of error in *ab initio* calculations:

1. The Born-Oppenheimer approximation
2. The use of an incomplete basis set
3. Incomplete correlation
4. The omission of relativistic effects

The heterocyclic molecules, which were studied in the current work, may adopt different tautomeric forms. In the case when the molecule exists in a gas phase as a mixture of more than one tautomer, the difference of energy between those tautomeric forms may be determined experimentally. Equilibrium between tautomers at room temperature is possible when those tautomers are very close in energy. In other cases, only theoretical calculations may provide information on relative energy of different forms of a molecule and hence, an information on the structure of a molecule which can be expected in an experiment. In this respect, modern quantum chemical methods that could provide this information with a possible high accuracy are very helpful in complementing many experimental studies. From the other side, the experimental data on the relative population (and hence the relative stability) of tautomers of the compound in inert environment (isolation conditions) provide very important data for verification of an accuracy of theoretical methods. The experimental conditions are important, in this case, since the high level calculations concern non-interacting molecules in the gas phase.

The relative energies of the energetically low-lying tautomers of DNA bases were theoretically studied by Piacenza et. al. using variety of different quantum chemical methods [149]. In particular, there were employed: Density Functional Theory (DFT) using the six functionals HCTH407, PBE, BP86, B-LYP, B3-LYP, and BH-LYP, and the *ab initio* methods: Hartree-Fock (HF), standard second-order Møller-Plesset perturbation theory (MP2), an improved version of the last method (SCS-MP2), quadratic configuration interaction including single and double excitations (QCISD) and perturbative triple corrections [QCISD(T)].

Good example, showing how accurate are the listed above methods (with respect to the experimental data), provided the computations concerning 2-pyridinone (**2PD**). In Figure 4.2 are presented the relative energies between the oxo and hydroxy forms of 2-pyridinone (**2PDo**) - 2-hydroxypyridine (**2PDh**) obtained in different calculations (according to Piacenza [149]).

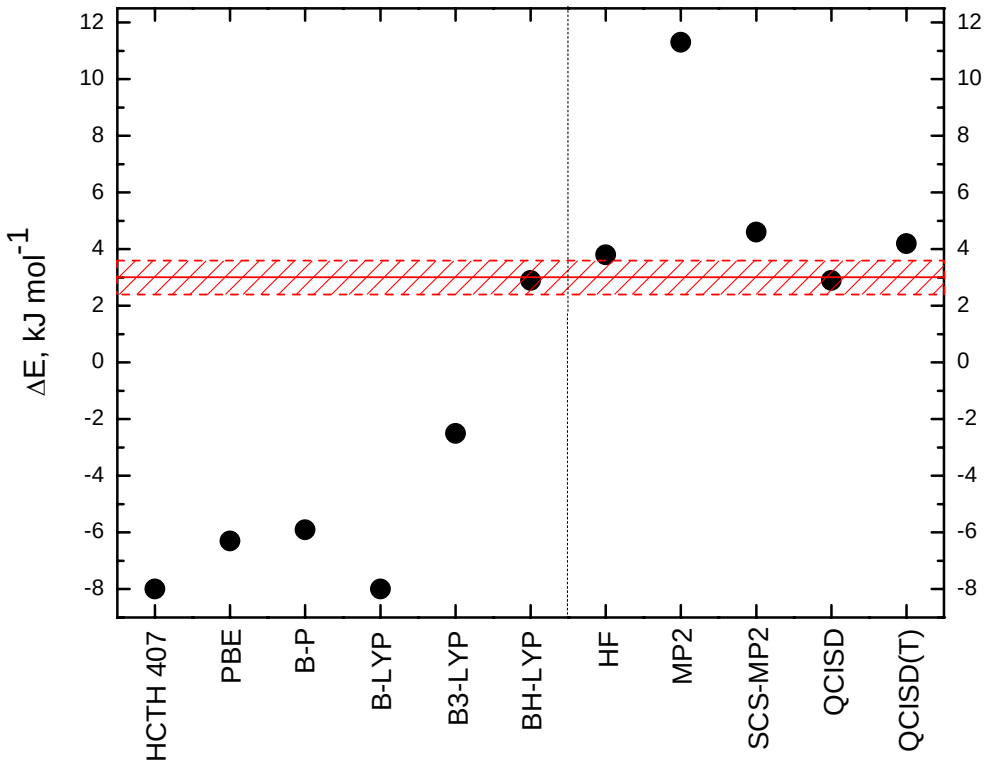

Figure 4.2. *Relative energies of 2-pyridone (**2PDo**) with respect to 2-hydroxypyridine (**2PDh**) obtained by various quantum chemical methods [TZV(2df,2dp) basis set] (according to Piacenza [149]). The area under a red grid displays the range of the energy in which the values of different experimental results were obtained.*

All DFT calculations predicted wrongly that the oxo tautomer of **2PD** is more stable than the hydroxy form, with the exception of calculations using BH-LYP functionals. The DFT(BH-LYP) calculation gave result close to the experimental value. The DFT(B3-LYP) calculations gave small deviation from experiment, but still a wrong sign of ΔE. So, the DFT methods underestimate the stability due to the aromatic character of the heterocyclic ring of the hydroxy tautomer. The experimental data obtained by Nowak et. al. for 2-pyridone using IR spectra in gas phase indicate that the hydroxy form is more stable than oxo form and the relative $\Delta E = -3.0 \pm 0.6$ kJ mol^{-1} [27] while Hatherley et al. obtained $\Delta E = -3.2$ kJ mol^{-1} with the use of microwave spectroscopy [150].

Although the MP2 method predicts correctly the relative stability of the isomers (i.e. the hydroxy form of the compound as a more stable), the energy difference is significantly overestimated (by 9 kJ mol^{-1}). As it will be shown further, the calculations carried out within the current work (presented in Table 5.1) provided the similar result.

More accurate are the results of theoretical predictions of the relative energies of the **2PDh** and **2PDo** forms obtained using the QCISD and QCISD(T) methods. The calculations carried out at these levels (previously by Piacenza and Grimme [149] and in the current work (Table 5.1)) yielded quite close value to the experimental data. One of the aims of the present work is to assess if these methods (QCISD and QCISD(T)) would predict accurately the energy differences between tautomers of other heterocyclic molecules, also.

The accumulated, up to now, theoretical data clearly indicate that the popular DFT and MP2 methods are not able to reproduce correctly the experimentally measured difference of energies of the tautomers with accuracy better than ca. 10 kJ mol^{-1}. Thus, it seems that the QCISD method gives the most accurate results for the heterocyclic compounds system.

4.2. Basis sets

One of the approximations inherent in all the *ab initio* methods is the introduction of a basis set. The smaller the basis, the poorer the representation. It is of prime importance to make the basis set as small as possible without compromising the accuracy, therefore many publications are dedicated to this problem [151-157].

The quantum-chemical calculations for molecules are carried out using LCAO MO (i.e. Linear Combination of Atomic Orbitals - Molecular Orbitals) approximation. This means that molecular orbitals are formed as a linear combination of atomic orbitals:

$$\psi_i = \sum_{\mu=1}^{n} c_{\mu i}\phi_\mu \,, \tag{22}$$

where ψ_i is molecular orbital, $c_{\mu i}$ are coefficients of linear combination, ϕ_μ are atomic orbitals and n is the number of atomic orbitals.

At early stage of the method development, the Slater Type Orbitals (STO) were used as basis functions due to their similarity to hydrogen-like orbitals. However, it turned out that the Slater functions are difficult to calculate. As an alternative solution, Gaussian Type Orbitals (GTO) have been introduced. The shape of an STO orbital could be approximated by summing up a number of GTOs:

$$GTO(\alpha, l, m, n; x, y, z) = Ne^{-\alpha r^2} x^l y^m z^n \,, \tag{23}$$

where N is a normalization constant, α is exponent, x, y and z are Cartesian coordinates and l, m and n are the exponents at Cartesian coordinates, $r^2=x^2+y^2+z^2$.

Since gaussians GTOs are not really orbitals, but simpler functions, in recent literature they are frequently called gaussian primitives.

The minimal basis set is the smallest possible set, i.e., it contains only one function per occupied atomic orbital in the ground state. The most popular minimal basis sets are the STO-nG, where n denotes number of primitives in the contraction.

In Pople's terminology [158-160], where the basis set structure is given for the whole molecule rather than particular atom, the notation emphasizes also a split valence (SV) nature of these sets. Symbols like n-ijG or n-ijkG can be encoded as: n - number of primitives for the inner shells; ij or ijk - number of primitives for contractions in the valence shell. The ij notations describe sets of valence double zeta quality and ijk sets of valence triple zeta quality.

The contractions related to valence shells are frequently augmented with other functions. The most popular are the polarization [161-165] and diffuse functions [166-168].

The polarization functions are simply functions having higher values of *l* (the orbital quantum number) than those present in occupied atomic orbitals for the corresponding atom. For the Pople's basis sets the following notation is used: n-ijG*, or n-ijkG* when polarization gaussians are added to a standard basis set on heavy atoms, and n-ijG**, or n-ijkG** are obtained by adding polarization p-type gaussian on the hydrogens. At present, the most precise manner is used to notate the basis set with polarization functions: n-ijkG(a,b), where a is the number and type of the gaussian on the heavy atoms, and b – on the hydrogens (for example, 6-311G(3d2f, 2p)).

The basis sets are also frequently augmented with the so-called diffuse functions. These gaussians have very small exponents and decay slowly with distance from the nucleus. Diffuse gaussians are usually of s and p type, however sometimes diffuse polarization functions are also used. Diffuse functions are necessary for correct description of anions and weak bonds (e.g. hydrogen bonds) and are frequently used for calculations of such properties as dipole moments, polarizabilities, etc.. For the Pople's basis sets the following notation is used: n-ij+G, or n-ijk+G when 1 diffuse s-type and p-type gaussian are added to a standard basis set on heavy atoms. The s- and p-type function has the same exponents in this case. The n-ij++G, or n-ijk++G are obtained by adding 1 diffuse s-type and p-type gaussian on heavy atoms and 1 diffuse s-type gaussian on hydrogens.

The number of contractions used to represent a single Slater atomic orbital (i.e. zeta, ζ) is a measure of the basis set's quality. This terms like single zeta (SZ), double zeta (DZ), triple zeta (TZ), quadruple zeta (QZ), etc. In the minimal basis set (i.e. SZ) only one basis function

(contraction) per Slater atomic orbital is used. DZ sets have two basis functions per orbital, etc. Since valence orbitals of atoms are more affected by forming a bond than the inner (core) orbitals, more basis functions should be assigned to describe valence orbitals. This prompted development of split-valence (SV) basis sets, i.e., basis sets in which more contractions are used to describe valence orbitals than core orbitals. So, DZP means double-zeta plus polarization, TZP stands for triple-zeta plus polarization, etc. Sometimes the number of polarization functions is given, e.g. TZDP, TZ2P, TZ+2P stands for triple-zeta plus double polarization. Letter V denotes split valence basis sets, e.g., DZV represents basis set with only one contraction for inner orbitals, and two contractions for valence orbitals.

Dunning has proposed a somewhat smaller set of primitives which yield good results [169]. The correlation consistent (cc, convention is to use small letters for the acronym, to distinguish it from Coupled Cluster, CC) basis sets are geared toward recovering the correlation energy of the valence electrons. The name correlation consistent refers to the fact that the basis sets are designed so that functions which contribute similar amounts of correlation energy are included at the same stage, independently of the function type. For example, the first d-function provides a large energy lowering, but the contribution from a second d-function is similar to that from the first f-function. The energy lowering from a third d-function is similar to that from the second f-function and the first g-function. Addition of polarization functions should therefore be done in the order: 1d, 2dlf and 3d2f lg. An additional feature of the cc basis sets is that the energy error from the sp-basis should be comparable to (or at least not exceed by) the correlation error arising from the incomplete polarization space and the sp-basis therefore also increases as the polarization space is extended. Several different sizes of cc basis sets are available in terms of final number of contracted functions. These are known by their acronyms: cc-pVDZ, cc-pVTZ, cc-pVQZ, cc-pV5Z and cc-pV6Z (correlation consistent polarized Valence Double/ Triple/ Quadruple/ Quintuple/ Sextuple Zeta). A step up in terms of quality increases each type of basis function by one, and adds a new type of higher-order polarization function.

4.3. Potential Energy Distribution (PED)

The interpretation of the experimental IR spectra is based on the assumption that if theoretically calculated wavenumbers and intensities of the IR bands are close to that observed experimentally, then forms of the vibrations calculated theoretically describe the real vibrations of the molecule with a good approximation. Information about the form of the vibrations of the molecule is obtained from normal vibration analysis. The forms of vibrations can be described by the elements of Potential Energy Distribution (**PED**) matrix.

The frequencies (or wavenumbers) of normal vibrations can be obtained within the harmonic approximation by solving the equation [170-171]:

$$F_q L_q = L_q \Lambda \tag{24}$$

where:

F_q is the force constant matrix expressed in "mass weighted" Cartesian coordinates *q;*

$q = M^{\frac{1}{2}} \Delta X$ (M – diagonal matrix of atomic masses, X - Cartesian coordinates, ΔX – nuclear displacements from the equilibrium positions).

Λ – diagonal matrix of eigenvalues λ_i; $\lambda_i = 4\pi^2 c^2 \tilde{\nu}_i^2$, (here c – speed of light in cms^{-1},

$\tilde{\nu}_i$ – wavenumber of i^{th} normal vibration in cm^{-1}),

L_q -is the matrix of forms of normal vibrations,

F_q can be obtained from the matrix of quadratic force constants expressed in Cartesian coordinates F_X from the equation:

$$F_q = M^{-\frac{1}{2}} F_X M^{-\frac{1}{2}}. \tag{25}$$

Then equation (24) can be rewritten:

$$M^{-\frac{1}{2}} F_X M^{-\frac{1}{2}} L_q = L_q \Lambda, \tag{26}$$

The normal vibrations are best described using the normal coordinates Q. In the normal coordinates the kinetic energy and potential energy operators adopt the diagonal form. The normal coordinates (Q) might be expressed by "mass weighted" Cartesian coordinates (q):

$$q = L_q Q. \tag{27}$$

Deformations of a molecule during vibrations (such as bond stretching, bending and torsion of angles) may be expressed in internal coordinates *S,* which can be defined for each molecule.

Matrix **B** allows transformation between Cartesian and internal coordinates:

$$S = \mathbf{B}X \tag{28}$$

Force constants matrix in internal coordinates (F_S) is connected with force constants matrix in Cartesian coordinates (F_X) by equation:

$$F_X = \mathbf{B}^{\mathbf{T}} F_S \mathbf{B}. \tag{29}$$

Pulay [172] proposed the procedure, where the normal coordinates are expressed by internal coordinates (S) using a transformation matrix L_S:

$$S = L_S Q \tag{30}$$

L_S matrix may be obtained from L_q matrix:

$$L_S = \mathbf{B} M^{\frac{1}{2}} L_q \tag{31}$$

The elements of L_S matrix are egenvectors of the Wilson equation:

$$\mathbf{G} F_S L_S = \Lambda L_S \tag{32}$$

and the G matrix:

$$\mathbf{G} = \mathbf{B} M^{-1} \mathbf{B}^{\mathrm{T}} \tag{33}$$

Such transformations of the force constants with respect to the Cartesian coordinates to the force constants with respect to the molecule-fixed internal coordinates allowed the normal-coordinate analysis to be performed as described by Schachtschneider [173].

Usually, the forms of the normal vibrations are expressed by vectors of potential energy distribution matrix (PED) [174, 175]. Elements of this matrix PED are defined by the formula:

$$\mathrm{PED}(i,j) = \frac{\sum_k F_s(j,k) L_S(k,j) L_S(j,i)}{\sum_k \sum_l F_S(k,l) L_S(k,i) L_S(l,i)}, \tag{34}$$

Where i – numbers of normal coordinates, j,k,l – numbers of internal coordinates.

In order to calculate the values of the PED matrix elements the specially designed programs were used. The first module was the program “Balga” which was created in Pulay’s group and the additional modules were written by L. Łapiński. In these calculations, matrices of the force constants in Cartesian coordinates F_X and Cartesian coordinates corresponding to the optimized geometry were taken from the Gaussian program output. The internal coordinates used in this analysis were defined following the recommendations of Pulay et al. [172]. The first step to analyze the normal vibration was calculation of the matrix **B** (matrix of transition between vector of internal and Cartesian coordinates). Using this matrix, it was possible to calculate the matrix of force constants in internal coordinates F_S according to equation (29). Then the G matrix was calculated (equation (33)). From the Wilson equation (32) the matrix of eigenvectors L_S (matrix of normal vibrations) was obtained. Then PED matrix could be calculated from equation (34).

The PED(*i,j*) values of PED matrix elements determine a percent of participation of vibration performed along *i*-th internal coordinate in potential energy of *i*-th normal vibration.

The matrix of the quadratic force constants F_X can be obtained in calculations made by modern quantum-mechanical programs such as Gaussian.

The next important step (beside calculation of frequencies of normal vibrations and corresponding intensities of the bands) is to determine which of the intramolecular vibrations take part in the given vibration, and an estimate of their participation.

4.4. Technical aspects

The structures of all species considered in the current work are presented in Section 3.2. The geometries of these forms were optimized using DFT method with B3LYP functional. Dunning's basis set cc-pVTZ, as well as 6-311++G(d,p) basis set were used in these calculations. Using the reference optimized geometries, the harmonic vibrational frequencies and IR intensities were calculated. To correct for the systematic shortcomings of the applied methodology (mainly for anharmonicity), the predicted vibrational wavenumbers were scaled down by a single factor of 0.98. The theoretical normal modes, calculated for the tautomers of the studied compounds were analyzed by carrying out the potential energy distribution (PED) calculation. The internal coordinates used in this analysis are listed in Tables in the Appendix. Potential energy distribution (PED) matrices [175] have been calculated and the elements of these matrices greater than 10% are given in Tables in the Appendix.

In this work, the theoretical calculations were performed using different basis sets: cc-pVTZ, cc-pVDZ as well as 6-31++G(d,p). The relative energies, harmonic vibrational frequencies and IR intensities were calculated for all tautomeric forms of the compounds studied in the current work. Our observations show that the theoretically simulated IR spectra calculated using different basis sets do not differ much between each other.

The experimental spectrum of 2-hydroxypyridine, which is a product of oxo→hydroxy photoreaction, presented in Figure 4.3 (trace a), is compared with the spectra calculated using density functional theory at the cc-pVTZ (trace b), cc-pVDZ (trace c) and at 6-31G++(d,p) (trace d) levels, obtained under the harmonic approximation, for the geometry optimized at DFT(B3LYP)/6-311++(d,p) level. The general agreement between the experimental and the calculated spectra is good, suggesting a close match between the theoretically optimized geometry of 2-hydroxypyridine and the structure of the molecule in the matrix. In spite of

the good agreement between the experimental and calculated spectra, as usual the theoretical frequencies are slightly overestimated, mainly due to neglect of anharmonicity. The scaling factor of 0.98 was used in order to reduce the average deviations of the scaled theoretical frequencies from the experimentally observed ones. Hence, the cc-pVTZ calculations predict the frequencies a little closer to experiment than those performed with the cc-pVDZ and 6-31++(d,p) basis sets (see Figure 4.3). In practical terms this means that the 6-31++(d,p) basis set (which requires a substantially smaller computational effort) can be used instead of the more extended cc-pVTZ basis to further investigate heterocyclic compounds without any significant loss of quality in the theoretical predictions.

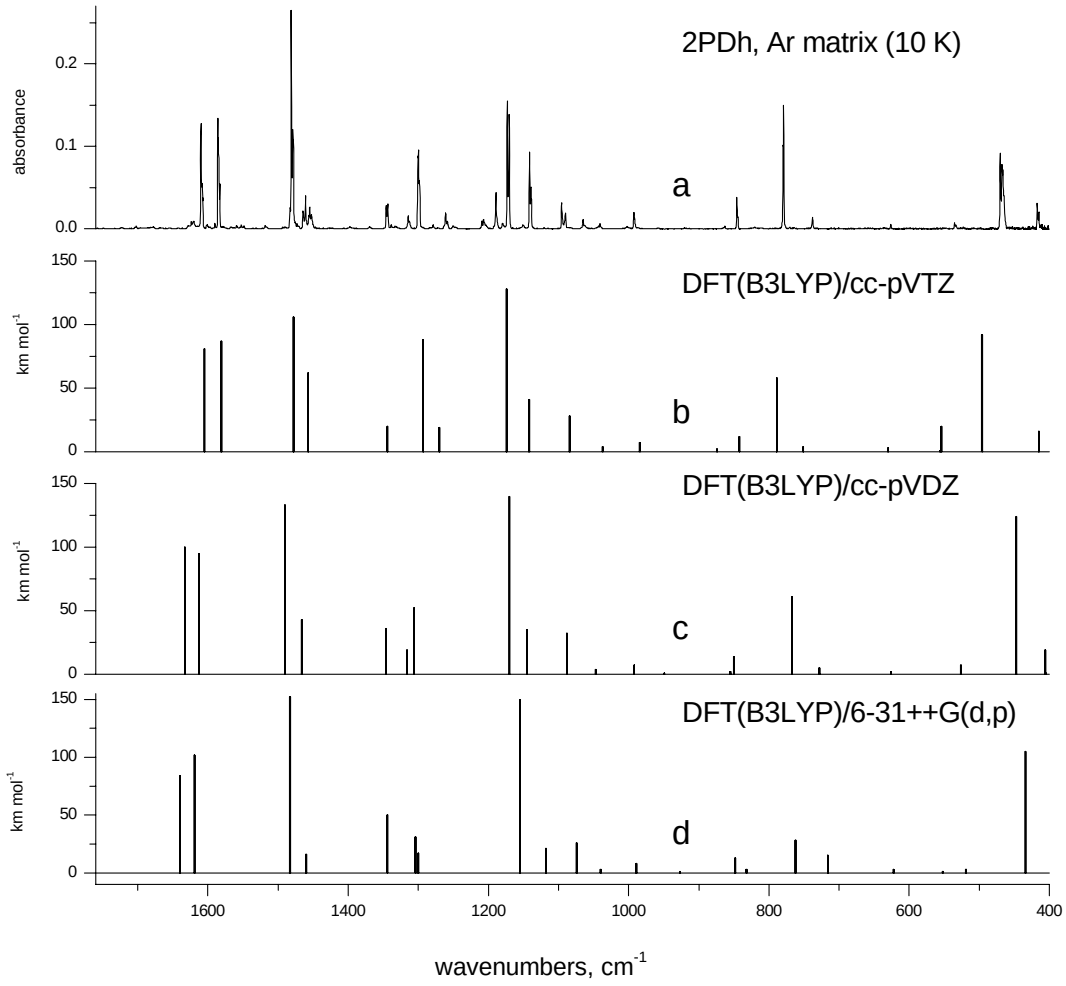

Figure 4.3. *Comparison of the (a) IR spectrum of 2-hydroxypyridine* ***2PDh*** *isolated in an argon matrix at 10 K with (b) the spectra calculated at DFT(B3LYP)/cc-pVTZ, (c) DFT(B3LYP)/cc-pVDZ and (d) DFT(B3LYP)/6-31++G(d,p) levels of theory at geometry optimized using the DFT(B3LYP)/6-311++G(d,p) method. The calculated wavenumbers were scaled by the single factor of 0.98.*

As it has been shown earlier, the DFT method reproduces well the infrared spectra but provides less reliable values of relative electronic energies. That is why the relative energies of the most stable isomeric forms of were also calculated using the MP2, QCISD and QCISD(T) methods. The MP2 energy calculations were performed not only at the DFT(B3LYP) optimized geometry, but also at geometry optimized at the MP2 level. For the 2-pyridinone-2-hydroxypyridine system (Table 5.1), ΔE_{el} was also calculated using the coupled-cluster method [144, 145] with single, double, and noniterative triple excitations [CCSD(T)]. Both cc-pVDZ and cc-pVTZ basis sets were utilized in these calculations.

In order to compute the Gibbs free energy differences between the hydroxy and oxo tautomers, the relative electronic energies were corrected for thermal and entropy terms using the harmonic oscillator and rigid rotor approximations. The temperature parameter used in these calculations was equal to the temperature of evaporation of a compound during matrix deposition. For a tautomerization reaction, the ΔpV and $p\Delta V$ terms equal zero, hence the Gibbs free energy difference between tautomers (ΔG) equals the Helmholtz free energy difference (ΔF).

All the calculations in the current work were carried out using the Gaussian 03 program [176].

5. Results and discussion

5.1. Thermodynamic parameters of tautomeric interconversions

Irrespective of the type of tautomeric system, a prototropic interconversion between two tautomeric forms is quantitatively described by a tautomeric equilibrium constant, K_T, which is frequently also used in the form $pK_T = -\log K_T$.

For rearrangements caused by the intramolecular proton transfer, the equilibrium constant K_T is defined as the concentration ratio or, equivalently, the percentage content ratio of the two tautomers, T_i and T_j, that are in tautomeric equilibrium. In equation (35), $[T_i]$ and $[T_j]$ denote the concentrations of T_i and T_j, and x is the percentage content of T_i.

$$K_T = \frac{T_i}{T_j} = \frac{x}{(100 - x)} \tag{35}$$

The mole ratio of the tautomers in the low-temperature matrix could be determined by several methods. The simplest and most commonly applied (also for tautomerism in the gas phase) is an approximate method where it was assumed that absolute intensities (integral absorption coefficients) of the bands due to the stretching vibration of the OH and NH groups are very simmilar (it concerns the case of oxo-hydroxy tautomerism). With this assumption, the ratio of integral intensities of these absorption bands is an estimation of the relative concentration of the tautomers:

$$\frac{[\text{hydroxy}]}{[\text{oxo}]} \cong \frac{I(OH)}{I(NH)} \tag{36}$$

According to the second and more precise method, the ratio of tautomers is obtained using the ratio of the sums of the integral intensities of all experimentally observed bands of both tautomers, scaled by the sum of the theoretically determined absolute intensities of the corresponding bands (equation 37):

$$\frac{[\text{hydroxy}]}{[\text{oxo}]} \cong \frac{\sum I(\text{hydroxy})}{\sum A^{th}(\text{hydroxy})} \cdot \frac{\sum A^{th}(\text{oxo})}{\sum I(\text{oxo})}, \tag{37}$$

where $\sum I(\text{tautomer})$ - is the sum of the integral intensities of the bands observed in the spectrum of the tautomer, $\sum A^{th}(\text{tautomer})$ - is the sum of the theoretically predicted absolute intensities of the corresponding bands.

The third method of determination of the ratio of tautomers in a matrix may be applied only for molecules for which the phototautomeric reaction occurs and all the molecules in the oxo form have been transformed into the hydroxy form under irradiation of the matrix with the UV-light. In the case when this conversion occurred with the 100% efficiency, the ratio between the tautomers can be obtained applying the equation:

$$\frac{[\text{hydroxy}]}{[\text{oxo}]} \cong \frac{\text{I(hydroxy)}}{\text{I*(hydroxy)} - \text{I(hydroxy)}}, \tag{38}$$

where I(hydroxy) is the integral intensity of the chosen absorption band of the hydroxy form before irradiation of the matrix, I*(hydroxy) is the intensity of this band after irradiation.

This three methods described above has been used simultaneously to estimate ratio of the tautomers of 4-pyrimidinone in an Ar matrix [28], the obtained results are very similar: [hydroxy] : [oxo] =0.42, 0.45, 0.48, respectively for the three methods described above.

Tautomeric equilibrium can be described by such thermodynamic parameters as:

- the relative internal energies (ΔE),
- the relative enthalpies (ΔH),
- the relative Gibbs free energies (ΔG),
- the relative free Helmholtz energy (ΔF) of tautomers.

For monomolecular tautomerization process $\Delta p=\Delta V=0$ (it is isobaric and isochoric process), hence $\Delta F= \Delta G$ and the difference of the free energy ΔF can be related with the difference of the free enthalpy ΔH:

$$\Delta F=\Delta G=\Delta H-T\Delta S, \tag{39}$$

ΔS is the entropy change during tautomeric transformation of the molecule.

The change of entropy during proton shift in a molecule is usually small, therefore often ΔS is neglected, and then the difference of internal energy can be approximated by enthalpy change: $\Delta E=\Delta H\approx\Delta G$ [177].

In the case when the influence of the environment disturbing the tautomeric equilibrium is negligibly small, the tautomer equilibrium constant $K_T = \frac{T_i}{T_j}$ is related with the difference of the free Helmholtz energy ΔF by the relation

$$K_T = \frac{T_i}{T_j} = e^{-\Delta F/RT}, \tag{40}$$

where R is the gas constant, T is the temperature.

So the method of determination of ΔF_{exp} on the basis of the spectrum of the compound isolated in a low-temperature matrix is:

$$\Delta F_{\exp} = F_{hydroxy} - F_{oxo} = -RT \ln \frac{[\text{hydroxy}]}{[\text{oxo}]} \tag{41}$$

As it was mentioned, the entropy term value is close to zero, and ΔH can be expressed by difference of the electronic energy ΔE_{el} of the tautomers and difference of zero point vibrational energy ΔE_{zpe}:

$$\Delta H \cong \Delta E_{el} + \Delta E_{zpe} \tag{42}$$

Here ΔE_{el} is the energy which is obtained from theoretical calculations; ΔE_{zpe} can be estimated from all (3N-6) vibrational frequencies of the molecule ν_i determined experimentally or theoretically:

$$\Delta E_{zpe} = 1/2 \sum_{i}^{3N-6} h\nu_i \tag{43}$$

The difference between electronic energies of tautomers obtained in calculation, ΔE_{el}, can be compared with experimentally determined ratio of tautomers:

$$RT \ln([T_i]/[T_j]) \cong \Delta E_{el} + \Delta E_{zpe} \tag{44}$$

The difference of the free Helmholtz energy ΔF comes from the electronic and vibrational contribution:

$$\Delta F \cong \Delta E_{el} + \Delta F^{vib}, \tag{45}$$

where ΔF^{vib} - the difference of the free energy which is due to vibrations of the molecule.

Then,

$$RT \ln([T_i]/[T_j]) = \Delta E_{el} + \Delta F^{vib} \tag{46}$$

The F^{vib} value can be estimated using calculated theoretically or determined experimentally frequencies of all (3N-6) molecular vibrations ν_i:

$$F^{vib} = -RT \ln \left[\prod_{i=1}^{3N-6} (1 - e^{-h\nu_i/kT}) \, e^{-h\nu_i/kT} \right] \tag{47}$$

Applying equation (46) one can obtain an accurate value of the electronic energy difference of the tautomers using only experimental data. This value can be compared with the theoretically calculated ΔE_{el}. Such comparison allows experimental verification of the methods of quantum chemistry.

As it has been mentioned already, the ratio of the tautomers in the low-temperature matrix corresponds to the equilibrium of the gas phase in the temperature of the sublimation of the compound (temperature of the oven). It has been proved on the example of the 2-pyridinone, which has been studied in the gas phase and in the matrix. Figure 5.1 shows the high frequency region of these spectra, where the bands corresponding to both forms, hydroxy and oxo, where observed. The ratio of the intensities of the bands which correspond to the νOH and νNH vibrations is almost the same in the spectrum of gaseous sample and in the matrix.

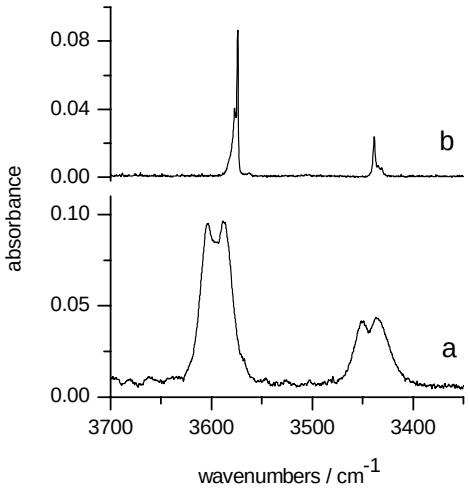

Figure 5.1. *The high frequency region of the IR spectra of 2-pyridinone: (a) in the gas phase (T=473 K) and (b) in an argon matrix.*

The spectra in gas phase were taken in several temperatures. ΔE was obtained from the slope of the obtained Van Hoff relation:

$$\ln\frac{\mathrm{I(OH)}}{\mathrm{I(NH)}} = \frac{\Delta \mathrm{E}}{\mathrm{R}} \cdot \frac{1}{T} - \frac{\Delta \mathrm{S}}{\mathrm{R}} + \mathrm{const}\,, \tag{48}$$

To determine ΔE by this method, it is no need to make any assumption for absolute intensities for the bands. The values of ΔE_{el} obtained from the experiments in the gas phase and in the matrix are: -2.1 ± 0.6 and -2.4 ± 0.6 kJ mol^{-1}, respectively [27]).

5.2. Systems with single heterocyclic ring

2-pyridinone

2-pyridinone is the simplest heterocyclic compound which exhibits prototropic oxo-hydroxy tautomerism (Figure 5.2). Both tautomers exist in similar amount when the molecule is in inert environment. The tautomerism 2-hydroxypyridine/2-pyridinone (the tautomers are denoted here as **2PDh** and **2PDo**, respectively) is frequently considered to be the prototype for oxo-hydroxy tautomerization processes in heterocyclic compounds [178-180]. Also, in this work, 2-hydroxypyridine / 2-pyridinone has served as a model system for studies of prototropic tautomerism of heterocyclic compounds structurally related to this compound.

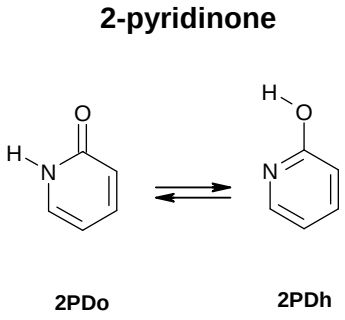

Figure 5.2. *Reaction of oxo-hydroxy tautomerization in 2-pyridinone.*

Numerous studies were devoted to estimation of the tautomeric equilibrium of this system in pure crystalline state and in different solutions [178-179]. Those studies resulted in a conclusion that tautomeric equilibrium strongly depends on the environment. In the crystalline state and in solutions with polar solvents the oxo form strongly dominates, while in diluted solutions with nonpolar solvents both forms were detected. Several experimental results showed that the tautomeric equilibrium in gas phase differs significantly. A variety of methods was applied to determine the tautomeric equilibrium and free energy difference between the hydroxy and the oxo forms of 2-pyridinone. Among these methods were: IR spectroscopy, UV spectroscopy [181-183], X-ray [184], UV photoelectron spectroscopy [186], microwave spectroscopy [150], and IR spectroscopy in inert gas matrices [27]. These measurements led to the conclusion that the free energy difference between the hydroxy form and the oxo form (see Figure 5.2) is 2÷3 kJ mol^{-1} in favor of the hydroxy form of this compound.

The first attempt to estimate the ratio of the tautomers of 2-pyridinone in the gas phase was made by Levin and Rodionova [116]. They estimated the [hydroxy]:[oxo] ratio in the vapors of

2-pyridinone at 573 K as 2 : 1. Their findings were followed by Beak et al. [181-183], who estimated the [hydroxy]:[oxo] ratio at 412 K as 2.6 : 1.

Beak et al. [181-183], who investigated the gas-phase tautomeric equilibria of 2-pyridinone using UV and IR spectroscopy, estimated the free Helmholtz energy difference ΔF = F(hydroxy) – F(oxo) = -3.2 kJ mol^{-1}. Brown et al. [184] performed the X-ray photoelectron spectroscopy (X-ray PES) studies of the gas-phase tautomeric equilibria of 2-pyridinone. Having assumed equal ionization cross sections for both tautomers, they evaluated the free energy differences as -2.4 kJ mol^{-1} (at 403 K) in favor of the hydroxy form.

The internal energy difference (ΔE) between **2PDo** and **2PDh** forms (see Figure 5.2) of this compound in the gas phase was experimentally determined in a reliable way by Hatherley et al. [150]. These authors investigated the tautomerism of the **2PDo** ↔ **2PDh** system by microwave spectroscopy. From the relative intensities of the observed microwave absorption bands and using the measured values of the dipole moments, Hatherley et al. estimated the energy difference between the ground states of the two (hydroxy and oxo) tautomers to be ΔE = -3.2 kJ mol^{-1} (the hydroxy form is more stable). Earlier, the results of infrared investigation of gaseous **2PD** at variable temperature were reported by Nowak et al. [27]. From the van't Hoff relation (see equation 48) the energy difference ΔE between the ground states of the two tautomers was estimated to be equal -3.0 ± 0.6 kJ mol^{-1}. The results obtained by Hatherley et al. are in good agreement with this value.

The studies of 2-pyridinone isolated in low-temperature matrices have been carried out previously in the research group of M.J. Nowak in Warsaw. The IR spectra of the compound obtained in the current work are in full agreement with the spectra of previous report; however, spectra reported in this work are obtained with better spectral resolution [185]. This studies showed, that after deposition of the matrix, both tautomeric forms – oxo and hydroxy coexist in the matrix, but the dominating is the hydroxy tautomer. The infrared spectrum of 2-pyridinone monomers isolated in an argon matrix is presented in Figure 5.3. During deposition of the matrix, solid 2-pyridinone was heated in a micro-oven to 340 K. In the high-frequency region of the IR spectrum, two bands were observed at 3574 and 3438 cm^{-1}, in spectral positions of the characteristic bands due to the stretching vibrations of OH and NH groups. These bands originate from the hydroxy and oxo tautomers of the compound, respectively. A low intensity of νNH band (at 3438 cm^{-1}), alongside the much stronger νOH band (at 3574 cm^{-1}) indicates that a small fraction of **2PD** molecules adopt the oxo **2PDo** form.

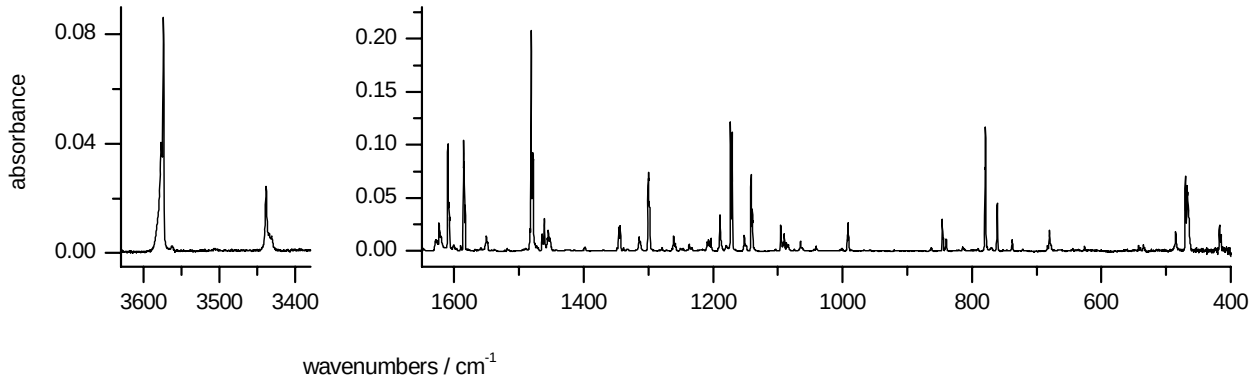

Figure 5.3. *The IR spectrum of 2-pyridinone isolated in an Ar matrix.*

The IR spectroscopy with combination of matrix isolation technique is a method which allows estimating values of relative populations of **2PDo** and **2PDh** forms of 2-pyridinone. A quite reliable measure of the ratio of tautomers in the matrix might be obtained from the ratio of the sums of intensities of all observed IR bands of a tautomer, scaled by the sums of their theoretically predicted intensities (see equation 37).

To apply this formula, the IR spectra of both tautomers (oxo and hydroxy) must be separated. The phototautomerization phenomenon was used to separate the spectra of 2-pyridinone. The change of the intensities of the IR bands after irradiation of the matrix with UV ($\lambda > 295$ nm) was a good criterion used to assign the absorption bands to the spectra of oxo and hydroxy tautomers.

Upon UV ($\lambda > 295$ nm) irradiation of the monomers of the 2-pyridinone isolated in an Ar matrix, the bands originating from the oxo tautomeric form of the compound decreased. The band due to the νNH vibration (at 3438 cm^{-1}) has disappeared completely; instead, the intensity of the νOH due to the stretching vibration of the OH group has increased (Figure 5.4). This observation allowed to postulate that the oxo (**2PDo**)→hydroxy (**2PDh**) photoreaction (Figure 5.2) occurred for the monomers of 2-pyridinone isolated in a low-temperature matrix.

The effect of UV irradiation is shown on the example of the high frequency part of IR spectra of 2-pyridinone isolated in an Ar matrix. The spectra obtained before and after irradiation are presented in Figure 5.4. The photoprocess induced by UV ($\lambda > 295$ nm) irradiation of monomeric 2-pyridinone lead to the total conversion of the oxo form **2PDo** into the hydroxy tautomer **2PDh**.

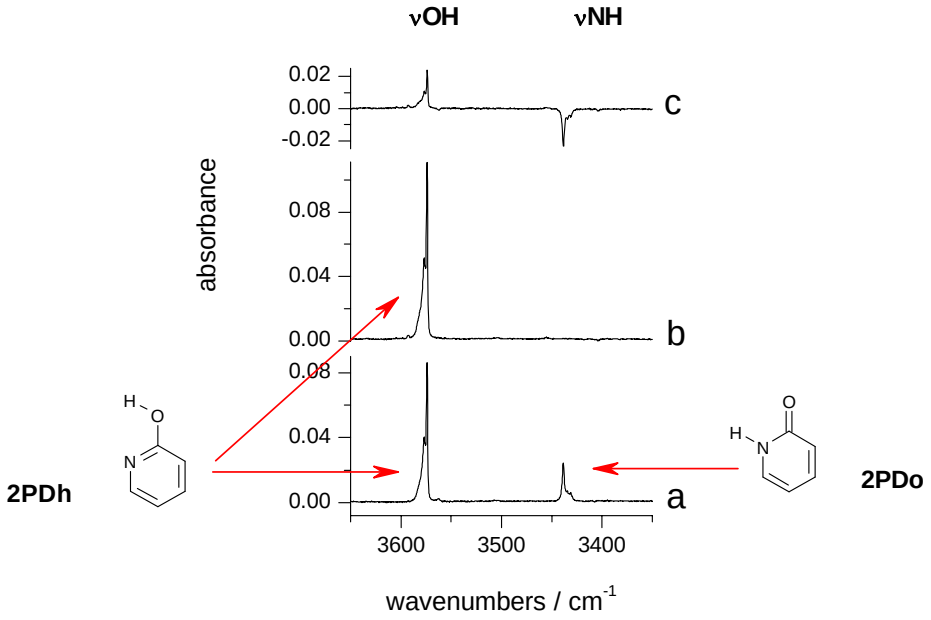

Figure 5.4. *High-frequency regions of the infrared spectra of 2-pyridinone (**2PD**) isolated in Ar matrices: (a) spectrum recorded after deposition of the matrix, (b) spectrum recorded after 1h of UV (λ > 295 nm) irradiation, and (c) difference spectrum, trace b minus trace a. The IR bands present in this spectral range are due to νOH and νNH vibrations and are characteristic of the hydroxy and oxo tautomers, respectively.*

In the low-frequency region of the IR spectra of 2-pyridinone, the most characteristic and an intensive band due to the stretching vibration of CO group (νC=O) at 1704 cm^{-1} was observed before irradiation of the matrix with UV light. After UV (λ > 295 nm) irradiation of the matrix, the behavior of this band is analogous to that at 3438 cm^{-1} (due to νNH vibration) – the band vanished completely, as it can be seen in the left panel of Figure 5.5.

The right panel of Figure 5.5 demonstrates the effect of irradiation of the matrix at the 1650-400 cm^{-1} region of the IR spectra. The bands originating from the oxo tautomer of 2-pyridinone (which vanish upon UV irradiation) in the spectrum recorded after deposition of the matrix are connected with the negative peaks of the difference spectrum (trace c in Figure 5.5) by red dotted lines. The bands directed downwards in the difference spectrum show decrease of intensity after irradiation of the matix with UV (λ > 295 nm) light.

At the same time, the bands due to the hydroxy tautomer increase after irradiation with UV (λ > 295 nm) light, in the difference spectrum this bands are directed upwards. In the low-frequency region of the IR spectra, the characteristic band was found at 470 cm^{-1}. It is due to the torsion vibration of the OH group (τOH). In this case, τOH participates in normal modes of two absorption bands: one very weak band at 535 and another, at 470 cm^{-1}, which are easy

recognizable in this region of the spectra (Figure 5.5). These bands originate from the hydroxy form of 2-pyridinone and increase in intensity after irradiation of the matrix.

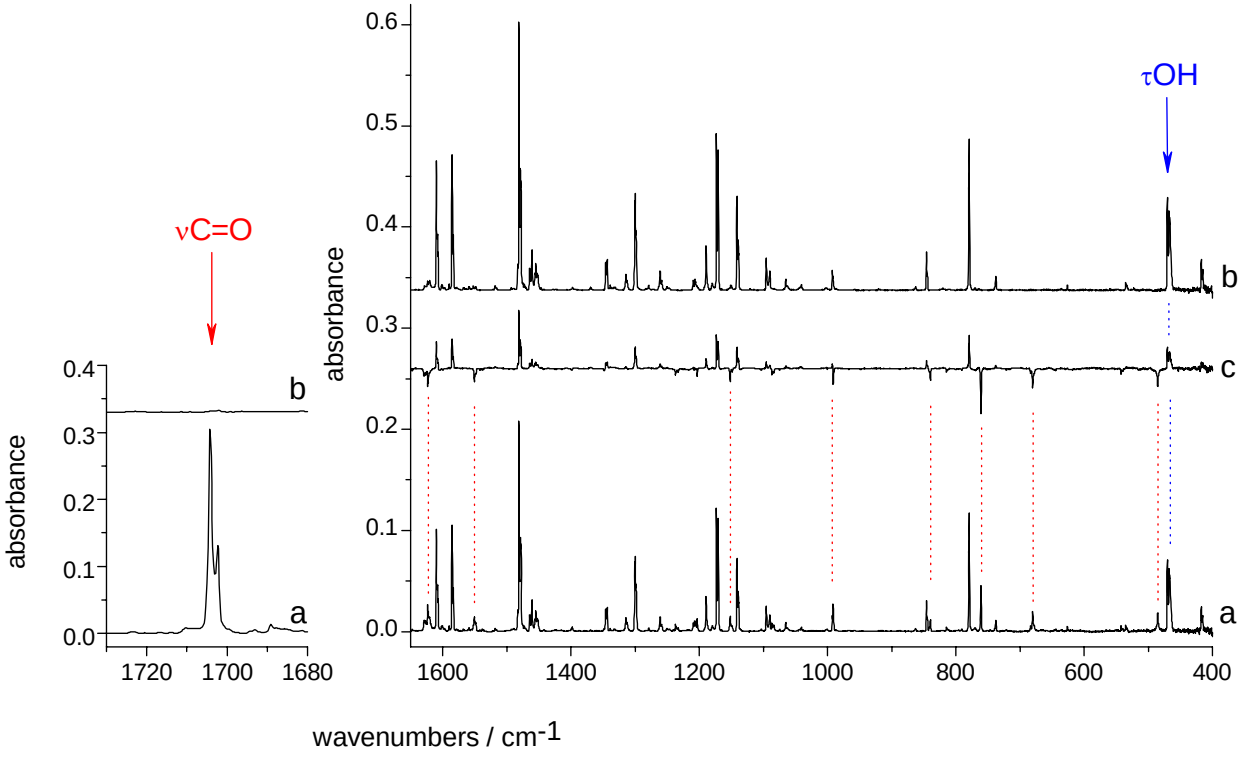

Figure 5.5. *Fragments of the IR spectrum of 2-pyridinone (**2PD**) isolated in an Ar matrix: (a) spectrum recorded after deposition of the matrix; (b) spectrum recorded after 1h of UV (λ > 295 nm) irradiation, (c) difference spectrum: spectrum b minus spectrum a. The bands directed downwards indicate the positions of the weak absorption bands present in the initial spectrum and vanishing upon UV (λ > 295 nm) irradiation. These bands are the spectral signatures of the oxo **2PDo** tautomer. The bands directed upwards indicate the positions of the bands originating from the hydroxy tautomer; these bands growing upon UV (λ > 295 nm) irradiation.*

Hence, the spectrum recorded after irradiation was the pure spectrum of 2-hydroxypyridone. The pure spectrum of the oxo form was obtained by subtracting the spectrum recorded upon irradiation (divided by an appropriate scale factor) from the initial spectrum of the mixture of the tautomers. These extracted spectra are compared with the spectra theoretically predicted for the oxo and hydroxy tautomers of 2-pyridinone at DFT(B3LYP)/cc-pVTZ level (Figure 5.6). These two experimental spectra are well reproduced by the results of the theoretical predictions of the spectra of form oxo (Figure 5.6 traces a, b) and of form hydroxy (Figure 5.6 traces c, d), respectively.

Assignment of the observed absorption bands to the theoretically predicted normal modes of oxo and hydroxy tautomers of the compound is given in the Tables A2 and A3 in the Appendix.

The agreement between the frequencies and intensities of the bands observed experimentally and predicted theoretically is very good. Table A2 contains experimental wavenumbers and relative integral intensities of the bands decreasing upon UV irradiation of the matrix compared with wavenumbers, absolute intensities and potential energy distribution (PED) calculated for the **2PDo** tautomer. Table A3 contains analogous experimental data of the bands increasing upon UV irradiation compared with wavenumbers, absolute intensities and PED calculated for the **2PDh** tautomer. The symmetry coordinates used in the normal mode analysis are provided in Table A1 in the Appendix.

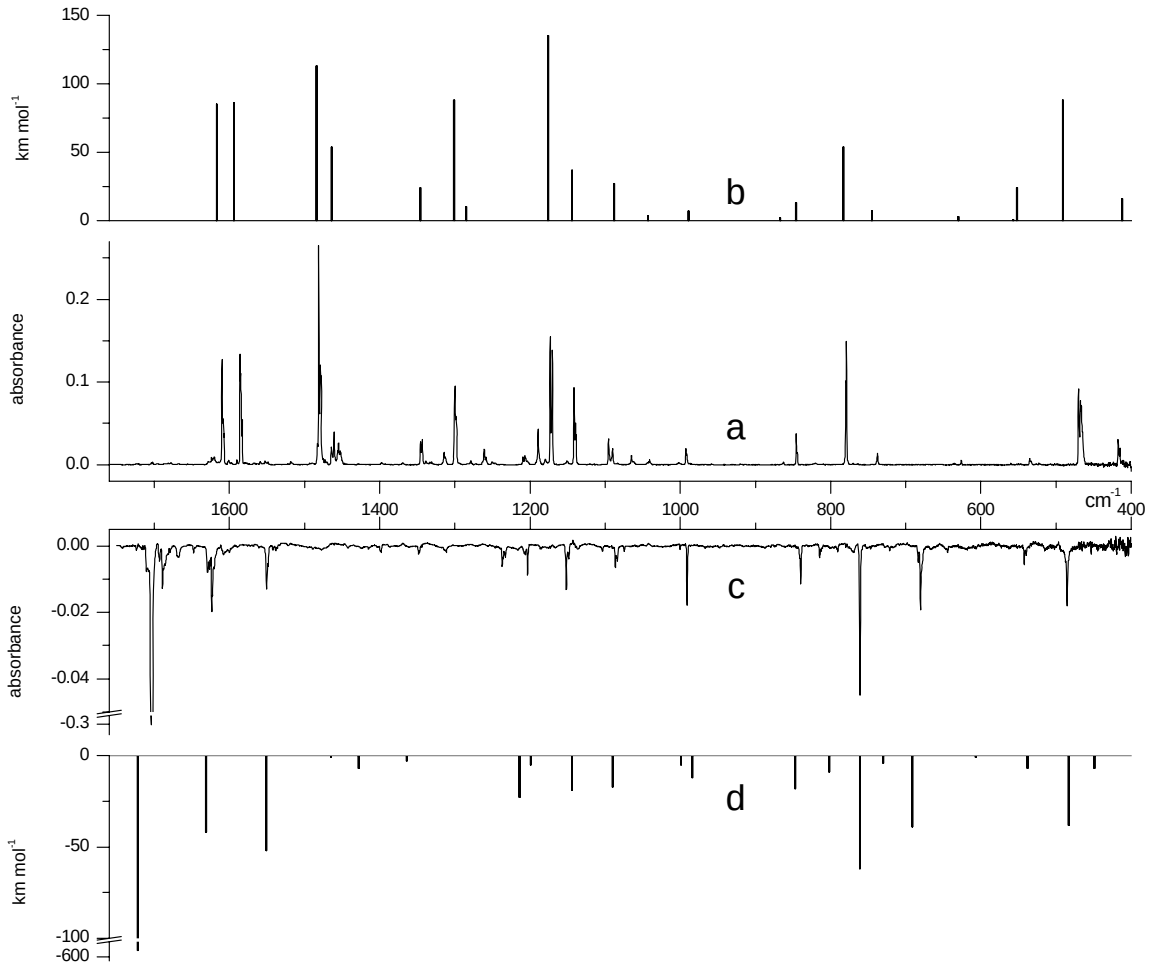

Figure 5.6. *Comparison of the separated spectra of two tautomers existing in an Ar matrix: (a) spectrum corresponding to the hydroxy tautomer (the bands significantly increasing upon UV irradiation, $\lambda > 295$ nm), (c) spectrum corresponding to the oxo tautomer (the bands which disappeared after irradiation of the matrix with UV light, $\lambda > 295$ nm), with the spectra calculated at the DFT(B3LYP)/cc-pVTZ level for the hydroxy (**2PDh**) tautomer (trace b) and the oxo (**2PDo**) tautomer of 2-pyridinone (trace d). The calculated wavenumbers were scaled by a factor of 0.98.*

For the first time the IR spectra of 2-pyridinone tautomers isolated in Ar matrix were interpreted in Ref. [27]. The authors obtained the [hydroxy]:[oxo] ratio for 2-pyridinone isolated in Ar and N_2 matrices equal to 2.80 : 1 and 2.99 : 1, respectively. In this estimation, the theoretical intensities A^{th} predicted at the SCF/6-31G** level were used.

In the current work, the ratio of the tautomers was estimated in a similar way (equation 37), but using the higher level of theory than in previous report: B3LYP/cc-pVTZ level. The relative contribution of both tautomeric forms has been estimated as: [hydroxy]:[oxo] = 2.8 : 1 in an Ar matrix (Table 5.2 in the next section).

The **2PDo** ↔ **2PDh** equilibrium has served as a test for theoretical calculations of relative stability of tautomers [178-180]. Almost all quantum chemical methods have been applied in order to predict the difference of energy of these tautomers, as it was described in Section 4.

The relative energies of the oxo and hydroxy tautomers of 2-pyridinone were studied by Piacenza et. al. using different computational methods [149]. The calculations carried out within the current work are presented in Table 5.1. The results of these calculations are in good agreement with the previous results gained by Piacenza ([149], see also Figure 4.2 and Table 5.1).

The QCISD and QCISD(T) calculations of the relative energies of the **2PDh** and **2PDo** tautomers (carried out by Piacenza and Grimme [149], as well as those carried out in the current work, presented in Table 5.1), are in good proximity to the experimentally measured value of ΔE *(*$\Delta E_{exp} \approx$ -3 kJ mol^{-1}, the hydroxy form is most stable).

Table p5.1: *Calculated electronic energy difference ΔE_{el} = ΔE_{el}(hydroxy) - ΔE_{el}(oxo), internal energy difference ΔE = ΔE(hydroxy) - ΔE(oxo) and free Helmholtz energy difference ΔF = ΔF(hydroxy) - ΔF(oxo) between the hydroxy and oxo tautomers of 2-pyridinone/2-hydroxypyridine (kJ mol^{-1}).*

method	**ΔE_{el}**	**$\Delta E=\Delta H$ [a] (at 340 K)**	**$\Delta F=\Delta G$ [a] (at 340 K)**
B3LYP/cc-pVTZ//B3LYP/cc-pVTZ	2.52	1.83	2.40
MP2/cc-pVDZ//MP2/cc-pVDZ	-10.70	-11.20	-10.54
MP2/cc-pVTZ//MP2/cc-pVTZ	-11.76	-12.26	-11.72
MP2/cc-pVDZ//B3LYP/cc-pVTZ	-10.44	-11.13	-10.56
MP2/cc-pVTZ//B3LYP/cc-pVTZ	-11.82	-12.51	-11.94
CCSD(T)/cc-pVDZ//B3LYP/cc-pVTZ	-5.76	-6.45	-5.88
CCSD(T)/cc-pVTZ//B3LYP/cc-pVTZ	-6.48	-7.17	-6.60
QCISD/cc-pVDZ// B3LYP/cc-pVTZ	-2.50	-3.19	-2.62
QCISD/cc-pVTZ// B3LYP/cc-pVTZ	-3.32	-4.01	-3.44
QCISD(T)/cc-pVDZ// B3LYP/cc-pVTZ	-4.79	-5.48	-4.91
QCISD(T)/cc-pVTZ// B3LYP/cc-pVTZ	-5.49	-6.18	-5.61
experiment [27]	-2.5±0.6 [b]	-3.0 ± 0.6[b]	-2.9±0.5 [c]

The results of theoretical calculation are taken from Ref. [185].

[a] Vibrational contributions to the theoretical values of ΔE and ΔF were calculated at the DFT(B3LYP)/cc-pVTZ level, except for calculations carried out at the MP2/cc-pVDZ//MP2/cc pVDZ and MP2/cc-pVTZ//MP2/cc-pVTZ levels where vibrational contributions were calculated using MP2/cc-pVDZ//MP2/cc-pVDZ and MP2/cc-pVTZ//MP2/cc-pVTZ methods, respectively.

[b] The value of ΔE_{el} was estimated by subtraction from the experimentally measured ΔF [27]; the ΔZPE = -0.54 kJ mol^{-1} value calculated at the DFT(B3LYP)/cc-pVTZ level.

[c] The value of ΔF was experimentally estimated using of the ratio of oxo and hydroxy tautomers trapped from the gas phase (at 340K) into a low-temperature Ar matrix.

4-Pyrimidinone

The structure of 4-pyrimidinone (**4PM**) is similar to that of 2-pyridinone. It differs only by a number of nitrogen atoms in heterocyclic ring (nitrogens are in 1 and 3 position of the ring), while a H-N-C=O fragment is the same (Figure 5.7).

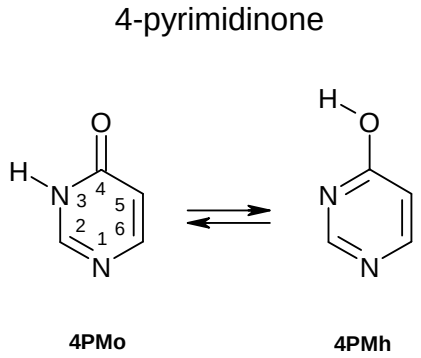

Figure 5.7. *Oxo-hydroxy tautomerism in 4-pyrimidinone.*

Numerous theoretical and experimental investigations concerned evaluation of the oxo-hydroxy tautomerism of 4-pyrimidinone. It was found by Nowak et al. that in the solid state this molecule exists only in the oxo form [26]. It was in accordance with earlier X-ray studies of crystalline compound [187]. Chevrier et al. [188] found that tautomeric equilibrium of this compound in solutions depends on the solvent polarity. Beak et al. [182] investigated 4-pyrimidinone in the gas phase and found two coexisting forms: oxo and hydroxy. They estimated the tautomeric equilibrium [hydroxy]:[oxo] = 0.55 at 500 K. A similar ratio of the tautomeric forms was observed by Nowak [28, 189] in inert gas matrices. The authors estimated the ratio applying equation 37 (see Section 5.1), and it was equal to 0.43, 0.45, 0.46 and 0.34 for the Ne, Ar, N_2 and Xe matrices, respectively (in this case, the theoretically predicted intensities A^{th} at the SCF/6-21G level were used in assessment of the ratio of tautomers). The difference in obtained values of the ratio of tautomers reflects the accuracy of the used methods. The obtained value was $\Delta F = 2.4 \pm 0.3$ kJ mol^{-1} in favor of the oxo form of 4-pyrimidinone (measurements in an Ar matrix) [28].

Sanchez et al. estimated the free energy difference ΔF ($\Delta F_{hydroxy} - \Delta F_{oxo}$) by Free Jet Absorption Millimeterwave Spectroscopy [190]. On the basis of obtained relative intensities of the observed absorption bands and measured dipole moments the authors obtained $\Delta F = 2.1$ kJ mol^{-1} (the oxo form is more stable).

The IR spectra of 4-pyrimidinone isolated in low-temperature inert matrices have been studied earlier in Nowak group [26, 28, 189]. It was demonstrated that the matrix-isolated compound exists as a mixture of the oxo and hydroxy tautomeric forms. The authors discovered, that upon UV ($\lambda > 295$ nm or $\lambda = 308$ nm) irradiation of the matrix the predominant oxo form converts into the hydroxy form. This intramolecular proton transfer photoreaction allowed separating the IR spectra of the two tautomers. The bands which intensity increased during UV irradiation were attributed to the spectrum of 4-hydroxypyrimidine (**4PMh**), while the decreasing bands to the spectrum of 4-pyrimidinone (**4PMo**).

In the current work, the IR spectra of 4-pyrimidinone isolated in an Ar matrix were also studied. The results were analogous to the previously reported [28, 189]; however, the new spectra were obtained with a better resolution [185]. This studies confirmed, that after deposition of the matrix, both tautomeric forms – oxo and hydroxy are present simultaneously, and that the dominating is the oxo tautomer (unlike the 2-pyridinone, where the hydroxy form was the dominating).

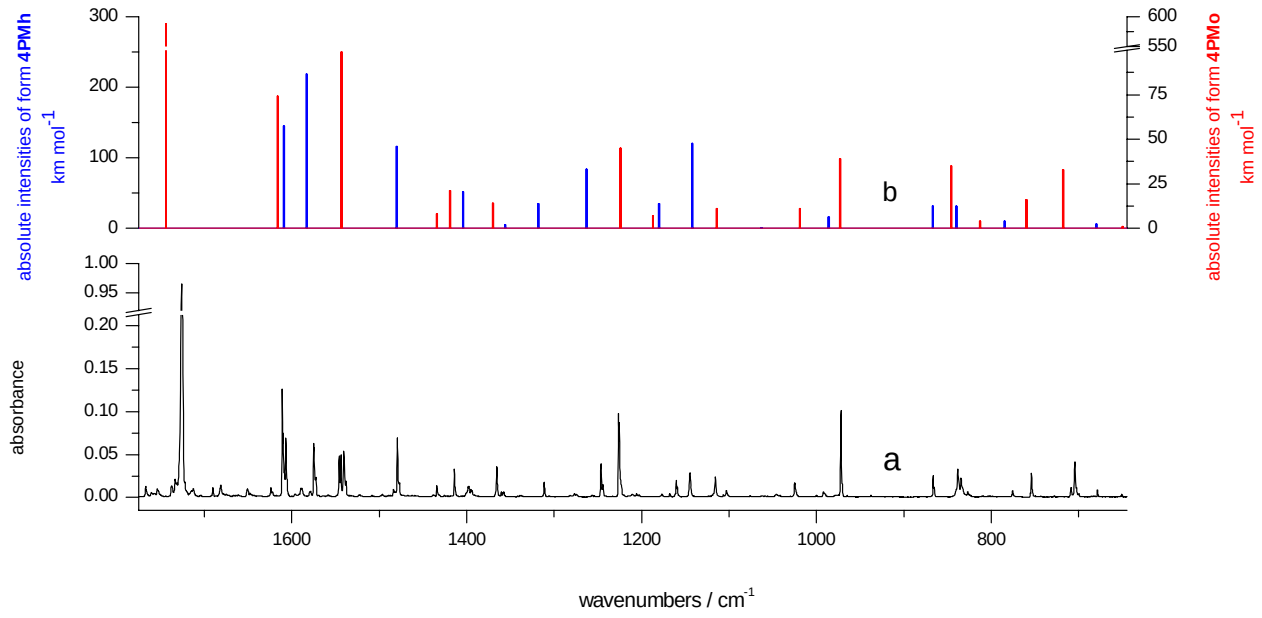

Figure 5.8. *The IR spectrum of 4-pyrimidinone isolated in an Ar matrix (trace a) compared with the results of theoretical simulations of the spectra (trace b): blue sticks for the hydroxy tautomer (**4PMh**) and red sticks for the oxo tautomer (**4PMo**). Two different ordinate scales are used to reflect the ratio between hydroxy and oxo tautomers in the theoretical spectrum. The calculated, at DFT(B3LYP)/cc-pVTZ level, wavenumbers were scaled by the single factor of 0.98.*

The infrared spectrum of 4-pyrimidinone monomers isolated in an argon matrix is presented in Figure 5.8 and compared with the results of theoretical simulations of the spectra of the oxo and hydroxy tautomers of the compound at DFT(B3LYP)/cc-pVTZ level. As it is seen, the agreement between the frequencies and intensities predicted theoretically at DFT(B3LYP)/cc-pVTZ level and the experimentally observed spectrum is very good.

In the high-frequency region, two bands due to the OH and NH stretching vibrations of the hydroxy and oxo form, respectively, were observed at 3562 and 3428 cm^{-1}. A low intensity of νOH band (at 3562 cm^{-1}), alongside the stronger νNH band (at 3428 cm^{-1}) confirms that a dominating form is the oxo form **4PMo** of the compound (Figure 5.9 trace a). For the 4-pyrimidinone, the oxo form predominates in the gas phase and in the matrix and this form is more stable than the hydroxy tautomer.

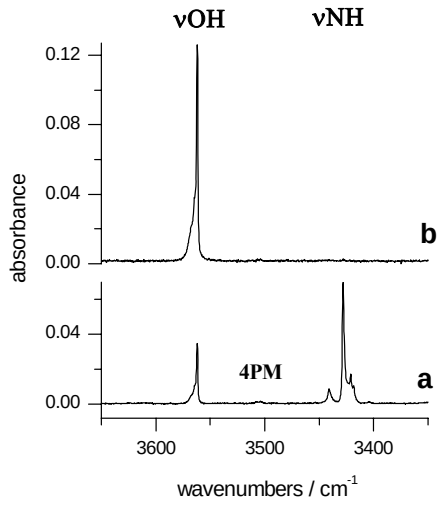

Figure 5.9. *High-frequency region of the infrared spectrum of 4-pyrimidinone (**4PM**) isolated in an Ar matrix: (a) spectrum recorded after deposition of the matrix and (b) spectrum recorded after 2 h of UV (λ > 300 nm) irradiation. The IR bands present in this spectral range are due to νOH and νNH vibrations and are characteristic of the hydroxy and oxo tautomers, respectively.*

Upon UV (λ > 300 nm) irradiation of the monomers of the 4-pyrimidinone isolated in an Ar matrix, the photoprocess leading to a total conversion of the oxo form of the compound into the hydroxy form occurred. The band originating from the oxo tautomeric form like νNH (at 3428 cm^{-1}) disappeared completely, whereas the band due to νOH (at 3562 cm^{-1}) originating from the hydroxy tautomer increased in the intensity (Figure 5.9).

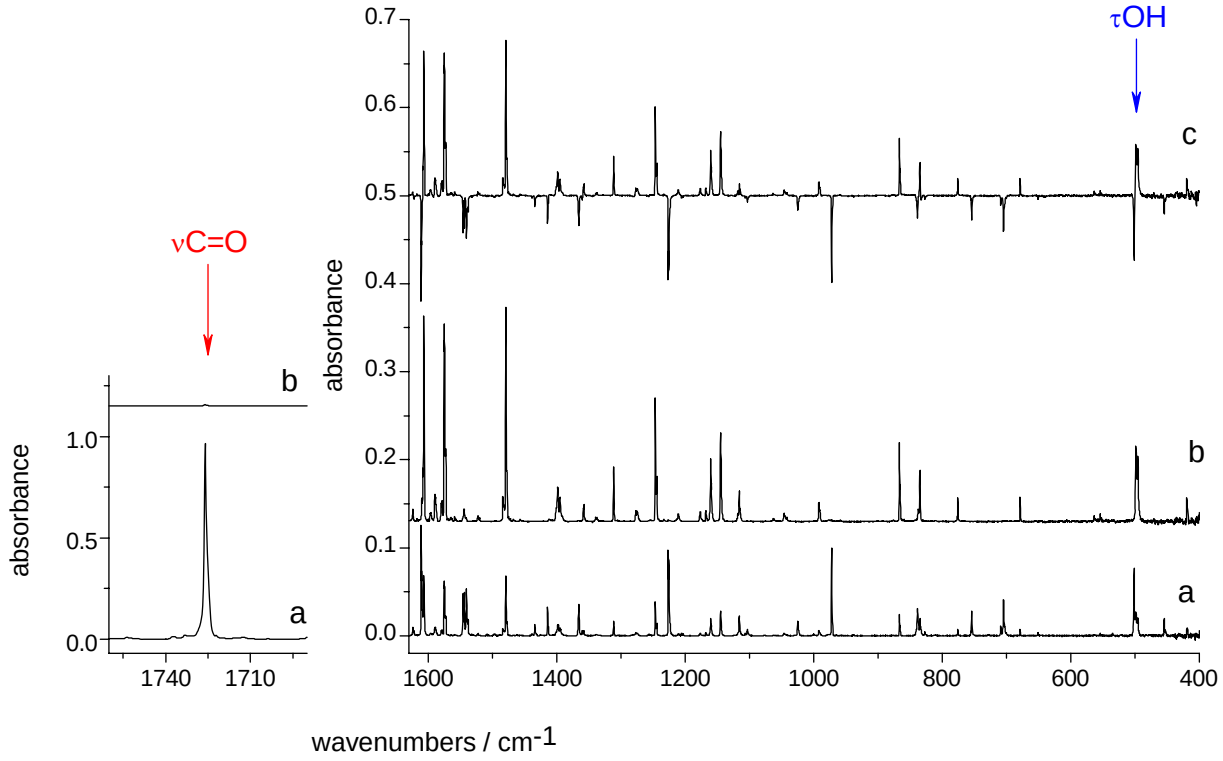

Figure 5.10. *Fragments of the IR spectra of 4-pyrimidinone (**4PM**) isolated in an Ar matrix: (a) spectrum recorded after deposition of the matrix; (b) spectrum recorded after 2 h of UV (λ > 300 nm) irradiation, (c) difference spectrum: spectrum b minus spectrum a. The bands directed downwards indicate the positions of the absorption bands which are vanishing upon UV (λ > 300 nm) irradiation. These bands are the spectral signatures of the oxo **4PMo** tautomer. The bands directed upwards indicate the positions of the bands originating from the hydroxy tautomer; these bands are growing upon UV (λ > 300 nm) irradiation.*

In the low-frequency region of the IR spectra of 4-pyrimidinone, the band due to the stretching vibration of CO group (νC=O) at 1726 cm^{-1} was observed before irradiation with UV light and vanished completely after UV (λ > 300 nm) irradiation of the matrix (Figure 5.10, left panel).

The right panel of Figure 5.10 demonstrates the effect of irradiation of the matrix at the 1650-400 cm^{-1} region of the IR spectra. The bands originating from the oxo tautomer of 4-pyrimidinone (which are vanish upon UV irradiation) are directed downwards in the difference spectra (trace c) showing its decreasing manner after irradiation of the matix with UV (λ > 300 nm) light. The bands due to the hydroxy tautomer increase after irradiation with UV (λ > 300 nm) light, in the difference spectrum this bands are directed upwards.

On the basis of this observation one can postulate that the oxo → hydroxy (**4PMo → 4PMh**) photoreaction (Figure 5.7) occurred for the monomers of 4-pyrimidinone isolated in a low-temperature matrix.

Using the numerical subtraction of the spectra, recorded before and after UV irradiation, it was possible to separate the spectra of the two tautomers (oxo and hydroxy) of the compound. Due to the reliable separation of the IR spectra of the tautomers, a quite precise [hydroxy] : [oxo] ratio and, hence, the free energy difference of the tautomers was possible to estimate.

As it was demonstrated in Figure 5.8, the IR spectra of 4-pyrimidinone recorded in this work are very well reproduced by the theoretical calculation carried out at DFT(B3LYP)/cc-pVTZ level for this compound. The absorption bands in the spectra of tautomers have been assigned to normal vibrations theoretically simulated at DFT(B3LYP)/cc-pVTZ level (previously the spectra were interpreted by comparison with the spectra predicted at HF/3-21G level [28, 189]). The full interpretation of the IR spectra of 4-pyrimidinone is presented in the Appendix. Assignment of the observed absorption bands to the theoretically predicted normal modes of oxo and hydroxy tautomers of the compound is given in Tables A5 and A6. Experimental wavenumbers and relative integral intensities of the bands due to the oxo form compared with wavenumbers, absolute intensities and potential energy distribution (PED) calculated for the **4PMo** tautomer is given in Table A5. Table A6 contains analogous experimental data of the bands due to the hydroxy tautomer compared with wavenumbers, absolute intensities and PED calculated for the **4PMh** tautomer. The symmetry coordinates used in the normal mode analysis are provided in Table A4 in the Appendix.

Using the absolute intensities of the absorption bands obtained at QCISD/cc-pVTZ level of theory, and the intensities of the respective bands observed in the experimental spectra of 4-pyrimidinone isolated in an Ar matrix (see equation 37 in Section 5.1), the ratio of [hydroxy]:[oxo] tautomers have been calculated, and it equals to 1 : 2.1. The free energy difference have been estimated as $\Delta F = 2.4 \pm 0.3$ kJ mol^{-1} in favor to the oxo tautomer (Table 5.2).

Theoretical calculations were carried out in this work to predict the tautomeric equilibrium. The electronic energies of **4PMo** and **4PMh** tautomers were calculated at QCISD/cc-pVDZ or QCISD(T)/cc-pVDZ levels using the geometries of the respective tautomers optimized at DFT(B3LYP)/cc-pVTZ level. The results of such calculations were compared with experimental measurements. The results of the QCISD/cc-pVDZ or QCISD(T)/cc-pVDZ calculations (presented in Table 5.2) showed that these methods quite correctly predict the increase of the relative stability of the oxo tautomer of **4PM** in comparison to the tautomeric equilibrium in **2PD**. Whereas for **2PD** the hydroxy tautomer is more stable and in the gas phase the ratio of the hydroxy and oxo forms was experimentally determined as 2.8 : 1, the tautomeric equilibrium **4PMo** ↔ **4PMh** is somewhat different, and the ratio of hydroxy and oxo tautomers is 1 : 2.1 (Table 5.2).

The QCISD and QCISD(T) calculations of the relative energies of the **4PMh** and **4PMo** tautomers (presented in Table 5.2), yielded good approximations to the experimentally measured value of ΔF *(*$\Delta F_{exp} \approx 2.4$ kJ mol^{-1}).

Table 5.2: *Experimental and theoretically calculated free energy differences between the hydroxy and oxo tautomers of 2-pyridinone, 4-pyrimidinone and 2-pyrazinone (kJ mol^{-1}).*

compounds	ΔE_{el} [a]	$\Delta F=\Delta G$ [b] at T	$\Delta F_{exp}=\Delta G_{exp}$ at T	T Kelvin	Experimental ratio of hydroxy and oxo forms (at T) [hydroxy]:[oxo]
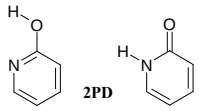 **2PD**	-2.50 (-4.79)	-2.62 (-4.91)	-2.9 ± 0.5	340	2.8 : 1
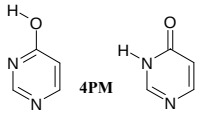 **4PM**	4.02 (2.09)	4.19 (2.26)	2.4 ± 0.3	400	1 : 2.1
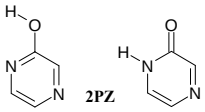 **2PZ**	-5.26 (-6.78)	-5.19 (-6.71)	-8.0 ± 1.0	360	14 : 1

[a] ΔE_{el} difference of electronic energies ($E_{hydroxy}$-E_{oxo}) calculated at the QCISD/cc-pVDZ or QCISD(T)/cc-pVDZ (given in parenthesis) levels at geometry optimized using the DFT(B3LYP)/cc-pVTZ method. The results of QCISD(T)/cc-pVDZ calculation is taken from ref. [185].

[b] $\Delta F=\Delta G$ difference of free Helmholtz = free Gibbs energies ($F_{hydroxy}$-F_{oxo}) calculated using the ΔE_{el} values and ΔE_{ZPE} corrections obtained on the basis of the DFT(B3LYP)/cc-pVTZ calculations.

2-Pyrazinone

2-Pyrazinone is an analog of 2-pyridinone with heterocyclic ring containing two nitrogen atoms in *para* position (Figure 5.11).

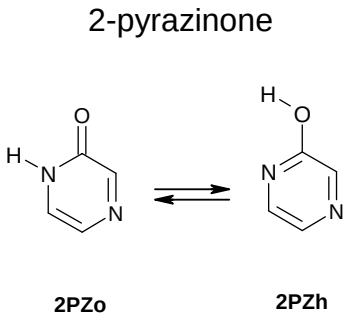

Figure 5.11. *Tautomeric equilibrium oxo-hydroxy in 2-pyrazinone*

Tautomerism of 2-pyrazinone isolated in low-temperature inert gas matrices has been investigated earlier by Nowak et. al by means of IR spectroscopy [191]. The UV-induced phototautomeric reaction has been used to separate the IR spectra of the oxo and hydroxy tautomers of this compound, but only a few bands due to the oxo form were observed. Because of difficulties in the assigning the bands to the oxo or hydroxy tautomer of the 2-pyrazinone, the [hydroxy] : [oxo] ratio for this compound was estimated using simplest method of estimation of the ratio of tautomers, described by the equation 36 (in Section 5.1). The obtained ratio [hydroxy] : [oxo] was equal to 8.6.

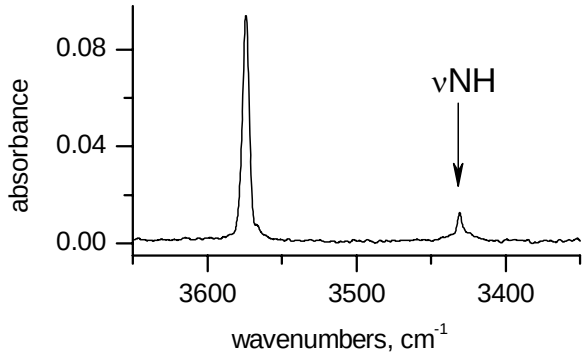

Figure 5.12. *High-frequency regions of the infrared spectra of 2-pyrazinone (**2PZ**) isolated in Ar matrixes. The IR bands present in this spectral range are due to νOH and νNH vibrations and are characteristic of the hydroxy and oxo tautomers, respectively.*

The results of the current work are similar [185]. For 2-pyrazinone isolated in an Ar matrix the hydroxy form of the compound was found to dominate significantly over the oxo form. In the IR spectrum of this compound, isolated in Ar matrix, only traces of the few most intense bands originating from the oxo form: at 3431 (Figure 5.12), 1711 (Figure 5.14), and much weaker bands at 792, 688, 552 and 391 cm^{-1} (Figure 5.13) were observed. Those bands were identified using the irradiation procedure with UV light ($\lambda > 340$ nm).

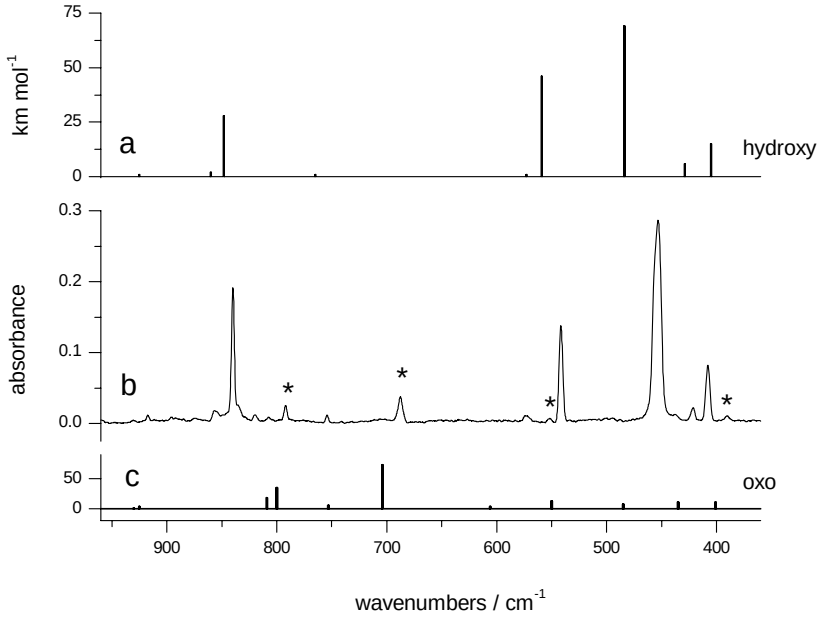

Figure 5.13. *Fragment of the IR spectrum of 2-pyrazinone (**2PZ**): (a) IR spectrum of the hydroxy tautomer **2PZh** predicted theoretically. (b) Experimental spectrum recorded after deposition of the matrix. Asterisks indicate the positions of the weak absorption bands present in the initial spectrum and vanishing upon UV ($\lambda > 340$ nm) irradiation. These bands are due to the oxo tautomer (**2PZo**) of the compound; (c) IR spectrum of the oxo tautomer **2PZo** predicted theoretically. The calculations were carried out at the DFT(B3LYP)/cc-pVTZ level and the obtained wavenumbers were scaled by the single factor of 0.98.*

Upon UV ($\lambda > 340$ nm) irradiation of the monomers of the 2-pyrazinone isolated in an Ar matrix, the photoprocess, which converts the oxo form of the compound into hydroxy form occurred. Due to the phototautomeric reaction the IR bands corresponding to the oxo form vanished. The band at 3431 cm^{-1} (which is due to νNH vibration) originating from the oxo tautomeric form, which was very weak after deposition of the matrix, has completely disappeared (see Figure 5.14). However, the increase of the intensities of the bands due to the hydroxy form was so small that a reliable determination of the value of tautomer ratio [hydroxy]:[oxo] based on the method applying equation 38 (in Section 5.1) was not possible.

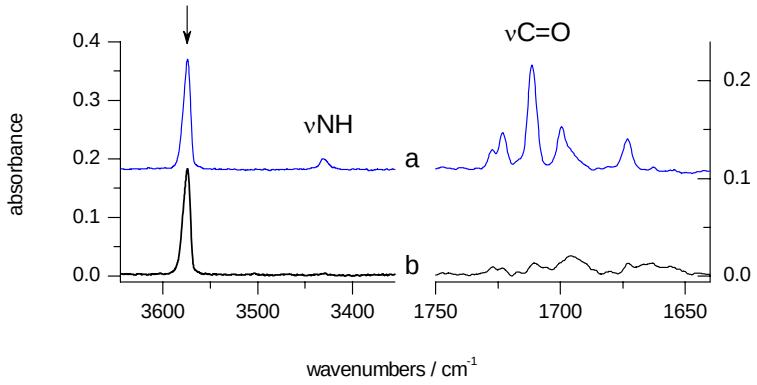

Figure 5.14. *Fragments of the IR spectra of 2-pyrazinone illustrating the effect of UV (λ > 340 nm) irradiation. (a) Spectrum recorded after deposition of the matrix. The arrow indicates the position of the absorption band due to hydroxy tautomer (**2PZh**) of the compound; (b) IR spectrum obtained after UV irradiation. Upon irradiation, the bands due to the oxo tautomer (**2PZo**) vanished. This effect indicates the presence of a small amount of the oxo tautomer in the freshly deposited matrix.*

Assignment of the observed absorption bands to the theoretically predicted normal modes at DFT(B3LYP)/cc-pVTZ level of oxo and hydroxy tautomers of 2-pyrazinone is given in Tables A8, A9 in the Appendix. This assignment was based on the comparison between experimental and theoretically predicted spectra. Almost all observed bands of the hydroxy form were interpreted, but only 8 bands in the spectrum of the oxo form could be attributed to this form. The two bands at 3431 and 1726 cm^{-1} due to the oxo form could be easily assigned because they appear in such spectral positions where the most intense characteristic bands were already observed for 2-pyridinone and 4-pyrimidinone. In the spectra of the oxo forms of these compounds the strong bands observed near, 3420 cm^{-1} were assigned to the stretching vibration of the NH group νNH and the bands near 1720 cm^{-1} were interpreted as originating from the in-plane stretching C=O vibration νCO.

The relative concentration of hydroxy and oxo forms of 2-pyrazinone was estimated using the obtained in the experiment integral intensities of the bands at 3575, 1546, 1119, 840, 454, 408 cm^{-1} from the spectrum of the hydroxy form and the bands at 3431, 1711, 792, 688 cm^{-1} from the spectrum of the oxo form scaled by the intensities of the respective bands obtained in the theoretical calculations at the DFT(B3LYP)/cc-pVTZ level (according to equation 37, Section 5.1). The obtained ratio [hydroxy] : [oxo] was equal to 14 : 1 (see Table 5.2).

The increase of the relative stability of the hydroxy tautomer of 2-pyrazinone, with respect to the corresponding values obtained for **2PD**, was well predicted theoretically at QCISD and QCISD(T) levels. Not only shifts of tautomeric equilibria of **2PZo↔2PZh** with respect to

the equilibrium in **2PDo↔2PDh**, but also the absolute values of the computed energy differences between the oxo and hydroxy tautomers of 2-pyrazinone are in fair agreement with experiment (see Table 5.2). These results showed that the QCISD and QCISD(T) methods are able to provide reliable relative energies of tautomers not only for the particular case of **2PDo↔2PDh** but also for other heterocyclic compounds. The results of theoretical and experimental estimations of the free energy difference between the hydroxy and oxo forms of 2-pyrazinone are presented in Table 5.2.

Upon examination of the experimental and theoretical results it is seen that the gas-phase tautomeric equilibria of heterocyclic compounds depend on the number of heterocyclic N atoms and on the relative position of the two nitrogen atoms in the ring. This dependency is presented in Figure 5.15, where it is possible to observe a systematic shift of the tautomeric equilibrium from the dominance of the oxo form (for **4PM**) via the mixture of the oxo and hydroxy forms to the dominance of the hydroxy form (**2PZ**) of the compounds.

One of the aims on this work was to determine the influence of direct attachment of benzene ring to heterocyclic molecules on their tautomeric equilibria. The tautomeric equilibrium determined for “parent molecules” with one six-membered ring served as a reference value. In the next chapter the results of experimental and theoretical investigations concerning analogs of 2-pyridinone, 2-pyrazinone and 4-pyrimidinone with a benzene ring fused with a heterocyclic ring will be presented.

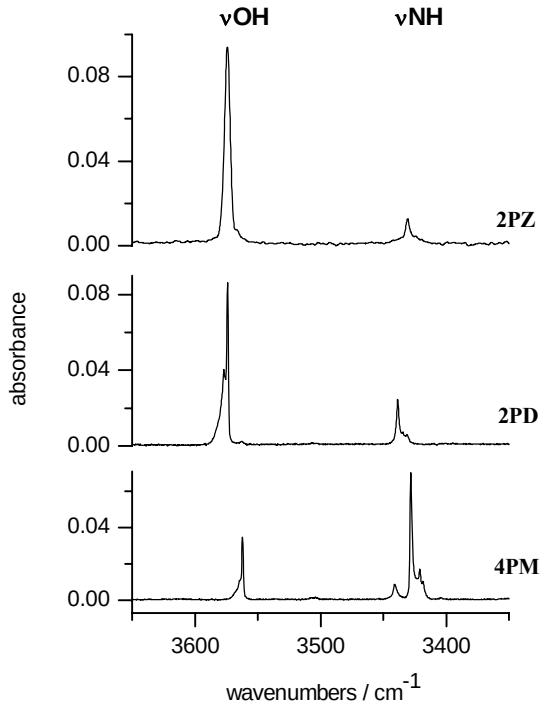

Figure 5.15. *Juxtaposition of high-frequency regions of the IR spectra of 2-pyrazinone (**2PZ**), 2-pyridinone (**2PD**), and 4-pyrimidinone (**4PM**) isolated in argon matrices. The IR bands presented in this spectral range are due to vOH and vNH vibrations and are characteristic of the hydroxy and oxo tautomers, respectively.*

5.3. Systems with fused heterocyclic and benzene rings

In the following section, the QCISD and QCISD(T) methods were used to predict gas-phase tautomeric equilibria for a series of the compounds: 2-quinolinone (**2QL)**, 1-isoquinolinone (**1IQ)**, 3-hydroxyisoquinoline (**3IQ)**, 4-quinazolinone (**4QZ)**, and 2-quinoxalinone (**2QX)**. No report on reliable experimental or theoretical studies of tautomerism of these systems was available to date. These compounds are analogous to those considered above (with a single heterocyclic ring), but with a benzene ring directly attached to a heterocyclic six-membered ring. The results of such calculations are compared with the experimental observations of the gas-phase equilibrium of tautomers trapped in low-temperature matrices.

2-Quinoxalinone

2-quinoxalinone is a compound which contains a benzene ring fused with a heterocyclic ring in position C5-C6 of 2-pyrazinone (Figure 5.16).

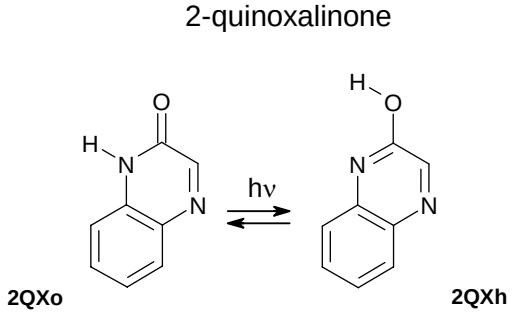

Figure 5.16. *Reaction of tautomerization oxo-hydroxy in 2-quinoxalinone*

The tautomerism of 2-quinoxalinone is determined by positions of labile hydrogen atom in the pyrazine ring of the molecule. The relative energies of the tautomeric forms of 2-quinoxalinone were calculated at the QCISD and QCISD(T) levels [185]. These calculations predict that the oxo tautomer **2QXo** (see Figure 5.16) is the most stable. Hydroxy tautomer **2QXh** is higher in energy by $\Delta E = 14.43$ kJ mol^{-1} (QCISD) or 11.34 (QCISD(T)), with respect to the energy of the oxo tautomer **2QXo**. Hence, for the gaseous 2-quinoxalinone at 450 K, the tautomeric form **2QXo** is expected to dominate, whereas tautomer **2QXh** can be populated only in a very small amount.

The studies of IR spectra of 2-qunoxalinone isolated in low-temperature Ar matrices confirm the theoretical results that majority of molecules of this compound adopt the oxo (**2QXo**) form [185]. The high-frequency region of the infrared spectrum of 2-qunoxalinone monomers isolated in an argon matrix is presented in Figure 5.17. In this fragment of the spectrum, two bands were observed: one at 3420 cm^{-1} is due to the NH stretching vibrations of the oxo form, and another, a weak band at 3568 cm^{-1} is due to the stretching vibration of the OH group of the hydroxy form. The frequency of these bands due to the stretching νNH and νOH vibrations is close to that of the corresponding νNH and νOH bands, which were observed in the IR spectrum of 2-pyrazinone isolated in an Ar matrix at 3431 and 3574 cm^{-1}, respectively (see Figure 5.21). Another characteristic band originating from the hydroxy form is due to the torsion vibration of OH group. In this case τOH participates in normal modes of two absorption bands at 533 and 501 cm^{-1} (see Figure 5.19 and Table B3 in the Appendix). The presence of the bands due to vibrations of OH group in the initial spectrum indicates that a small amount of the hydroxy tautomer **2QXh** is present in the low-temperature matrix (after deposition).

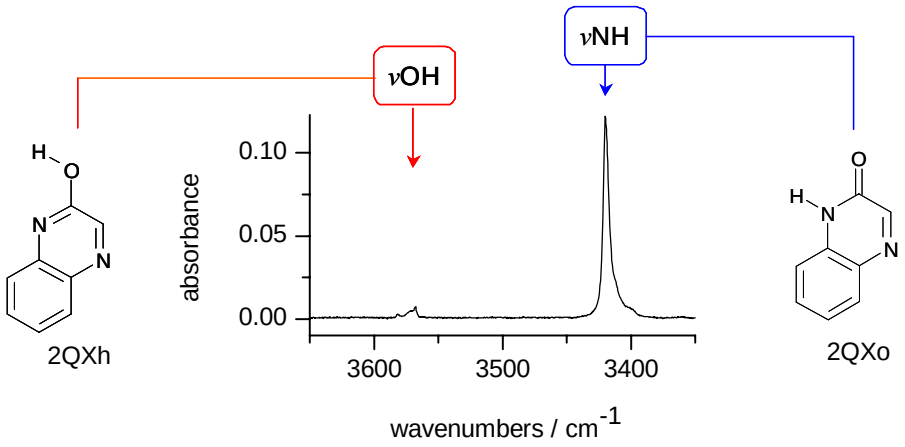

Figure 5.17. *High-frequency region of the IR spectrum of 2-quinoxalinone (**2QX**) isolated in an Ar matrix. The IR bands present in this spectral range are due to vOH and vNH vibrations and are characteristic of the hydroxy and oxo tautomers, respectively.*

Other very weak bands due to the hydroxy **2QXh** tautomer were identified in the IR spectrum thanks to the effect of UV irradiation of the matrix. Upon such irradiation, the molecules in the oxo form converted into the hydroxy tautomer and the IR spectrum of this latter form increased many times (see Figure 5.18).

Upon UV (λ > 335 nm) irradiation of the monomers of the 2-qunoxalinone isolated in an Ar matrix, the bands originating from the oxo tautomeric form of the compound decreased. The band

due to the νNH vibration (at 3420 cm^{-1}) has decreased, instead, the intensities of the bands , due to the stretching and torsion vibrations of the OH group (νOH at 3568 cm^{-1} and τOH at 533 and 501 cm^{-1}, which are characteristic of the hydroxy tautomer), has increased. The most striking changes in the spectra during irradiation concern the decrease of the intensity of the bands originating from the oxo form. The changes of the intensities of the IR bands upon UV irradiation are more clearly illustrated in the difference spectrum (Figure 5.18), where the positive peaks correspond to the increasing bands of the hydroxy form and the negative peaks to the decreasing bands of the oxo form. On the basis of this observation one can postulate that the oxo → hydroxy (**2QXo→2QXh**) photoreaction occurred for the monomers of 2-qunoxalinone isolated in a low-temperature matrix.

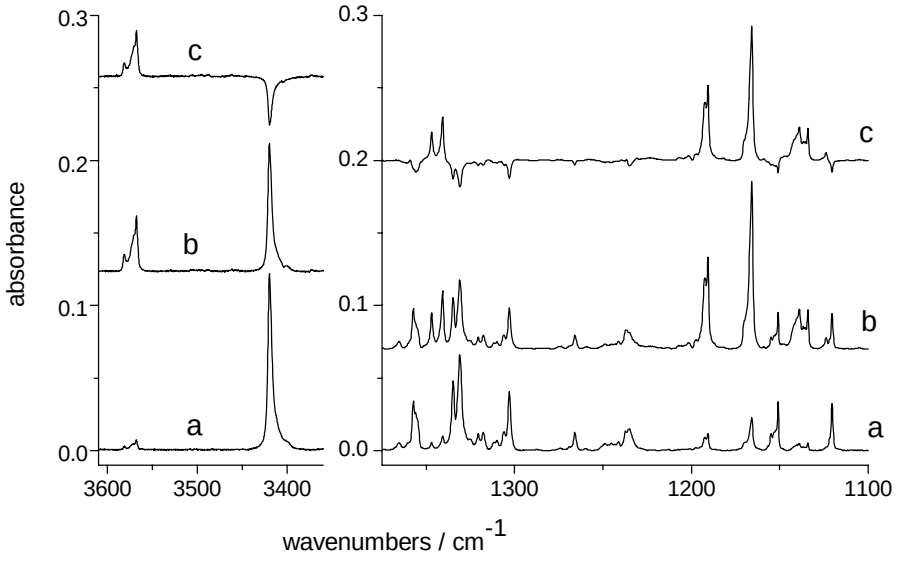

Figure 5.18 *Fragments of the IR spectrum of 2-quinoxalinone (**2QX**) isolated in an Ar matrix: (a) spectrum recorded after deposition of the matrix; (b) spectrum recorded after 6.5 h of UV (λ > 335 nm) irradiation, (c) difference spectrum: spectrum b minus spectrum a. The bands directed upwards indicate the positions of the weak absorption bands present in the initial spectrum and growing upon UV (λ > 335 nm) irradiation. These bands are the spectral signatures of the hydroxy 2QXh tautomer.*

Without this photoeffect, it would be very difficult to identify the bands due to the hydroxy **2QXh** tautomer in the initial IR spectrum of the compound. Having the observed IR bands assigned to either the oxo form or the hydroxy form, the ratio of the tautomers in the matrix was assessed using sums of integrated intensities of the bands which were identified in the spectra of the hydroxy and oxo forms, and sums of absolute intensities of the corresponding bands calculated at the DFT(B3LYP)/cc-pVTZ level (see equation 37 in Section 5.1). As a result, the ratio of the hydroxy and oxo forms of 2-qunoxalinone in an Ar matrix was estimated to be

equal to 1:40. The ratio of tautomers trapped in a low-temperature matrix is believed to be equal to the ratio of these forms in the gas phase from which the matrix was formed, as it was demonstrated earlier on an example of 2-pyridinone, where tautomerism of the **2PDh ↔ 2PDo** system was studied for the compound in the gas phase as well as for the compound isolated in low-temperature matrixes.

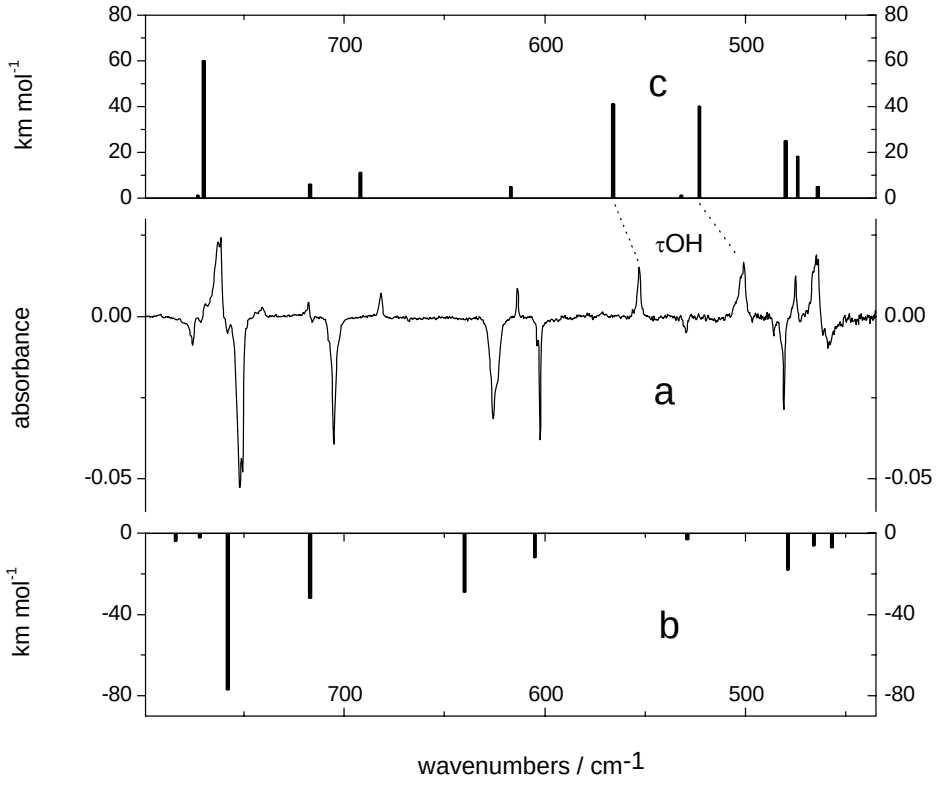

Figure 5.19. *Comparison of experimentally observed absorption bands of 2-qunoxalinone isolated in an Ar matrix: (a) difference spectrum, the bands correspond to: directed upwards are due to the hydroxy tautomer* ***2QXh*** *(significantly increasing upon UV (λ > 335 nm) irradiation (the bands connected with dotted lines are due to the τOH vibration), directed downwards are due to the oxo tautomer* ***2QXo*** *(decreasing upon UV (λ > 335 nm) irradiation), with the spectra calculated at the DFT(B3LYP)/cc-pVTZ level for (b) the oxo (**2QXo**) tautomer and (c) the hydroxy (**2QXh**) tautomer of the compound. The calculated wavenumbers were scaled by a factor of 0.98.*

Hence, on the basis of the ratio of the hydroxy and oxo forms isolated in an Ar matrix, the experimental difference of free energies of the two tautomers can be estimated using the equation 46 (see Section 5.1). The result of such an assessment is presented in Table 5.3, where obtained free energy difference ΔF_{exp} is compared with the results of theoretical predictions. As can be seen, the agreement between the experimental and theoretically predicted

ΔF values is quite satisfactory. Theory (at the QCISD level) and experimental estimations provide the value $\Delta F \approx 14$ kJ mol^{-1}, in favor of the significantly more stable **2QXo** oxo tautomer.

Due to the effect of UV irradiation of monomers of the 2-qunoxalinone, it was possible to separate the spectra of two tautomers, and to assign the observed absorption bands to the theoretically predicted normal modes of oxo and hydroxy forms of the compound. This assignment is present in Figure 5.19, and in Figure 5.20 where the extracted spectrum of photoproduct compared with spectra theoretically predicted at DFT(B3LYP)/cc-pVTZ level. The agreement between the frequencies and intensities of the experimentally observed bands and predicted theoretically is very good, in this level of theory. The positions and intensities of the bands (compared with corresponding experimental values) for oxo and hydroxy tautomers are presented in Table B2 and B3 in the Appendix. The theoretical bands have been assigned to the normal modes gained by using internal coordinates presented in Table B1 in the Appendix.

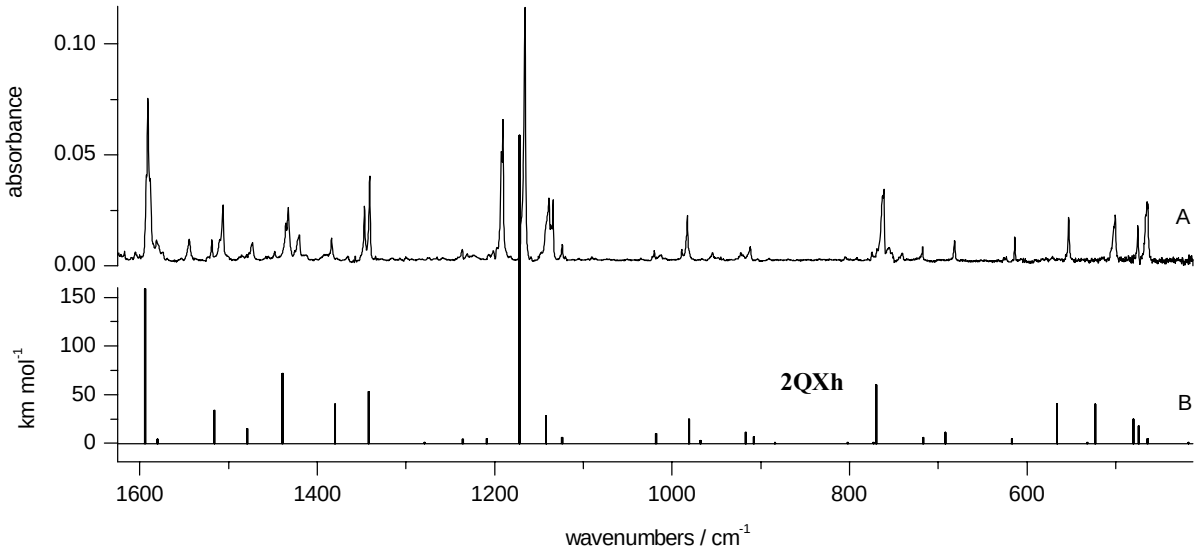

Figure 5.20. *(A) Infrared spectrum of the photoproduct generated upon 6.5 h of UV (λ > 335 nm) irradiation of 2-quinoxalinone isolated in an Ar matrix. The spectrum of the unreacted substrate of the photoreaction (the oxo tautomer* ***2QXo****) has been removed by electronic subtraction. (B) Infrared spectrum of the hydroxy tautomer* ***2QXh*** *theoretically predicted at the DFT(B3LYP)/cc-pVTZ level. The calculated wavenumbers were scaled by the single factor of 0.98.*

The experimental observation of a strong dominance of the oxo form of **2QX** is in sharp contrast to the observations of tautomeric equilibrium in 2-pyrazinone (**2PZ**), a one-ring analog of 2-quinoxalinone. For the **2PZ**, the dominating form is the hydroxy tautomer. Comparison of the [hydroxy]:[oxo] ratio in **2QX** (1:40) with the corresponding ratio for **2PZ** (14:1) shows the magnitude of the difference in tautomeric equilibria in these two related compounds. This is

illustrated by a substantial difference of relative intensities of the bands due to the νOH and νNH vibrations observed in the IR spectra recorded for both compounds isolated in Ar matrixes (see Figure 5.21). Such a sizable shift of tautomeric equilibrium, introduced by a direct attachment of benzene ring to the heterocyclic ring of **2PZ**, is also predicted theoretically. The results of theoretical and experimental estimations of the free energy difference between the hydroxy and oxo forms of **2PZ** are compared in Table 5.3 with the corresponding ΔF values obtained for **2QX**.

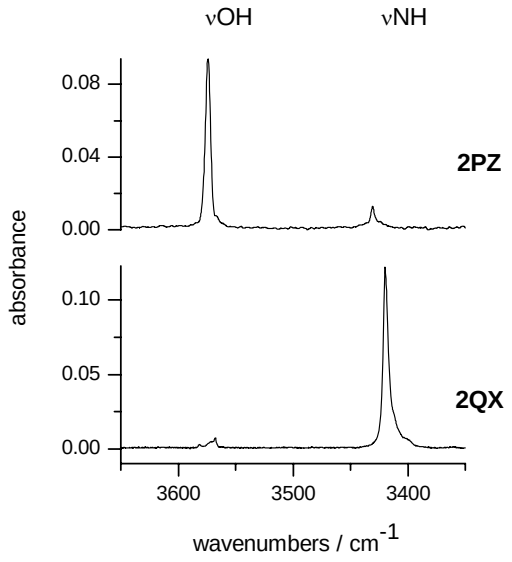

Figure 5.21. *High-frequency regions of the infrared spectra of 2-pyrazinone (**2PZ**), and 2-quinoxalinone (**2QX**) isolated in Ar matrixes. The IR bands present in this spectral range are due to νOH and νNH vibrations and are characteristic of the hydroxy and oxo tautomers, respectively.*

2-Quinolinone (carbostyril)

2-Quinolinone (or carbostyril) is a compound which contains a benzene ring fused with a heterocyclic ring in position C5-C6 of 2-pyridinone.

2-Quinolinone can exist in two forms, referred to as the oxo **2QLo** and hydroxy **2QLh** tautomers (Figure 5.22). These two forms may interconvert by H-atom transfer between the oxygen atom and the nitrogen atom of the pyridine ring.

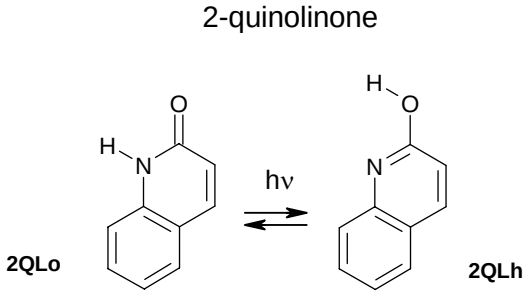

Figure 5.22. *Reaction of tautomerization oxo-hydroxy in 2-quinolinone*

The electronic properties and absorption spectra of the tautomers of 2-quinolinone have been investigated by several authors [181, 192-194]. These studies refer to the widely cited gas calorimetric measurement results, [181] which claim that the hydroxy **2QLh** form of gaseous 2-quinolinone is lower in energy (by 1.2 kJ mol^{-1}) than the oxo **2QLo** tautomer of the compound. As it will be shown further, the experimental results obtained in this work demonstrate that the data reported by Beak [181] are not correct. In the experiments on 2-quinolinone molecules in seeded supersonic jet expansions [194], the observed spectra of dispersed fluorescence (DF) and of fluorescence excitation (FE) were more intense for the hydroxy tautomer **2QLh** than for the oxo form **2QLo**. This observation might suggest that (in agreement with Beak's report [181]) the population of the **2QLh** tautomer in the gas phase is greater than the population of **2QLo**. However, the transition moments between S_0 and S_1 states can be very different for both tautomers in question, and conclusion about relative populations of the tautomers based on DF and FE spectra can be misleading.

Calculations carried out at QCISD or QCISD(T) levels predict the oxo form of 2-quinolinone (**2QL**) to be more stable than the hydroxy tautomer (see Table 5.3). At the QCISD level of theory the predicted value of the free energy difference between the **2QLh** and **2QLo** forms is as high as 16 kJ mol^{-1}. This value is even higher than ΔF predicted (at the same theory level) for the 2-quinoxalinone (**2QX**) system (discussed in the paragraph above). Similarly, the calculations

carried out at the QCISD(T) level predict also a larger difference in stabilities of the hydroxy and oxo forms (in favor of the oxo tautomer) in the case of **2QL**, in comparison with the corresponding value obtained for **2QX** (Table 5.3).

Table 5.3. *Experimental and theoretically calculated free energy differences between the hydroxy and oxo tautomers of 2-pyridinone, 2-quinolinone, 2-pyrazinone and 2-quinoxalinone (kJ mol^{-1})*

compounds	R(C-N)[a] Å	ΔE_{el}[b]	$\Delta F=\Delta G$[c] at T	$\Delta F_{exp}=\Delta G_{exp}$ at T	T Kelvin	Experimental ratio of hydroxy and oxo forms (at T) [hydroxy]:[oxo]
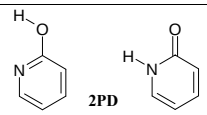 **2PD**	1.408	-2.50 (-4.79)	-2.62 (-4.91)	-2.9 ± 0.5	340	2.8 : 1
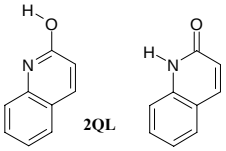 **2QL**	1.393	15.65 (12.84)	15.70 (12.89)	17 ± 1.5	450	1 : 95
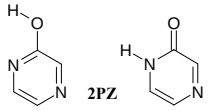 **2PZ**	1.400	-5.26 (-6.78)	-5.19 (-6.71)	-8.0 ± 1.0	360	14 : 1
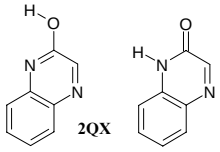 **2QX**	1.382	14.43 (11.34)	14.65 (11.56)	14 ± 1.0	450	1 : 40

[a] Distance between C and N atoms in the H-N-C=O fragment of the oxo tautomer. The value has been obtained by geometry optimization carried out at the DFT(B3LYP)/cc-pVTZ level.

[b] ΔE_{el} difference of electronic energies ($E_{hydroxy}$-E_{oxo}) calculated at the QCISD/cc-pVDZ or QCISD(T)/cc-pVDZ (given in parenthesis) levels at geometry optimized using the DFT(B3LYP)/cc-pVTZ method. The results of QCISD(T)/cc-pVDZ calculation is taken from ref. [185].

[c] $\Delta F=\Delta G$ difference of free Helmholtz = free Gibbs energies ($F_{hydroxy}$-F_{oxo}) calculated using the ΔE_{el} values and ΔE_{ZPE} corrections obtained on the basis of the DFT(B3LYP)/cc-pVTZ calculations.

These predictions are in nice agreement with experimental observations [185]. In the IR spectrum of **2QL** isolated in an Ar matrix, the bands indicating the presence of a very tiny amount of the hydroxy tautomer are barely detectable and the whole spectrum is dominated strongly by the bands due to the oxo form. In the freshly deposited matrix, two bands due to the oxo form could be easily assigned because they appear in such spectral positions where the most intense characteristic bands were already observed in the oxo tautomers of 2-pyridinone, 4-pyrimidinone and 2-pyrazinone. In the spectra of 2-quinolinone the strong band observed at 1702 cm^{-1} was interpreted as originating from the stretching C=O vibration (νCO). In the high-frequency region of the spectrum of **2QL** monomers isolated in an Ar matrix (Figure 5.23), the band at 3428 cm^{-1} was assigned to the stretching vibration of the NH group νNH. In this spectrum, the absorption at the usual position of a band due to νOH vibration is extremely weak. Nevertheless, using methods similar to those applied for the case of **2QX**, it was possible to assess the relative populations of the **2QLh** and **2QLo** tautomers of 2-quinolinone in the matrix (1:95) and to estimate experimentally the ΔF for this compound (Table 5.3).

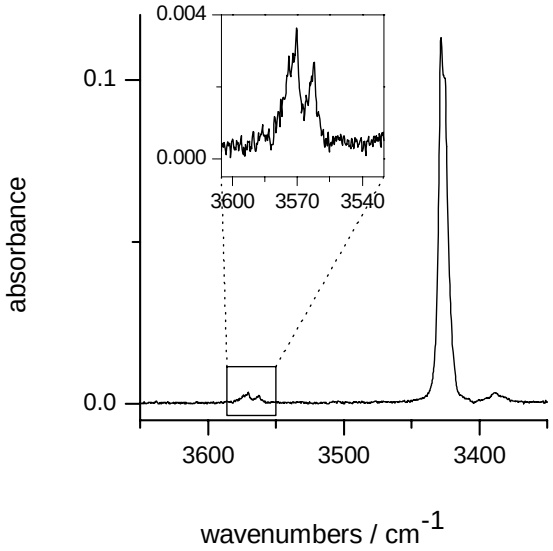

Figure 5.23. *High-frequency region of the infrared spectra of 2-quinolinone (**2QL**) isolated in Ar matrix. The IR bands present in this spectral range are due to νOH and νNH vibrations and are characteristic of the hydroxy and oxo tautomers, respectively.*

The comparison of the experimental IR spectrum of 2-quinolinone isolated in a low-temperature Ar matrix with the spectrum theoretically predicted (at the DFT(B3LYP)/cc-pVTZ level) for isomer oxo (**2QLo**) is presented in Figure 5.24. Good agreement between the patterns of

experimental and theoretical spectra supports the conclusion that the oxo tautomeric form **2QLo** is adopted by 2-quinolinone monomers isolated in an Ar matrix. Assignment of the observed absorption bands to the theoretically predicted normal modes of tautomer **2QLo** of the compound is given in Table B5 in the Appendix.

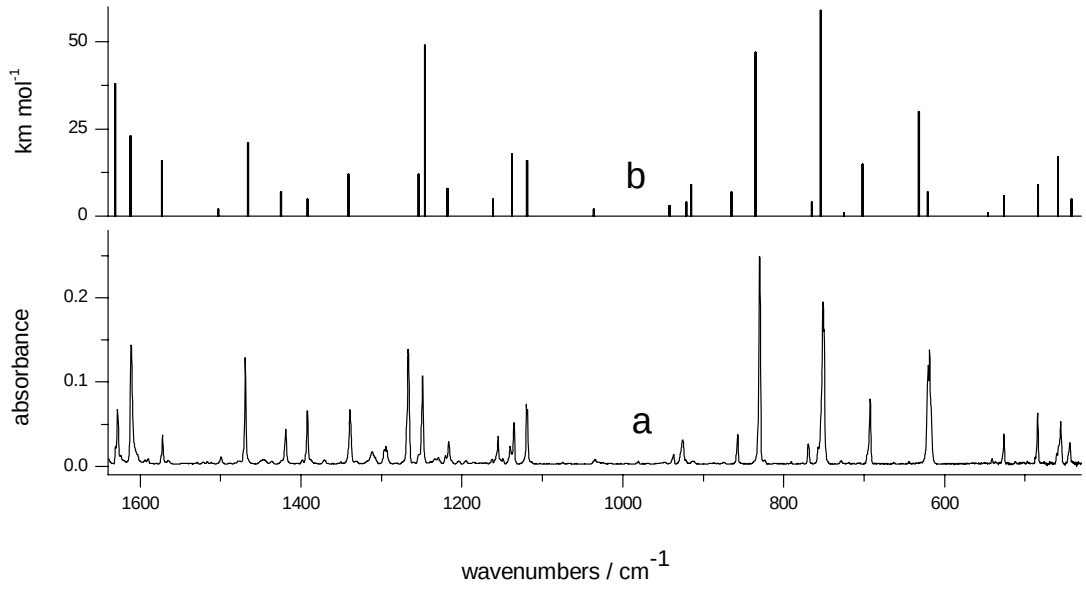

Figure 5.24. *The low-region fragment of the IR specta of 2-quinolinone (**2QL**) isolated in an Ar matrix: (a) spectrum recorded after deposition of the matrix; (b) IR spectrum of the oxo tautomer **2QLo** theoretically predicted at the DFT(B3LYP)/cc-pVTZ level. The calculated wavenumbers were scaled by the single factor of 0.98.*

UV ($\lambda > 320$ nm) irradiation of the matrix-isolated monomers of 2-quinolinone led to the decrease of the bands belonging to the spectrum of the oxo form and to the increase of the (initially very weak) bands of the spectrum of the hydroxy tautomer (Figure 5.25). The increase of the intensities of the bands corresponding to the stretching vibration at 3570 cm^{-1} and torsion vibration at 551 and 502 cm^{-1} of OH group is evidence that the hydroxy **2QLh** form arise as a product of this photoreaction. Hence, the main photochemical process observed for monomeric 2-quinolinone can be reliably interpreted as a proton transfer **2QLo** → **2QLh** reaction (Figure 5.22).

The infrared spectrum of 2-quinolinone irradiated with UV light is presented in Figure 5.25 (trace b) and compared with the results of theoretical simulations of the spectra of the hydroxy tautomer of the compound at DFT(B3LYP)/cc-pVTZ level (trace d). As it seen, the agreement

between the frequencies and intensities predicted theoretically and the experimentally observed spectrum is good.

However, in the IR spectra of irradiated 2-quinolinone, alongside with the bands originating from the hydroxy **2QLh** form of the compound, some bands are present which are difficult to interpret. It is possible, that these bands are due to the species, which are products of reactions of decomposition of studied compound, which take place during irradiation of the matrix. In Figure 5.25 these bands are marked with asterisks.

Because of this reason, not all the bands arising during UV irradiation could be unequivocally assigned to the spectrum of the hydroxy tautomer **2QLh**.

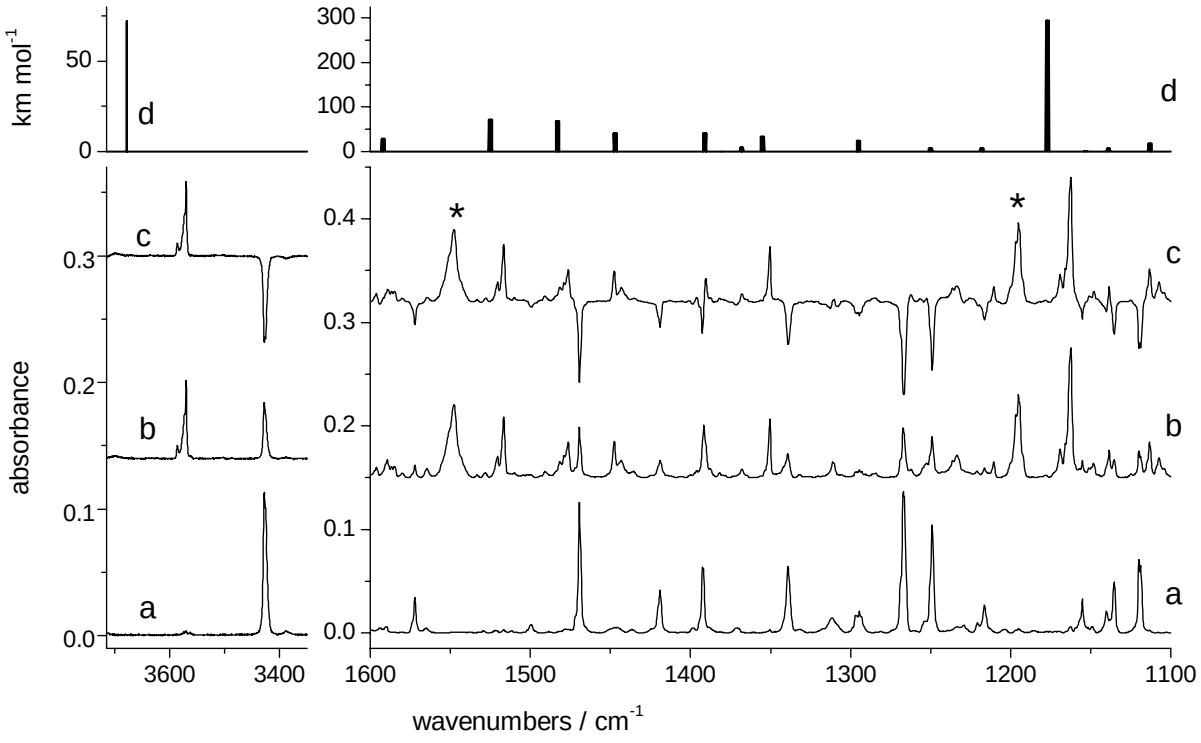

Figure 5.25. *Fragments of the IR spectra of 2-quinolinone (**2QL**) isolated in an Ar matrix: (a) spectrum recorded after deposition of the matrix; (b) spectrum recorded after 4.5 h of UV (λ > 320 nm) irradiation, (c) difference spectrum: spectrum b minus spectrum a. The bands directed downwards indicate the positions of the absorption bands present in the initial spectrum and decreasing upon UV (λ > 320 nm) irradiation (bands due to the oxo **2QLo** form), the bands directed upwards indicate the positions of the weak absorption bands present in the initial spectrum and growing upon UV (λ > 320 nm) irradiation (bands due to the hydroxy **2QLh** tautomer). Asterisks indicate the bands due to the unidentified secondary photoproduct; (d) IR spectrum of the hydroxy tautomer **2QLo** theoretically predicted at the DFT(B3LYP)/cc-pVTZ level. The calculated wavenumbers were scaled by the single factor of 0.98.*

The values of the ratio of the hydroxy and oxo tautomers of the compound, presented in Table 5.3, were compared with the corresponding data obtained for 2-pyridinone (**2PD**), a single-ring analogue of **2QL**. From this comparison (as well as from the graphical comparison of the high-frequency regions of the IR spectra of **2PD** and **2QL**, presented in Figure 5.26), it is evident that direct attachment of a benzene ring to the C(5)-C(6) bond of the **2PD** ring leads to a dramatic shift of the tautomeric equilibrium in favor of the higher stability of the oxo tautomer. The experimental observations of tautomeric equilibrium in **2QL** (well supported by the results of theoretical calculations) sharply contradict the previous report by Beak [181] where the energy difference between **2QLh** and **2QLo** was (unfortunately erroneously) estimated to be -1.2 kJ mol^{-1}, in favor of the hydroxy form. At this point, mentioning the pair of compounds 2-thiopyridine and 2-thioquinoline (analogous to **2PD** and **2QL**, but with sulfur atom replacing oxygen atom) seems also to be noteworthy. Whereas for 2-thiopyridine [35] the thiol form dominates strongly (with the thiol : thione ratio in an Ar matrix equal to 27 : 1), for 2-thioquinoline [37] the thione form was found to be significantly more stable and the thiol:thione ratio was estimated in this latter case to be equal to 1 : 7.7. This shows that attachment of a benzene ring considerably shifts the tautomeric equilibrium not only for the oxo compounds (with structure similar to **2PD**), but also for the corresponding thione compounds. One can treat a thiol tautomer as an analogue of a hydroxy form and a thione tautomer as an analogue of an oxo form, then one can say that for both thione and oxo compounds the direction of a change in tautomeric equilibrium, between the "parent" compounds and benzo-annelated derivatives, is the same. For species such as 2-quinoxalinone, 2-quinolinone, and 2-thioquinoline, the stabilities of the oxo or thione tautomers (with respect to the hydroxy or thiol forms) are significantly higher than those for the single-ring compounds 2-pyrazinone, 2-pyridinone, and 2-thiopyridine.

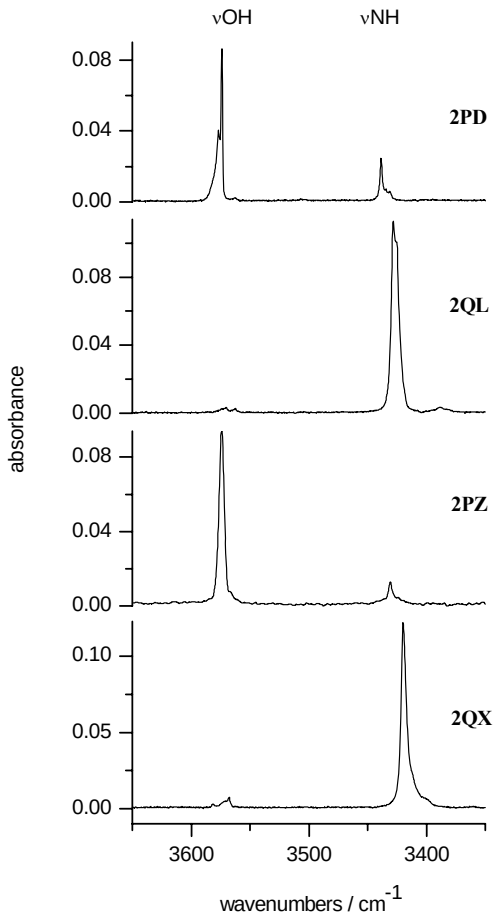

Figure 5.26. *High-frequency regions of the infrared spectra of 2-pyridinone (**2PD**), 2-quinolinone (**2QL**), 2-pyrazinone (**2PZ**), and 2-quinoxalinone (**2QX**) isolated in Ar matrices. The IR bands present in this spectral range are due to vOH and vNH vibrations and are characteristic of the hydroxy and oxo tautomers, respectively.*

1-Isoquinolinone (isocarbostyril)

1-Isoquinolinone (or isocarbostyril, **1IQ**) is an isomer of 2-quinolinone (**2QL**). Although both compounds (**1IQ** and **2QL**) have the same structural elements, 2-pyridinone **2PD** and a directly fused benzene ring, they differ by the position at which the benzene ring is attached to **2PD**. For **2QL**, the benzene ring is fused at the C(5)-C(6) bond of **2PD** (which is formally a double bond in the structure of the **2PDo** form). In the case of **1IQ**, the benzene ring is attached at the C(3)-C(4) bond (double in the **2PDo** structure) (Figure 5.27). Using the position of the benzene ring with respect to the N-C-O fragment as a criterion, **1IQ** (as **4QZ**, see next paragraph) can be considered as a group of compounds structurally different from **2QX** and **2QL**, discussed in previous paragraphs.

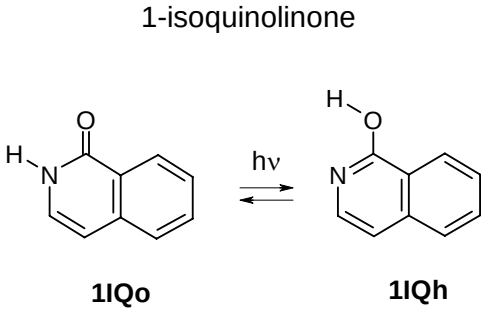

Figure 5.27. *Reaction of tautomerization oxo-hydroxy in 1-isoquinolinone.*

Theoretical calculations, carried out at QCISD and QCISD(T) levels, predict for 1-isoquinolinone **1IQ** that tautomeric forms of this compound should differ in energy by more than 20 kJ mol^{-1} (Table 5.4). For this compound, the oxo form was predicted to be the significantly more stable tautomer. Such a big calculated energy difference for **1IQ** should preclude experimental observation of the less stable tautomers. Indeed, in the experimental investigations on **1IQ** isolated in low-temperature Ar matrix, no IR bands which could indicate the presence of any amounts of the hydroxy forms were detected [185]. This is illustrated in Figure 5.28, where at the usual spectral position of a νOH band no absorption is visible.

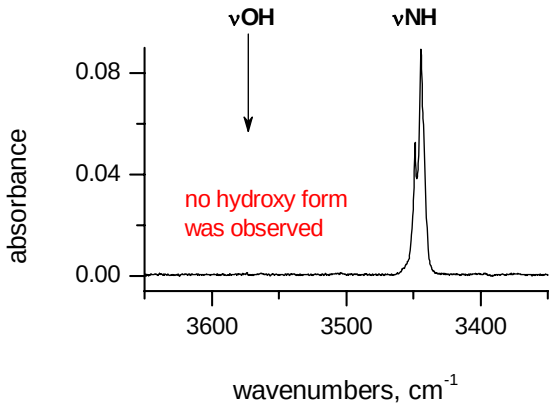

Figure 5.28. *High-frequency region of the infrared spectrum of 1-isoquinolinone (**1IQ**) isolated in an Ar matrix. The IR band presented in this spectral range is due to vNH vibration and is characteristic of the oxo tautomers. No trace of band due to the vOH of the hydroxy form was observed.*

The comparison of the experimental IR spectrum of 1-isoquinolinone isolated in a low-temperature Ar matrix with the spectrum theoretically predicted (at the DFT(B3LYP)/cc-pVTZ level) for isomer oxo (**1IQo**) supports the conclusion that the molecules of this compound occur only in its oxo form in the freshly deposited matrix. This comparison is presented in the in Figure 5.29, where one can see a very good agreement between the patterns of experimental and theoretical spectra.

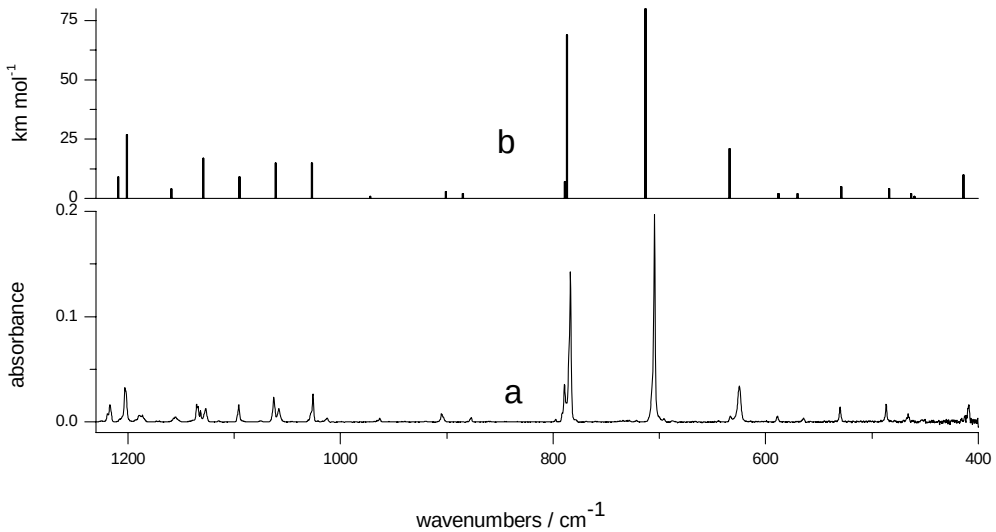

Figure 5.29. *The low-region fragment of the IR spectrum of 1-isoquinolinone (**1IQ**) isolated in an Ar matrix: (a) spectrum recorded after deposition of the matrix; (b) IR spectrum of the oxo tautomer of **1IQo** theoretically predicted at the DFT(B3LYP)/cc-pVTZ level. The calculated wavenumbers were scaled by the single factor of 0.98.*

UV (λ > 320 nm) irradiation of the monomers of the 1-isoquinolinone isolated in an Ar matrix stimulated the photoprocess leading to a conversion of the oxo form of the compound into hydroxy form. This photoreaction led to the decrease of the bands belonging to the spectrum of the oxo form and to the growth of the bands of the spectrum of the hydroxy tautomer (Figures 5.30 and 5.31).

The bands originating from the oxo tautomeric form (νNH at 3444 cm^{-1}) of the compound decreased, whereas the bands originating from the hydroxy tautomer arised. Among them appeared easily recognizable bands due to the νOH (at 3572 cm^{-1}, see Figure 5.30), and due to the τOH (at 3572 cm^{-1}, see Figure 5.31) vibrations. This observation supports the conclusion that the oxo → hydroxy (**1Iqo → 1IQh**) photoreaction (Figure 5.27) occurred for the monomers of 1-isoquinolinone isolated in a low-temperature matrix.

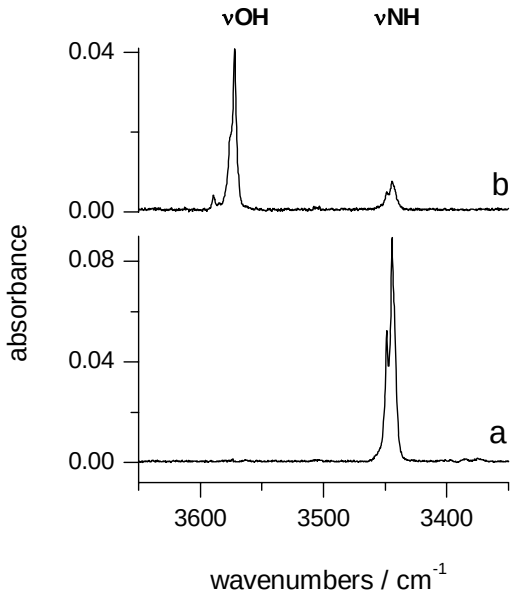

Figure 5.30. *High-frequency region of the infrared spectrum 1-isoquinolinone (**1IQ**) isolated in an Ar matrix: (a) spectrum recorded after deposition of the matrix and (b) spectrum recorded after 1.5 h of UV (λ > 320 nm) irradiation.*

Having two spectra (recorded before and after UV irradiation) of matrices containing different relative populations of the oxo and the hydroxy forms of 1-isoquinolinone, it was possible to extract (by subtracting the initial spectra due to the oxo tautomer) the spectra of the hydroxy tautomer of the compound. These two separated experimental spectra of tautomers are well reproduced by the results of the theoretical predictions of the spectra of form oxo **1IQo** and hydroxy **1IQh** (Figure 5.31). The absorption bands in the spectra of both tautomers have been

assigned to normal modes theoretically calculated at DFT(B3LYP)/cc-pVTZ level (see Appendix, Tables B7 and B8).

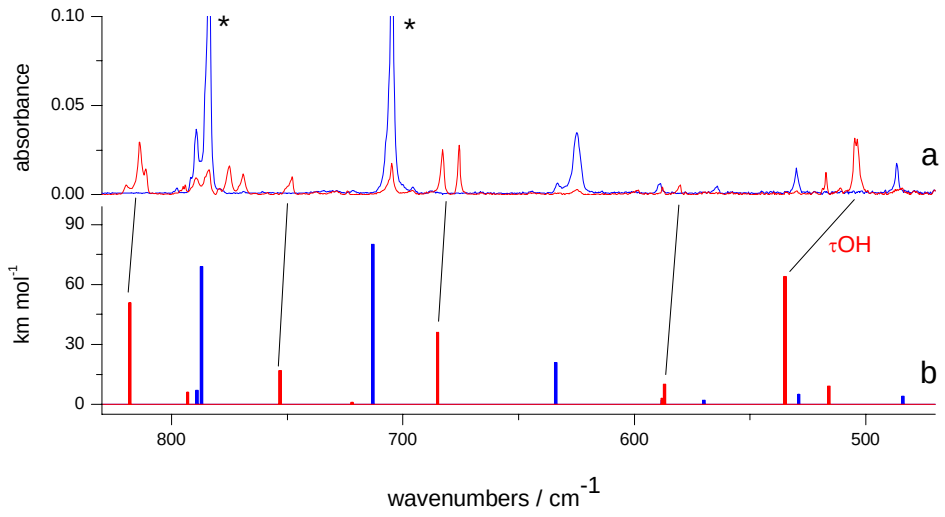

Figure 5.31. *Panel (a). Fragments of the experimental spectra of 1-isoquinolinone: (blue line) recorded after deposition of the matrix, (red line) generated upon UV (λ > 320 nm) irradiation. Panel (b). The corresponding fragments of the spectra calculated at the DFT(B3LYP)/cc-pVTZ level for the following: (blue) the oxo tautomer (1IQo) and (red) the hydroxy tautomer (1IQh) of 1-isoquinolinone. The calculated wavenumbers were scaled by a factor of 0.98. Asterisks indicate the bands intensities of which reach out of the scale.*

The results of theoretical estimation of the free energy difference between the hydroxy and oxo forms of 1-isoquinolinone are given in Table 5.4. Free energy difference cannot be obtained from experiment; it is only estimated as higher than the value obtained for the limit of detection of rare tautomer.

Table 5.4. *Experimental and Theoretically Calculated Free Energy Differences Between the Hydroxy and Oxo Tautomers of 2-Pyridinone, 1-Isoquinolinone, 4-Pyrimidinone and 4-Quinazolinone (in kJ mol^{-1})*

compounds	R(C-N)[a] Å	ΔE_{el}[b]	$\Delta F=\Delta G$[c] at T	$\Delta F_{exp}=\Delta G_{exp}$ at T	T Kelvin	Experimental ratio of hydroxy and oxo forms (at T) [hydroxy]:[oxo]
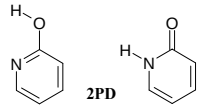 2PD	1.408	-2.50 (-4.79)	-2.62 (-4.91)	-2.9 ± 0.5	340	2.8 : 1
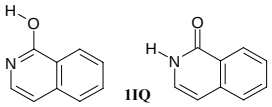 1IQ	1.391	23.97 (21.17)	23.68 (20.88)	>17	420	hydroxy form not observed
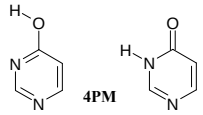 4PM	1.415	4.02 (2.09)	4.19 (2.26)	2.4 ± 0.3	400	1 : 2.1
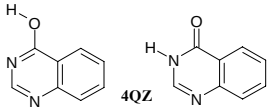 4QZ	1.399	28.79 (25.77)	28.78 (25.76)	>17	470	hydroxy form not observed

[a] Distance between C and N atoms in the H-N-C=O fragment of the oxo tautomer. The value has been obtained by geometry optimization carried out at the DFT(B3LYP)/cc-pVTZ level.

[b] ΔE_{el} difference of electronic energies ($E_{hydroxy}$-E_{oxo}) calculated at the QCISD/cc-pVDZ or QCISD(T)/cc-pVDZ (given in parenthesis) levels at geometry optimized using the DFT(B3LYP)/cc-pVTZ method. The results of QCISD(T)/cc-pVDZ calculation is taken from ref. [185].

[c] $\Delta F=\Delta G$ difference of free Helmholtz = free Gibbs energies ($F_{hydroxy}$-F_{oxo}) calculated using the ΔE_{el} values and ΔE_{ZPE} corrections obtained on the basis of the DFT(B3LYP)/cc-pVTZ calculations.

4-Quinazolinone

4-quinazolinone (**4QZ**) is a compound which contains a benzene ring fused with a heterocyclic ring in position C3-C4 of 4-pyrimidinone (Figure 5.32). It was mentioned previously, that 4-quinazolinone is an analogous compound with 1-isoquinolinone (**1IQ**). The applied criterion is the position of the benzene ring with respect to the N-C-O fragment. In both compounds (**4QZ** and **1IQ**), the benzene ring is attached in the same position C3-C4 to the single-ring compound: 4-pyrimidinone in the case of 4-quinazolinone, and 2-pyridinone in the case of 1-isoquinolinone.

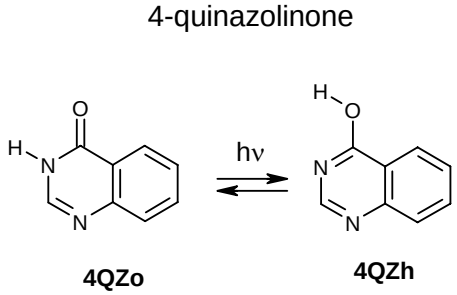

Figure 5.32. *Reaction of tautomerization oxo-hydroxy in 4-quinazolinone*

Theoretical calculations, carried out for **4QZ** at QCISD and QCISD(T) levels, predict (as it was in the case of **1IQ**) that tautomeric forms of this compound should differ in energy by more than 25 kJ mol^{-1} (Table 5.4). For **4QZ**, the oxo form was predicted to be the significantly more stable tautomer. Free energy differences as big as those calculated for **4QZ** (by analogy with **1IQ**) should preclude experimental observation of the less stable tautomers. Figure 5.33 presents a high-frequency region of 4-quinazoline isolated in an Ar matix. This figure illustrates that there is no absorption in the spectral position typical of νOH. It indicates the absence of detectable amount of the molecules in the hydroxy **4QZh** form in the matrix.

Hence, on the basis of experimental and theoretical data, one can conclude that attachment of a benzene ring at a position such as in **4QZ** and **1IQ** leads to very pronounced (even more pronounced than was the case for **2QL** and **2QX**) relative stabilization of oxo tautomeric forms. Although for the "parent", single-ring compounds (**4PM** and**2PD**) the hydroxy tautomers are well populated, the populations of the hydroxy forms of **4QZ** and **1IQ** in the gas phase must be so low that no traces of these tautomers could be found for **1IQ** and **4QZ** trapped from the gas into low-temperature matrices [185].

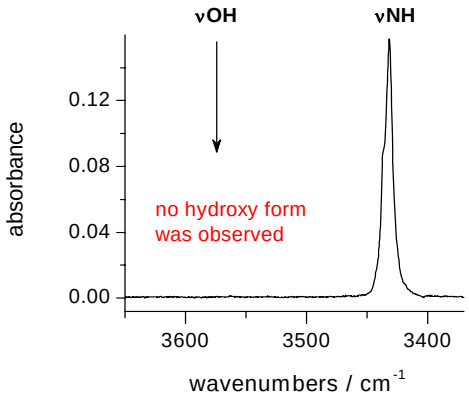

Figure 5.33. *High-frequency region of the infrared spectra of 4-quinazolinone (**4QZ**) isolated in Ar matrices. The IR band presented in this spectral range is due to vNH vibration and is characteristic of the oxo tautomers. No trace of band due to the vOH of hydroxy form was observed.*

The comparison of the experimental IR spectrum of 4-quinazolinone isolated in a low-temperature Ar matrix with the spectrum theoretically predicted (at the DFT(B3LYP)/cc-pVTZ level) for isomer oxo (**4QZo**) is presented in Figure 5.34. A very good agreement between the patterns of experimental and theoretical spectra supports the conclusion that the oxo tautomeric form **2QLo** is adopted by 4-quinazolinone monomers isolated in an Ar matrix. Assignment of the observed absorption bands to the theoretically predicted normal modes of tautomer **4QZo** of the compound is given in Table B10 in the Appendix.

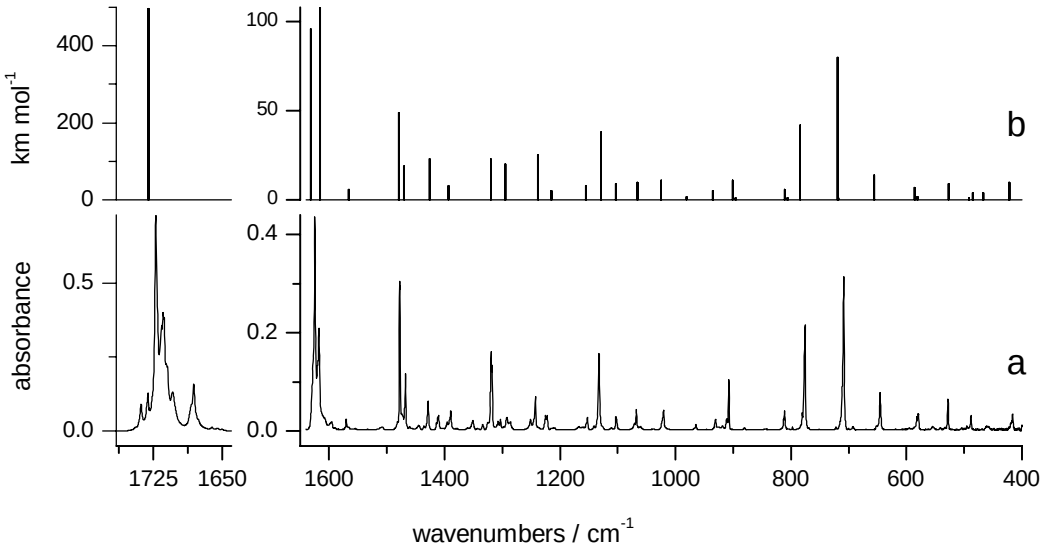

Figure 5.34. *Comparison of (a) the experimental spectrum of isolated 4-quinazolinone in an Ar matrix (after deposition), the bands are due to the oxo form **4QZo,** with (b) the theoretical spectrum of the oxo tautomer **4QZo** of 4-quinazolinone calculated at the DFT(B3LYP)/cc-pVTZ level. Theoretical wavenumbers were scaled by a factor of 0.98.*

The irradiation of the monomers of 4-quinazolinone isolated in an Ar matrix with UV ($\lambda > 295$ nm) light leads to decreasing of the bands belonging to the spectrum of the oxo form, and to arising of the new bands of the spectrum of the hydroxy tautomer. Particularly, the band due to the νNH vibration at 3432 cm^{-1}, which is a characteristic of the oxo tautomer, has decreased, whereas the bands due to the νOH vibration (at 3561 cm^{-1}) and τOH at 530 cm^{-1} originating from the hydroxy tautomer, have arised (Figures 5.35 and 5.36). The frequency of these bands due to the νOH and τOH vibrations is close to that of the corresponding νOH band at 3562 cm^{-1}, and of τOH bands (at 535 and 470 cm^{-1}), which were observed in the IR spectrum of 4-pyrimidinone isolated in an Ar matrix. On the basis of the spectra of 4-quinazolinone, recorded before and after UV irradiation of the matrices, one can conclude that the oxo → hydroxy (**4QZo → 4QZh**) phototautomeric reaction occurs also for monomers of 4-quinazolinone isolated in a low-temperature matrix (Figure 5.32), as it was in the case of the bicyclic heterocycles considered in previous paragraphs. This photoreaction converts the oxo forms (**4QZo**) into the hydroxy tautomer (**4QZh**).

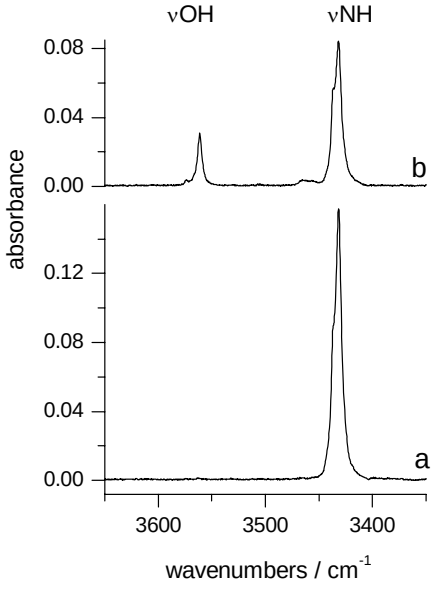

Figure 5.35. *High-frequency regions of the infrared spectra of 4-quinazolinone (**4QZ**) isolated in an Ar matrix: (a) spectrum recorded after deposition of the matrix and (b) spectrum recorded after 4.5 h of UV ($\lambda > 300$ nm) irradiation. The IR bands present in this spectral range are due to νOH and νNH vibrations and are characteristic of the hydroxy and oxo tautomers, respectively.*

A minor product emerging after UV irradiation of the matrix and coexisting with the dominating photoproduct **4QZh** has a characteristic, comparatively broad band at 2250 and 2138 cm^{-1}. The spectral position and complex pattern with many maxima indicate that this band may be originating from the conjugated ketene. The most characteristic band in the spectra of ketenes is a very strong band due to the "antisymmetric" stretching vibration of the –C=C=O group at the same region of IR spectra.

The experimental difference of free energies of the two tautomers ΔF_{exp} was estimated as larger than 17 kJ mol^{-1}. The results of experimental and theoretical assessments of ΔF are presented in Table 5.4. As can be seen, theoretically obtained value of ΔF is above the experimentally estimated lower limit of this value. Theory (at the QCISD level) and experimental estimations provided the conclusion that of **4QZo** oxo tautomer is significantly more stable.

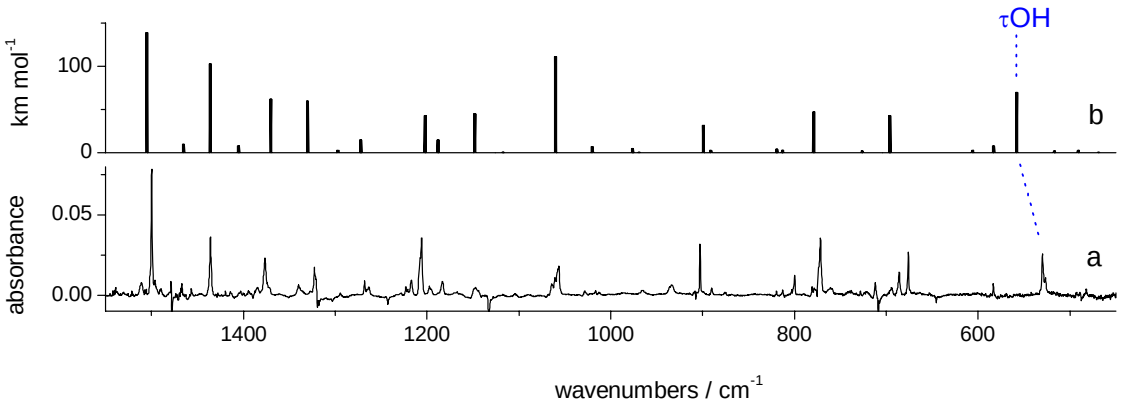

Figure 5.36. *Comparison of (a) the extracted spectrum of the photoproduct obtained after UV irradiation of 4-quinazolinone in an Ar matrix, with (b) the theoretical spectrum of the hydroxy tautomer* ***4QZh*** *of 4-quinazolinone calculated at the DFT(B3LYP)/cc-pVTZ level. Theoretical wavenumbers were scaled by a factor of 0.98.*

Because of bands originating from the minor photoproduct, the assignment of the bands due to the hydroxy **4QZh** tautomer of 4-quinazolinone needed more attention. The IR spectrum of hydroxy form was extracted by a numerical subtraction of the bands originating from the oxo form of the compound (see Figure 5.36).

The assignment of the observed absorption bands due to the hydroxy tautomer of the 4-quinazolinone to the theoretically calculated normal modes of the form 4QZh is given in Table B11 in the Appendix.

The values of the ratio of the hydroxy and oxo tautomers of 4-quinazolinone (and 1-isoquinolinone, see previous section), presented in Table 5.4, were compared with the corresponding data obtained for 4-pyrimidinone (4PM) (or 2-pyridinone **2PD** in the case of 1-isoquinolinone **1IQ**), a single-ring analogue of 4-pyrimidinone (and 1-isoquinolinone). From this comparison (as well as from the graphical comparison of the high-frequency regions of the IR spectra of **4PM** and **4QZ (2PD** and **1IQ)**, presented in Figure 5.37, it is evident that direct attachment of a benzene ring to the C(5)-C(6) bond of the **4PM** (and **2PD)** ring leads to a dramatic shift of the tautomeric equilibrium in favor of the higher stability of the oxo tautomer.

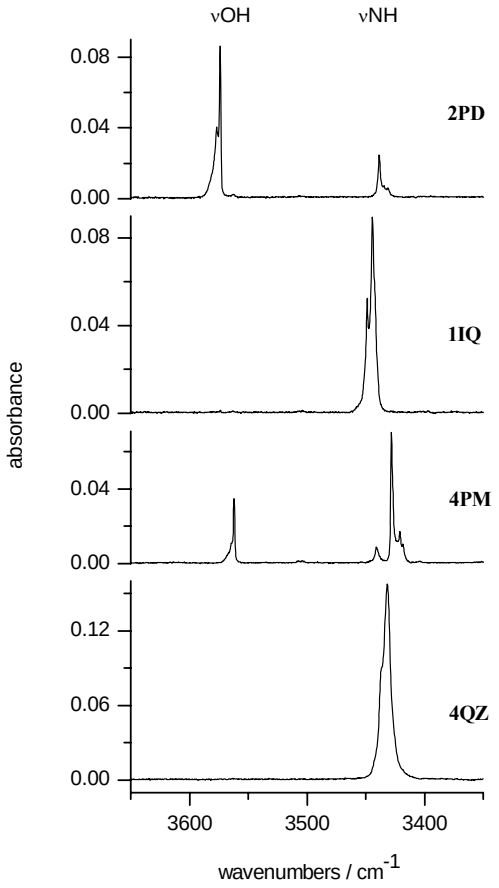

Figure 5.37. *High-frequency regions of the infrared spectra of 2-pyridinone (**2PD**), 1-isoquinolinone (**1IQ**), 4-pyrimidinone (**4PM**), and 4-quinazolinone (**4QZ**) isolated in Ar matrixes. The IR bands present in this spectral range are due to vOH and vNH vibrations and are characteristic of the hydroxy and oxo tautomers, respectively.*

3-Hydroxyisoquinoline

Alongside 2-quinolinone **2QL** and 1-isoquinolinone **1IQ**, which are two compounds built of benzene and **2PD** subunits fused together, there exists also a third isomer, 3-hydroxyisoquinoline (**3IQ**). This latter compound **3IQ** is built by a fusion of the benzene ring with 2-pyridinone **2PD** at the C(4)-C(5) bond (Figure 5.38). However, it does not seem that **3IQ** is just a third isomer, which should be similar in its properties to **2QL** and **1IQ**. The very fact that in **2QL** and **1IQ** benzene is attached at one of the double bonds of the **2PDo** form, whereas in **3IQ** the two rings are fused at the C(4)-C(5) bond of **2PD** (formally single in **2PDo**), turned out to be of crucial importance for stabilization of the **3IQo** tautomer. For the hydroxy form of **3IQ**, the single- and double bond system in both rings is regularly aromatic, but the single and double-bond system in the oxo **3IQo** tautomer does not contribute well to the stabilization of this form. This destabilization is reflected in the results of theoretical prediction of relative energies of the **3IQh** and **3IQo** tautomers.

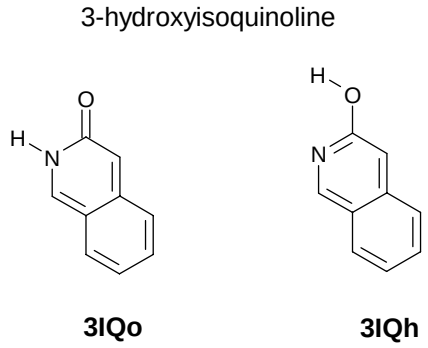

Figure 5.38. *Two tautomeric forms (oxo and hydroxy) of 3-hydroxyisoquinoline*

The energy of **3IQh** was calculated at both QCISD and QCISD(T) levels to be lower by 29 kJ mol^{-1} than the energy of the **3IQo** form (Table 5.5). Such a big calculated energy difference for **3IQ** should preclude experimental observation of the less stable tautomers. The experimental observations on **3IQ** monomers isolated in an Ar matrix are in full agreement with the theoretical predictions [185]. Only the hydroxy **3IQh** form was experimentally observed in an Ar matrix after deposition, with the **3IQo** population (if any) below the detection limits. This is reflected in the high-frequency region of the infrared spectrum of **3IQ** (Figure 5.39), where only the νOH band is observed and no absorption is detectable at the usual position of the νNH band.

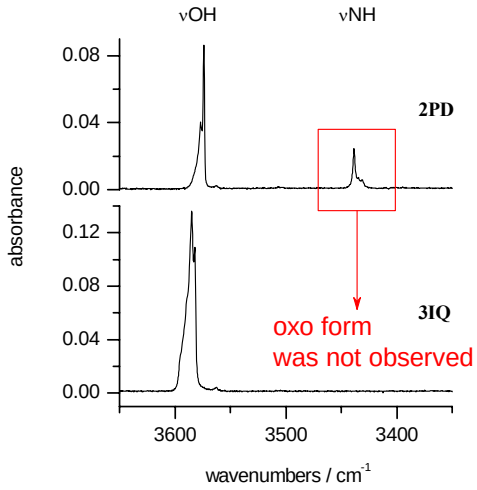

Figure 5.39. *High-frequency regions of the infrared spectra of 2-pyridinone (**2PD**) and 3-isoquinolinone (**3IQ**) isolated in Ar matrixes. The IR bands present in this spectral range are due to vOH and vNH vibrations and are characteristic of the hydroxy and oxo tautomers, respectively.*

The comparison of the experimental IR spectrum of 3-hydroxyisoquinoline isolated in a low-temperature Ar matrix with the spectrum theoretically predicted (at the DFT(B3LYP)/cc-pVTZ level) for isomer hydroxy (**3IQh**) confirms the conclusion, that the hydroxy tautomeric form **3IQh** is adopted by 3-hydroxyisoquinoline monomers isolated in an Ar matrix. It is presented in Figure 5.40, where a very good agreement between the patterns of experimental and theoretical spectra is illustrated. Assignment of the observed absorption bands to the theoretically predicted normal modes of tautomer **3IQh** of the compound is given in Table B13 in the Appendix.

After irradiation of the monomers of 3-hydroxyisoquinoline with UV light ($\lambda > 275$ nm), no changes in the intensities of the IR bands were observed on the time scale of an hour, and no indication of arising of a new substrate as a photoproduct. Hence, the spectrum recorded after irradiation was the pure spectrum of 3-hydroxyisoquinoline.

Table 5.5. *Experimental and theoretically calculated free energy differences between the hydroxy and oxo tautomers of 2-tyridinone and 3-hydroxyisoquinoline (in kJ mol^{-1}).*

compounds	R(C-N)[a] Å	ΔE_{el}[b]	$\Delta F=\Delta G$[c] at T	$\Delta F_{exp}=\Delta G_{exp}$ at T	T Kelvin	Experimental ratio of hydroxy and oxo forms (at T) [hydroxy]:[oxo]
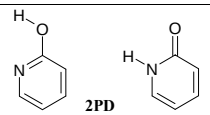 2PD	1.408	-2.50 (-4.79)	-2.62 (-4.91)	-2.9 ± 0.5	340	2.8 : 1
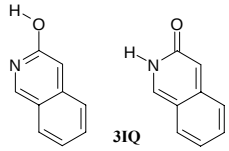 3IQ	1.427	-29.54 (-29.00)	-29.34 (-28.80)	< -17	420	oxo form not observed

[a] Distance between C and N atoms in the H-N-C=O fragment of the oxo tautomer. The value has been obtained by geometry optimization carried out at the DFT(B3LYP)/cc-pVTZ level.

[b] ΔE_{el} difference of electronic energies ($E_{hydroxy}$-E_{oxo}) calculated at the QCISD/cc-pVDZ or QCISD(T)/cc-pVDZ (given in parenthesis) levels at geometry optimized using the DFT(B3LYP)/cc-pVTZ method. The results of QCISD(T)/cc-pVDZ calculation is taken from ref. [185].

[c] $\Delta F=\Delta G$ difference of free Helmholtz = free Gibbs energies ($F_{hydroxy}$-F_{oxo}) calculated using the ΔE_{el} values and ΔE_{ZPE} corrections obtained on the basis of the DFT(B3LYP)/cc-pVTZ calculations.

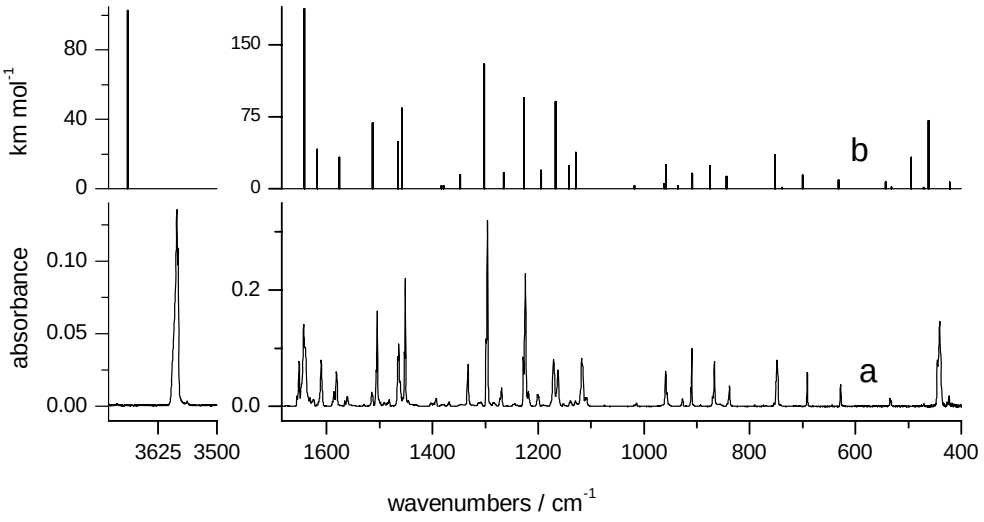

Figure 5.40. *Comparison of (a) the experimental spectrum of isolated 3-hydroxyquinoline in an Ar matrix, the bands are due to the hydroxy form* ***3IQh*** *before UV irradiation with (b) the theoretical spectrum of the hydroxy tautomer* ***3IQh*** *of 3-hydroxyquinoline calculated at the DFT(B3LYP)/cc-pVTZ level. Theoretical wavenumbers were scaled by a factor of 0.98.*

The systematic survey of tautomerism of benzo-annelated derivatives of 2-pyridinone, 4-pyrimidinone, and 2-pyrazinone revealed a substantial influence of fusion with a benzene ring on the oxo-hydroxy equilibrium. It was shown, using experimental and theoretical methods, that (except for a special case of 3-hydroxyisoquinoline) benzo-annelation leads to significant stabilization of the oxo tautomers with respect to the hydroxy forms. In the case of 3-hydroxyisoquinoline, the attachment of a benzene ring to 2-pyridinone shifts the equilibrium towards the hydroxy tautomer. The theoretical results of all calculations carried out in this work are in good agreement with the experimental data.

This effect was demonstrated for 2-quinolinone, 1-isoquinolinone, 2-quinoxalinone, and 4-quinazolinone. A similar shift of a tautomeric equilibrium has recently been theoretically predicted for cytosine and its benzo-fused derivative [196]. It seems probable that an effect of the same nature contributes to greater stabilization of the oxo forms (relative to the hydroxy tautomers) of hypoxantine and allopurinol (see next paragraph, and [195, 197]) with respect to a corresponding tautomeric equilibrium in 4-pyrimidinone. In all of these cases, extension of a π-electron system (being a consequence of direct attachment of a second ring) seems to be the crucial factor. The results described in the present work should contribute to better understanding of a link between aromaticity and tautomerism [198].

5.4. Systems with fused heterocyclic six- and five-membered rings

Allopurinol and hypoxanthine are important compounds due to their biological functions. Both molecules are bicyclic. One of the rings of these compounds has the structure of 4-pyrimidinone while the second is five-membered with two nitrogen atoms; it is pyrazole in the case of allopurinol and imidazole in the case of hypoxanthine. Pyrazole and imidazole are heterocyclic aromatic compounds and they are attached to the double bond of 4-pyrimidinone. Therefore, one may expect, having in mind the conclusions from the previous section, that for allopurinol and hypoxanthine the oxo-hydroxy tautomeric ratio should be shifted in favor of the oxo form with respect to the tautomeric ratio observed for 4-pyrimidinone.

The biological activity of both compounds is described in the Introduction (Section 1.2). Hypoxanthine forms nucleoside - inosine. 9-Methylhypoxanthine is a model compound of inosine; the methyl group mimics the sugar moiety.

Allopurinol

The tautomerism of allopurinol is determined by the positions of two labile hydrogen atoms in the molecule. For this compound, there are 9 tautomers with canonical structures (see Figure 5.41).

The crystal structure of allopurinol has been determined using three-dimensional X-ray data [199]. This X-ray structure analysis has revealed that the oxo form **AI** (see Figure 5.41) is the preferred tautomer in the crystal. The Raman and IR spectra recorded for crystalline allopurinol indicated also the presence of the oxo tautomers in the solid state [200]. Electronic absorption, dispersed fluorescence, and fluorescence excitation spectra were measured for this compound in aqueous solutions of different pH [201]. These studies showed that in water solutions the molecules of allopurinol adopt oxo **AI** tautomeric form. Coexistence of the oxo-N(1)H (**AI**) and the oxo-N(2)H (**AII**) tautomers of allopurinol (see Figure 5.41 for atom numbering) in DMSO solution was suggested on the basis of the ^{13}C NMR spectroscopic measurements [202].

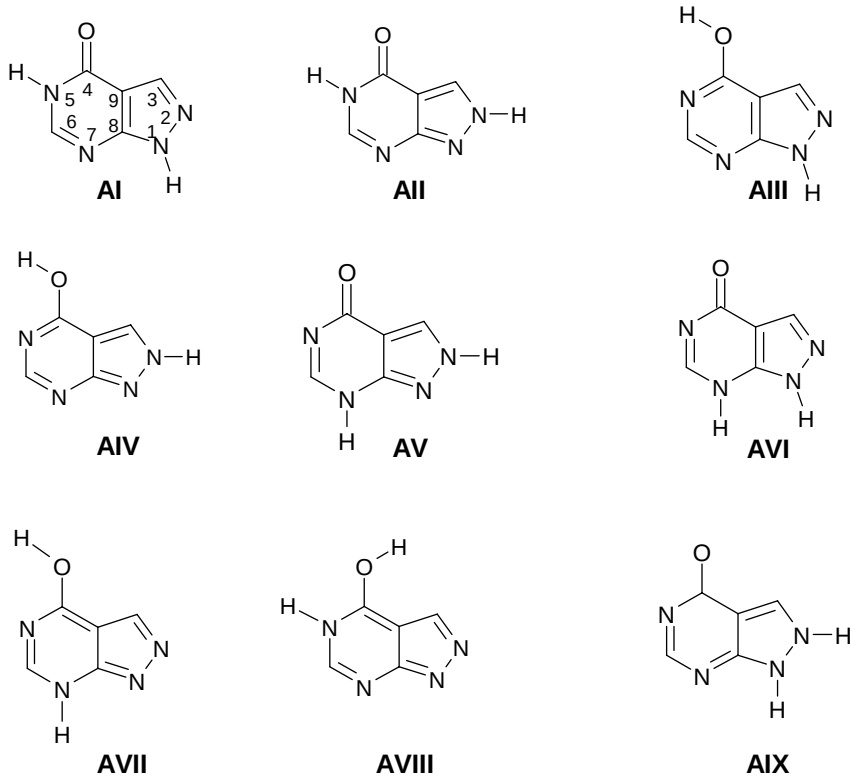

Figure 5.41. *Canonical tautomeric forms of allopurinol. Forms* ***AIIIa*** *and* ***AIVa*** *refer to the rotamers with hydroxyl group directed towards N(5) atom, while forms* ***AIIIb*** *and* ***AIVb*** *are rotamers with hydroxyl group directed to C(3) atom.*

The theoretical calculations were carried out by Costas [203] at DFT level with the BP86 and B3LYP exchange-correlation functionals, and the DZVP and 6-31++G(d,p) basis sets. These studies demonstrate that **AI** and **AII** forms of allopurinol are the most stable oxo forms, but the relative energy of the **AII** is higher by a 15.4 kJ mol^{-1}, with respect to **AI** tautomer.

The relative energies of the tautomeric forms of allopurinol were calculated in the current work at the DFT(B3LYP), MP2, and QCISD levels. These calculations predicted that the oxo tautomer **AI** with one of the labile hydrogens attached to N(1) and the other to N(5) nitrogen atoms is the most stable form. The relative energies of five other tautomers which were calculated in the current work (**AII**, **AIII**, **AIV**, **AV**, **AVI**) are given in Table 5.5.

Table 5.5. *Relative electronic (ΔE_{el}), zero-point vibrational (ΔZPE) and total ($\Delta E_{total} = \Delta E_{el} + \Delta ZPE$) energies (kJ mol^{-1}) of allopurinol isomers.*

	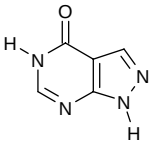	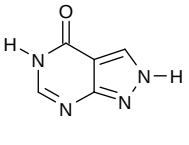	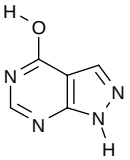	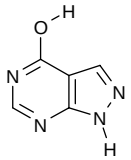	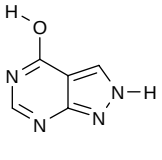	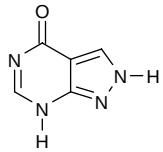	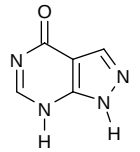	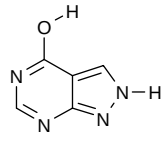
	AI	**AII**	**AIIIa**	**AIIIb**	**AIVa**	**AV**	**AVI**	**AIVb**
ΔE_{el}(DFT)	0	14.8	23.2	47.8	52.3	53.5	76.5	82.0
ΔZPE(DFT)	0	0.0	-0.5	-1.6	-0.4	-1.4	-3.5	-2.0
ΔE_{el}(DFT)+ ΔZPE(DFT)	0	14.8	22.7	46.2	51.9	52.1	73.0	80.0
ΔE_{el}(MP2)	0	11.4	20.1					
ΔE_{el}(MP2)+ ΔZPE(DFT)	0	11.4	19.6					
ΔE_{el}(QCISD)	0	15.5	27.7		55.5			
ΔE_{el}(QCISD)+ ΔZPE(DFT)	0	15.5	27.2		55			

The energy of the form **AI** was taken as reference. The results of DFT (using the B3LYP functional) and MP2 calculations obtained using 6-31++G(d,p) basis set; the results of QCISD obtained using cc-pVDZ basis set (geometry optimized at DFT(B3LYP)/cc-pVDZ level).

The forms **AVII**, **AVIII** and **AIX** (not listed in this table) are very high in energy (by more than 100 kJ mol^{-1}) and can be safely ruled out from further discussion. Among the low-energy isomers of allopurinol, the oxo tautomer **AII** is higher in energy by 15.5 kJ mol^{-1} (QCISD), with respect to the energy of the oxo tautomer **AI**. The energy difference between the most stable hydroxy form **AIIIa** and tautomer **AI** is considerably high and is equal 27.7 kJ mol^{-1} (QCISD). Theoretical calculations carried out earlier by several authors at a lower level [203, 204] give a similar results of relative energies of allopurinol tautomers. Hence, for the gaseous allopurinol at ca. 450 K, the tautomeric form **AI** is expected to dominate, whereas tautomer **AII** can be populated only in a very small amount. The thermal population of any of the hydroxy tautomers should be so low that these forms would not be detectable either in the gas phase or in the low-temperature matrices [195].

The infrared spectrum of allopurinol monomers isolated in an argon matrix is presented in Figure 5.42 (trace a). In the high-frequency region, two bands due to the NH stretching vibrations of the oxo form were observed at 3491 and 3432/3430 cm^{-1}. These bands should correspond to the νN1H vibration in the pyrazole ring and to the νN5H vibration in the pyrimidine ring, respectively. The frequency of the latter band due to the stretching N5H vibration is very close to that of the corresponding νN3H band (3428 cm^{-1}), which was observed in the IR spectrum of 4-pyrimidinone isolated in an Ar matrix (see Section 5.2, [189]). It indicates that this band is due to the stretching vibration of the NH group in the pyrimidine ring. No absorption was found in frequency range 3650 – 3550 cm^{-1}, where the bands due to the OH stretching vibrations should be expected.

Another evidence that the oxo form is dominant is a very intense band at 1747 cm^{-1} which was interpreted as originating from the stretching C=O vibration νCO of the oxo tautomer of allopurinol (see Figure 5.42, trace a).

The absence of the νOH band in the IR spectrum of allopurinol and the presence of a band due to the νCO vibration indicate that only oxo tautomer (or tautomers) of the compound exist(s) in the Ar matrix after its deposition.

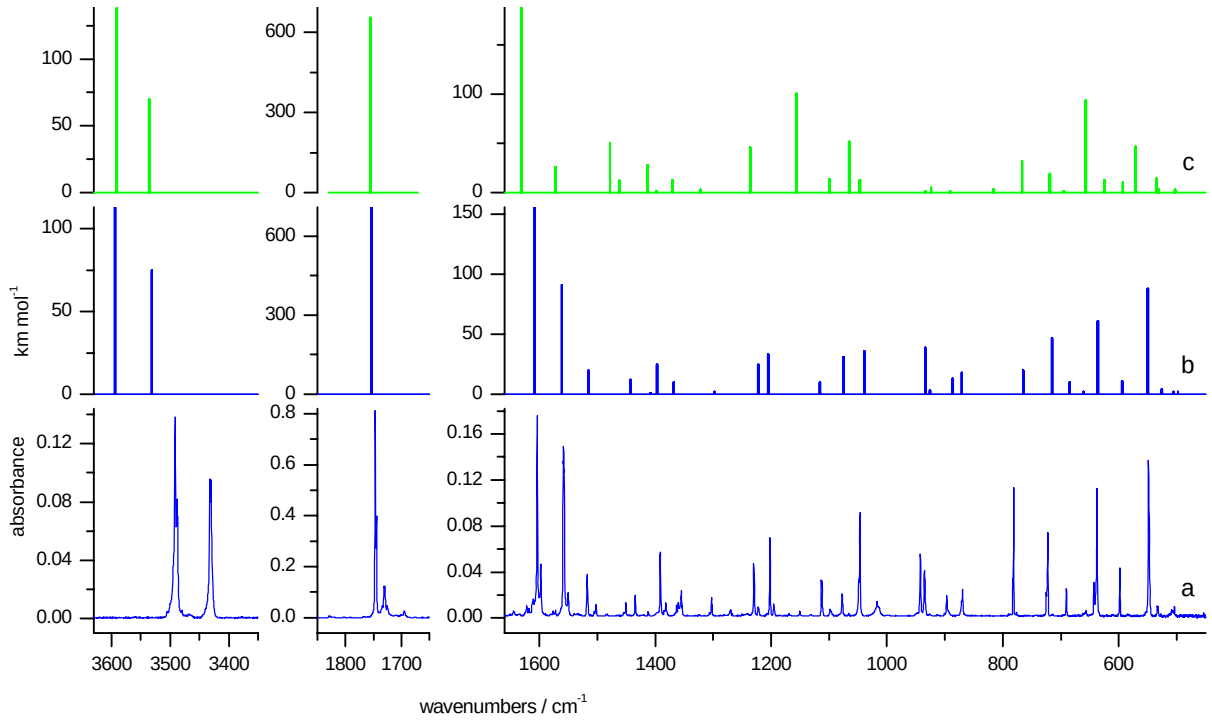

Figure 5.42. *Comparison of (a) the experimental IR absorption spectrum of allopurinol isolated in an Ar matrix with (b) the spectrum of the oxo tautomer* ***AI*** *and (c) the spectrum of the oxo tautomer* ***AII*** *theoretically simulated at the DFT(B3LYP)/6-31++G(d,p) level. The calculated wavenumbers were scaled by a factor of 0.98.*

The comparison of the experimental IR spectrum of allopurinol isolated in a low-temperature Ar matrix with the spectrum theoretically predicted (at the DFT(B3LYP)/6-31++G(d,p) level) for isomer **AI** is presented in Figure 5.42 (trace b). Good agreement between the patterns of experimental and theoretical spectra supports the conclusion that the oxo tautomeric form **AI** is adopted by allopurinol monomers isolated in an Ar matrix. Assignment of the observed absorption bands to the theoretically predicted normal modes of tautomer **AI** of the compound is given in Table C2 in Appendix. Comparison of the experimental spectrum of allopurinol with the spectra calculated for tautomers **AI** and **AII** does not allow assigning unequivocally any band, in the whole mid-IR range, to tautomer **AII**. Hence, there are no clear spectral signatures of the presence of this form in a low-temperature Ar matrix. On the other hand, the presence of a very small amount of allopurinol adopting the tautomeric form **AII** cannot be excluded based on the present experimental observations.

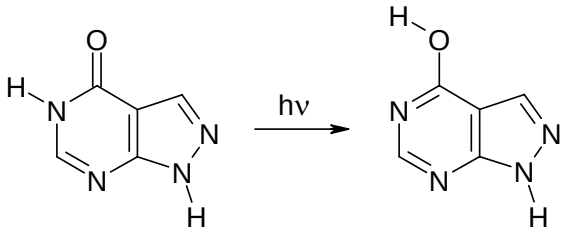

Figure 5.43. *Phototautomeric reaction observed for allopurinol.*

Upon UV (λ > 230 nm) irradiation of the monomers of the compound isolated in an Ar matrix, all the bands of the initial spectrum (including the most intense νC=O band at 1747 cm^{-1}) decreased, whereas a new spectrum of photoproduct(s) emerged (see Figure 5.44). The appealing feature of this new spectrum is the presence of the band at 3559 cm^{-1}, which can be assigned to the stretching vibration of the OH group (νOH). The position of this band is quite similar to that of the νOH band found previously at 3564 cm^{-1} in the spectrum of 4-hydroxypyrimidine (see Section 5.2, [189, 26, 28]). On the basis of this observation one can postulate that the oxo → hydroxy (**AI→AIII**) photoreaction (Figure 5.43) occurred for the monomers of allopurinol isolated in a low-temperature matrix. Photoreactions of the same type were described earlier (see Sections 5.2 and 5.3 of the current work). Photoreaction is analogous to that observed for matrix-isolated 4-pyrimidinone [26, 28, 29].

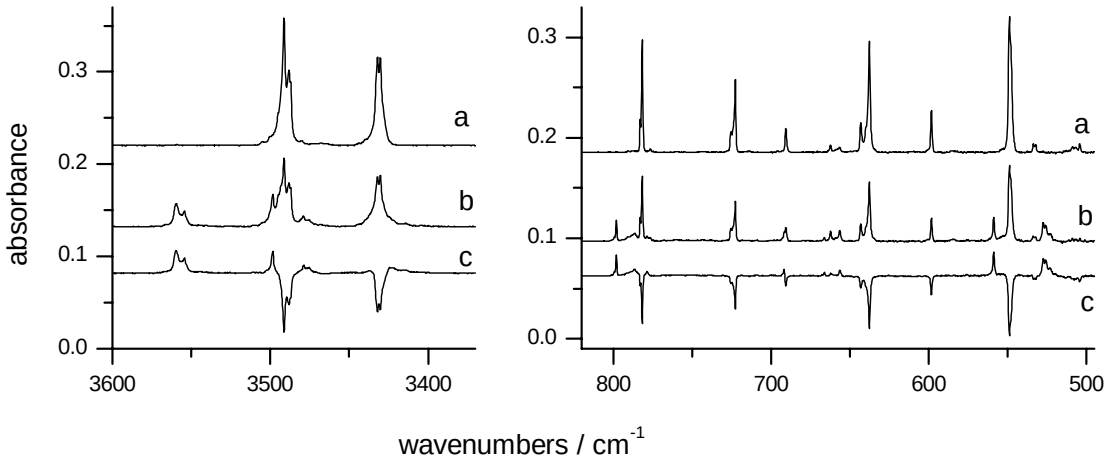

Figure 5.44. *Portions of the IR spectrum of allopurinol isolated in an Ar matrix recorded: (a) after deposition; (b) after 4 h of UV (λ > 230 nm) irradiation; (c) difference spectrum: trace b minus trace a.*

The photoprocess induced by UV ($\lambda > 230$ nm) irradiation of monomeric allopurinol did not lead to total conversion of the oxo form **AI** into the hydroxy tautomer **AIIIa** (for the structure see Figure 5.43). Upon prolonged (4 h) UV irradiation the intensities of the IR bands due to **AI** substrate decreased to 48% of their initial values. Hence, 52% of the **AI** form was converted into photoproduct(s) (Figure 5.44). The extracted spectrum of the photoproduct(s) is compared in Figure 5.45 with the spectrum of the hydroxy form **AIIIa** theoretically predicted at the DFT(B3LYP)/6-31++G(d,p) level. Good overall agreement between these two spectra supports the conclusion that the main photogenerated species is tautomer **AIII**. No such agreement was observed between the experimental spectrum of the photoproduct(s) and the theoretical spectra of other hydroxy isomers; e.g. form **AIVa** (see Figure 5.45, trace c). The assignment of the observed absorption bands to the theoretically calculated normal modes of the form **AIIIa** is given in Table C3 in Appendix.

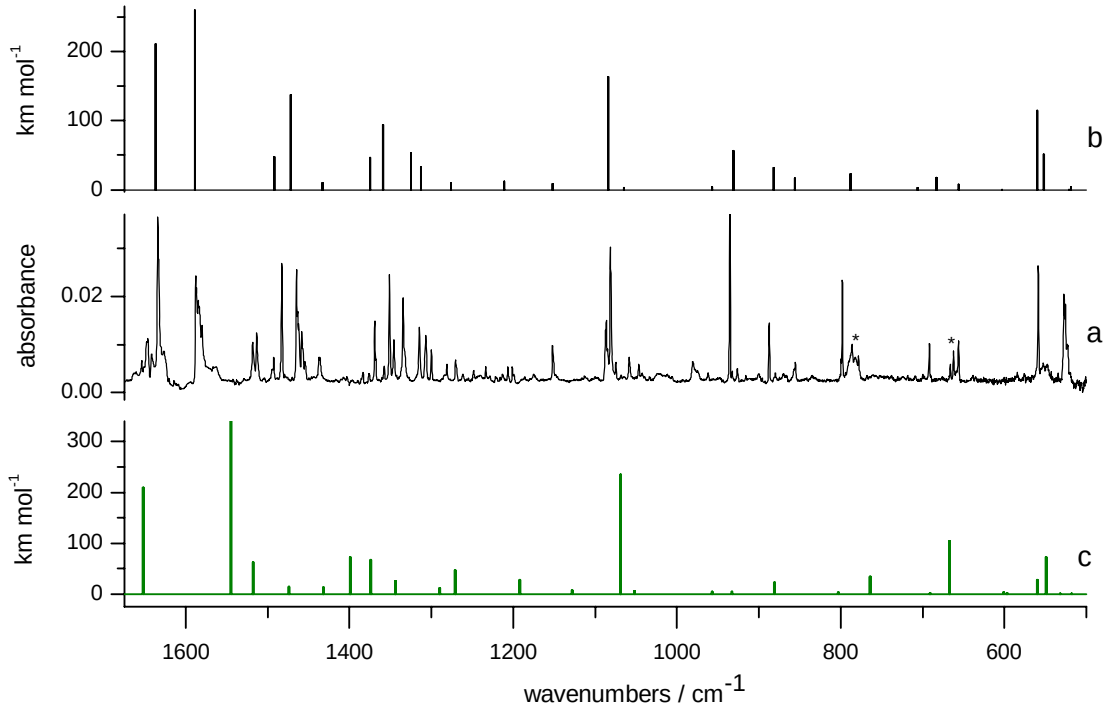

Figure 5.45. *Comparison of (a) the experimental spectrum of the photoproducts generated upon UV ($\lambda > 230$ nm) irradiation of allopurinol isolated in an Ar matrix with (b) the spectrum of the hydroxy tautomeric form* ***AIIIa*** *and with (c) the spectrum of the hydroxy tautomeric form* ***AIVa****, theoretically simulated at the DFT(B3LYP)/6-31++G(d,p) level. The calculated wavenumbers were scaled by a factor of 0.98. Asterisks in the experimental spectrum point to the bands which indicate UV-induced creation of the ketene form with the open pyrimidine ring. The spectrum of unreacted oxo tautomer* ***AI*** *was subtracted.*

A minor product emerging after UV irradiation of the matrix and coexisting with the dominating photoproduct **AIII** has a characteristic, comparatively broad band at 2153 cm^{-1} (Figure 5.46). The frequency, complex pattern with many maxima, and high absolute intensity are typical of a band due to the "antisymmetric" stretching vibration of the –C=C=O group [28, 29, 205]. The conjugated ketene may be formed after photohemical opening of the six-membered ring. The conjugated ketene can exist in several possible stable isomeric forms; one of them is presented in Figure 5.46. For this structure, an extremely intense (1116 km mol^{-1}) band due to –C=C=O "antisymmetric" stretching vibration with frequency 2159 cm^{-1} was theoretically predicted at the DFT(B3LYP) level. Analogous calculations carried out for other possible stable isomeric forms of open-ring conjugated ketene resulted in predictions of equally strong IR bands at nearly the same (±20 cm^{-1}) frequency. The comparison between the experimental observation with the theoretically predicted frequency and intensity of the band due to –C=C=O "antisymmetric" stretching vibration suggests that a ring-opening reaction occurs for allopurinol upon UV irradiation. The low intensity of the band at 2153 cm^{-1} in the experimental spectrum and its high absorption coefficient indicate that only small fraction of allopurinol molecules was converted to the open-ring ketene structure upon UV irradaition.

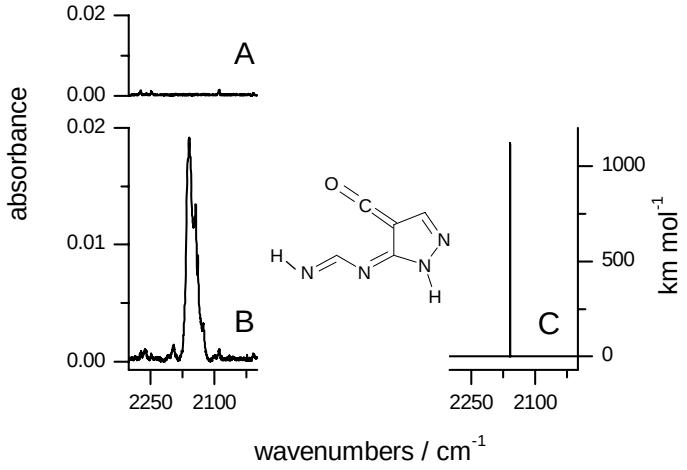

Figure 5.46. *The spectral range where the band due to the "antisymmetric" vibration of the ketene –C=C=O group should be expected. A: fragment of IR spectrum of allopurinol recorded after deposition of matrix; B: the spectrum recorded after UV irradiation of the matrix; C: the spectrum theoretically simulated at the DFT(B3LYP)/6-31++G(d,p) level with the corresponding ketene structure. The calculated wavenumber was scaled by a factor of 0.98.*

As it was mentioned already, the phototautomeric reaction observed for allopurinol did not lead to the total conversion of the initial oxo forms of the compounds into the corresponding hydroxy forms. The possible reasons for that are described in Section 5.6.

9-Methylhypoxanthine

9-Methylhypoxanthine is a molecule of hypoxanthine with methyl group at the N(9) position. Methylation at the N(9) nitrogen atom fixes the form of hypoxanthine in which the compound is present in inosine. In 9-methylhypoxanthine, the number of possible tautomeric forms is significantly reduced with respect to hypoxanthine itself (see Figure 5.47). For this species, there is only one labile hydrogen atom (comparing with hypoxanthine, where there are two labile hydrogen atoms, see next section), which can be attached to either the oxygen atom or to one of the nitrogen atoms of the pyrimidine ring.

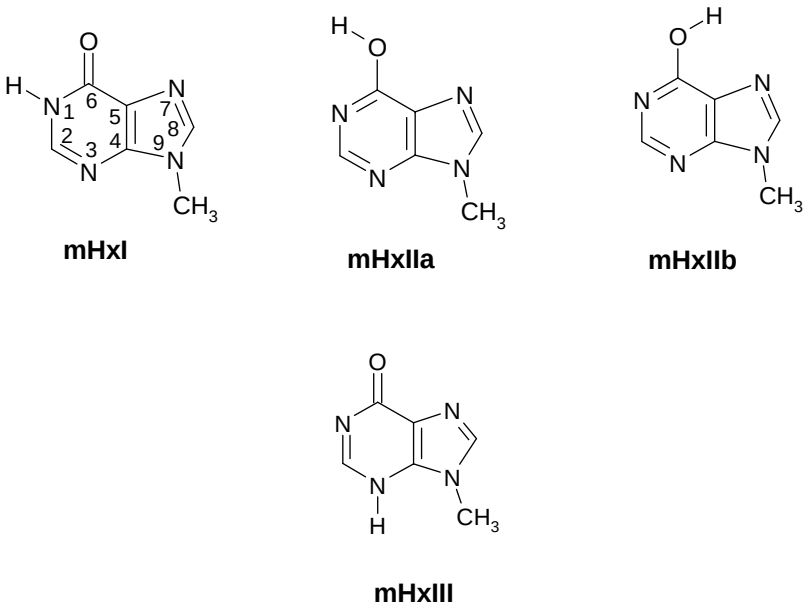

Figure 5.47. *Possible tautomeric forms of 9-methylhypoxanthine.*

The experimental physicochemical investigations on inosine and the model hypoxanthine derivatives substituted at N(9) atom (such as 9-methylhypoxanthine) concerned mostly the organometallic complexes of these species [206, 207]. The photoelectron spectra of gaseous hypoxanthines methylated at different positions (including 9-methylhypoxanthine) have been measured by Lin and co-workers [208]. Although this type of measurements gives usually only rough information about tautomerism, the authors concluded that the oxo forms of the investigated species predominate. As for inosine, its structure in the solid state has been determined using the X-ray crystallographic methods [209].

Theoretical calculations, carried out in the present work at DFT, MP2 and QCISD levels, showed that there are two low-energy forms of 9-methylhypoxanthine: the oxo-N(1)H-tautomer

and the hydroxy tautomer (the tautomers are denoted here as **mHxI** and **mHxII**, respectively), whereas the third tautomeric form **mHxIII** is much higher in energy (see Table 5.7). The oxo-N(1)H tautomer **mHxI** was predicted at all applied levels of theory to be the most stable form. The energy of the hydroxy forms **mHxIIa** and **mHxIIb** was calculated to be 10–19 kJ mol^{-1} higher.

Table 5.7. *Relative electronic (ΔE_{el}), zero-point vibrational (ΔZPE) and total ($\Delta E_{total}=\Delta E_{el}+\Delta ZPE$) energies (kJ mol^{-1}) of 9-methylhypoxanthine isomers.*

	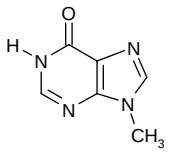	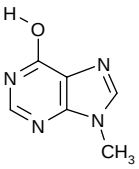	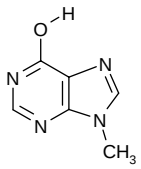	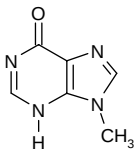
	mHxI	**mHxIIa**	**mHxIIb**	**mHxIII**
ΔE_{el}(DFT)	0	13.6	18.8	85.9
ΔZPE(DFT)	0	0.0	0.1	-3.7
ΔE_{el}(DFT)+ ΔZPE(DFT)	0	13.6	18.9	82.2
ΔE_{el}(MP2)	0	10.3	15.1	
ΔE_{el}(MP2)+ ΔZPE(DFT)	0	10.3	15.2	
ΔE_{el}(QCISD)	0	13.6	18.2	87.1
ΔE_{el}(QCISD)+ ΔZPE(DFT)	0	13.6	18.3	82.4

The energy of the form **mHxI** was taken as reference. The results of DFT (using the B3LYP functional) and MP2 calculations obtained using 6-31++G(d,p) basis set; the results of QCISD obtained using cc-pVDZ basis set (geometry optimized at DFT(B3LYP)/cc-pVDZ level).

In the high frequency range (3600–3400 cm^{-1}) of the experimental spectrum of 9-methylhypoxanthine isolated in an Ar matrix (Figure 5.48), two bands were observed. The high-intensity band, assigned to the N1H stretching vibration was found at the frequency 3433 cm^{-1}, similar to the frequencies of analogous bands in the spectra of allopurinol and 4-pyrimidinone. The lower-intensity band was detected at the frequency 3557 cm^{-1}, characteristic of the stretching vibration of the OH group. This picture strongly suggests that two tautomeric forms of 9-methylhypoxanthine were trapped into a low-temperature Ar matrix: oxo and hydroxy (unlike allopurinol, where only oxo tautomer was detected in the freshly deposited Ar matrix) [195]. Based on the observed ratio of intensities of the experimental νOH and νNH bands and taking into

account the calculated absolute intensities of these bands, equal 106 and 68 km mol^{-1}, respectively, the ratio of populations of the oxo and hydroxy tautomers was estimated as 11.7:1. Equation 37 was used for this purpose (see Section 5.1).

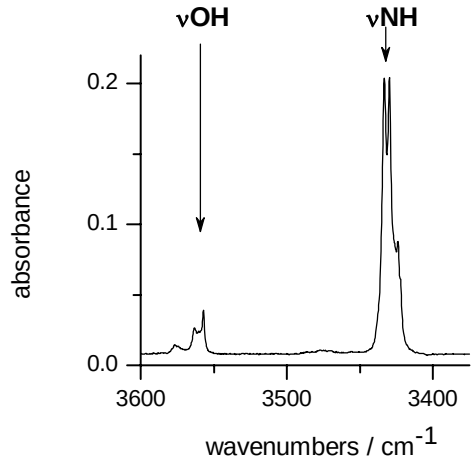

Figure 5.48. *High-frequency region of the infrared spectrum of 9-methylhypoxanthine isolated in an Ar matrix. The IR bands presented in this spectral range are due to νOH and νNH vibrations and are characteristic of the hydroxy and oxo tautomers, respectively.*

Assuming that the relative population of 9-methylhypoxanthine isomers, characteristic of the gaseous phase equilibrium prior to deposition, is retained in the matrix, it is possible to estimate the difference in energies between the two forms. The temperature of the oven used for deposition of 9-methylhypoxanthine in this study was equal to ca. 480 K. At this temperature the observed ratio of tautomers (11.7:1) corresponds, according to the Boltzmann distribution, to the energy difference of 9.8 kJ mol^{-1}. This value is in a good correspondence with the energy difference 13.6 kJ mol^{-1} calculated by QCISD approach (see Table 5.7).

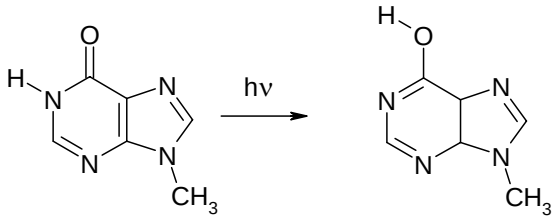

Figure 5.49. *Phototautomeric reaction observed for 9-methylhypoxanthine*

UV (λ > 270 nm) irradiation of the matrix-isolated monomers of 9-methylhypoxanthine led to the decrease of the bands belonging to the spectrum of the oxo form (the bands due to the νC=O vibration at 1750 cm^{-1} and due to the νNH vibration at 3433 cm^{-1}, which are characteristic of the oxo form of the compound) and to the increase of the (initially very weak) bands of

the spectrum of the hydroxy tautomer (Figure 5.50). The increasing of the intensity of the band at 3559 cm^{-1}, which can be assigned to the stretching vibration of the OH group (νOH) indicates that after irradiation of the matrix the oxo → hydroxy photoreaction occurred for the monomers of 9-methylhypoxanthine isolated in a low-temperature matrix.

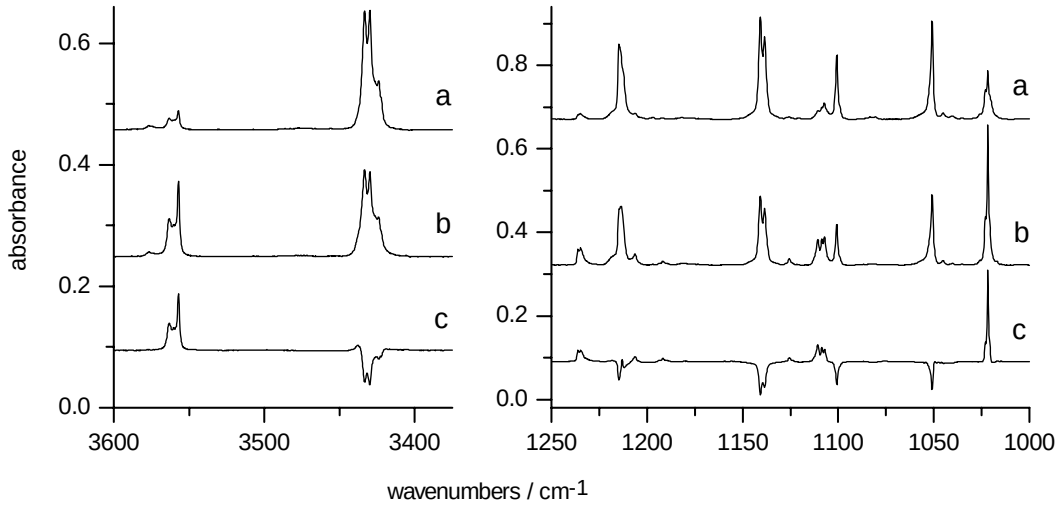

Figure 5.50. *Portions of the IR spectrum of 9-methylhypoxanthine isolated in an Ar matrix: (a) after deposition of the matrix; (b) after 12 h of UV (λ > 270 nm) irradiation; (c) difference spectrum: trace b minus trace a.*

Having two spectra (recorded before and after UV irradiation) of matrices containing different relative populations of the oxo-N(1)H and the hydroxy forms of 9-methylhypoxanthine, it was possible to separate (using numerical subtraction) the spectra of the two tautomers of the compound and to assign the observed absorption bands to the theoretically predicted normal modes of oxo and hydroxy forms of the compound. These separated spectra are compared (in Figures 5.51 and 5.52) with the spectra calculated (at the DFT(B3LYP)/6-31++G(d,p) level) for tautomers oxo **mHxI** and hydroxy **mHxII**. Identification of the substrate of the photoreaction as form **mHxI** and the photoproduct as tautomer **mHxII** is strongly supported by the good agreement between the experimental and theoretical IR spectra. Hence, the main photochemical process observed for monomeric 9-methylhypoxanthine can be reliably interpreted as a proton transfer **mHxI** → **mHxII** reaction (Figure 5.49). The positions and relative intensities of the absorption bands found in the experimental spectra of both tautomers are compared with the theoretically predicted wavenumbers and absolute intensities of the bands in Tables C5 and C6

in the Appendix. The theoretically obtained bands have been assigned to the normal modes, which were presented using internal coordinates given in Table C4 in the Appendix.

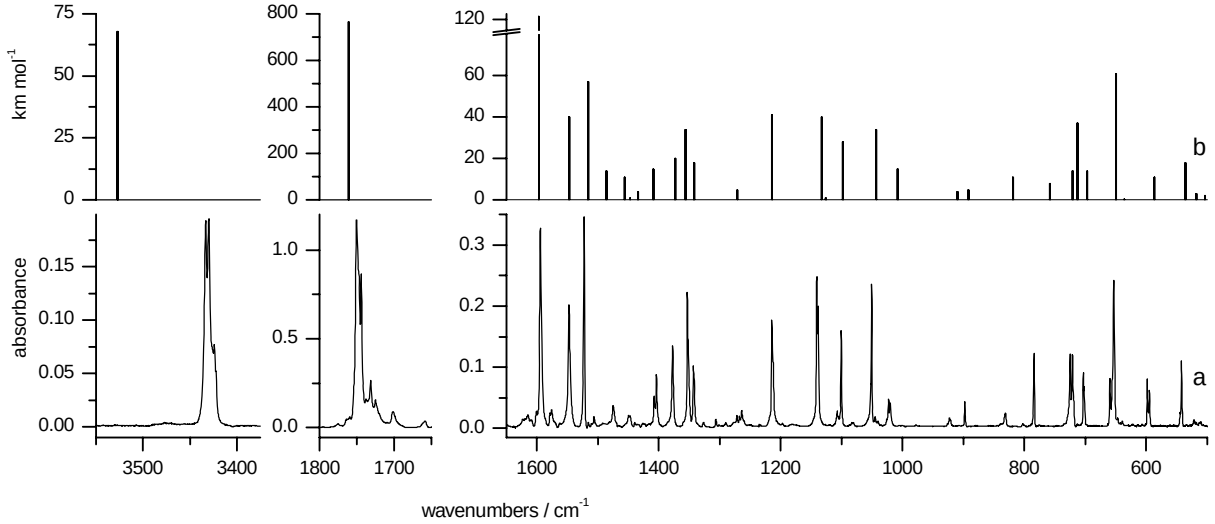

Figure 5.51. *Comparison of (a) the extracted experimental spectrum of the bands due to the oxo tautomer of 9-methylhypoxanthine dominating in the Ar matrix before UV irradiation with (b) the theoretical spectrum of the oxo tautomer* ***mHxI*** *of 9-methylhypoxanthine calculated at the DFT(B3LYP)/6-31++G(d,p) level. Theoretical wavenumbers were scaled by a factor of 0.98.*

It does not seem very likely that both rotamers **mHxIIa** and **mHxIIb** are generated upon UV irradiation. The theoretically predicted spectrum of form **mHxIIb** does not reproduce well the experimental spectrum of the photoproduct(s) (see the comparison shown in Figure 5.52). Form **mHxIIb** is predicted to be higher in energy by 5 kJ mol^{-1}, with respect to form **mHxIIa** and the barrier between these two forms was calculated (at the DFT (B3LYP)/6-31++G(d,p) level) to be 35 kJ mol^{-1}.

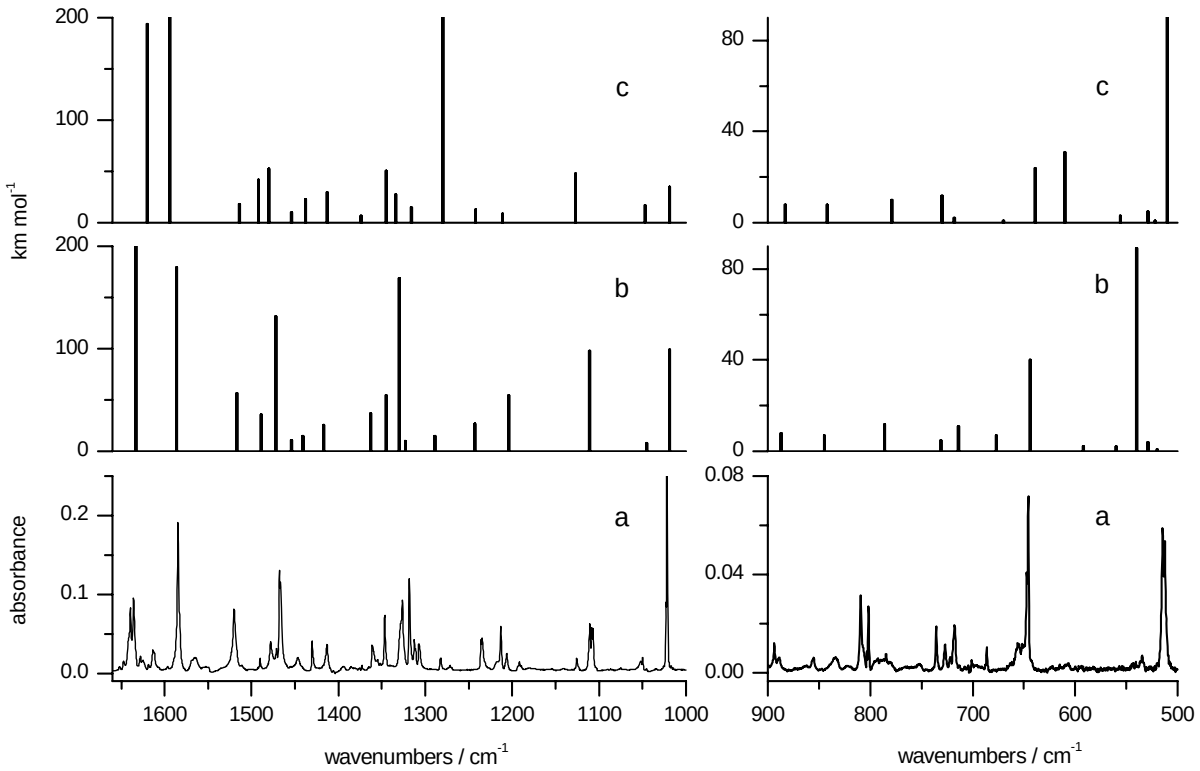

Figure 5.52. *Comparison of (a) the extracted spectrum of the bands due to the main photoproduct (the hydroxy tautomer) generated upon UV (λ > 270 nm) irradiation of 9-methylhypoxanthine isolated in an Ar matrix with (b) the theoretical spectrum of the hydroxy isomer* ***mHxIIa*** *and (c) the theoretical spectrum of the hydroxy isomer* ***mHxIIb****. The theoretical spectra were calculated at the DFT(B3LYP)/6-31++G(d,p) level. The calculated wavenumbers were scaled by a factor of 0.98.*

Similarly as it was in the case of allopurinol, a minor product emerging after UV irradiation of the matrix and coexisting with the dominating photoproduct **mHxII** was detected. A small amount of the open-ring conjugated ketene occurred also for 9-methylhypoxanthine, and it has a characteristic, comparatively broad band at 2151 cm^{-1} due to the "antisymmetric" stretching vibration of the –C=C=O group (Figure 5.53). The conjugated ketene can exist in several possible stable isomeric forms, the theoretical simulation spectra (at DFT(B3LYP) level) in the Figure 5.53 was calculated for one of possible forms, and this form is presented in in the right part of the figure. For this structure, an extremely intense (1082 km mol^{-1}) band due to –C=C=O "antisymmetric" stretching vibration with frequency 2169 cm^{-1} was theoretically predicted at the DFT(B3LYP) level. Analogous calculations carried out for other possible stable isomeric forms of open-ring conjugated ketene 9-methylhypoxanthine resulted in predictions of equally strong IR bands at nearly the same (±20 cm^{-1}) frequency. The comparison between

the experimental observation with the theoretically predicted frequency and intensity of the band due to –C=C=O "antisymmetric" stretching vibration suggests that a ring-opening reaction occurs for 9-methylhypoxanthine upon UV irradiation.

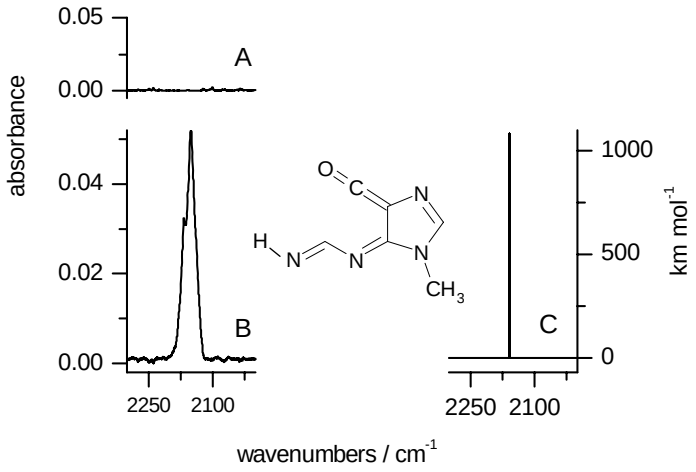

Figure 5.53. *The spectral range where the bands due to the "antisymmetric" vibrations of the ketene –C=C=O group should be expected. (A) part of IR spectrum of 9-methylhypoxanthine recorded after deposition of matrix ; (B) the spectrum recorded after UV irradiation of the matrix; (C) the spectrum theoretically simulated at the DFT(B3LYP)/6-31++G(d,p) level and the structure of ketene. The calculated wavenumber was scaled by a factor of 0.98.*

Hence, upon irradiation of the matrix with UV light, the oxo form of 9-methylhypoxanthine existing in the matrix converts into hydroxy tautomeric form (as it was illustrated in Figure 5.49). As it was in the case of allopurinol, the oxo → hydroxy phototautomeric reaction observed for 9-methylhypoxanthine did not lead to the total conversion of the initial oxo forms of the compounds into the corresponding hydroxy forms. Most probably, that for this compound the reaction of phototautomerism is reversible and as a result of irradiation the photostationary state is obtained (see Section 5.6).

Hypoxanthine

Hypoxanthine is a purine base and consists of two heterocyclic rings: one is six-membered and has the structure of 4-pyrimidinone and the second has a five-membered structure of imidazole ring with two nitrogen atoms. Hypoxanthine (**Hx**) exhibits oxo-hydroxy tautomerism and tautomerism which is related with proton shift in the imidazole ring N9H ↔ N7H. Eight stable neutral tautomeric forms can be drawn: four oxo forms and four hydroxy forms. For each hydroxy form, except hydroxy-N1H, two rotameric forms may exist, depending on the position of the OH group. The structures of possible tautomers of hypoxanthine (**Hx**) are presented in Figure 5.54.

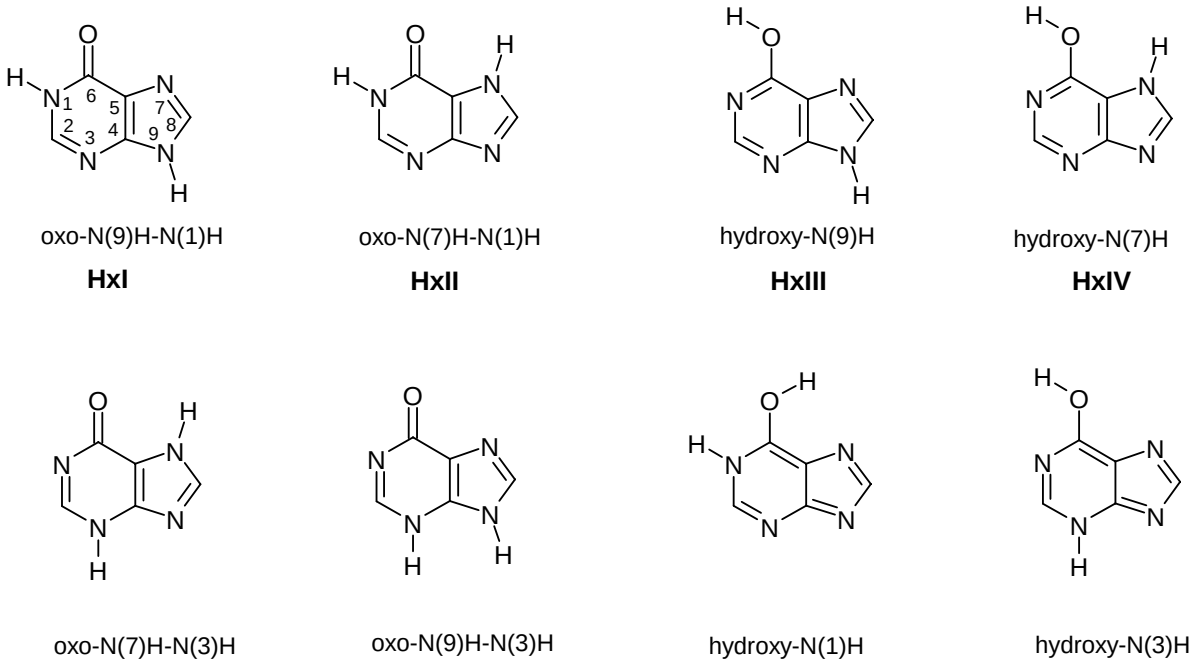

Figure 5.54. *Possible tautomeric forms of hypoxanthine.*

A variety of computational methods, including semi-empirical and ab initio, has been applied in order to predict the relative energy of different tautomers of hypoxanthine. In the gas phase, semi-empirical methods have predicted that the oxo-N(9)-H (form **HxI**) is more stable than oxo-N(7)-H (form **HxII**) by about 4 kJ/mol [222, 223]. However, the results of ab initio and density functional methods indicate that the form oxo-N(7)-H (**HxII**) is the most stable tautomer. Within the limits of the latter calculation, Costas et. al [210] reported the energetic stability, structural and electronic properties for 13 possible isomers of neutral hypoxanthine calculated at the DFT(BP)/DZVP level of theory. It was found that the most stable is oxo-N(7)-H (**HxII**)

tautomer, whereas the oxo-N(9)-H (**HxI**) form is predicted to be higher in energy only by 3.5 kJ mol^{-1}. For the hydroxy-N(9)-H (**HxIII**) and the hydroxy-N(7)-H (**HxIV**) tautomers of hypoxanthine, the calculated energies are significantly higher (by 24.8 and 34.8 kJ mol^{-1}, respectively) than the energy of the most stable oxo-N(7)-H form. Hernandes [204] reported the calculated (at MP2 and DFT level of theory) energy difference for seven isomeric forms of hypoxanthine. According to the calculations performed at the MP2/6-31+G(d,p) level the oxo-N(7)-H tautomer should be the most stable, the oxo-N(9)-H form is predicted to be higher in energy by 3.8 kJ mol^{-1}; for hydroxy-N(9)-H and the hydroxy-N(7)-H tautomers the calculated energies are significantly higher (by 11.7 and 21.3 kJ mol^{-1}, respectively) than the energy of the most stable oxo-N(7)-H form. Similar values of the relative energies of hypoxanthine tautomers were obtained at the MP2/6-31++G(d,p), [211] DFT(B3LYP)/6-311++G(d,p) [212] and DFT(B3LYP)/6-31+G(d,p) [204] levels of theory.

Hence, all results of ab initio and density functional methods predicted that the oxo-N(7)-H (**HxII**) form is the most stable tautomer. However, the theoretical Monte Carlo calculations of the thermodynamic properties of water solutions of hypoxanthine [213] showed that in water environment the oxo-N(9)-H (**HxI**) tautomer would only be slightly favored as compared with the oxo-N(7)-H form. According to these results, for neutral hypoxanthine in aqueous solutions, the populations of both tautomers should be similar.

In this work, the relative stabilities of seven isomeric forms of hypoxanthine were studied at different levels of theory. Calculations were made for two oxo tautomers [oxo-N(7)-H and oxo-N(9)-H] and for five hydroxy forms [two rotamers of hydroxy-N(7)-H tautomer, two rotamers of hydroxy-N(9)-H tautomer and form hydroxy-N(1)-H], the structures of which are shown in Table 5.8. The results of calculations at the DFT/6-31++G(d,p) and MP2/cc-pVDZ levels (see Table 5.8) indicate that the oxo tautomer (**HxII**) is the most stable. The difference in electronic energies due to proton shift between nitrogens N7 (**HxII**) and N9 (**HxI**) is small (3.5 kJ mol^{-1} at DFT and 3.2 kJ mol^{-1} at MP2 levels of theory). The calculations made at QCISD level of theory (cc-pVDZ basis set) predicted that oxo-N(9)-H tautomer has the lowest energy (with energy difference about -0.1 kJ mol^{-1} between oxo-N(7)-H and oxo-N(9)-H tautomers). When the difference between zero-point-energy of these tautomers was taken into account then the QCISD calculations indicate that the form oxo-N(7)-H is slightly more stable (by 0.1 kJ mol^{-1}). The relative energies of seven tautomers calculated in the current work are summarized in Table 5.8.

Table 5.8. *Relative electronic (ΔE_{el}), zero-point vibrational (ΔZPE) and total ($\Delta E_{el}+\Delta ZPE$) energies (kJ mol^{-1}) of hypoxanthine tautomers.*

method	**T a u t o m e r i c f o r m s**						
	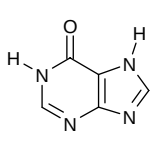	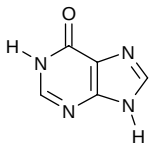	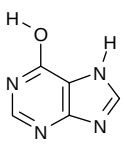	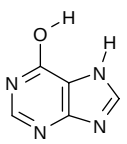	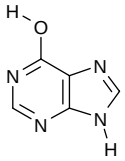	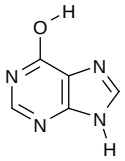	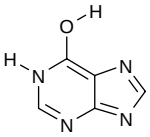
	HxII	**HxI**	**HxIV**		**HxIII**		
ΔE_{el}(DFT)	0	3.5	28.2	65.4	17.5	23.2	83.6
ΔZPE(DFT)	0	0.2	1.0	4.0	0.3	0.3	1.5
ΔE_{el}(DFT)+ΔZPE(DFT)	0	3.7	29.2	69.4	17.8	23.5	85.1
ΔE_{el}(MP2)	0	3.2	24.1		13.5		
ΔE_{el}(MP2)+ΔZPE(DFT)	0	3.4	25.1		13.8		
ΔE_{el}(QCISD)	0	-0.1	27.7		13.8		
ΔE_{el}(QCISD)+ΔZPE(DFT)	0	0.1	28.7		14.1		

The energy of the form **HxII** oxo-N(7)-H was taken as reference. The results of DFT (using the B3LYP functional) and MP2 calculations obtained using 6-31++G(d,p) basis set (geometry optimized at DFT(B3LYP)/ 6-31++G(d,p) level); the results of QCISD obtained using cc-pVDZ basis set (geometry optimized at DFT(B3LYP)/cc-pVDZ level).

A variety of experimental measurements, including ultraviolet spectroscopy [214], ultraviolet photoelectron spectroscopy [208], IR spectroscopy in inert gas matrix [215] and X-ray [216], have led to different conclusions on hypoxanthine tautomerism. Ultraviolet photoelectron spectra of hypoxanthine in the gas phase indicate the high stability of the oxo-N(7)-H tautomer than the oxo-N(9)-H form [208]. In crystal, hypoxanthine exists in the oxo-N(9)-H tautomeric form [Munns]. In the case of xanthine, a dioxypurine, the oxo-N(7)H form is predicted to be the dominant tautomer present in the gas phase and in aqueous media [217, 218]. Neutron diffraction studies pointed out that in the crystalline phase the molecules of hypoxanthine exist predominantly in oxo-N(9)-H tautomeric form with an approximately planar purine ring; however, a minor contribution from other tautomers of hypoxanthine could not be excluded with certainty [216].

Tautomerism involving change of position of a proton within the five-membered imidazole ring has been studied on the basis of spectroscopic investigations of neutral hypoxanthine in solutions. [219, 220, 214] These studies suggest that the relative population of the tautomeric species is strongly dependent on the solvent dielectric constant.

The experimental matrix-isolation studies performed hitherto [211, 221, 215] suggested that monomers of hypoxanthine isolated in low-temperature matrices adopt predominantly the oxo-N(7)-H and oxo-N(9)-H tautomeric forms. Spectral signatures of a small amount (less than 5%) of hydroxy form [211, 215] were also reported. Hence, although these experimental studies suffered from technical imperfections and provided no reliable method for distinguishing between the IR bands due to different tautomers, they seemed to confirm the theoretical predictions.

The infrared spectrum of hypoxanthine monomers isolated in and argon matrix, recorded in the present study [197], is not quite identical to the spectra reported previously [211, 221, 215]. The most striking difference concerns the region 3520 – 3400 cm^{-1}, where the bands due to N-H stretching vibrations are expected. The band at 3464 cm^{-1} was reported in all of the previous papers as the strongest absorption in this range. However, in the IR spectra recorded within the current work no absorption appears at this frequency (see Figure 5.55). This shows that a significant amount of species other than hypoxanthine monomers was present in matrices reported by other authors [211, 221, 215]. The presence of some impurities was also indicated by appearance of 15 other IR bands reported by other authors but missing in the spectra recorded within the current work.

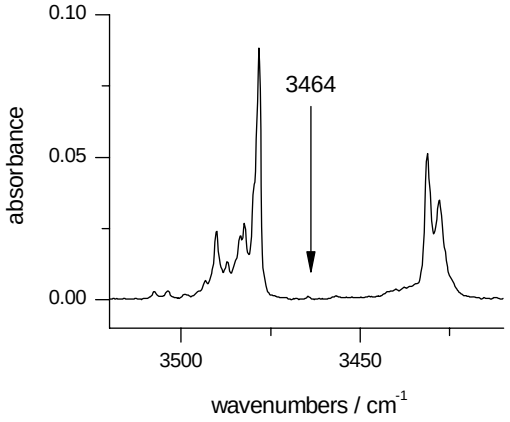

Figure 5.55. *The high-frequency region of the IR spectrum of hypoxanthine isolated in an Ar matrix. Arrow indicates the position of the absorption band reported by other authors but absent in the spectra collected within the present work.*

According to the theoretical calculations of relative energies of tautomeric forms of hypoxanthine, both oxo-N(9)-H form (**HxI**) and oxo-N(7)-H form (**HxII**) should be populated in the gas phase in comparable quantities, with somewhat higher population of the latter tautomer. Such a predominance of the oxo-N(7)-H tautomer in the gas phase was previously observed by means of UV photoelectron spectroscopy [208]. As a consequence, these oxo forms (**HxII** and **HxI**) should be also trapped into a low-temperature matrix.

The infrared spectrum of hypoxanthine monomers isolated in an argon matrix is presented in Figures 5.55 and 5.56. In the high-frequency region, two split bands due to the NH stretching vibrations of the oxo forms of the compound were observed at 3490/3478 and 3431/3428 cm^{-1}. These bands should correspond to the stretching vibration of the NH groups which belong to the pyrazole and pyrimidine rings, respectively. The frequency of the latter band due to the stretching N1H vibration is very close to that of the corresponding νN3H band (3428 cm^{-1}), which was observed in the IR spectrum of 4-pyrimidinone isolated in an Ar matrix (see Section 5.2, [189]). It indicates that this band is due to the stretching vibration of the NH group in the pyrimidine ring.

In the region 1800-1600 cm^{-1} of the IR spectra of isolated hypoxanthine, two strong bands due to the stretching vibration of the C=O group (νC=O) were observed at 1753 and 1735cm^{-1}. This point out that oxo forms of the studied compound are populated in a low-temperature matrix after deposition. The comparison of the experimental spectrum of hypoxanthine monomers with the theoretical spectra calculated for the oxo-N(9)-H form (**HxI**) and for the oxo-N(7)-H form (**HxII**) presented in Figure 5.56 strongly suggest that both these tautomeric forms are present in the low-temperature matrix.

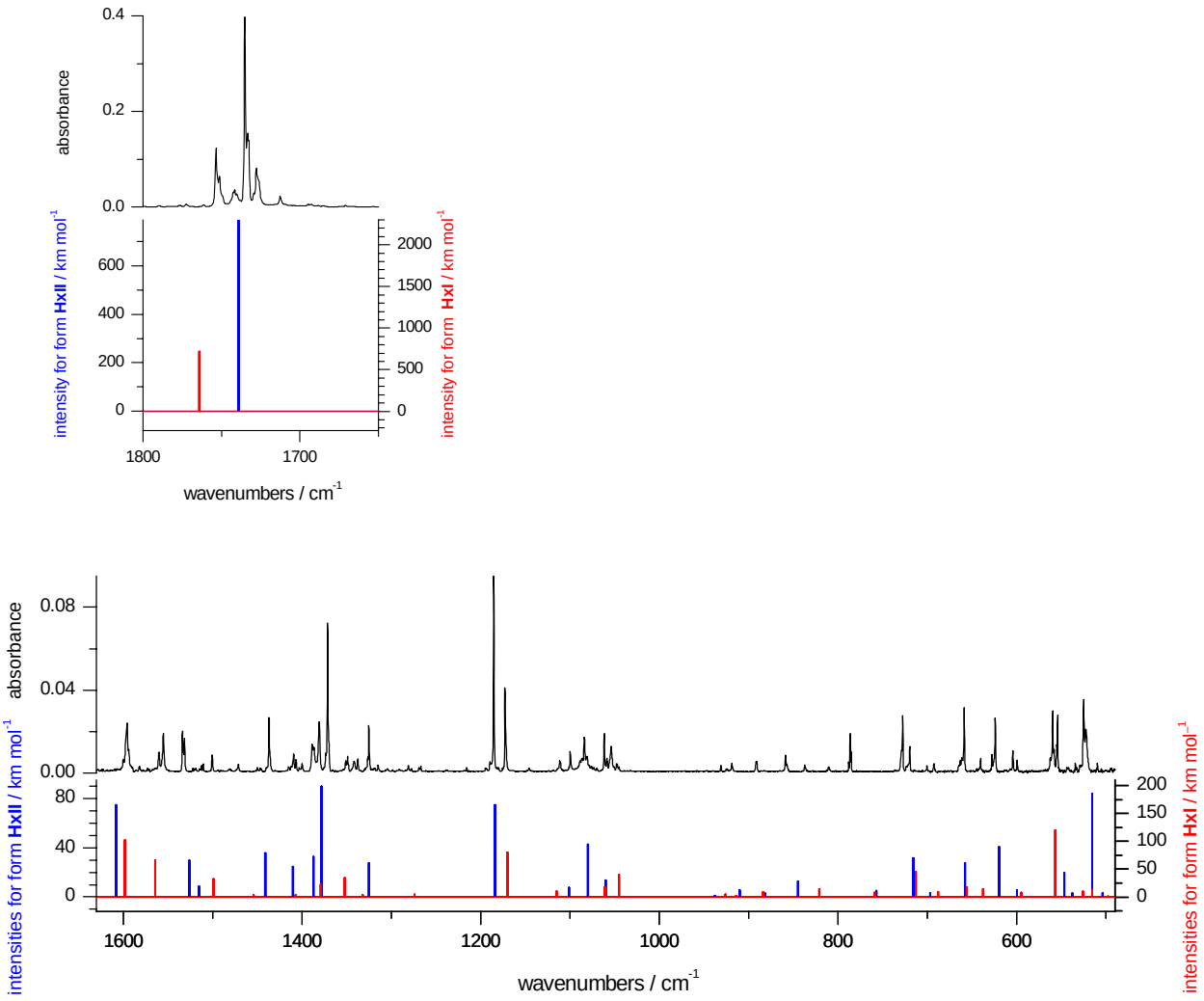

Figure 5.56. *The IR spectrum of hypoxanthine isolated in an Ar matrix (10 K) compared with the results of theoretical simulations of the spectra: (blue sticks) for the oxo-N(7)-H (**HxII**) tautomer and (red sticks) for the oxo-N(9)-H (**HxI**) tautomer. The calculated (at DFT(B3LYP)/6-31++G(d,p) level) wavenumbers were scaled by the single factor of 0.98.*

Upon UV ($\lambda > 270$ nm) irradiation of matrix-isolated hypoxanthine, one set of IR bands substantially decreased in intensity, whereas the bands belonging to another set were almost unchanged (Figure 5.57). For example, the band due to the stretching vibration of the C=O group (νC=O) observed at 1753 cm^{-1} decreased strongly, but a band due to the same type of vibration, found at 1735 cm^{-1} (corresponding to the band in the theoretical spectrum of the other oxo tautomer) did not. Comparison with the spectra theoretically predicted at the DFT(B3LYP)/6-31++G(d,p) level (Figures 5.56 and 5.57) suggests that these two bands should be assigned to the oxo tautomers **HxI** and **HxII**, respectively. The lower frequency of the νC=O vibration in molecules adopting the oxo-N(7)-H form **HxII** reflects the effect of

the hydrogen-bond-like (but much weaker than a typical hydrogen bonding) interaction between the N(7)-H proton and the oxygen atom of the C=O group. Also the analysis of other regions of IR spectra (presented in Figure 5.57) recorded before and after UV (λ > 270 nm) irradiation confirms the assignment of structure **HxI** to the form being the substrate significantly consumed in the photoreaction induced by exposure to UV (λ > 270 nm) light.

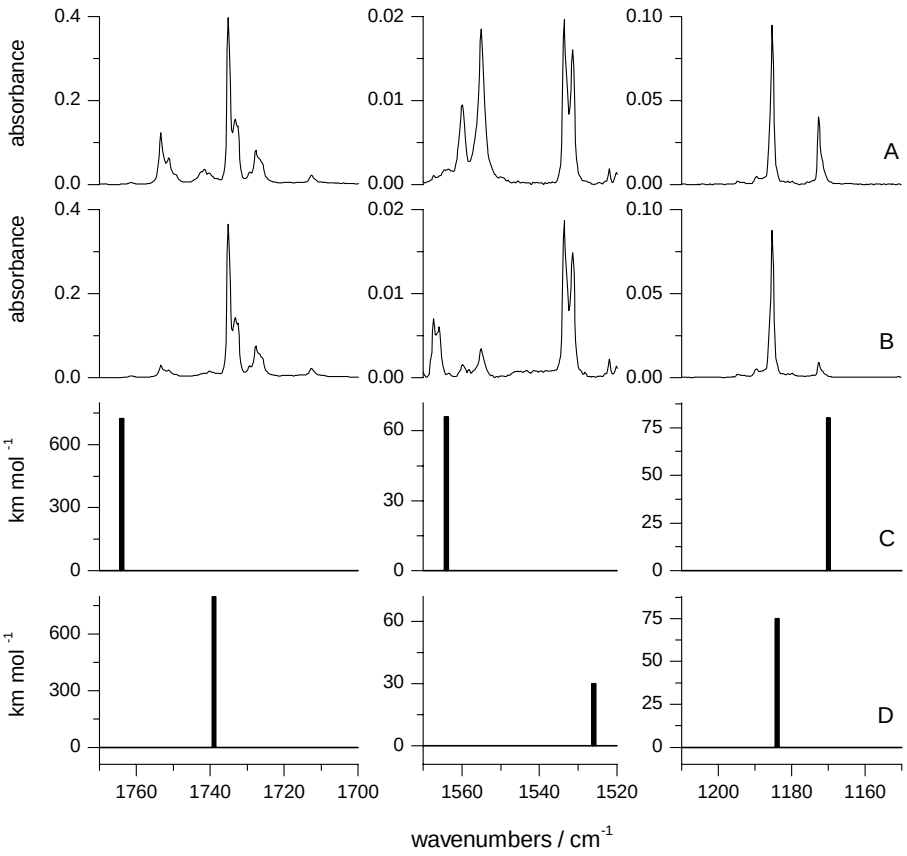

Figure 5.57. *Fragments of the IR spectrum of hypoxanthine isolated in an Ar matrix: (A) after deposition of the matrix, (B) after 4 h of UV (λ > 270 nm) irradiation; compared with corresponding fragments of the spectrum calculated at the DFT(B3LYP)/6-31++G(d,p) level for (C) the oxo-N(9)-H (**HxI**) tautomer and (D) the oxo-N(7)-H (**HxII**) tautomer of the compound. The calculated wavenumbers were scaled by a factor of 0.98.*

Decrease of the population of form **HxI** was accompanied by generation of a photoproduct. If the photoreaction consuming tautomer **HxI** is a phototautomeric reaction presented in Figure 5.58, then the photoproduct generated in this photoprocess should have the hydroxy-N(9)-H structure **HxIII**. It is noteworthy, that the bands due to the product of the phototransformation of form **HxI** grow at the positions of very weak absorptions present already (see Figure 5.59) in the spectrum

collected before exposure of the matrix to UV ($\lambda > 270$ nm) light. One of these bands was observed at 3566/3561 cm^{-1} that is at a frequency typical for the O-H stretching vibrations (νOH). Analogous (νOH) bands in the spectra of the hydroxy forms of related compounds such as allopurinol and 9-methylhypoxanthine, were found at very similar frequencies: 3564 cm^{-1} and 3557 cm^{-1}, respectively (see previous paragraphs). These experimental facts strongly suggest that the photoproduct is the hydroxy-N(9)-H form **HxIII** and that a very small amount of this tautomer were present in the Ar matrix before any irradiation.

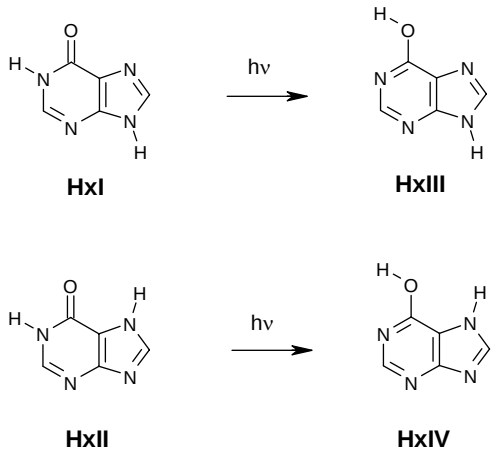

Figure 5.58. *Unimolecular oxo → hydroxy photoreactions in hypoxanthine*

On the basis of the effects induced by UV ($\lambda > 270$ nm) irradiation of matrix-isolated hypoxanthine it was possible to assign the bands found in the IR spectrum of the compound to the separated spectra of the oxo-N(9)-H (**HxI**), oxo-N(7)-H (**HxII**) and hydroxy-N(9)-H (**HxIII**) tautomeric forms. For most of the observed IR bands, this assignment could be done in the unequivocal manner; somewhat less certain assignments concern cases of significant overlap of bands due to two or three tautomers. The spectrum of the bands substantially decreasing during UV ($\lambda > 270$ nm) irradiation (decreasing in the same manner as the νC=O band at 1753 cm^{-1}) is graphically presented in Figure 5.60 trace C. The spectrum of the bands decreasing only slightly during UV ($\lambda > 270$ nm) irradiation (behaving in the same manner as the νC=O band at 1735 cm^{-1}) is shown in Figure 5.60 trace A. These spectra were extracted by electronic subtractions of the spectra recorded before and after irradiation of the matrix. These two experimental spectra are well reproduced by the results of the theoretical predictions of the spectra of form **HxI** (Figure 5.60 trace D) and of form **HxII** (Figure 5.60 trace B), respectively. The very

good agreement between experimental and theoretical spectra presented in Figure 5.60 leaves no doubt about the correctness of identification of forms **HxI** and **HxII**.

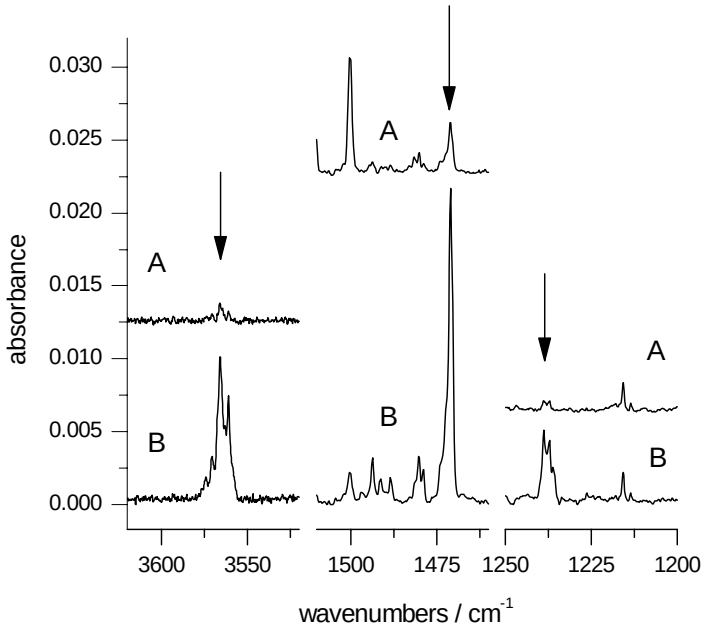

Figure 5.59. *Fragments of the IR spectrum of hypoxanthine isolated in an Ar matrix: (A) after deposition of the matrix, (B) after 4 h of UV (λ > 270 nm) irradiation. Arrows indicate the positions of the weak absorption bands present in the initial spectrum and growing upon UV (λ > 270 nm) irradiation. These bands are the spectral signatures of the hydroxy-N(9)-H (**HxIII**) tautomer.*

The list of IR bands observed in the initial spectrum of hypoxanthine isolated in a low-temperature Ar matrix is given in Table C9 in the Appendix. These bands are assigned to a particular tautomeric form **HxI**, **HxII** or **HxIII** and interpreted by comparison with the spectra calculated at the DFT(B3LYP)/6-31++G(d,p) level. The theoretical spectra of tautomers of hypoxanthine are presented in the Appendix in Tables C11-C14. These tables provide also detailed PED analysis of the calculated normal modes.

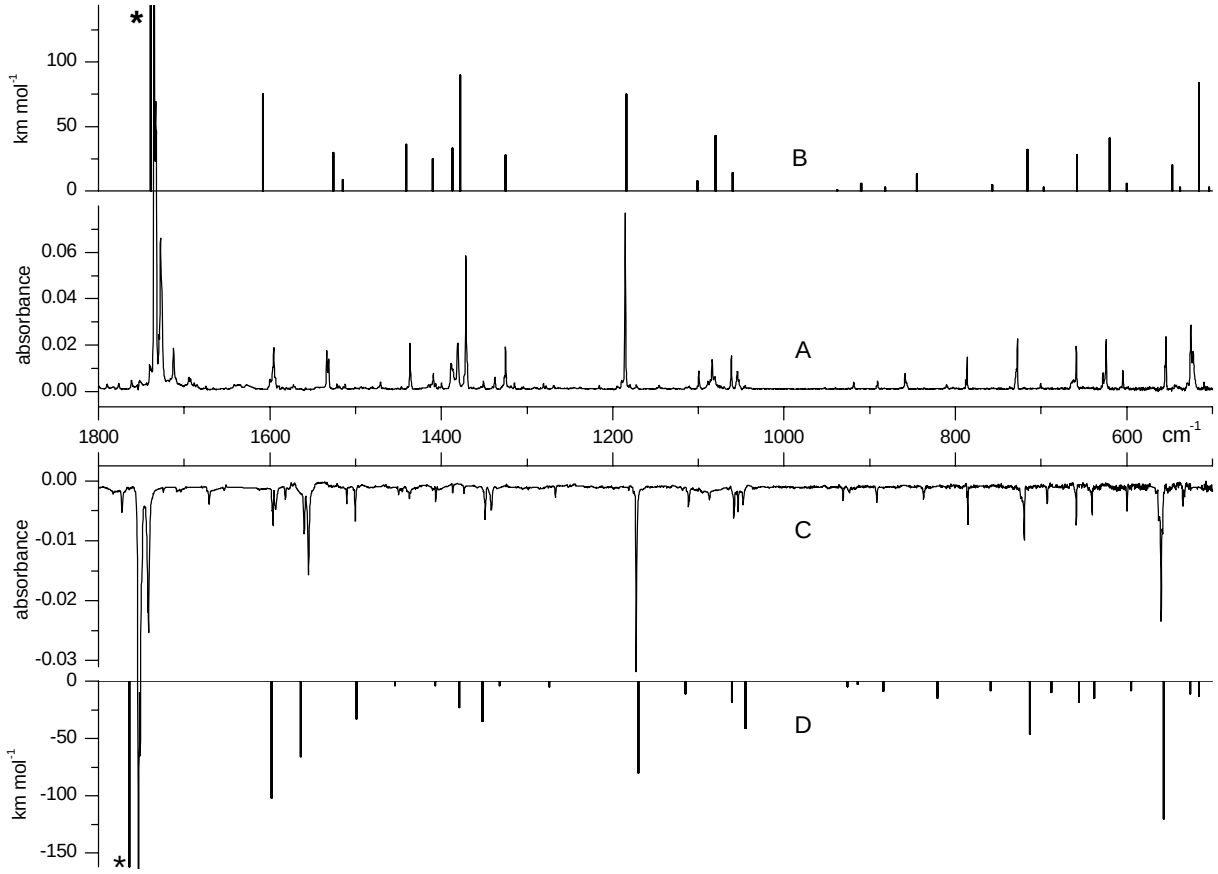

Figure 5.60. *Comparison of the spectra of two substrates of the observed photoreactions: (C) spectrum of the bands significantly decreasing upon UV (λ > 270 nm) irradiation (showing the same behavior as the band at 1753 cm^{-1} presented in Figure 5.56), (A) spectrum of the bands only slightly decreasing upon UV (λ > 270 nm) irradiation (showing the same behavior as the band at 1753 cm^{-1} presented in Figure 5.56), with the spectra calculated at the DFT(B3LYP)/6-31++G(d,p) level for (B) the oxo-N(7)-H (**HxII**) tautomer and (D) the oxo-N(9)-H (**HxI**) tautomer of hypoxanthine. The calculated wavenumbers were scaled by a factor of 0.98. Asterisks indicate the bands intensities of which reach out of the scale.*

An attempt was made to estimate the ratio of tautomers of hypoxanthine trapped in the low-temperature Ar matrix. The ratio of populations of the oxo-N(9)-H (**HxI**) and the oxo-N(7)-H (**HxII**) forms was estimated using equation 37 (see Section 5.1), using sums of intensities of experimental bands that could be safely assigned to the oxo-N(9)-H and the oxo-N(7)-H forms, and sums of the absolute intensities of corresponding bands in the spectra theoretically calculated for these two tautomers. The obtained value is k_1= [**HxI**] : [**HxII**] = 0.51.

The strongly overlapping bands due to N-H stretching vibrations (see Table C9) were not taken into account in this assessment. Assuming that the observed ratio of tautomers (k_1=0.51) corresponds to the frozen gas-phase equilibrium at the temperature of evaporation of the compound (T=500 K), the free energy difference between the two oxo forms was estimated as

ΔF=2.8 kJ mol^{-1} in favor of form **HxII**. This value is higher than theoretical predictions at QCISD/ cc-pVDZ//DFT(B3LYP)/6-31++G(d,p) levels by 2.7 kJ mol^{-1} (Table 5.8).

In the case of oxo – hydroxy tautomeric equilibrium, the situation is more complicated. Because of small initial population of the hydroxy-N(9)-H form **HxIII**, infrared bands due to this tautomer are very weak. Hence, the assessment of k_2= [**HxIII**] : [**HxI**] using the same method as in the case of k_1 would suffer from substantial uncertainty. Nevertheless, such an effort was undertaken and the resulting ratio of the hydroxy-N(9)-H form to the oxo-N(9)-H form was k_2= [**HxIII**] : [**HxI**] = 0.1 ± 0.03.

Such values of k_1 and k_2 mean, that after deposition of the matrix tautomers **HxII**, **HxI** and **HxIII** are present in the ratio of 1 : 0.51 : 0.05.

Another method has also been applied in order to assess the relative population of tautomeric form **HxIII**. This approach was based on the changes of populations of the oxo-N(9)-H form **HxI** and hydroxy-N(9)-H form **HxIII** during the transformation **HxI** → **HxIII**, induced by UV (λ > 270nm) light. Consumption of form I and generation of form III can be described by equation (49),

$$[\mathbf{HxI}]_i - [\mathbf{HxI}]_f = [\mathbf{HxIII}]_f - [\mathbf{HxIII}]_i \qquad (49)$$

where: $[\mathbf{HxI}]_i$ and $[\mathbf{HxIII}]_i$ are populations of forms **HxI** and **HxIII** before UV irradiations,

$[\mathbf{HxI}]_f$ and $[\mathbf{HxIII}]_f$ are populations of forms **HxI** and **HxIII** after UV irradiations.

Equation 49 is strictly valid as far as the **HxI** → **HxIII** conversion is quantitative.

On the basis of the experimental spectra, collected before and after UV (λ > 270 nm) irradiation, the following values were obtained: $[\mathbf{HxIII}]_f : [\mathbf{HxIII}]_i$ = 8.3 and $[\mathbf{HxI}]_f : [\mathbf{HxI}]_i$ = 0.24.

By combination of these relations with equation 49, the ratio of populations of forms **HxIII** and **HxI** was assessed,

$$k_2' = \frac{[\mathbf{HxIII}]_i}{[\mathbf{HxI}]_i} = \frac{1 - \dfrac{[\mathbf{HxI}]_f}{[\mathbf{HxI}]_i}}{\dfrac{[\mathbf{HxIII}]_f}{[\mathbf{HxIII}]_i} - 1} = 0.1 \qquad (50)$$

Because upon exposure of matrix-isolated hypoxanthine to UV (λ > 270 nm) light the oxo → hydroxy phototautomeric reaction was accompanied by a minor photodecomposition process (see the spectral signatures in the Figures 5.61 and 5.62), the value k_2' must be treated as an upper limit of the ratio of forms **HxIII** and **HxI** in the Ar matrix before any irradiation. Nevertheless, as it

could be seen, both methods of evaluation of relative population of form **HxIII** gave the same values $k_2 = k_2^{'} = 0.1$.

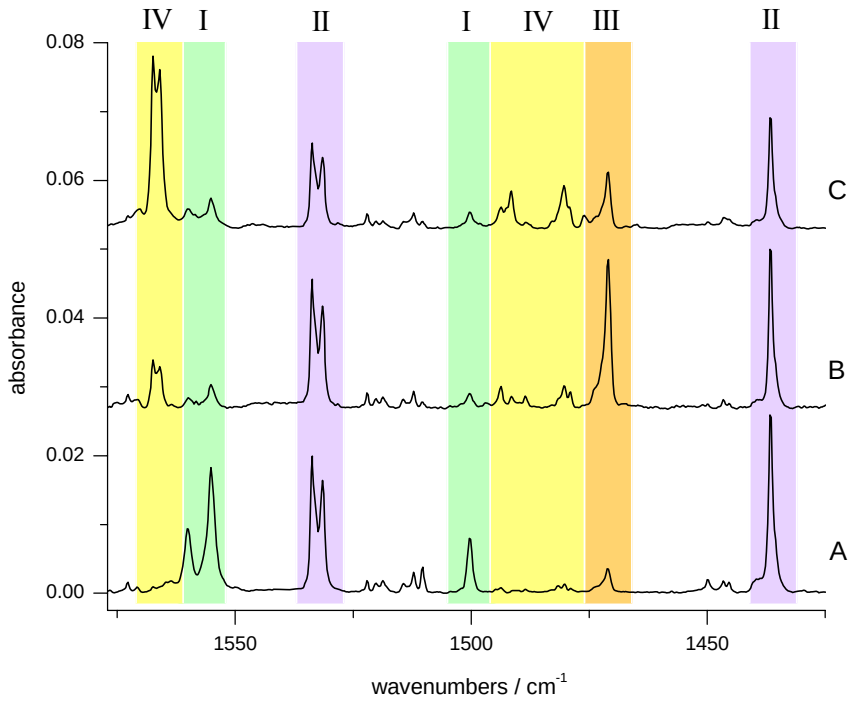

Figure 5.61. *Fragment of the IR spectrum of hypoxanthine isolated in an Ar matrix: (A) after deposition of the matrix; (B) after 4 h of UV (λ > 270 nm) irradiation; (C) recorded in a separate experiment after 2 h of UV (λ > 230 nm) irradiation of the matrix. Infrared bands due to different tautomers of hypoxanthine are marked with different color of the background: (green) oxo-N(9)-H (**HxI**); (violet) oxo-N(7)-H (**HxII**); (orange) hydroxy-N(9)-H (**HxIII**); (yellow) hydroxy-N(7)-H (**HxIV**). Intensities of the bands recorded in the two experiments are normalized by the factor correcting for the slightly different amount of the compound deposited in both experiments.*

For the temperature T=500K and the ratio of tautomers **HxII** : **HxIII** = 0.05 the free energy difference between forms **HxII** and **HxIII** is equals to 12.5 ± 1 kJ mol^{-1} in favor of oxo-N(7)-H form **HxII**. This value corresponds nicely to the energy difference for tautomers **HxII** and **HxIII** calculated at the MP2/6-31++(d,p) level (ΔE + ΔZPE = 13.8 kJ mol^{-1}) and QCISD/cc-pVDZ// DFT(B3LYP)/ 6-31++G(d,p) level (ΔE + ΔZPE = 14.1 kJ mol^{-1}), see Table 5.8.

The oxo-hydroxy equilibrium **HxI** : **HxIII** observed within N(9)-H tautomers of hypoxanthine is quite similar to that obtained for 9-methylhypoxanthine (see previous paragraph). For the latter compound, the ratio of the oxo and hydroxy tautomers trapped in an Ar matrix was 11.7 : 1, whereas for hypoxanthine the analogous ratio was approximately equal **HxI** : **HxIII** = 10 : 1. It

could be anticipated that tautomerism, in which N(1) and O atoms are directly involved, would not be significantly influenced by the replacement of the hydrogen atom by a methyl group at the remote N(9) position. Hence, it is not surprising that the experimentally estimated difference of free energies (9.8 kJ mol^{-1} at T=480K) of the hydroxy and oxo tautomers of 9-methyl-hypoxanthine is so similar to the corresponding value obtained for the hydroxy (**HxIII**) and oxo-N(9)-H (**HxI**) tautomers of hypoxanthine (9.6 kJ mol^{-1} at T=500K).

Whereas irradiation of matrix-isolated hypoxanthine with UV (λ > 270 nm) light led only to slight consumption of the oxo-N(7)-H tautomer **HxII** and to generation of correspondingly small amount of the hydroxy-N(7)-H form **HxIV**, the phototautomeric **HxII** → **HxIV** transformation was considerably more pronounced when the matrices were exposed to shorter-wavelength UV (λ > 230 nm) light, see Figure 5.62. The spectra shown in Figure 5.61 demonstrate the dependency of relative effectiveness of **HxII** → **HxIV** and **HxI** → **HxIII** phototautomeric reactions on the wavelength of UV light used for irradiation. The bigger amount of the hydroxy-N(7)-H tautomer **HxIV** generated upon UV (λ > 230 nm) irradiation is evidenced by much higher intensity of the band at 1567/1566 cm^{-1} (Figure 5.61 trace C), in comparison to the intensity of this band in the spectrum recorded after irradiation of the matrix with UV (λ > 270 nm) light (Figure 5.61 trace B). The IR band at 1566 cm^{-1} is a very characteristic feature, which can reliably be assigned to the spectrum of the hydroxy-N(7)-H form **HxIV**.

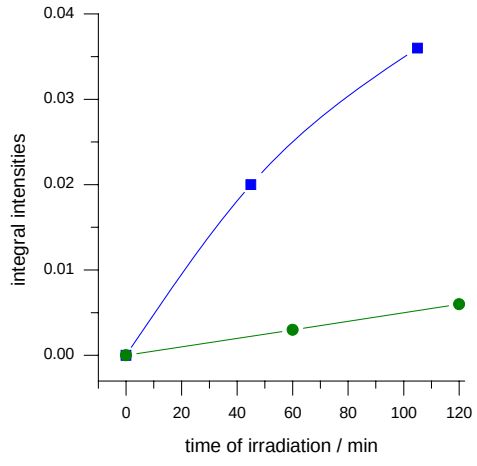

***Figure 5.62**. The change of the intensity of the band at 1566 cm^{-1} with time of irradiation: after irradiation with λ > 270 nm light - green trace; after irradiation with λ > 230 nm light- blue trace. This band is a characteristic feature of the hydroxy-N(7)-H form (**HxIV**) in the IR spectra of hypoxanthine.*

The experimental spectra of photoproducts generated upon UV (λ > 230 nm) irradiation and upon UV (λ > 270 nm) irradiation are compared in Figure 5.63 with the spectra theoretically predicted for the hydroxy tautomers **HxIII** and **HxIV**. This comparison supports the conclusion that exposure of matrix-isolated hypoxanthine to UV light leads to phototautomeric reactions **HxI** → **HxIII** and **HxII** → **HxIV** (Figure 5.58), with the first process relatively more effective upon (λ > 270 nm) irradiation and the second process more pronounced upon (λ > 230 nm) irradiation. The bands which could be reliably assigned to the spectra of hydroxy tautomers **HxIII** and **HxIV** are listed in Table C10 in the Appendix. These bands are also compared with the results of theoretical predictions and interpreted in terms of DFT-calculated normal modes.

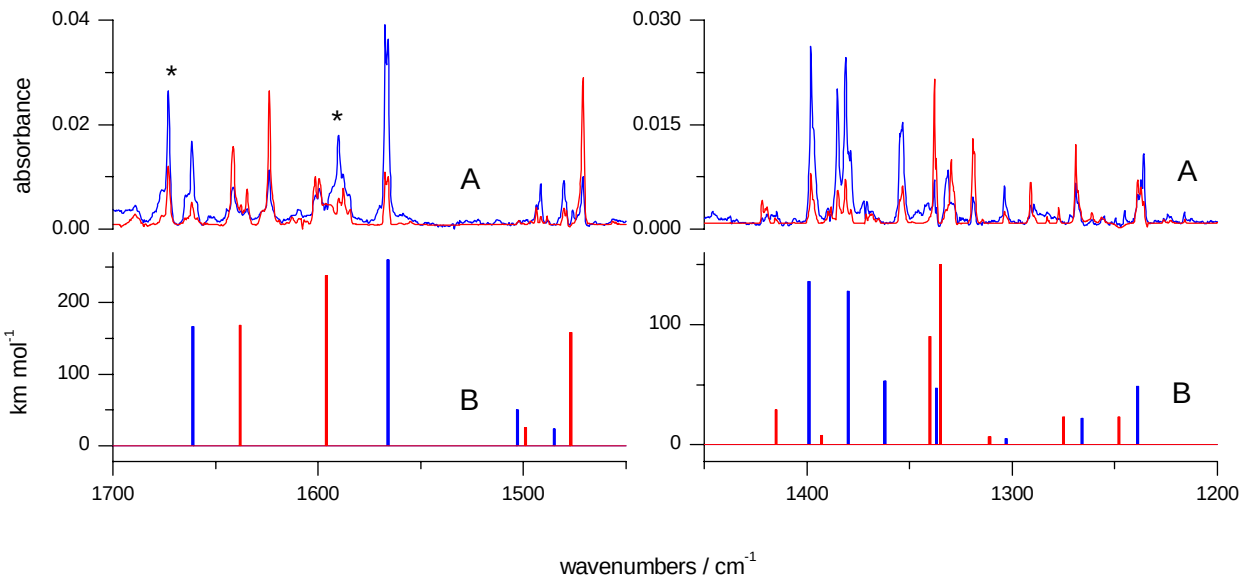

Figure 5.63. *Panel (A). Fragments of the experimental spectra of photoproducts: (red line) generated upon UV (λ>270 nm) irradiation, (blue line) generated upon UV (λ>230 nm) irradiation. The spectra of the oxo-N(9)-H (**HxI**) and oxo-N(7)-H (**HxII**) tautomers were removed by electronic subtraction from the spectra recorded after UV irradiation. Panel (B). The corresponding fragments of the spectra calculated at the DFT(B3LYP)/6-31++G(d,p) level for: (red) the hydroxy-N(9)-H tautomer (**HxIII**) and (blue) the hydroxy-N(7)-H tautomer (**HxIV**) of hypoxanthine. The calculated wavenumbers were scaled by a factor of 0.98. Asterisks indicate the bands due to unidentified photoproducts other than the hydroxy tautomers **HxIII** and **HxIV**.*

Alongside the IR bands, which should be assigned to photoproducts **HxIII** and **HxIV**, several other bands appear in the spectra recorded after UV irradiation. One of these IR absorptions (a broad and structured feature at 2144 cm^{-1}) indicates photogeneration of the open-ring conjugated ketene (Figure 5.64). Analogous bands (due to "antisymmetric" stretching vibrations of the –C=C=O group) were observed at 2153, 2151 and 2139 cm^{-1} in the IR spectra of UV-irradiated allopurinol, 9-methylhypoxanthine and 4-pyrimidinone, respectively (see Sections 5.2 and 5.4). Other bands (e.g. those shown in Figure 5.63) indicating occurrence of unidentified phototransformations accompanying the **HxII** → **HxIV** and **HxI** → **HxIII** phototautomerism were observed at: 2144, 1673, 1590, 1476, 1355/1353, 1137, 822 and 718 cm^{-1}. These bands appeared already upon UV (λ > 270 nm) irradiation of matrix-isolated hypoxanthine. The yield of unidentified photoproducts, other than the hydroxy tautomers **HxIII** and **HxIV**, was higher when the shorter-wavelength UV (λ > 230 nm) light was used. Photogeneration of these species was even more pronounced when matrices were exposed to unfiltered light of the high-pressure mercury lamp (λ > 200 nm).

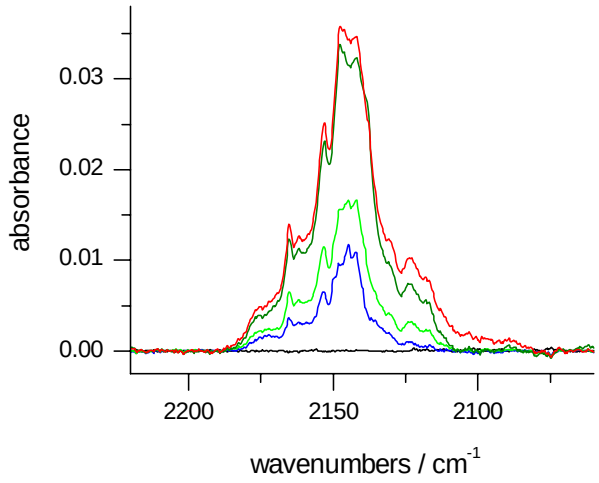

Figure 5.64. *The spectral range where the bands due to the "antisymmetric" vibrations of the ketene -C=C=O group should be expected. Progress of UV irradiation of hypoxanthine isolated in an Ar matrix: the black trace corresponds to the IR spectrum recorded after deposition of the matrix; blue and green traces correspond to the spectra recorded after 45 and 105 min irradiation of the matrix with UV light using cutoff filter λ > 230 nm, respectively; olive and red traces correspond to the spectra recorded after further irradiation (60 and 120 min, respectively) of the matrix with UV light without any filter (λ > 200 nm).*

5.5. N-hydroxypyridine-2(1H)-thione

N-hydroxypyridine-2(1*H*)-thione (**Np**) (other names are omadine or pyrithione) is known as a candidate for a good photochemical precursor of hydroxyl radicals (·OH). This compound has been used as a photochemical source of ·OH radicals in a number of studies on oxidative damage of DNA [95-98]. It was observed that hydroxyl radicals were photogenerated already upon UV ($\lambda > 350$ nm) irradiation. These mild photochemical conditions constitute an obvious advantage of *N*-hydroxypyridine-2(1*H*)-thione as a precursor. On the other hand, Aveline and coworkers [102-104] claimed that *N*-hydroxypyridine-2(1*H*)-thione was a nonspecific hydroxyl radical generator, and beside the ·OH radical cleavage, this compound undergoes other primary photoprocesses, which are pH-dependent [102-104].

N-Hydroxypyridine-2(1*H*)-thione (**Np**) is known under commercial name 2-mercaptopyridine *N*-oxide. These two names correspond to structures **NpI** and **NpII**, respectively (see Figure 5.65). The possibility of the molecule to adopt structures **NpI** and **NpII**, differing only by the position of the labile hydrogen atom, is caused by prototropic tautomerism. Hence, for the compound in the gas phase, an equilibrium reflecting (in terms of Boltzmann's distribution) relative stabilities of forms **NpI** and **NpII** should be expected. In the current work, relative energies of forms **NpI** and **NpII** were calculated at the MP2/6-311++G(d,p) and QCISD/6-31++G(d,p) levels. The results of these calculations made for several isomers of the compound are presented in Table 5.9. The *N*-hydroxy form **NpI** was predicted to be substantially more stable (by ca. 30 kJ mol^{-1}) than the *N*-oxide form **NpIIa**. Crystallographic investigation by Bond and Jones demonstrated that in the solid state the compound adopts the *N*-hydroxy thione form **NpI** [224].

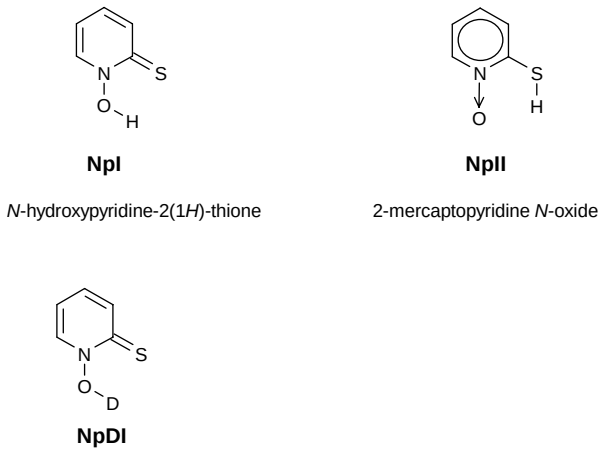

Figure 5.65. *Structures of N-hydroxypyridine-2(1H)-thione, its deuterated derivative and 2-mercaptopyridine N-oxide.*

Table 5.9. *Relative electronic (ΔE_{el}), zero-point vibrational (ΔZPE) and total ($\Delta E_{el}+\Delta ZPE$) energies (kJ mol^{-1}) of N-hydroxypyridine-2(1H)-thione (**Np**) isomers.*

calculation method	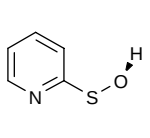	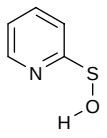	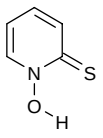	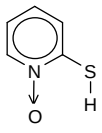	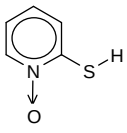
	NpIIIb	**NpIIIa**	**NpI**	**NpIIa**	**NpIIb**
ΔE_{el}(DFT)	-53.8	-56.4	0.0	28.5	42.0
ΔZPE(DFT)	2.7	2.9	0.0	8.0	6.8
ΔE_{el}(DFT)+ΔZPE(DFT)	-51.1	-53.5	0.0	36.5	48.8
ΔE_{el}(MP2)	-66.7	-66.9 [a]	0.0	21.1	31.9
ΔE_{el}(MP2)+ΔZPE(DFT)	-64.0	-64.0	0.0	29.1	38.7
ΔE_{el}(QCISD) [b]	-85.0	-81.6	0.0	24.8	35.3
ΔE_{el}(QCISD)[b]+ΔZPE(DFT)	-82.3	-78.7	0.0	32.8	42.1

The energy of the form **NpI** was taken as reference. The DFT(B3LYP) and MP2 calculations were carried out using the 6-311++G(d,p) basis set.

[a] Nonplanar structure, torsion angles: τ(HOSC)=55.7^0, τ(OSCN)=32.5^0

[b]QCISD calculations were carried out using the 6-31++G(d,p) basis set at geometry optimized at the DFT(B3LYP)/6-311++G(d,p) level.

β(H9-O8-S7) = 106.9º
β(O8-S7-C2) = 100.3º
τ(H9-O8-S7-C2) = 95.4º
τ(O8-S7-C2-N1) = 169.5º

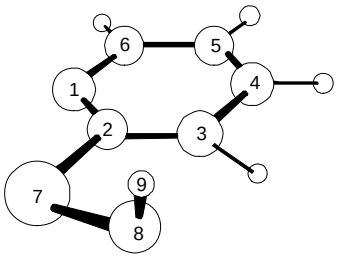

IIIb

The geometries of five isomers of *N*-hydroxypyridine-2(1*H*)-thione (presented in Table 5.9) were fully optimized using the MP2 and DFT(B3LYP) methods. Another four isomeric forms of the compounds were also taken into consideration, but the geometry optimization showed that there are no local minima for this forms, all of them were converted into another isomers of *N*-hydroxypyridine-2(1*H*)-thione (**Np**). The results were as follows:

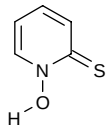

Energy minimization by optimization of geometry of this rotamer of form **NpI** led to a barrierless convergence to structure **NpI** with intramolecular hydrogen bond O-H···S.

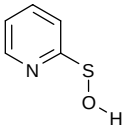

Upon optimization this structure converts to form **NpIIIa** (see Table 5.9);

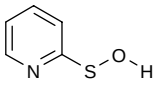
and
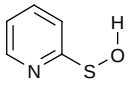

upon optimization both structures convert to form **NpIIIb** (see Table 5.9).

For isomer **NpII**, the energy of its rotameric form **NpIIb**, with SH group rotated by 180° the energy was predicted to be higher (by ca 10 kJ mol^{-1}, see Table 5.9) than the energy of the rotamer of **NpIIa**. The difference in energy reflects stabilization of the latter form by an interaction of the -SH hydrogen atom with the lone electron pair of the N→O oxygen atom. Due to analogous reasons, form **NpI** (as it is presented in Figure 5.65) should be lower in energy with respect to its rotamer with OH group rotated by 180°. This latter form turned out not to correspond to a minimum on the potential energy surface.

The results presented in Table 5.9 suggest also that form **NpIII** should be substantially more stable (by ca. 64 – 82 kJ mol^{-1}) than form **NpI**. However, *N*-hydroxypyridine-2(1*H*)-thione cannot easily change the configuration of its atoms and adopt form **NpIII**. In fact, though form **NpIII** is built of the same set of atoms as *N*-hydroxypyridine-2(1*H*)-thione, it should be treated as another compound (2-hydroxysulfanyl-pyridine). Transformation of **NpI** (or **NpII**) into **NpIII** would involve breaking of the N-O bond, which is quite stable in the ground electronic state of *N*-hydroxypyridine-2(1*H*)-thione. Nevertheless, comparison of calculated energies of forms **NpI** and **NpIII** is interesting and it seems to be important for the sake of interpretation of experimental occurrences observed in this work.

Taking into account the results of the theoretical predictions of relative energies of forms **NpI** and **NpII**, one can expect that in the gas phase at moderate temperatures the *N*-hydroxy isomer **NpI** should strongly dominate. As a consequence, isomer **NpI** should be the almost exclusively populated in the low-temperature matrices [231]. In Figure 5.66 the infrared spectra of monomers of *N*-hydroxypyridine-2(1*H*)-thione and of the deuterated isotopologue of *N*-hydroxypyridine-2(1*H*)-thione isolated in a low-temperature Ar and N_2 matrices are presented.

Comparing these spectra with the spectra theoretically predicted [at the DFT(B3LYP)/6-311++G(d,p) level] for isomer **NpI** and deuterated form **NpDI** one can see that the theoretically simulated spectra are in good agreement with the experimentally recorded spectra of N-hydroxypyridine-2(1H)-thione (Figure 5.66). The assignment of the IR bands observed in the experimental spectra of N-hydroxypyridine-2(1H)-thione isolated in low-

temperature matrices to the theoretically calculated normal modes for the form **NpI** is given in Table D2 in the Appendix,

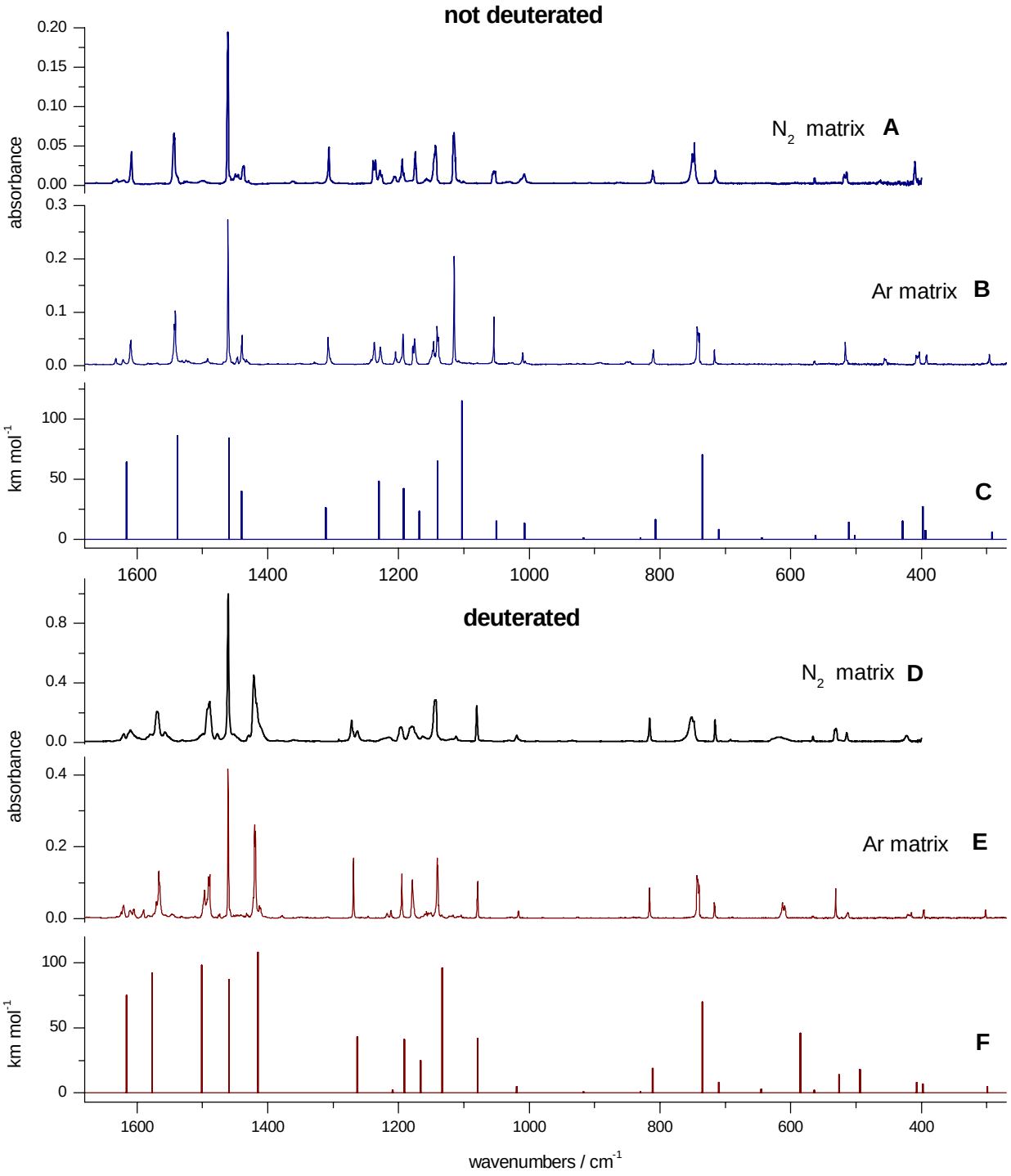

Figure 5.66. *Experimental IR spectra of N-hydroxypyridine-2(1H)-thione isolated in Ar marix (trace B) and in N_2 matrix (trace A); its deuterated isotopologue isolated in Ar matrix (trace E) and in N_2 matrix (trace D), compared with the spectra calculated at the DFT(B3LYP)/6-311++G(d,p) level for form* ***NpI*** *(trace C) and for deuterated form* ***NpDI*** *(trace F). The theoretical wavenumbers were scaled by the single factor of 0.98.*

whereas the analogous assignment concerning the deuterated isotopologue **NpDI** is presented in Table D3 in the Appendix. The theoretical bands have been assigned to the normal modes gained by using internal coordinates presented in Table D1 in the Appendix.

The calculated spectrum of 2-mercaptopyridine *N*-oxide (form **NpII**) reproduces the experimentally recorded spectra of *N*-hydroxypyridine-2(1*H*)-thione slightly less accurately than the spectrum calculated for **NpI** (Figure 5.67). However, the identification of the species isolated in low-temperature matrices, when based on comparison of experimental spectra with the spectra calculated for **NpI** and **NpII**, would not be unambiguous. In this respect, conclusions based on calculations of relative energies of isomers **NpI** and **NpII** seem to be much more reliable.

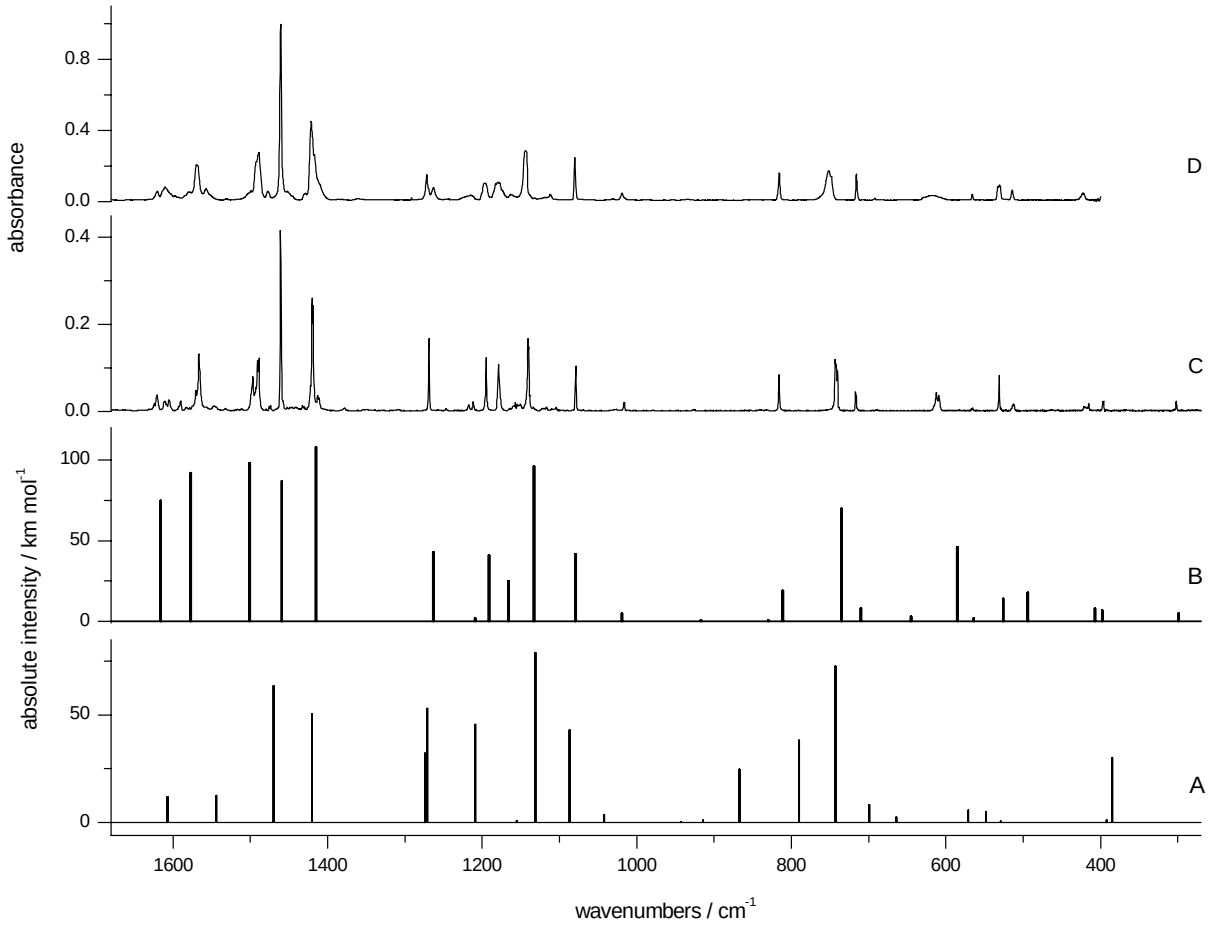

Figure 5.67. *Experimental IR spectra of N-hydroxypyridine-2(1H)-thione isolated in an Ar matrix (trace C) and in a N_2 matrix (trace D), compared with the spectra calculated at the DFT(B3LYP)/6-311++G(d,p) level for form* ***NpI*** *(trace B) and for 2-mercaptopyridine N-oxide* ***NpII*** *(trace A). The theoretical wavenumbers were scaled by the single factor of 0.98.*

The characteristic feature of the IR spectra of monomeric *N*-hydroxypyridine-2(1*H*)-thione (**NpI**) is the obvious lack of a well-defined band (see Figure 5.68) due to the stretching vibration of the free OH group (νOH). For isolated compounds without intramolecular hydrogen bonds [225], such band is expected in the spectral range 3650 – 3550 cm^{-1}. If an intramolecular hydrogen bond (involving OH group) exists in a molecule, then the νOH band is significantly shifted towards lower wavenumbers. This effect is accompanied by a substantial broadening of such νOH band [225].

In the spectrum obtained after deposition of the low-temperature matrix (Figure 5.68), in 2800 – 2400 cm^{-1} spectral range, a broad band was observed and interpreted as νOH band due to vibration of OH group involved in intramolecular hydrogen bond. The observed IR spectra of monomeric *N*-hydroxypyridine-2(1*H*)-thione demonstrated that the intramolecular –O-H···S=C hydrogen bond in **NpI** is quite a strong interaction leading to a very pronounced broadening and low-wavenumber shift of the νOH band.

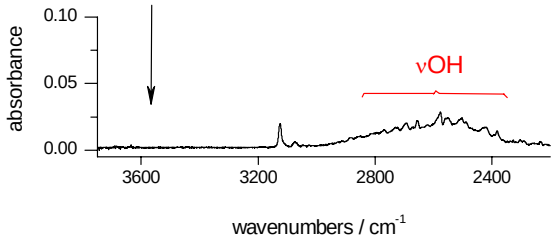

Figure 5.68. *High-frequency region of the infrared spectra of N-hydroxypyridine-2(1H)-thione isolated in a N_2 matrix recorded after deposition of the matrix. The arrow indicates the spectral position where the band due to the stretching vibration of OH group not involved in a hydrogen bond should appear.*

Upon UV irradiation of the low-temperature Ar or N_2 matrices containing monomers of **NpI** photogeneration of two products was observed. The relative yield of these two photoproducts was found to be dependent on the wavelengths of the light used for irradiation (Figs 5.69).

When the longer-wavelength light was applied (λ > 385 nm for Ar and λ > 345 nm for N_2 matrices), one of the products was generated. Figure 5.69 (traces B at left panel and E at right panel) illustrate the high-frequency region of IR spectra of *N*-hydroxypyridine-2(1*H*)-thione after longer-wavelength irradiation. In the IR spectrum of this species, no sharp band due to νOH vibration was found. Instead, a very broad and long-wavelength shifted absorption was observed at ca. 3050 cm^{-1}, see Figure 5.69. This shows that (similarly to the case of the precursor **NpI**) also in the structure of the photoproduct in question, the OH group interacts with a lone-electron pair of a heteroatom.

When the matrices were irradiated with shorter-wavelength UV light ($\lambda > 345$ nm – Ar or $\lambda > 295$ nm – N_2) photogeneration of a second product was observed (traces C and F in Figure 5.69). This was indicated by appearance of a new spectrum with a characteristic band at 3577 cm^{-1} (Ar) or 3566 cm^{-1} (N_2). Such sharp bands are typical of OH stretching vibrations of OH groups not involved in a hydrogen bond. If a deuterated isotopologue **NpDI** was used as a precursor, analogous UV ($\lambda > 345$ nm or $\lambda > 295$ nm) irradiation led to generation of a photoproduct characterized by an IR spectrum (Figure 5.70) with the band at 2643 cm^{-1} (Ar) or 2636 cm^{-1} (N_2). Such bands are typical of stretching vibrations of a free OD group, not involved in a hydrogen bond.

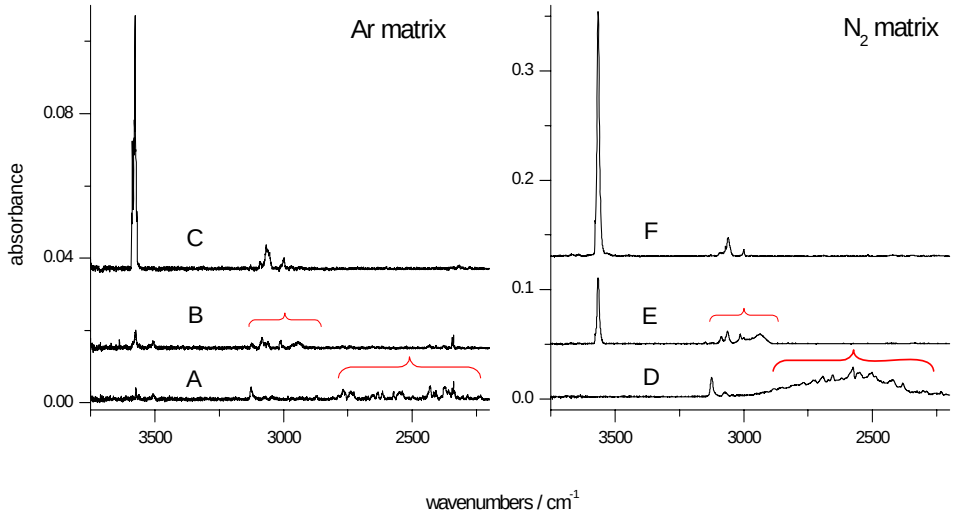

Figure 5.69. *High-frequency region of the infrared spectra recorded in an Ar (left panel) matrix: (A) of N-hydroxypyridine-2(1H)-thione recorded after deposition of the matrix, (B) of the first photoproduct recorded after 100 minutes of UV ($\lambda > 385$ nm) irradiation, (C) of the second photoproduct recorded after subsequent 50 minutes of UV ($\lambda > 345$ nm) irradiation; and in N_2 (right panel): (D) of N-hydroxypyridine-2(1H)-thione recorded after deposition of the matrix, (E) of the first photoproduct recorded after 15 minutes of UV ($\lambda > 345$ nm) irradiation, (F) of the second photoproduct recorded after subsequent 15 minutes of UV ($\lambda > 295$ nm) irradiation.*

Figure 5.71 demonstrates the changes that occur in the low-frequency region of the IR spectra upon UV irradiation of the low-temperature matrices. In an Ar matrix, after UV irradiation with $\lambda > 385$ nm, the bands of the IR spectra due to the initial substrate are decreasing (traces A and B in Figure 5.71), at the same time new bands appear due to the first product of the photoreaction. As it was shows earlier (Figure 5.69), this photoproduct is characterized by an intramolecular hydrogen bond. After subsequent irradiation with shorter wavelength, the bands due to both initial substrate and first photoproduct disappeared completely, whereas the bands due to the second photoproduct appear (traces C in Figure 5.71). The high-frequency region of the IR spectra after

UV irradiation of the matrix indicates that no intramolecular hydrogen bond occurs in this species (Figure 5.69 traces C and F).

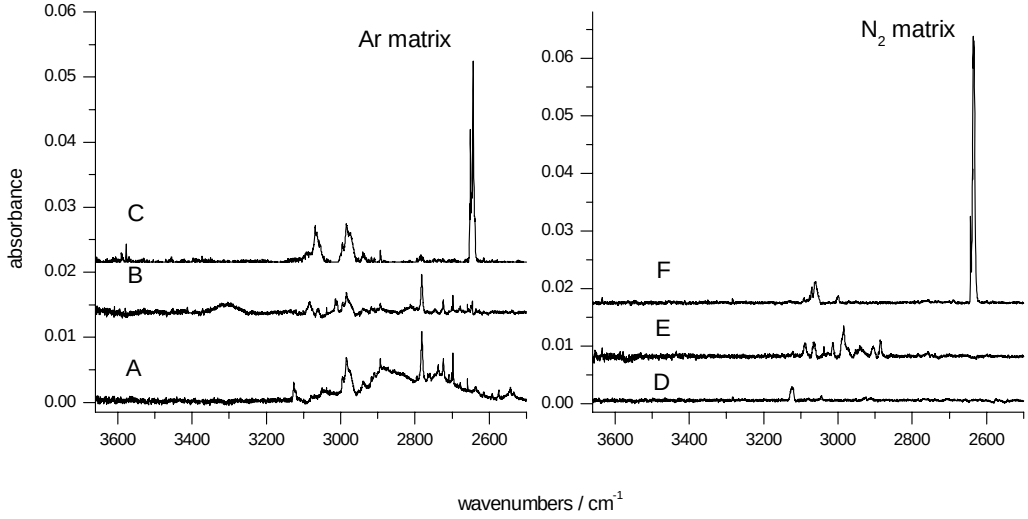

Figure 5.70. *High-frequency region of the infrared spectra recorded in an Ar (left panel) matrix: (A) of deuterated N-hydroxypyridine-2(1H)-thione recorded after deposition of the matrix, (B) of the first photoproduct recorded after 9 minutes of UV (λ > 360 nm) irradiation, (C) of the second photoproduct recorded after subsequent 20 minutes of UV (λ > 300 nm) irradiation; and in N_2 (right panel): (D) of deuterated N-hydroxypyridine-2(1H)-thione recorded after deposition of the matrix, (E) of the first photoproduct recorded after 15 minutes of UV (λ > 360 nm) irradiation, (F) of the second photoproduct recorded after subsequent 20 minutes of UV (λ > 300 nm) irradiation.*

In a N_2 matrix, 15 min. of irradiation with $\lambda > 345$ nm leads to complete vanishing of the bands due to the initial substrate. As can be seen in Figure 5.71 (traces E and F), two types of the bands due to the photoproducts appear: one type increases and the second type vanishes completely upon subsequent irradiation of the matrix with shorter-wavelength irradiation ($\lambda > 295$ nm). Described spectral changes demonstrated that also in N_2 matrix two different photoproducts were generated upon UV irradiation. The first product (that was observed in an Ar matrix after UV irradiation with longer-wavelength) is characterized by a very broad band at 3050 cm^{-1} and thus, involves the intramolecular hydrogen bond; the second product is identical to the photoproduct of irradiation of Ar matrix with shorter-wavelength and has no intramolecular hydrogen bonds. The bands due to this second photoproduct increase in the intensities after shorter-wavelength irradiation (trace F in Figure 5.71); this species is a final product of the photoreactions that occur in *N*-hydroxypyridine-2(1*H*)-thione monomers isolated in low-temperature matrices.

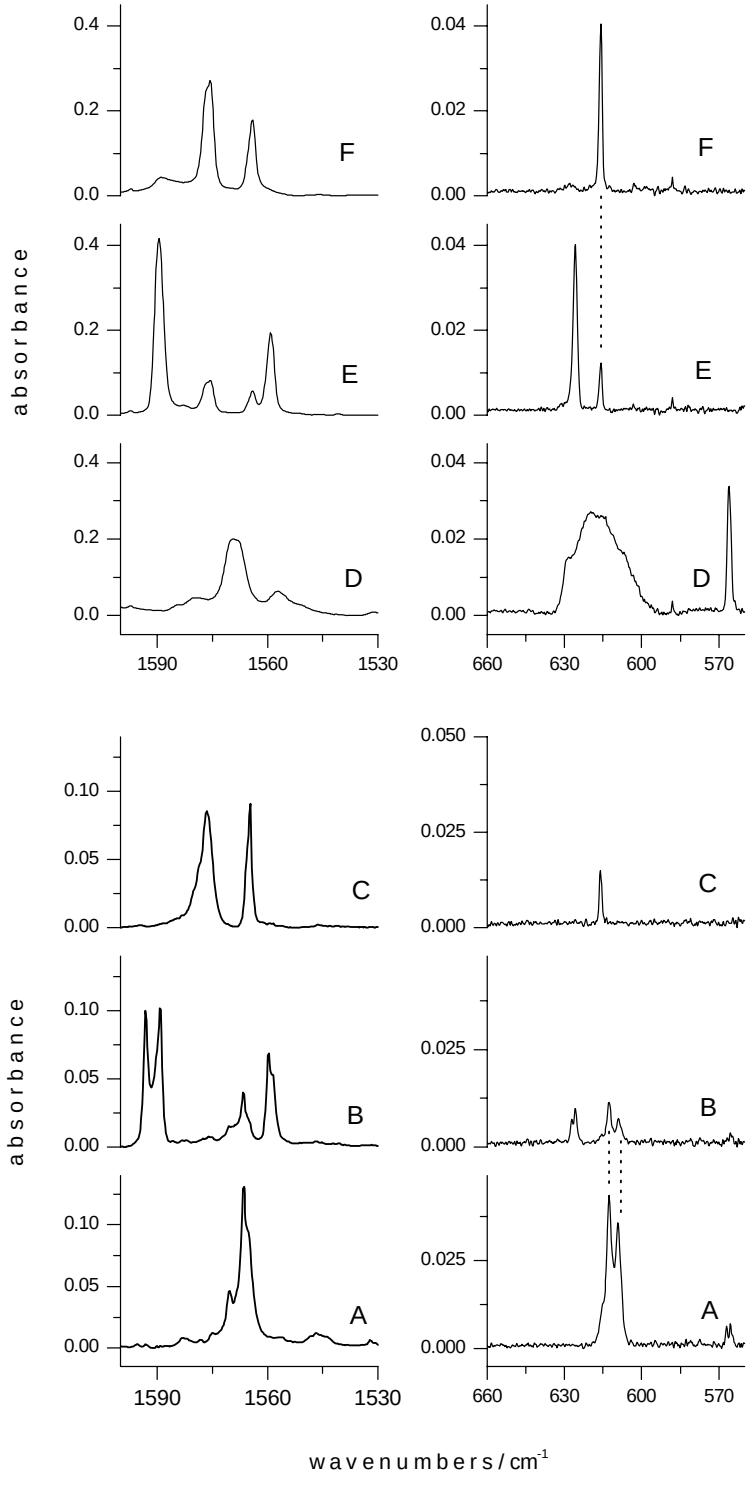

Figure 5.71. *Fragments of the IR spectrum of N-hydroxypyridine-2(1H)-thione isolated in an Ar matrix; (A) spectrum recorded after deposition of the matrix; (B) spectrum recorded after 100 minutes of UV (λ > 385 nm) irradiation, (C) spectrum recorded after subsequent 50 minutes of UV (λ > 345 nm) irradiation. Corresponding fragments of the IR spectrum of N-hydroxypyridine-2(1H)-thione isolated in a N_2 matrix; (D) spectrum recorded after deposition of the matrix; (E) spectrum recorded after 15 minutes of UV (λ > 345 nm) irradiation, (F) spectrum recorded after subsequent 15 minutes of UV (λ > 295 nm) irradiation.*

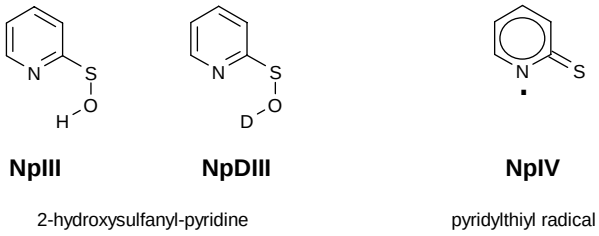

Figure 5.72. *2-Hydroxysulfanyl-pyridine, its deuterated analog and pyridythyil radical.*

The observed sharp bands in high-frequency region of the IR spectra after shorter-wavelength UV ($\lambda > 345$ nm or $\lambda > 295$ nm) irradiation may originate from the stretching vibration of the O-H bond in the ·OH radical. This supposition would follow the known pattern of photochemical behavior of *N*-hydroxypyridine-2(1*H*)-thione in solution. This compound is known to be a photochemical source of hydroxyl radicals.

The experimental observations might suggest that upon shorter-wavelength UV irradiation the bond between the OH group and the rest of the molecule breaks and free ·OH (or ·OD) radical is photogenerated. Hence, the candidates for the final products of photochemical transformations of matrix-isolated *N*-hydroxypyridine-2(1*H*)-thione would be: (1) the hydroxyl radical ·OH or ·OD, and (2) the pyridylthiyl radical **NpIV** (see Figure 5.72).

An UV-induced process having hydroxyl radical as well as pyridylthiyl radical as final products must involve movement of the smaller fragment outside the matrix cage, so that the two radicals are separated in matrix. This did not seem to be an improbable occurrence. Hydroxyl radicals were previously generated by *in situ* photolysis of matrix-isolated precursors such as H_2O_2 and HONO [226-229]. The IR bands due to the stretching vibration of the O-H bond in the ·OH radical were observed at 3554 cm^{-1} (Ar) [226], 3548 cm^{-1} (Ar) [230] and 3547 cm^{-1} (N_2). If ·OH radicals were involved in a hydrogen bond, then the position of the νOH band was shifted towards lower wavenumbers (significantly lower than 3500 cm^{-1}) [227].

In comparison to the experimental data collected within the previous works on ·OH radicals generated by *in situ* photolysis of matrix-isolated precursors [226-228], the spectral positions of the νOH bands observed (within the current work) in the spectra of the final products of UV-induced transformations of *N*-hydroxypyridine-2(1*H*)-thione were considerably higher [3577cm^{-1} (in an Ar matrix) and 3566 cm^{-1} (in a N_2 matrix)]. This does not support (and seems to contradict) the interpretation of the final steps of UV-induced changes of *N*-hydroxypyridine-2(1*H*)-thione in terms of generation of free hydroxyl radicals separated in the matrix lattice from pyridylthiyl radicals **NpIV**.

The possibility of UV generation of pyridylthiyl radical **NpIV** should be proven by identification of the IR spectrum obtained in matrices after short wavelength irradiation. The experimental spectra of the final photoproduct were compared with theoretically predicted IR spectra of two alternate possible photoproducts: pyridylthiyl radical **IV** and 2-hydroxysulfanyl-pyridine **NpIII** (see Figure 5.72). The results are shown in Figure 5.73. The spectra predicted for both putative photoproducts **NpIV** and **NpIII** reproduce quite well the experimental spectrum of the final photoproduct in the range 1600 – 500 cm^{-1}, however, the theoretical spectrum of radical **IV** did not contain the intensive band at ca. 350 cm^{-1} (which is due to the torsion vibrations of the OH group (τOH)).

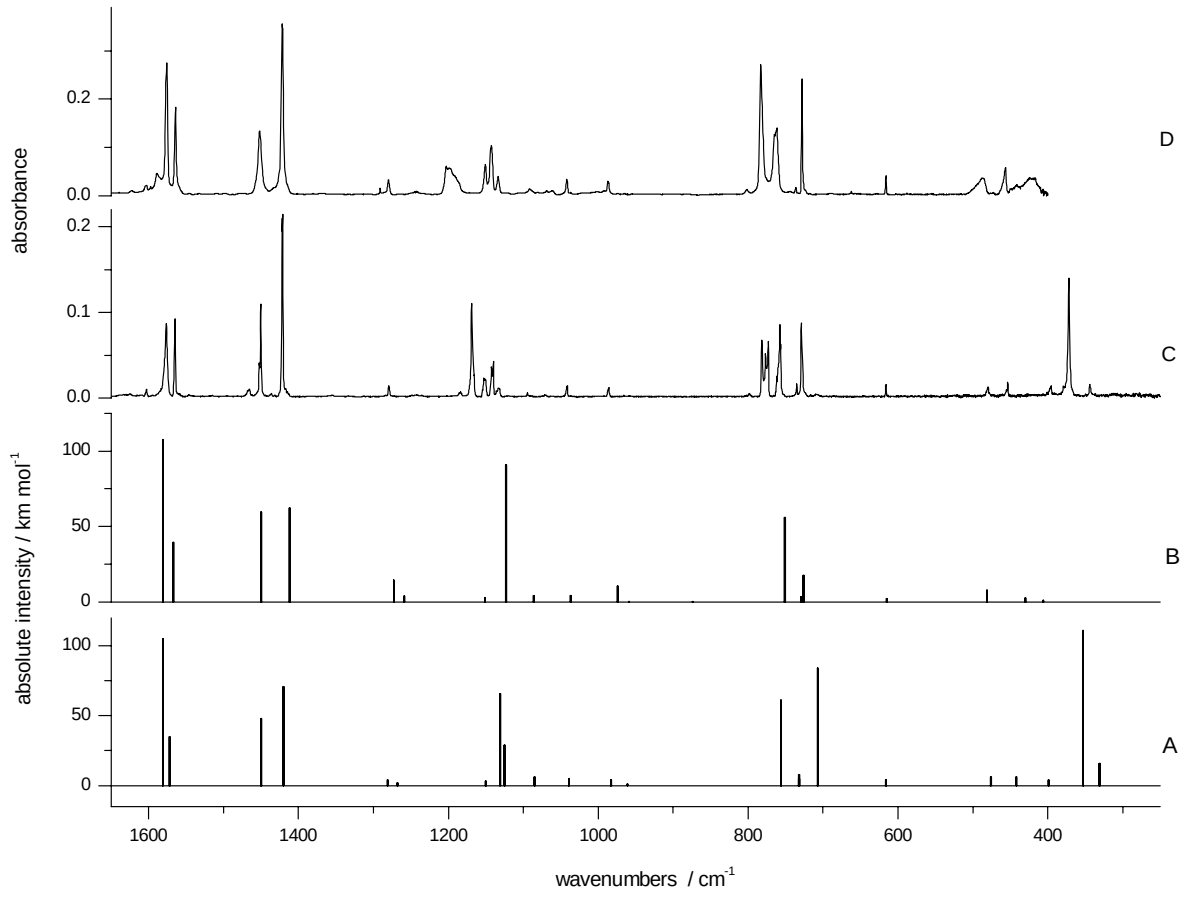

Figure 5.73. *Infrared spectra of the final photoproduct generated upon UV irradiation of N-hydroxypyridine-2(1H)-thione isolated in an Ar matrix (C) or in a N_2 matrix (D); infrared spectra calculated at the DFT(B3LYP)/6-311++G(d,p) level for* ***NpIIIb*** *(trace A) and pyridilthiyl radial* ***NpIV*** *(trace B). The theoretical wavenumbers were scaled by the single factor of 0.98.*

The structure of the final product may be conclusively proven by considering the effects of UV irradiation of *N*-hydroxypyridine-2(1*H*)-thione **I** and its deuterated derivative **DI**. If the final

products of the photochemical transformations of matrix-isolated *N*-hydroxypyridine-2(1*H*)-thione were hydroxyl radicals and pyridylthiyl radicals **NpIV**, then the spectra recorded after prolonged exposure of **NpI** or **NpDI** to UV ($\lambda > 345$ nm or $\lambda > 295$ nm) light, should consist of the spectrum of pyridylthiyl radical **NpIV** (see Figure 5.73) and a single band due to the stretching vibration of OH or OD bond. Hence, except for the νOH and νOD bands, the spectra of the final photoproducts generated from **NpI** and from **NpDI** should be **identical**, regardless whether the compound was deuterated or not. Therefore, the identity (or lack of it) of the spectra (below 2500 cm^{-1}) recorded after prolonged $\lambda > 345$ nm (or $\lambda > 295$ nm) irradiation of **NpI** and the spectra recorded after analogous irradiation of **NpDI** should be a very important observation, crucial for the analysis of the photochemical changes of **NpI**.

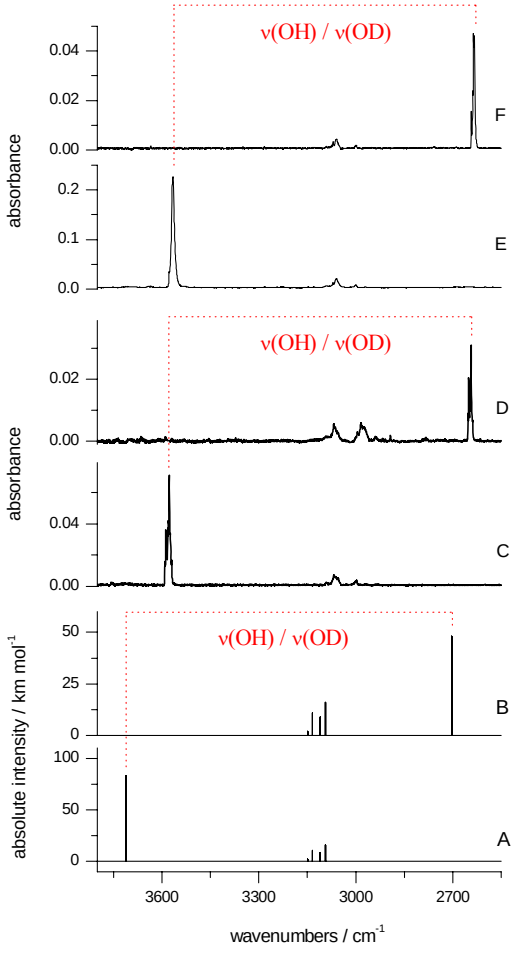

Figure 5.74. *High-frequency region of the IR spectra of the final photoproduct generated upon UV irradiation of N-hydroxypyridine-2(1H)-thione isolated in an Ar matrix (C) or in a N_2 matrix (E); infrared spectra of the final photoproduct generated upon UV irradiation of the deuterated isotopologue of N-hydroxypyridine-2(1H)-thione isolated in an Ar matrix (D) or in a N_2 matrix (F); infrared spectra calculated at the DFT(B3LYP)/6-311++G(d,p) level for* ***NpIIIb*** *(trace A) and for* ***NpDIIIb*** *(trace B). The theoretical wavenumbers were scaled by the single factor of 0.98.*

The IR spectra of the final products of the UV-induced transformations of **NpI** and of **NpDI**, isolated in Ar matrices, are presented in Figures 5.74 and 5.75. It is apparent that most of the bands in these spectra are placed at the same (or very similar) position, regardless of the initial substrate **NpI** or **NpDI**. One of the differences, concerning the νOH and νOD bands (Figure 5.74), found respectively at 3577 and 2643 cm^{-1}, and could be explained in terms of the pair of hydroxyl and pyridylthiyl radicals isolated separately in a matrix. But the spectra shown in Figure 5.75 (traces C and D) differ also by the positions of other absorptions. One of the pairs of such absorptions appears at the standard position of bands due to in-plane bending vibrations of the OH or OD groups (βOH or βOD). The band in spectrum C was observed at 1169 cm^{-1}, whereas the band in spectrum D was found at 863 cm^{-1}. A second pair of such bands, which can be interpreted as originating from out-of-plane torsions of the OH or OD groups (τOH or τOD), appear at 372 cm^{-1} (spectrum C) and 282 cm^{-1} (spectrum D). Comparison of the spectra recorded after prolonged UV (λ > 345 nm or λ > 295 nm) irradiation of **NpI** (Figure 5.75 trace E) and **NpDI** (Figure 5.75 trace F) isolated in N_2 matrices yields the same picture. Correctness of the assignment of the βOH and τOH bands (indicated in Figure 5.75) is supported by their broadening and shift towards higher-wavenumbers, when Ar matrix environment was replaced by solid N_2.

Appearance of the βOH / βOD as well as τOH / τOD bands (by which the spectra of product(s) generated from **NpI** differ from the spectra of product(s) generated from **NpDI**) strongly contradicts the hypothesis that the final products of the photochemical changes of *N*-hydroxypyridine-2(1*H*)-thione could be the ·OH radical and the pyridylthiyl radical **NpIV**.

In search of an alternative interpretation of the UV-induced transformations of matrix-isolated *N*-hydroxypyridine-2(1*H*)-thione (observed by FTIR spectroscopy), theoretical simulations of infrared spectra have been carried out [at the DFT(B3LYP)/6-311++G(d,p) level], for a number of trial structures of the photoproducts. By this method the final product photogenerated from **NpI** has been identified as the form **NpIIIb**. The spectra calculated for this species (as well as for its deuterated isotopologue **NpDIIIb**) are compared (in Figures 5.74 and 5.75) with the experimental spectra recorded after prolonged UV (λ > 345 nm or λ > 295 nm) irradiation of matrix-isolated **NpI** or **NpDI**. The general agreement between the experimental and theoretical spectra is very good. This is true for non-deuterated species **NpIIIb** as well as for deuterated **NpDIIIb**. Identity of the experimental spectra of the final products photogenerated from non-deuterated **NpI** and deuterated **NpDI** precursors, except for bands due to νOH, βOH, τOH and νOD βOD, τOD, is well reproduced in theoretical simulations. Also the isotope shifts of the νOH / νOD, βOH / βOD and τOH / τOD bands are well theoretically predicted. In the structure of **NpIIIb**, the OH group is

not involved in an intramolecular hydrogen bond. Hence, in agreement with experimental observation, the IR band due to νOH vibration is predicted at high wavenumbers. The frequencies and integrated intensities of the bands observed in the IR spectra of the final product of the photoinduced transformations of **NpI** (and **NpDI**) are collected in Tables D4 and D5 (in the Appendix). In these tables the experimental spectra are interpreted by comparison with frequencies, intensities and normal mode forms theoretically predicted for **NpIIIb** and **NpDIIIb**.

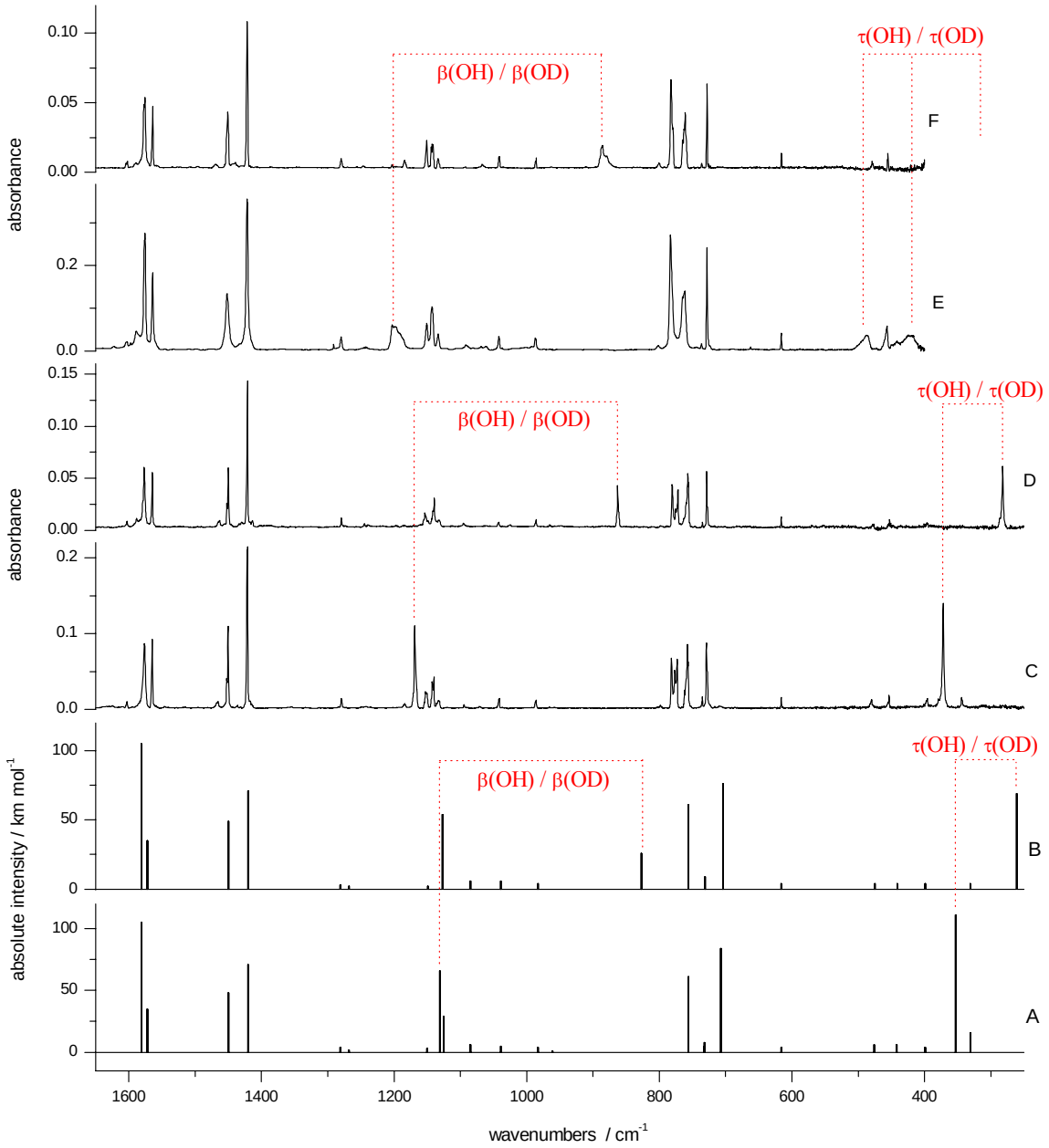

Figure 5.75. *Infrared spectra of the final photoproduct generated upon UV irradiation of N-hydroxypyridine-2(1H)-thione isolated in an Ar matrix (C) or in a N_2 matrix (E); infrared spectra of the final photoproduct generated upon UV irradiation of the deuterated isotopologue of N-hydroxypyridine-2(1H)-thione isolated in an Ar matrix (D) or in a N_2 matrix (F); infrared spectra calculated at the DFT(B3LYP)/6-311++G(d,p) level for* ***NpIIIb*** *(trace A) and for* ***NpDIIIb*** *(trace B). The theoretical wavenumbers were scaled by the single factor of 0.98.*

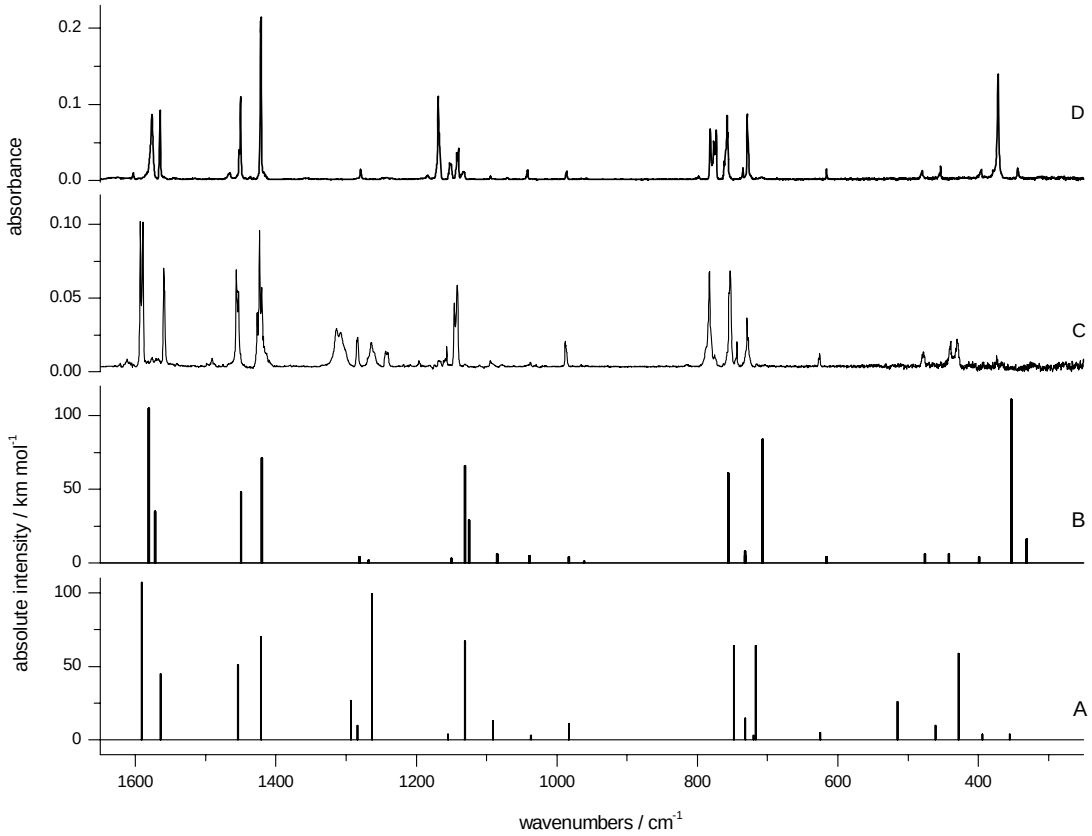

Figure 5.76. *Infrared spectra of the intermediate product (C) and the final photoproduct (D) generated upon UV irradiation of N-hydroxypyridine-2(1H)-thione isolated in an Ar matrix; infrared spectra calculated at the DFT(B3LYP)/6-311++G(d,p) level for* ***NpIIIa*** *(trace A) and for* ***NpIIIb*** *(trace B). The theoretical wavenumbers were scaled by the single factor of 0.98.*

Identification of the final product of photochemical changes of matrix-isolated *N*-hydroxypyridine-2(1*H*)-thione provided also a hint for identification of the intermediate product appearing in the course of UV-irradiation of **NpI**. Following the progress of the UV-induced reaction it was easy to observe that the spectra of the intermediate and the final photoproducts are quite similar (see Figure 5.76). The similarity of the IR spectra suggested that the two photogenerated species must have very similar structures. This requirement is best fulfilled by form **NpIIIa** as a candidate for the structure of the intermediate photoproduct. Forms **NpIIIa** and **NpIIIb** differ only by a rotation of the OH group with respect to the 2-pyridinethione frame. However, the rotation of the OH has one important consequence: there is an intramolecular hydrogen bond in **NpIIIa**, but in **NpIIIb** there are no intramolecular hydrogen bonds. That is why the sharp bands due to stretching vibrations of free OH (or OD) groups were observed in the IR spectra of the final product, whereas in the spectrum of the intermediate product the broad νOH

and νOD bands were observed at much lower wavenumbers (Figure 5.77), indicating involvement of the OH and OD groups in a hydrogen bond.

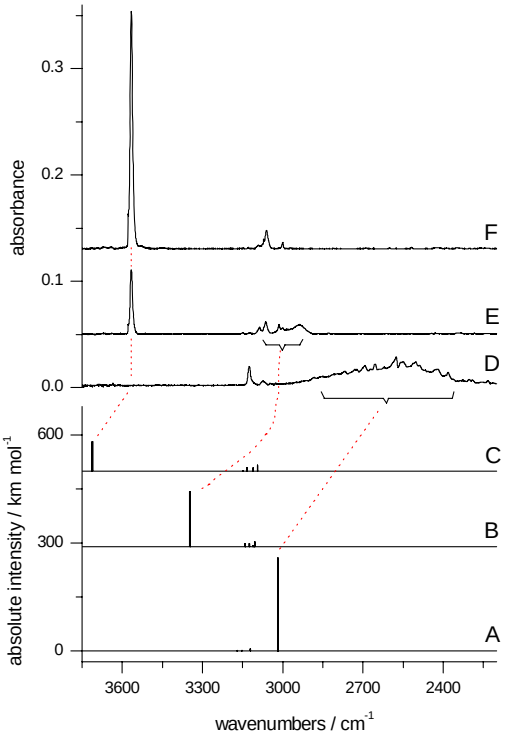

Figure 5.77. *High-frequency region of the infrared spectra of N-hydroxypyridine-2(1H)-thione isolated in a N_2 matrix recorded: (D) after deposition of the matrix, (E) after 15 minutes of irradiation with UV(λ > 345 nm) light, (F) after subsequent 15 minutes of irradiation with UV(λ > 295 nm) light. The corresponding fragments of the spectra calculated at the DFT(B3LYP)/6-311++G(d,p) level for* ***NpI*** *(trace A), for* ***NpIIIa*** *(trace B) and for* ***NpIIIb*** *(trace C). The theoretical wavenumbers were scaled by the single factor of 0.98.*

Another evidence that the intermediate photoproduct has the structure of **NpIIIa** provides the analysis of the spectra obtained during irradiations with the light of different wavelengths. Figure 5.78 presents juxtaposed fragments of the spectra which were obtained at different stages of UV irradiation and the IR spectra theoretically simulated at DFT(B3LYP)/6-311++G(d,p) level for isomeric forms **NpI**, **NpIIIa** and **NpIIIb**. As it can be seen from the figure, the spectral position of the experimentally observed bands corresponding to the intermediate and the final photoproducts are in good agreement with the bands calculated for **NpIIIa** and **NpIIIb** isomers.

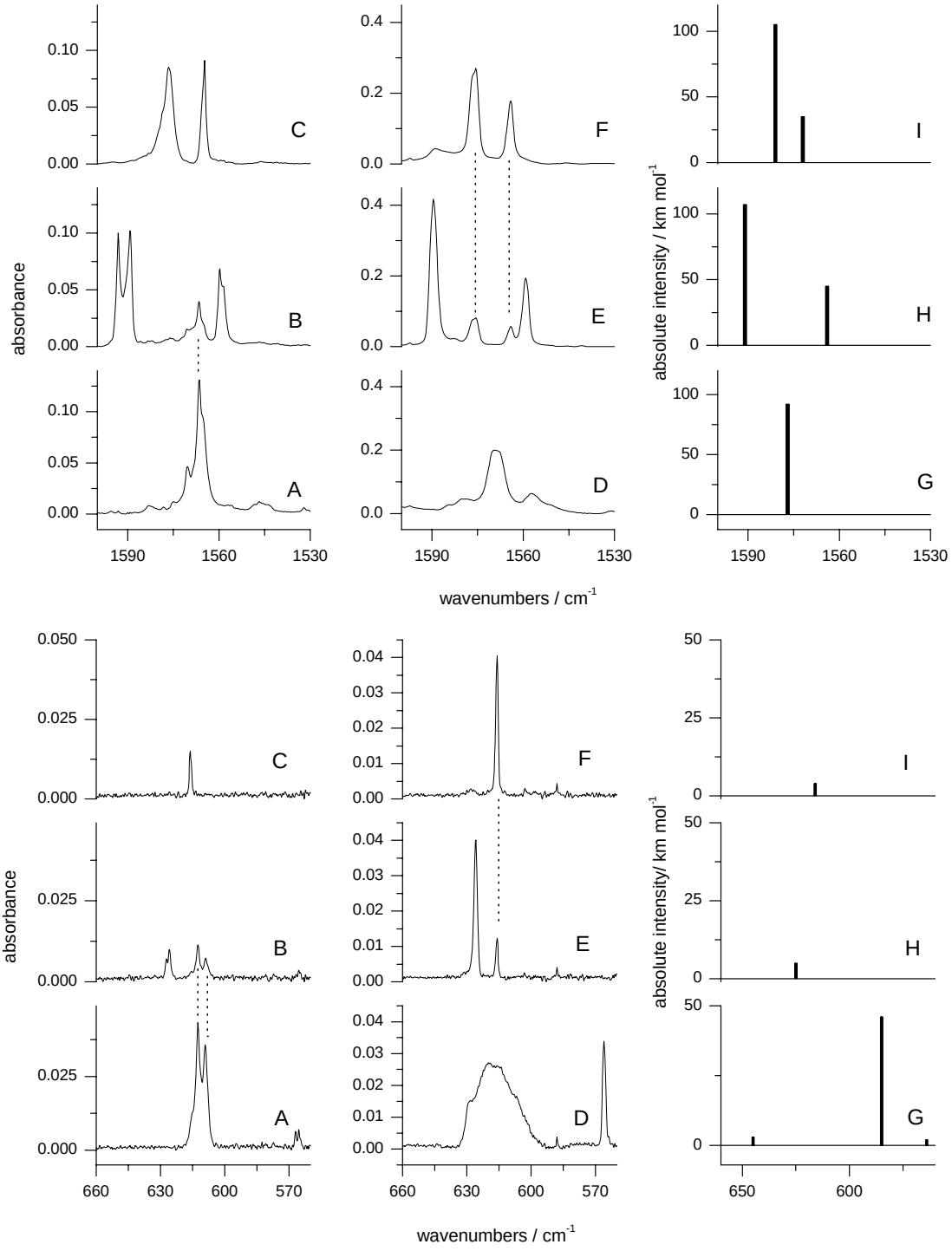

Figure 5.78. *Fragments of the IR spectrum of N-hydroxypyridine-2(1H)-thione isolated in an Ar matrix; (A) spectrum recorded after deposition of the matrix; (B) spectrum recorded after 100 minutes of UV (λ > 385 nm) irradiation, (C) spectrum recorded after subsequent 50 minutes of UV (λ > 345 nm) irradiation. Corresponding fragments of the IR spectrum of N-hydroxypyridine-2(1H)-thione isolated in a N_2 matrix; (D) spectrum recorded after deposition of the matrix; (E) spectrum recorded after 15 minutes of UV (λ > 345 nm) irradiation, (F) spectrum recorded after subsequent 15 minutes of UV (λ > 295 nm) irradiation. Vertical lines indicate bands due to the unreacted initial substrate (Ar matrix) or the final photoproduct (N_2 matrix). Corresponding fragments of the spectra calculated at the DFT(B3LYP)/6-311++G(d, p) level for* ***NpI*** *(G),* ***NpIIIa*** *(H), and* ***NpIIIb*** *(I). The theoretical wavenumbers were scaled by the single factor of 0.98.*

The extracted experimental spectra of the intermediate products photogenerated from **NpI** or **NpDI** are well reproduced by the spectra theoretically predicted for structures **NpIIIa** and **NpDIIIa**, respectively (see Figures 5.79 and 5.80). Also the magnitude of the isotope shift of νOH / νOD, βOH / βOD and τOH / τOD bands (indicated in figures) are well reproduced by theoretical calculations. However, the frequencies obtained for those modes are less accurately predicted than positions of other bands. This is due to high anharmonicity of vibrations of OH/OD group engaged in intramolecular hydrogen bond.

The correctness of the identification of the intermediate product as form **NpIIIa** as well as the assignment of structure **NpIIIb** to the final photoproduct is further supported by the fact that, although the experimental spectra of these two products are quite similar (see Figure 5.76), the details by which they differ (see Figure 5.78) are very well reproduced by the spectra calculated for **NpIIIa** and **NpIIIb**. The assignment of IR bands observed in the spectra of the intermediate product, appearing during UV irradiation of matrix isolated **NpI** or **NpDI**, to the frequencies and forms of the normal modes calculated for **NpIIIa** and **NpDIIIa** is given in Tables D6 and D7, in the Appendix.

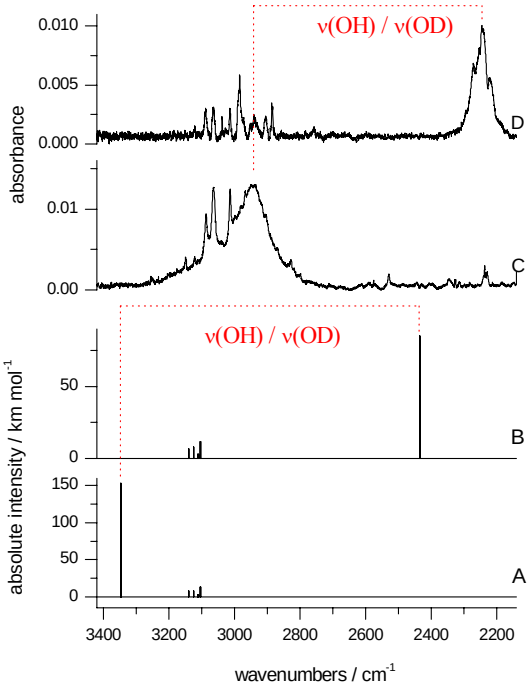

Figure 5.79. *Extracted infrared spectrum of the intermediate photoproduct generated upon UV irradiation of N-hydroxypyridine-2(1H)-thione isolated in a N_2 matrix (C); extracted infrared spectrum of the intermediate photoproduct generated upon UV irradiation of the deuterated isotopologue of N-hydroxypyridine-2(1H)-thione isolated in a N_2 matrix (D); infrared spectra calculated at the DFT(B3LYP)/6-311++G(d,p) level for* ***NpIIIa*** *(trace A) and for* ***NpDIIIa*** *(trace B). The theoretical wavenumbers were scaled by the single factor of 0.98.*

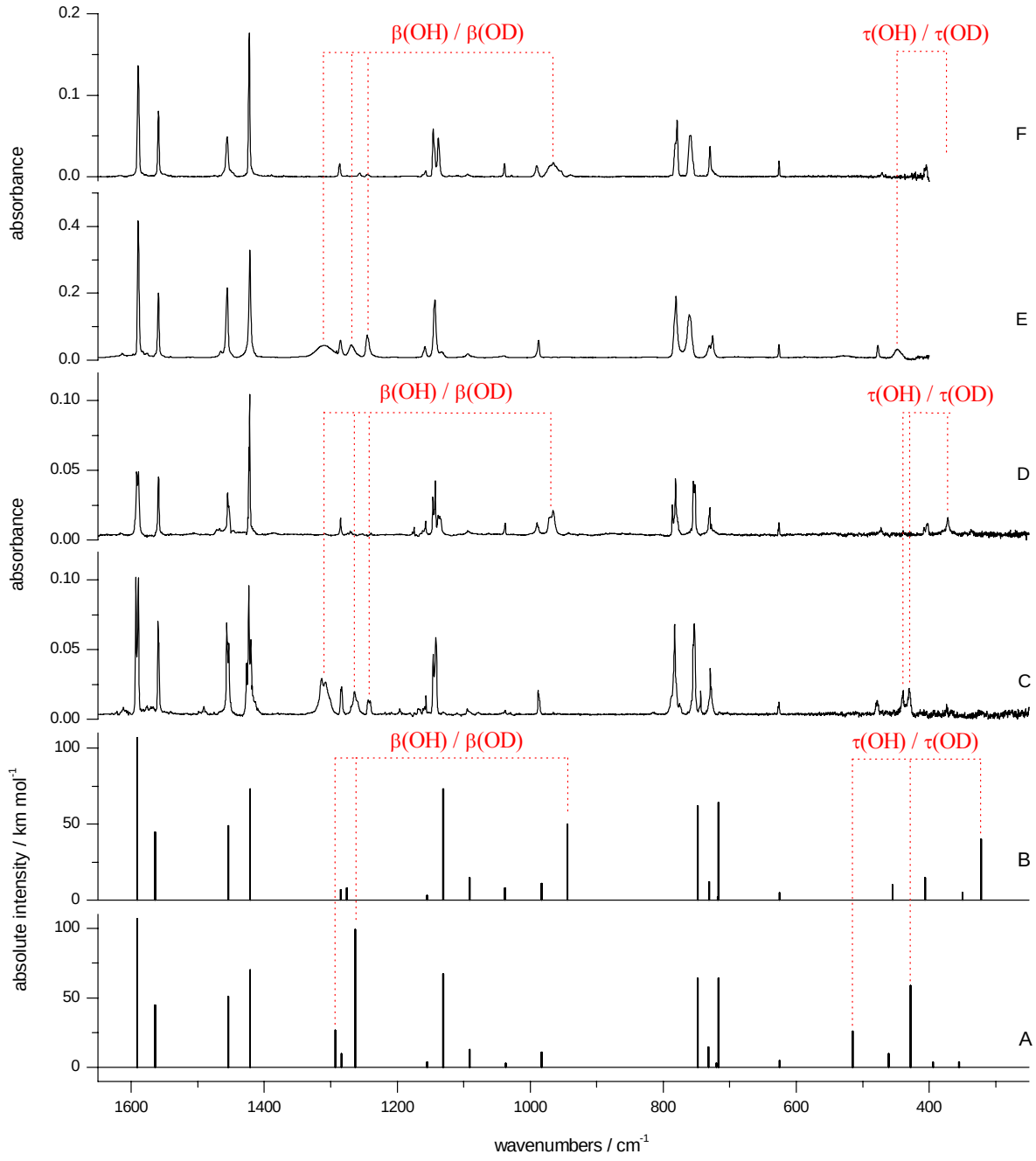

Figure 5.80. *Extracted infrared spectra of the intermediate photoproduct generated upon UV irradiation of N-hydroxypyridine-2(1H)-thione isolated in an Ar matrix (C) or in a N_2 matrix (E); extracted infrared spectra of the intermediate photoproduct generated upon UV irradiation of the deuterated isotopologue of N-hydroxypyridine-2(1H)-thione isolated in an Ar matrix (D) or in a N_2 matrix (F); infrared spectra calculated at the DFT(B3LYP)/6-311++G(d,p) level for* ***NpIIIa*** *(trace A) and for* ***NpDIIIa*** *(trace B). The theoretical wavenumbers were scaled by the single factor of 0.98.*

Described above experiments allowed unambiguous identification of the photoproducts obtained after UV irradiation of monomeric *N*-hydroxypyridine-2(1*H*)-thione isolated in matrices as two isomers of 2-hydroxysulfanyl-pyridine (**NpIIIa** and **NpIIIb)**. As far as we know, this compound has not been known previously and in the current work this thioperoxy derivative of pyridine was obtained for the first time. The photoprocesses leading to transformation of matrix-isolated *N*-hydroxypyridine-2(1*H*)-thione **NpI** into intermediate and final products (2-hydroxysulfanyl-pyridine in **NpIIIa** and **NpIIIb** forms) may be described according to the following scheme:

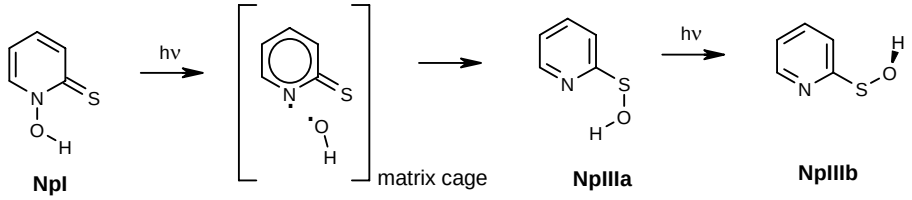

Figure 5.81. *Phototransformations of monomeric N-hydroxypyridine-2(1H)-thione isolated in low-temperature Ar or N2 matrices.*

In this scheme (Figure 5.81), the initial step concerns homolytic cleavage of the N-O bond of the *N*-hydroxypyridine-2(1*H*)-thione molecule excited by a near-UV photon. The released hydroxyl radical ·OH can be easily trapped, especially in a cage of a low-temperature matrix, by the sulfur atom of the pyridylthiyl radical **NpIV**. This recombination of the radicals yields a new compound 2-hydroxysulfanyl-pyridine **NpIII**, which can adopt two rotameric structures **NpIIIa** and **NpIIIb**. As it follows from experimental observations, breaking of the intramolecular hydrogen bond in **NpIIIa** and generation of **NpIIIb** requires some excess of the excitation energy. That is why for photogeneration of this latter form irradiation of the matrices with shorter-wavelength UV light was necessary. The interpretation described above is fully supported by a theoretical model based on theoretical CC2 calculations of the potential energy surfaces of the ground and first excited singlet electronic states of the system [231]. After electronic excitation of the monomeric *N*-hydroxypyridine-2(1*H*)-thione, the molecule envolves to the conical intersection of the potential energy surfaces of the excited and the ground states and then to the global minimum of the ground state corresponding to 2-hydroxysulfanyl-pyridine.

5.6. Reversibility of the phototautomeric reaction

Experimental results of UV irradiation of the isolated molecules, which consist of one or two heterocyclic rings: 2-pyridinone, 4-pyrimidinone, 2-pyrazinone, 2-quinolinone, 1-isoquinolinone, 2-quinoxalinone, 4-quinazolinone, and allopurinol, 9-methylhypoxanthine and hypoxanthine indicate that the oxo → hydroxy phototautomeric reaction occurs for monomers of these heterocycles. This photoreaction converts the oxo forms of these compounds into its corresponding hydroxy tautomers. The phototautomeric reactions observed for the bicyclic compounds mentioned above did not lead to the total conversion of the initial oxo forms of the compounds into the corresponding hydroxy forms. The spectra presented in Figures 5.18, 5.25, 5.30, 5.35, 5.44 and 5.50 of the current work support this observation. There are two possible reasons for that.

First, due to photoreversibility of the phototautomeric reaction, a concomitant hydroxy → oxo phototransformation occurred (together with the photoreaction transforming the oxo forms of the compounds into the hydroxy tautomer). In such a case the observed photoprocess would lead to a photostationary state.

The second reason, is that the phototautomeric reactions in 2-quinolinone, 1-isoquinolinone, and 4-quinazolinone were accompanied (to a greater or lesser extent, depending on the compound and wavelengths of the applied UV light) by competing photoreaction(s), partially consuming the reagent. As a rule, the progress of the phototautomeric reactions in 2-quinoxalinone **2QX**, 2-quinolinone **2QL**, 1-isoquinolinone **1IQ**, and 4-quinazolinone **4QZ** was considerably slower than was the case for single-ring compounds 2-pyridinone **2PD** and 4-pyrimidinone **4PM**. Although it was quite slow, the photoreaction induced by UV irradiation of the oxo **2QXo** form of 2-quinoxalinone seems to produce only one product: the hydroxy **2QXh** tautomer. This is illustrated (Figure 5.20 in Section 5.3) by a good agreement between the experimental IR spectrum growing in the course of UV irradiation (the spectrum of the photoproduced species) with the spectrum calculated at the DFT(B3LYP) level for the **2QXh** form.

Photoreversibility of the oxo → hydroxy phototautomerism of the type observed for the studied compounds was experimentally proven for the model system 4-pyrimidinone / 4-hydroxypyrimidine [195]. This model molecule has a six-membered ring and the possibility of the tautomerism involving pyrazole or imidazole ring is automatically excluded.

Both oxo and hydroxy forms of this model compound are populated in the gas phase and are trapped into a low-temperature Ar matrix (see Section 5.2, [26, 28]). Irradiation of matrix-isolated

4-pyrimidinone with UV ($\lambda > 270$ nm) light leads to an almost total conversion of the oxo form into the hydroxy tautomer (Figures 5.9 and 5.82). Upon subsequent UV ($\lambda > 230$ nm) irradiation partial recovery of the oxo tautomer occurred (Figure 5.82 traces b, c, d). The spectral signature of this reverse hydroxy → oxo photoprocess is the reappearance and increase of the νNH band (at 3428 cm^{-1}) and the νC=O band (at 1726 cm^{-1}), both characteristic of the IR spectrum of the oxo tautomer [29]. This was the first experimental observation of the photoreversibility of the oxo–hydroxy intramolecular phototautomerization in the compounds where the hydrogen atom is shifted between the N–H and C=O groups placed at alpha position with respect to each other.

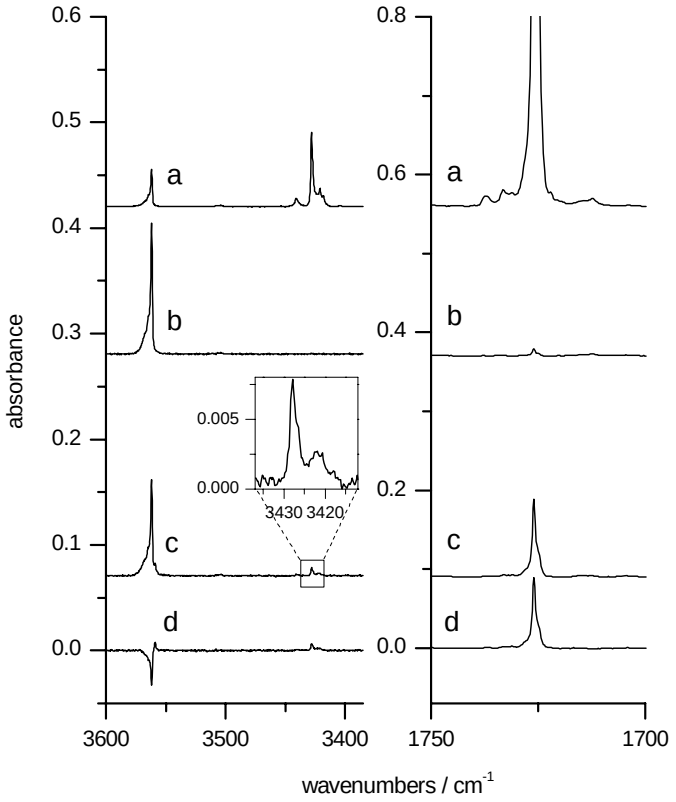

Figure 5.82 *Portions of the IR spectra of 4-pyrimidinone isolated in an Ar matrix: (a) after deposition of the matrix; (b) after UV irradiation with $\lambda > 270$ nm; (c) after UV irradiation with $\lambda > 230$ nm; (d) difference spectrum: trace c minus trace b.*

The phototautomeric reaction of the same type occurred also for the compounds, for which 4-pyrimidinone/4-hydroxypyrimidine is a model compound. The choice of an appropriate cutoff filter was guided by the fact that the oxo tautomeric forms of the compounds in question absorb at longer wavelengths than their hydroxy counterparts. The energies of 0-0 electronic transitions were previously determined by dispersed fluorescence and fluorescence excitation spectra, for

2-pyridinone, 4-pyrimidinone, and 2-quinolinone tautomers in supersonic jet expansions. The 0-0 lines in these spectra were found at 335 and 277 nm for **2PDo** and **2PDh** [128], at 328 and 283 nm for **4PMo** and **4PMh** [127], and at 344 and 319 nm for **2QLo** and **2QLh** [194], respectively. If the wavelength of the UV light used for irradiation of a matrix was such that only the oxo form was excited, then only the oxo → hydroxy transformation was induced and complete transformation of all the molecules into the hydroxy form was observed. In a dedicated experiment (carried out for **4PM**) [195], the first irradiation of the matrix (leading to total conversion of all the material to the hydroxy form) was followed by an irradiation with shorter wavelength UV light ($\lambda > 230$ nm). This led to partial recovery of the population of the oxo form (totally consumed during the first irradiation). Hence, the occurrence of the photoreaction in the hydroxy → oxo direction (accompanying the dominating oxo → hydroxy phototransformation) was demonstrated and the photoreversibility of the phototautomeric reaction was proven.

5.7. Aromaticity and tautomerism

Better understanding of the principles of the aromaticity may considerably facilitate the understanding of the tautomeric equilibrium [198]. Moreover, the aromaticity concept is a cornerstone to rationalize and understand the structure and thus the behavior of heterocyclic compounds [237-241].

The characteristics which distinguish aromatic from non-aromatic compounds have been realized for a very long time. Heteroaromatic compounds must accord with the general characteristics:

1. to be a cyclic structures with significant resonance energies;
2. their electronic structures have to be in agreement with Hückel's (4n + 2) π-electron rule. In agreement with Hückel's rule, cyclic delocalization of monocyclic systems with 4n+2 π-electrons leads to all the attributes of aromatic stabilization, in contrast to systems with 4n electrons, which are anti-aromatic and destabilized;
3. their rings have to possess diamagnetic currents;
4. they tend to react by substitution rather than addition;
5. the bond orders and lengths tend to be intermediate between single and double.

The degree of aromaticity of a ring has a profound influence on the properties of hydroxy substituents (and also of amino or mercapto substituents [233]). Phenol is weakly acidic, aniline much less so, and toluene almost not at all. Furthermore, there is no tendency for these benzenoid derivatives to tautomerize to their alternative tautomeric forms because of the loss of aromaticity that this would entail. The increased tendency toward proton loss from such substituents as OH, NH_2, and SH relative to their benzenoid congeners when situated α or γ to a pyridine-like nitrogen atom results in higher acidity and the possibility of tautomerism to an alternative form.

2-Hydroxypyridine could tautomerize in two fundamentally different ways: if the proton moves to the nitrogen, cyclic conjugation and hence aromaticity is preserved, whereas movement of the proton to a ring carbon is unfavorable; only the former process occurs and leads to the favored tautomeric form at equilibrium (Figure 5.83). As it has been mentioned above, the tautomeric equilibrium of pyridones and analogous compounds are highly dependent on the medium: this implies that aromatic stability also depend on the medium.

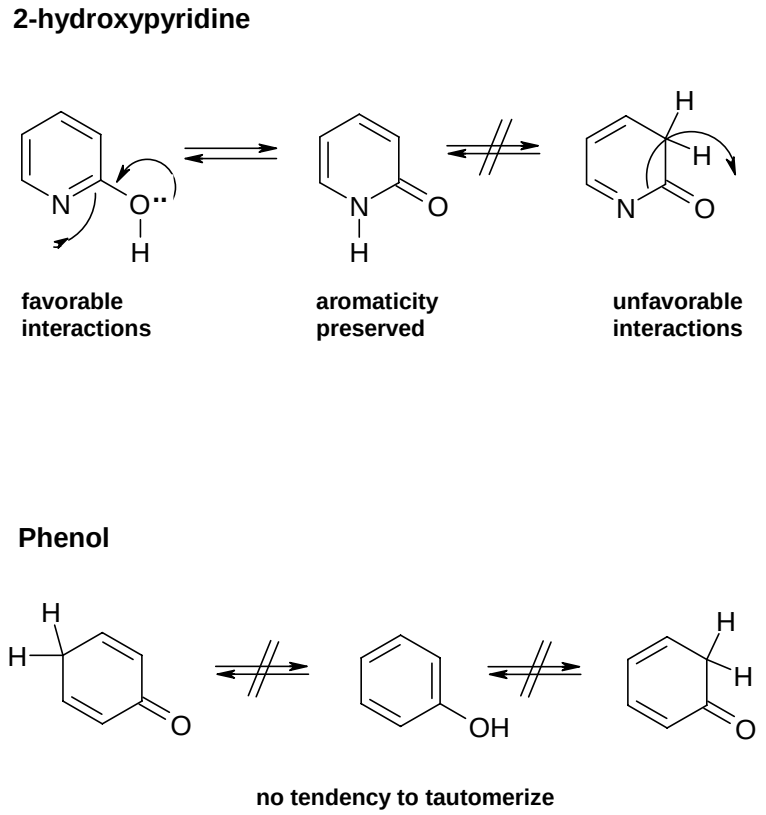

Figure 5.83. *Tautomerism in pyridines*

In the view of the basic importance of aromaticity, many scales of aromaticity have been proposed. The different "dimensions" of aromaticity can show different quantitative or qualitative values or variations for a given compound or series of compounds. The multidimensionality of aromaticity derives partly from the statistical treatment of the data matrices which are built up of variously defined aromaticity indices for many model systems.

Three major approaches to the quantization of aromaticity exist: (a) the increased thermodynamic stability of aromatic compounds is the basis of the energy scale. (b) the geometry of the ring was proposed as a criterion for the degree of aromaticity. Today, interand intramolecular bond length data are easily collected by routine X-ray measurements. On the basis of these measurements, the harmonic oscillator model of aromaticity (HOMA) concept has been successfully used as evidence of the aromatic character in many π-electron systems. This model relates the decrease of aromaticity to two geometric/energetic factors: one describing the bond length alternation (GEO) and the other describing the extension of the mean bond length (EN). (c) Magnetic property measurements led to a quantitative approach to aromaticity. Diamagnetic susceptibility was the first magnetic property studied in connection with the concept of resonance energy. More recently, ^{1}H NMR spectroscopy has become a tool in the study of ring currents in cyclic π-conjugated systems. More about aromaticity see [198, 232, 234-236].

6. Concluding discussion

Matrix isolation is a powerful tool for studying photochemical transformations occurring in isolated molecules exposed to the UV radiation. This work contains examples of unimolecular photochemical processes leading to the change of a structure of irradiated molecule. Several cases of phototautomeric oxo → hydroxy reaction were described and one example of formation of a new chemical compound, which formally is an isomer of the substrate molecule. Phototautomeric processes, described in this work, can be studied only under matrix-isolation conditions. In such an environment, thermodynamical equilibration practically does not take place (or it is extremely slow); hence, unstable tautomers trapped in the matrix can be easily characterized spectroscopically. The photochemical formation of a new compound – 2-hydroxy sulfanyl-pyridine, described in the last part of this work, most probably, occurred due to the matrix environment. Isolation of a substrate molecule in a matrix cage prevented fast detachment of photochemically formed ·OH radical, and allowed formation of a final product.

The change of a relative amount of tautomers in a matrix after irradiation allowed experimental determination of a ratio of tautomers frozen during formation of a matrix. The differences in ratios of tautomers measured for the compounds: 2-pyridinone, 4-pyrimidinone and 2-pyrazinone showed that tautomeric equilibria of these heterocyclic compounds depend on the number of heterocyclic N atoms and on the relative position of the two nitrogen atoms in the ring. A systematic shift of the tautomeric equilibrium from the dominance of the oxo form (for 4-pyrimidinone, **4PM**) via the mixture of the oxo and hydroxy forms (2-pyridinone **2PD**) to the dominance of the hydroxy form of the compounds (2-pyrazinone, **2PZ**) was illustrated in Figure 5.15 (in Section 5.2).

The tautomeric ratios measured for the bicyclic compounds which consist of a benzene ring connected to the heterocyclic ring in different positions (2-quinoxalinone **2QX**, 2-quinolinone **2QL**, 1-isoquinoline **1IQ**, 4-quinazolinone **4QZ**) strongly suggest that direct attachment of the benzene ring at one of the double bonds in the structure of **2PD**, **2PZ**, or **4PM** leads to a significant increase of stability of the oxo tautomers (**2QXo**, **2QLo**, **1IQo**, and **4QZo**), with respect to the corresponding hydroxy forms (**2QXh**, **2QLh**, **1IQh**, and **4QZh**). On the contrary, direct attachment of the benzene ring at the single bond in the structure of **2PD**, **2PZ**, or **4PM** leads to an increase of stability of the hydroxy tautomer (the case of 3-hydroxyisoquinoline **3IQh**), with respect to the corresponding oxo form (**3IQo**).

In an attempt to rationalize these observations, aromaticity of the tautomeric forms of **2PD**, **2PZ**, or **4PM** and their double-ring analogues was considered. The heterocyclic ring of

the hydroxy **2PDh** form is more aromatic than the ring of the oxo **2PDo** form; the same is true for analogous pairs of tautomers in **2PZ** and **4PM**. Certainly, higher aromatic character of the **2PDh** ring contributes to the stabilization of this form much more strongly than is the case for the **2PDo** form. The "least aromatic" fragment of the ring of oxo forms of these compounds (**2PDo**, **2PZo** or **4PMo**) is the N–C bond in the H–N–C=O group. This N–C bond has a single-bond character, which breaks the alternation of single and double bonds around the ring, and hence leads to decrease of its aromaticity.

Direct attachment of a benzene ring to a double bond of heterocyclic ring substantially extends the π-electron system of a molecule. Numerous π-electrons in **2QXo**, **2QLo**, **1IQo**, and **4QZo** can be shared all over the molecule, making also the heterocyclic rings of the oxo forms somewhat more aromatic. Hence, the single N-C bond in the H–N–C=O group should gain (in **2QXo**, **2QLo**, **1IQo**, and **4QZo**) a bit of a double bond character. It was shown that the length of this bond decreased in comparison with analogous N-C bond in single-ring compound. This result was obtained by geometry optimizations carried out for single-ring (**2PDo**, **2PZo**, and **4PMo**) as well as double-ring (**2QXo**, **2QLo**, **1IQo**, and **4QZo**) compounds. The calculations showed that, with the attachment of a benzene ring, the N–C bond (in H–N–C=O) gets systematically shorter (Tables 5.3 and 5.4). This suggests that the difference of aromaticity of the heterocyclic rings of the hydroxy and oxo tautomers is somewhat reduced in double ring compounds, in comparison to their single-ring analogues. Therefore, the stability advantage of the hydroxy forms, introduced by the aromaticity factor, should be much lower for double-ring systems than it was for single-ring species.

The influence of aromaticity can be best described when the oxo and hydroxy forms of formamide are taken as a reference. Formamide is the simplest possible system containing H-N-C=O fragment and for this compound (see Table 6.1) the aromaticity factors (in a sense discussed above) do not exist at all. As it results from experimental observations [31, 32] and theoretical calculations [149], the oxo tautomer of formamide is more stable (by at least 40 kJ mol^{-1}) than the hydroxy form of this compound. In 2-pyridinone, the higher stability of the oxo form of the amide group is balanced by the higher stability of the aromatic ring in the hydroxy form. The high difference of the aromaticity in favor of hydroxy form causes that the energy of both tautomers oxo (**2PDo**) and hydroxy (**2PDh**) are almost the same (ΔF = -3 kJ mol^{-1}). For **1IQ** where the aromaticity advantage of the hydroxy tautomer is noticeably reduced, the oxo tautomeric forms become again the most stable (Table 6.1). The same deduction can be made about tautomerism of **2QX**, **2QL**, and **4QZ**.

In case when pyrimidine and benzene rings are fused on a single bond, as it is in 3-hydroxyisoquinoline (**3IQ**), then aromaticity of the oxo form is even reduced, in comparison with parent compound 2-pyridinone, and therefore the hydroxy form (**3IQh**) is more stable. The length of N-C bond in **3IQo** is greater than in **2PDo** (Table 5.5).

Table 6.1 *Free energy difference between hydroxy and oxo tautomers of formamide, 2-pyridinone and 2-quinolinone.*

compound	**tautomers**	**ΔF = ΔF(hydroxy) - ΔF(oxo)**
formamide		ΔF ≈ 40 kJ mol^{-1} (calculated) [149]
2-pyridinone	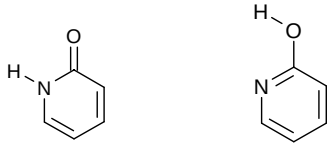	ΔF ≈ -3 kJ mol^{-1}
2-quinolinone	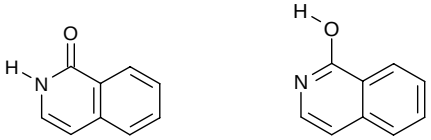	ΔF > 17 kJ mol^{-1} (experiment) ΔF ≈ 21 kJ mol^{-1} (calculated)

Purines, which contain five-membered second heterocyclic ring, also may be characterized by its aromatic properties. Hypoxanthine and allopurinol contain 4-pyrimidinone ring. In 4-pyrimidinone, the higher stability of the amide group in the oxo form is balanced by the higher stability of the aromatic ring in the hydroxy form. A big difference of the aromaticity in favor of hydroxy form causes that the energy of both tautomers oxo and hydroxy are almost the same (ΔF = 2.5 kJ mol^{-1}). For allopurinol and hypoxanthine, where the aromaticity advantage of the hydroxy tautomers is noticeably reduced, the oxo tautomeric forms become again the most stable (Table 6.2). In the case of allopurinol, the energy difference has to be very high, since in the initial spectra of the compound isolated in an Ar matrix, no signatures of hydroxy form were observed. The theoretical methods predict ΔF (for this system) to be approximately near 20 kJ mol^{-1}. For hypoxanthine and its methylated analogue (9-methylhypoxanthine) a tiny amount of hydroxy tautomer were observed after deposition of the matrix, the estimated values of ΔF are 9.8 and 12.5 kJ mol^{-1}, respectively.

Table 6.2. *Free energy difference between hydroxy and oxo tautomers of 4-pyrimidinone, allopurinol and hypoxanthine.*

compound	**tautomers**	**ΔF = ΔF(hydroxy) - ΔF(oxo)**
4-pyrimidinone	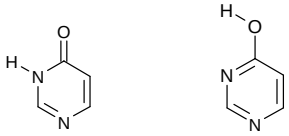	ΔF ≈ 2.5 kJ mol^{-1} (experiment)
allopurinol	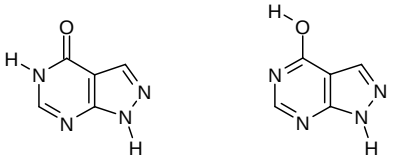	ΔF ≈ 20 kJ mol^{-1} (calculated)
hypoxanthine	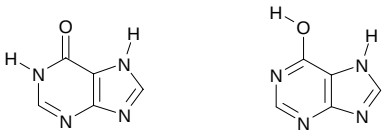	ΔF ≈ 9.6 kJ mol^{-1} (experiment)

Another factor may affect the stabilization of the tautomeric forms of the studied compounds. Intramolecular interactions contribute to the internal energy of a tautomer. In heterocyclic molecules in the oxo form, the very weak interactions exist between lone electron pair of oxygen and vicinal hydrogen from N-H group (in H-N-C=O). This very weak interaction is not a real hydrogen bond because of very unfavorable geometry for H-bond to be formed. Atoms from N-H group may interact, also, with lone electron pair from neighboring nitrogen.

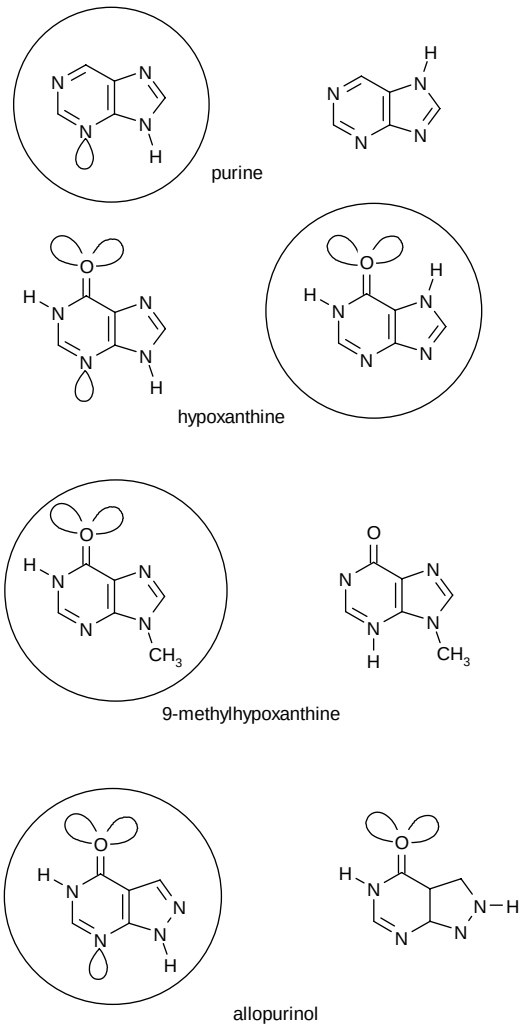

Figure 6.1. *Most stable oxo forms of purine, hypoxanthine, 9-methylhypoxanthine and allopurinol.*

In Figure 6.1 the oxo forms of purine, hypoxanthine, 9-methylhypoxanthine and allopurinol are presented with lone electron pairs attending in above mentioned intramolecular interactions. The most stable forms of these compounds are indicated with circles. In purine, the weak intramolecular interaction N(9)-H···N(3) exist only in the molecule in the form oxo-N(9)-H. As a consequence, only the N(9)-H tautomer, stabilized by this interaction, is populated in the gas phase and in low-temperature Ne, Ar and N_2 matrices [242-244].

The intamolecular interactions may explain tautomerism of hypoxanthine, which is related with proton shift in the imidazole ring N9H ↔ N7H. The oxo-N(7)-H tautomeric form was observed as a dominating isomer of the hypoxanthine isolated in an Ar matrices The second form which was populated it was the oxo-N(9)-H tautomer, in which the hydrogen atom is attached to another nitrogen atom within the imidazole ring. Both positions of the hydrogen atom, at N(7) or N(9) nitrogen atoms, are stabilized by weak interactions with the lone-electron pairs of O(6)

oxygen or N(3) nitrogen atoms, respectively. Apparently, the stabilizing interaction is stronger in the first case. This is due to a more favorable geometry of the quasi-ring closed by a N(7)-H····O(6) interaction. In this case a five-membered quasi-ring is closed by a hydrogen-bond-like interaction, whereas for tautomer oxo-N(9)-H, the quasi-ring is only four-membered. Moreover, in the tautomer oxo-N(7)-H, one of the lone-electron pairs of O(6) is directed towards the N(1)-H group. Such a favorable factor does not appear in the case of the oxo-N(9)-H-tautomer. In a similar way the existence of N(1)-H····O(6) interactions explains higher stability of the oxo-N(1)-H tautomer of 9-methylhypoxanthine. The most stable tautomer of allopurinol, the oxo-N(5)-H, N(1)H form, (different atom numbering in this molecule!) has two interacting N-H groups: N(5)-H····O(4) and N(1)-H····N(7). This is why only this form was observed in an Ar matrix. Juxtaposition of the results of the studies on tautomerism of purine, hypoxanthine 9-methylhypoxanthine and allopurinol demonstrates the role of the weak intramolecular interactions as an important factor governing tautomeric equilibria in purine bases.

In this work, it was demonstrated that upon UV irradiation the reaction of intramolecular proton transfer occurs in the studied compounds, which consist of one or two rings. In the studied compounds, the proton was transferred from nitrogen atom to oxygen in the six-membered heterocyclic ring. In the case of allopurinol, 9-methylhypoxanthine and hypoxanthine, along with oxo → hydroxy photoreaction, the accompanied process was observed which results, most probably, from the formation of ring-open species (conjugated ketenes).

The more complicate process, caused by UV light occurred for hypoxanthine. Upon UV-irradiation, two simultaneous photochemical processes were observed: reaction converting oxo-N7 form into hydroxy-N7 tautomer, and oxo-N9 form into corresponding hydroxy-N9 form. One of the photoproducts, the hydroxy form with N9-H group is populated upon UV irradiation with ($\lambda > 270$ nm), the second product the hydroxy form N7-H is a result of phototautomeric reactions relatively more effective upon $\lambda > 230$ nm irradiation.

In the current work, the IR spectra of the oxo-N(7)-H and of the oxo-N(9)-H tautomers of hypoxanthine were experimentally separated thanks to the UV induced transformations of both forms. The previous attempts to assign the observed IR bands to the spectra of tautomers oxo-N9 and oxo-N7 were based on a mere comparison with the spectra theoretically predicted for the two forms [211]. In comparison to such methods, the separation of the spectra done in the present work is much more reliable.

The studies of the photochemical transformations of *N*-hydroxypyridine-2(1*H*)-thione and its deuterated isotopologue allowed a conclusion, that the final product of the photoreaction is thioperoxy derivative of pyridine. This is the first report on generation of this species.

Experimental identification of the intermediate and final products of the UV-induced transformations of matrix-isolated *N*-hydroxypyridine-2(1*H*)-thione as the rotameric forms of 2-hydroxysulfanyl-pyridine (**NpIIIa** and **NpIIIb**, respectively), allowed proposition of a self-consistent scheme of the observed photoreaction (Figure 5.81). In this scheme, the initial step concerns homolytic cleavage of the N-O bond of the *N*-hydroxypyridine-2(1*H*)-thione molecule excited by a near-UV photon. The released hydroxyl radical ·OH can be easily trapped, especially in a cage of a low-temperature matrix, by the sulfur atom of the pyridylthiyl radical **NpIV**. This recombination of the radicals yields a new compound 2-hydroxysulfanyl-pyridine **NpIII**, which can adopt two rotameric structures **NpIIIa** and **NpIIIb**. As follows from experimental observations, breaking of the intramolecular hydrogen bond in **NpIIIa** and generation of **NpIIIb** requires some excess of the excitation energy. That is why for photogeneration of this latter form the irradiation of the matrixes with shorter-wavelength UV light was necessary.

In this work, the assignment of obtained IR spectra of almost all tautomeric forms of the studied compounds was carried out. This was performed as for tautomers initially present in low-temperature matrices, as for the spectra of photoproducts populated in the matrix upon UV irradiation. In this purpose, the experimental spectra were compared with the spectra theoretically simulated with help of quantum-mechanical calculations at DFT(B3LYP) level. The good agreement allowed assignment of experimental absorption bands to the normal modes calculated for theoretically predicted spectra. Theoretical analysis of the normal modes was carried out for each compound, and with help of calculated matrix elements of potential energy distribution, the forms of vibrations connected with absorption bands were described.

The relative electronic energies of the most stable tautomers of the studied molecules were theoretically estimated using QCISD method (for geometry optimized at the DFT(B3LYP) level).The comparison of obtained data with experimentally assessed values of ΔE showed that this method predicts well not only the shifts of tautomeric equilibria for the studied compounds, but provides also a reliable values (withing an accuracy of a few kJ mol^{-1}) for calculated energy differences between tautomers of a given compound. This method gave results closer to experiment than MP2 calculations for 2-pyridinone, however, it seems that for 9-methylhypoxanthine and hypoxanthine MP2 results are better. The accurate calculations of molecule stability needs more advanced theoretical method.

References

[1]. M.K. Shukla, J. Leszczynski, *J. Biomol. Struct.Dynam.* **25** (2007) 93.

[2]. J.L. Ravanat, T. Douki, J. Cadet, *J. Photochem. Photobiol. B* **63** (2001) 88.

[3]. J. Cadet, E. Sage, T. Douki, *Mutat. Res*. **571** (2005) 3.

[4]. G.P. Pfeifer, Y.-H. You, A. Besaratinia, *Mutat. Res*. **571** (2005) 19.

[5]. J.-M. L. Pecourt, J. Peon, B. Kohler, *J. Am. Chem. Soc.* **122** (2000) 9172.

[6]. C.E. Crespo-Hernández, B. Cohen, P.M. Hare, B. Kohler, *Chem. Rev.* **104** (2004) 1977.

[7]. L. Blancafort, M.A. Robb, *J. Phys. Chem. A* **108** (2004) 10609.

[8]. I.R. Gould, M.A. Vincent, I.H. Hillier, L.Lapinski, M.J. Nowak, *Spectrochem. Acta A* **48** (1992) 811.

[9]. A. Les, L. Adamowicz, M.J. Nowak, L. Lapinski, *Spectrochem. Acta A* **48** (1992) 1385.

[10]. M.J. Nowak, L. Lapinski, J.S. Kwiatkowski, J. Leszczynski, *J. Phys. Chem.* **100** (1996) 3527.

[11]. M.J. Nowak, L. Lapinski, D.C. Bienko, D. Michalska, *Spectrochem. Acta A* **53** (1997) 855.

[12]. R.P. Sinha, D.P. Hader, *Photochem. Photobiol. Sci.* **1** (2002) 225.

[13]. R.B.Setlow, W.L. Carrier, *J. Mol. Biol.* **17** (1966) 237.

[14]. W. Saenger, *Principles of Nucleic Acid Structures*; Springer-Verlag: New York, 1984.

[15]. J.D. Watson and F.H.C. Crick, *Nature* **171** (1953) 737.

[16]. M.D. Topal, and J.R. Fresco, *Nature* **263** (1976) 285.

[17]. G.V. Fazakerley, Z. Gdaniec, L.C. Sowers, *J. Mol. Biol.* **230** (1993) 6.

[18]. L. Lapinski, H. Rostkowska, A. Khvorostov, R. Fausto, M.J. Nowak, *J. Phys. Chem. A* **107** (2003) 5913.

[19]. S. Perun, A.L. Sobolewski, W. Domcke, *J. Phys. Chem. A* **110** (2006) 9031.

[20]. T. Schultz, E. Samoylova, W. Radloff, I.V. Hertel, A.L. Sobolewski, W. Domcke, *Science* **306** (2004) 1765.

[21]. S. Scheiner, *J. Phys. Chem. A* **104** (2000) 5898.

[22]. G.M. Chaban, M.S. Gordon, *J. Phys. Chem. A* **103** (1999) 185.

[23]. L.M. Salter, G.M. Chaban, *J. Phys. Chem. A* **106** (2002) 4251.

[24]. M.K. Shukla, J. Leszczynski, *J. Phys. Chem. A* **109** (2005) 7775.

[25]. M.K. Shukla, J. Leszczynski, *Int. J. Quantum Chem.* **105** (2005) 387.

[26]. M.J. Nowak, J. Fulara, and L. Lapinski, *J. Mol. Struct.* **175** (1988) 91.

[27]. M.J. Nowak, L. Lapinski, J. Fulara, A. Leś, L. Adamowicz, *J. Phys. Chem.* **96** (1992) 1562.

[28]. L. Lapinski, J. Fulara, M.J. Nowak, *Spectrochem. Acta A* **46** (1990) 61.

[29]. L. Lapinski, M.J. Nowak, A. Les, L. Adamowicz, *J. Am. Chem. Soc.* **116** (1994) 1461.

[30]. L. Lapinski, J. Fulara, R. Czerminski, M.J. Nowak, *Spectrochem. Acta A* **46** (1990) 1087.

[31]. G. Maier, J. Endres, *Eur. J. Org. Chem.* **2000** (2000) 1061.

[32]. F. Duvernay, A. Trivella, F. Borget, S. Coussan, J.P. Aycard, T. Chiavassa, *J. Phys. Chem. A* **109** (2005) 11155.

[33]. F. Duvernay, P. Chatron-Michaut, F. Borget, D.M. Birney, T. Chiavassa, *Phys. Chem. Chem. Phys.* **9** (2007) 1099.

[34]. F. Duvernay, T. Chiavassa, F. Borget, J.-P. Aycard, *J. Phys. Chem. A* **109** (2005) 6008.

[35]. M.J. Nowak, L. Lapinski, H. Rostkowska, A. Les, L. Adamowicz, *J. Phys. Chem*. **94** (1990) 7406.

[36]. M.J. Nowak, L. Lapinski, J. Fulara, A. Les, L. Adamowicz, *J. Phys. Chem*. **95** (1991) 2404.

[37]. D. Prusinowska, L. Lapinski, M.J. Nowak, L. Adamowicz, *Spectrochim. Acta A* **51** (1995) 1809.

[38]. A. Khvorostov, L. Lapinski, H. Rostkowska, and M.J. Nowak, *J. Phys. Chem. A* **109** (2005) 7700.

[39]. L. Lapinski, M.J. Nowak, R. Kołos, J.S. Kwiatkowski, J. Leszczyński, *Spectrochim. Acta A* **54** (1998) 685.

[40]. M.J. Nowak, L. Lapinski, and J. Fulara, *Spectrochim. Acta A* **45** (1989) 229.

[41]. L. Lapinski, M.J. Nowak, J. Fulara, A. Les, L. Adamowicz, *J. Phys. Chem.* **94** (1990) 6555.

[42]. H. Vranken, J. Smets, G. Maes, L. Lapinski, M.J. Nowak, *Spectrochim. Acta A* **50** (1994) 875.

[43]. F.H.C. Crick, L. Barnett, S. Brenner, R. J. Watts-Tobin, *Nature* **192** (1961) 1227.

[44]. S. Nishimura, D.S. Jones, H.G. Khorana, *J. Mol. Biol.* **13** (1965) 302.

[45]. T.H. Jukes, *Adv. Enzymol.* **47** (1978) 375.

[46]. R.W. Holley, G.A. Everett, J.T. Madison, A. Zamir, *J. Biol. Chem.* **240** (1965) 2122.

[47]. H. Grosjean, S. Auxilien, F. Constantinesco, C. Simon, Y. Corda, H.F. Becker, D. Foiret, A. Morin, Y.X. Jin, M. Fournier, J.L. Fourrey, *Biochimie* **78** (1996) 488.

[48]. L. Stryer, *Biochemistry*; 4th edition,W.H. Freeman and Company: New York: 1995.

[49]. J.L. Smith, *Curr. Opin. Struct. Biol.* **5** (1995) 752.

[50]. P.G. Reid, A.H. Watt, P.A. Routledge, and A.P. Smith, *Br. J. Clin. Pharmacol.* **23** (1987) 331.

[51]. M.H. Williams, R.B. Kreider, D.W. Hunter, C.T. Somma, L.M. Shall, M.L. Woodhouse, L. Rokitski, *Med. Sci. Sports Exerc.* **22** (1990) 517.

[52]. L. McNaughton, B. Dalton, J. Tarr, *Int. J. Sport Nutr.* **9** (1999) 333.

[53]. S. Spitsin, D.C. Hooper, T. Leist, L.J. Streletz, T. Mikheeva, H. Koprowskil, *Mult. Scler.* **7** (2001) 313.

[54]. A. Juhasz-Nagy, and D.M. Aviado, *J. Pharmacol. Exp. Ther.* **202** (1977) 683.

[55]. G. Haskó, M.V. Sitkovsky and C. Szabó, *Trends Pharmac. Sci.* **25** (2004) 152.

[56]. A. Wakai, D.C. Winter, J.T. Street, R.G. O'Sullivan, J.H. Wang, H.P. Redmond, *J. Surg. Res.* **99** (2001) 311.

[57]. R.L. Wortmann, *Curr. Opin. Rheumatol.* **17** (2005) 319.

[58]. R.L. Wortmann, *Curr. Opin. Rheumatol.* **14** (2002) 281.

[59]. E. Pea, *Contrib. Nephrol.* **147** (2005) 35.

[60]. G. Bellinghieri, D. Santoro, V. Savica, *Contrib. Nephrol.* **147** (2005) 149.

[61]. B.T. Emmerson, *New Engl. J. Med.* **334** (1996) 445.

[62]. N. Schlesinger, *Drugs* **64** (2004) 2399.

[63]. M.S. Cairo, M. Bishop, *Br. J. Haematol.* **127** (2004) 3.

[64]. M.T. Holdsworth, P. Nguyen, *Am. J. Health-Syst. Pharm.* **60** (2003) 2213.

[65]. F. Mellin, C. Monteil, M. Isabelle, B. Di Melgio, J.P. Henry, C. Thuillez, P. Mulder, *Free Radic. Biol. Med.* **37** (Suppl. 1) (2004) S39.

[66]. W. Guan, T. Osanai, T. Kamada, H. Hanada, H. Ishizaka, H. Onodera, A. Iwasa, N. Fujita, S. Kudo, T. Ohkubo, K. Okumura, *J. Cardiovasc. Pharmacol.* **41** (2003) 699.

[67]. N.A. Weimert, W.F. Tanke, J.J. Sims, *Ann. Pharmacother.* **37** (2003) 1708.

[68]. A. Movahed, K. Nair, T.F. Ashavaid, P. Kumar, *Can. J. Cardiol.* **12** (1996) 138.

[69]. R. Machado-Vieira, F. Kapczinski, D.O. Souza, D.R. Lara, J.C. Soares, *Bipolar Disord.* **7** (Suppl. 2) (2005) 73.

[70]. S. Akhondzadeh, A. Safarcherati, H. Amini, *Prog. Neuro-Psychopharmacol.* **29** (2005) 253.

[71]. H.J. Roth and H. Fenner, Arzneistoffe (3rd ed.), Deutscher Apotheker Verlag: Stuttgart, 2000, pp. 51–114.

[72]. K. Mekouar, J.F. Mouscadet, D. Desmaele, F. Subra, H. Leh, D. Savoure, C. Auclair and J. d'Angelo, *J. Med. Chem.* **41** (1998) 2846.

[73]. F. Zouhiri, M. Danet, C. Bernard, M. Normand-Bayle, J.F. Mouscadet, H. Leh, C.M. Thomas, G. Mbemba, J. d'Angelo and D. Desmaele, *Tetrahedron Lett.* **46** (2005) 2201.

[74]. Y. Pommier, A.A. Johnson and C. Marchand, *Nat. Rev. Drug. Discov.* **4** (2005) 236.

[75]. J. Polanski, F. Zouhiri, L. Jeanson, D. Desmaele, J. d'Angelo, J. Mouscadet, R. Gieleciak, J. Gasteiger, M.L. Bret, *J. Med. Chem.* **45** (2002) 4647.

[76]. R.S. Becker, S. Chakravorti, C.A. Gartner, M. de Graca Miguel, *J. Chem. Soc., Faraday Trans.* **89** (1993) 1007.

[77]. U. Brackmann, Lambdachrome® Laser Dyes, Lambda Physik GmbH: Göttingen, 1986.

[78]. B.B. Snavely, in: J.B. Birks (Ed.), *Organic Molecular Photophysics*, 1, John Wiley and Sons: London, 1973 Chapter 5.

[79]. C.V. Shank, A. Dienes, A.M. Trozzolo, J.A. Myer, *Appl. Phys. Lett.* **16** (1970) 405.

[80]. G.A. Reynolds, K.-H. Drexhage, *Opt. Commun.* **13** (1975) 222.

[81]. A.N. Fletcher, D.E. Bliss, J.M. Kauffman, *Opt. Commun.* **47** (1983) 57.

[82]. H.H. Grunhagen, H.T. Witt, *Z. Naturforsch. B* **25** (1970) 373.

[83]. R.P. Haughland, in K.D. Larison (Ed.), *Handbook of Fluorescent Probes and Research Chemicals*, Molecular Probes Inc, Eugene, USA, 1992.

[84]. J.M. Kauffiman, G.S. Bajwa, P.T. Litak, C.J. Kelley, R. Pai, *Proceedings of the Conference on Scintillating and Fiber Detectors*, 1997.

[85]. P.R. Selvin, T.M. Rana, and J.E. Hearst, *J. Am.Chem. Soc.* **116** (1994) 6029.

[86]. M. Li, P.R. Selvin, *Bioconjugate Chem.* **8** (1997) 127.

[87]. A. Rieutord, P. Prognon, F. Brion, G. Mahuzier, *Analyst* **122** (1997) 59R.

[88]. G. Jürgens, A. Hermann, D. Aktuna, W. Petek, *Clin. Chem.* **38** (1992) 853.

[89]. C. Tzougraki, C. Noula, R. Geiger, G. Kokotos, *Liebigs Ann. Chem.* **4** (1994) 365.

[90]. T. Besson, B. Joseph, P. Moreau, M.-C. Viaud, G. Coudert, G. Guillaumet, *Heterocycles* **34** (1992) 273.

[91]. C.J. Burrows, J.G. Muller, *Chem. Rev.* **98** (1998) 1109.

[92]. J. Cadet, M. Berger, T. Douki, J.-L. Ravanat, *Mutat. Res.* **531** (2003) 5.

[93]. E. Pelle, X. Huang, T. Mammone, K. Marenus, D. Maes, K. Frenkel, *J. Invest. Dermatol.* **121** (2003) 177.

[94]. C. Walling, *Acc. Chem. Res.* **8** (1975) 125.

[95]. B. Epe, D. Ballmaier, W. Adam, G. N. Grimm, C.R. Saha-Möller, *Nucleic. Acids Res.* **24** (1996) 1625.

[96]. S.G. Chaulk, J.P. Pezacki, A.M. MacMillan, *Biochemistry* **39** (2000) 10448.

[97]. D. Tobin, M. Arvanitidis, R.H. Bisby, *Biochem. Biophys. Res. Commun.* **299** (2002) 155.

[98]. W. Adam, D. Ballmaier, B. Epe, G.N. Grimm, C.R. Saha-Möller, *Angew. Chem. Int. Ed. Engl.* **34** (1995) 2156.

[99]. J. Boivin, E. Crepon, S. Zard, *Tetrahedron Lett.* **31** (1990) 6869.

[100]. D.H.R. Barton, J.C. Jaszberenyi, A.I. Morell, *Tetrahedron Lett.* **32** (1991) 311.

[101]. K.M. Hess, T.A. Dix, *Anal. Biochem.* **206** (1992) 309.

[102]. B.M. Aveline, I.E. Kochevar, R.W. Redmond, *J. Am. Chem. Soc.* **118** (1996) 10113.

[103]. B.M. Aveline, I.E. Kochevar, R.W. Redmond, *J. Am. Chem. Soc.* **118** (1996) 289.

[104]. B.M. Aveline, I.E. Kochevar, R.W. Redmond, *J. Am. Chem. Soc.* **118** (1996) 10124.

[105]. P.G.E. Evans, J.K. Sudgen, N.J. Van Abbe, *Pharm. Acta Helv.* **50** (1975) 94.

[106]. R.A. Neihof, C.A. Bailey, C. Patouillet, P.J. Hannan, *Arch. Environ. Contam. Toxicol.* **8** (1979) 355.

[107]. B.L. Barnett, H.C. Kretshmar, F.A. Hartman, *Inorg. Chem.* **16** (1977) 1834.

[108]. J. Blatt, S.R. Taylor, G.J. Kontoghiorghes, *Cancer. Res.* **49** (1989) 2925.

[109]. J. Balzarini, M. Stevens, E. De Clercq, D. Schols and C. Pannecouque, *J. Antimicrob. Chemother.* **55** (2005) 135.

[110]. L. Vegard, *Nature* **113** (1924) 716.

[111]. L. Vegard, *Nature* **114** (1924) 357.

[112]. E. Whittle, D.A. Dows, G.C. Pimentel, *J. Chem. Phys.* **22** (1954) 1943.

[113]. V.E. Bondybey, L.E. Brus, *Nonradiative processes in small molecules in low-temperature solids*; in *Advances in Chemical Physics*, Prigogine, R., Rice S.A., Eds.: John Wiley & Sons: New York, 1980, Vol.41.

[114]. A.R. Katritzky, MJ. Karelson, P.A. Harris, *Heterocycles* **32** (1991) 329.

[115]. A. Gordon, A.R. Katritzky, *Tetrahedron Lett.* **9** (1968) 2767.

[116]. E.S. Levin, G.N. Radionova; *Dokl. Chem.* (Eng. Transl.) **164** (1965) 910.

[117]. E.F. Caldin and V. Gold, *Proton-transfer Reactions*; Chapmann and Hall: London, 1975.

[118]. A. Douhal, *J. Phys. Chem.* **98** (1994) 13131.

[119]. A.B. Kotlyar, N. Borovok, S. Nachliet and M. Gutman, *Biochem.* **33** (1994) 873.

[120]. S. Lochbrunner, A. J. Wurzer, E. Riedle, *J. Chem. Phys.* **112** (2000) 10699.

[121]. S. Lochbrunner, K. Stock, E. Riedle, *J. Mol. Struct.*, **700** (2004) 13.

[122]. S. Nagaoka, J. Kusunoki, T. Fujibuchi, S. Hatakenaka, K. Mukai, U. Nagashima, *J. Photochem. Photobiol. A* **122** (1999) 151.

[123]. V. Guallar, V.S. Batista, W.H. Miller *J. Chem. Phys.* **113** (2000) 9510.

[124]. P.J. Wagner, *Acc. Chem. Res.* **4** (1971) 168.

[125]. P.J. Wagner, in *CRC Handbook of Organic Photochemistry and Photobiology*; Hoorspool, W. R., Ed.; CRC

[126]. A. Douhal, F. Lahmani, A. H. Zewail, *Chem. Phys.* **207** (1996) 477.

[127]. Y. Tsuchiya, T. Tamura, M. Fujii and M. Ito, *J. Phys. Chem.* **92** (1988) 1760.

[128]. M.R. Nimlos, D.F. Kelly and E.R. Bernstein, *J. Phys. Chem.* **93** (1989) 643.

[129]. A. Held and D.W. Pratt, *J. Am. Chem. Soc.* **112** (1990) 8629.

[130]. N. Akai, K. Ohno, M. Aida, *Chem. Phys. Lett.* **413** (2005) 306.

[131]. N. Akai, T. Harada, K. Shin-ya, K. Ohno, M. Aida, *J. Phys. Chem. A* **110** (2006) 6016.

[132]. N. Akai, K. Ohno, M. Aida, *J. Photochem. Photobiol. A* **187** (2007) 113.

[133]. L. Lapinski, M.J. Nowak, J.S. Kwiatkowski, J. Leszczynski, *J. Phys. Chem. A* **103** (1999) 280.

[134]. A.L. Sobolewski, W. Domcke, C. Dedonder-Lardeux and C. Jouvet, *Phys. Chem. Chem. Phys.* **4** (2002) 1093.

[135]. A.L. Sobolewski and W. Domcke, *Chem. Phys.* **259** (2000) 181.

[136]. W. Domcke and A.L. Sobolewski, *Science* **302** (2003) 1693.

[137]. C. Dedonder-Lardeux, C. Jouvet, S. Perun, A. L. Sobolewski, *Phys. Chem. Chem. Phys.* **5** (2003) 5118.

[138]. J. Wei, A. Kuczman, J. Reidel, F. Renth and F. Temps, *Phys. Chem. Chem. Phys.* **5** (2003) 315.

[139]. G. Karmas, P. Spoeri, *J. Am. Chem. Soc.* **74** (1952) 1580.

[140]. T. Kanakahara, Y. Takagi, *Heterocycles* **9** (1978) 1733.

[141]. R.G. Jones, *J. Am. Chem. Soc.* **71** (1949) 78.

[142]. C. Møller, M.S. Plesset, *Phys. Rev.* **46** (1934) 618.

[143]. J.A. Pople, M. Head-Gordon, K. Raghavachari, *J. Chem. Phys.* **87** (1987) 5968.

[144]. E.A. Salter, G.W. Trucks, R.J. Bartlett, *J. Chem. Phys.* **90** (1989) 1752.

[145]. J. Gauss, J.F. Stanton, R.J. Bartlett, *J. Chem. Phys.* **95** (1991) 2623.

[146]. R.G. Parr, W. Yang, *Density-functional Theory of Atoms and Molecules*; Oxford University Press: New York, 1989.

[147]. A. Becke, *Phys. Rev.* **A38** (1988) 3098.

[148]. C.T. Lee, W.T. Yang, R.G. Parr, *Phys. Rev. B* **37** (1988) 785.

[149]. M. Piacenza, S. Grimme, *J. Comput. Chem.* **25** (2004) 83.

[150]. L.D. Hatherley, R.D. Brown, P.D. Godfrey, A.P. Pierlot, W. Caminati, D. Damiani, S. Melandri, L.B. Favero, *J. Phys. Chem.* **97** (1993) 46.

[151]. R. Ahlrichs, P.R. Taylor, *J. Chem. Phys.* **78** (1981) 315.

[152]. J. Andzelm, M. Klobukowski, E. Radzio-Andzelm, Y. Saski, H. Tatewaki, *Gaussian Basis Sets for Molecular Calculations*; ed. S. Huzinaga; Elsevier: Amsterdam, 1984.

[153]. T.H. Dunning, P.J. Hay, *Gaussian basis sets for molecular calculations*; in: *Modern Theoretical Chemistry*, Vol. 3; ed. H.F. Schaefer, III, pp. 1-28, Plenum Press, New York, 1977.

[154]. D. Feller, E.R. Davidson, *Chem. Rev.* **86** (1986) 681.

[155]. D. Feller, E.R. Davidson, *Basis Sets for Ab Initio Molecular Orbital Calculations and Intermolecular Interactions*; pp.1-43, in *Reviews in Computational Chemistry*, eds. Kenny B. Lipkowitz and Donald B. Boyd,VCH, N.Y., 1990.

[156]. R. Poirier, R. Kari, I.G. Csizmadia, *Handbook of Gaussian Basis Sets*; Elsevier Science, N.Y., 1985.

[157]. S. Wilson, *Basis sets*; in *Ab-initio Methods in Quantum Chemistry*, ed. K.P. Lawley; Wiley: Chichester, 1987.

[158]. R. Ditchfield, W.J. Hehre and J.A. Pople, *J. Chem. Phys.* **54** (1971) 724.

[159]. W.J. Hehre, R. Ditchfield and J. A. Pople, *J. Chem. Phys.* **56** (1972) 2257.

[160]. V.A. Rassolov, M.A. Ratner, J.A. Pople, P.C. Redfern and L.A. Curtiss, *J. Comp. Chem.* **22** (2001) 976.

[161]. T.H. Dunning Jr., *J. Chem. Phys.* **90** (1989) 1007.

[162]. M.M. Francl, W.J. Pietro, W.J. Hehre, J.S. Binkley, M.S. Gordon, D.J. DeFrees, J.A. Pople, *J. Chem. Phys.* **77** (1982) 3654.

[163]. M. Gutowski, F.B. Van Duijneveldt, G. Chalasinski, L. Piela, *Mol. Phys*. **61** (1987) 233.

[164]. K. Jankowski, R. Becherer, P. Scharf, H. Schier, R. Ahlrichs, *J. Chem. Phys.* **82** (1985) 1413.

[165]. R. Krishnan, J.S. Binkley, R. Seeger, J.A. Pople, *J. Chem. Phys*. **72** (1980) 650.

[166]. T. Clark, J. Chandrasekhar, G.W. Spitznagel, P.V.R. Schleyer, *J. Comp. Chem.* **4** (1983) 294.

[167]. M.J. Frisch, J.A. Pople, J.S. Binkley, *J. Chem. Phys.* **80** (1984) 3265.

[168]. J.E. Del Bene, *J. Comput. Chem.* **10** (1989) 603.

[169]. D.E. Woon, T.H. Dunning, Jr. *J. Chem. Phys.* **98** (1993) 1358.

[170]. E.B. Wilson, J.C. Decius, P.C. Cross, *Molecular Vibrations*; McGraw-Hill, N.Y., 1955.

[171]. B. Wojtkowiak, M. Chabanel, *Spektroskopia molekularna*; PWN: Warszawa, 1984.

[172]. P. Pulay, G. Fogarasi, F. Pang, J.E. Boggs, *J. Am. Chem. Soc.* **101** (1979) 2550.

[173]. J.H. Schachtschneider, Technical Report, Shell Development Co., Emeryville, CA, 1969.

[174]. S. Califano, *Vibrational States*; Wiley: N.Y., 1976.

[175]. G. Keresztury, G. Jalsovszky, *J. Mol. Struct.* **10** (1971) 304.

[176]. M.J. Frisch, G.W. Trucks, H.B. Schlegel, G.E. Scuseria, M.A. Robb, J.R. Cheeseman, J.A. Montgomery Jr., T. Vreven, K.N. Kudin, J.C. Burant, J.M. Millam, S.S. Iyengar, J. Tomasi, V. Barone, B. Mennucci, M. Cossi, G. Scalmani, N. Rega, G.A. Petersson, H. Nakatsuji, M. Hada, M. Ehara, K. Toyota, R. Fukuda, J. Hasegawa, M. Ishida, T. Nakajima, Y. Honda, O. Kitao, H. Nakai, M. Klene, X. Li, J.E. Knox, H.P. Hratchian, J.B. Cross, V. Bakken, C. Adamo, J. Jaramillo, R. Gomperts, R.E. Stratmann, O. Yazyev, A.J. Austin, R. Cammi, C. Pomelli, J.W. Ochterski, P.Y. Ayala, K. Morokuma, G.A. Voth, P. Salvador, J.J. Dannenberg,

V.G. Zakrzewski, S. Dapprich, A.D. Daniels, M.C. Strain, O. Farkas, D.K. Malick, A.D. Rabuck, K. Raghavachari, J.B. Foresman, J.V. Ortiz, Q. Cui, A.G. Baboul, S. Clifford, J. Cioslowski, B.B. Stefanov, G. Liu, A. Liashenko, P. Piskorz, I. Komaromi, R.L. Martin, D.J. Fox, T. Keith, M.A. Al-Laham, C.Y. Peng, A. Nanayakkara, M. Challacombe, P.M.W. Gill, B. Johnson, W. Chen, M.W. Wong, C. Gonzalez, J.A. Pople, *Gaussian 03*, revision C.02; Gaussian, Inc.: Wallingford, CT, 2004.

[177]. G.-S. Li, M.F. Ruiz-López, M.-S. Zhang, B. Maigret, *J. Mol. Struct. (THEOCHEM)* **422** (1998) 197.

[178]. C. Krebs, H.J. Hofmann, H.J. Köhler, C. Weiss, *Chem. Phys. Lett.* **69** (1980) 537.

[179]. J.S. Kwiatkowski, T.J. Zielinski, R. Rein, *Advan. Quantum Chem.* **18** (1986) 85.

[180]. J.S. Kwiatkowski, R.J. Barlett, W.B. Person, *J. Am. Chem. Soc.* **110** (1988) 2353.

[181]. P. Beak, *Accounts. Chem. Res.* **10** (1977) 186.

[182]. P. Beak, F.S. Fry, J. Lee, F. Steele, *J. Am. Chem. Soc.* **98** (1976) 171.

[183]. P. Beak, F.S. Fry, *J. Am. Chem. Soc.* **95** (1973) 1700.

[184]. R.S. Brown, A. Tse, J.C. Vederas, *J. Am. Chem. Soc.* **102** (1980) 1174.

[185]. A. Gerega, L. Lapinski, M. J. Nowak, A. Furmanchuk, and J. Leszczynski, *J. Phys. Chem. A* **111** (2007) 4934.

[186]. C. Guimon, G. Garrabe, G. Pfister-Guillouzo, *Tetrahedron Lett.* **20** (1979) 2585.

[187]. S. Furnberg, J. Sollbakk, *Acta Chem. Scand*. **24** (1970) 3230.

[188]. M. Chevrier, O. Bensaude, J. Guillerez and J.-E. Dubois, *Tetrahedron Lett.* **21** (1980) 3359.

[189]. L. Lapinski, M.J. Nowak, A. Leś, L. Adamowicz, *Vibration. Spectrosc.* **8** (1995) 331.

[190]. R. Sanchez, B.M. Guiliano, S. Melandri, L.B. Favero and W. Caminati, *J. Am. Chem. Soc.* **129** (2007) 6287.

[191]. L. Lapinski, M.J. Nowak, J. Fulara, A. Leś and Ludwik Adamowicz, *J. Phys. Chem.* **96** (1992) 6250.

[192]. A. Held, D.F. Plusquellic, J.L. Tomer, D.W. Patt, *J. Phys. Chem.* **95** (1991) 2877.

[193]. W.M.F. Fabian, K.S. Niederreiter, G. Uray, W. Stadlbauer, *J. Mol. Struct.* **477** (1999) 209.

[194]. M.R. Nimlos, D.F. Kelley, E.R. Bernstein, *J. Phys. Chem.* **91** (1987) 6610.

[195]. A. Gerega, L. Lapinski, I. Reva, H. Rostkowska, M.J. Nowak, *Biophys. Chem.* **122** (2006) 123.

[196]. O. Huertas, J.R. Blas, I. Soteras, M. Orozco, F.J. Luque, *J. Phys. Chem. A* **110** (2006) 510.

[197]. A. Gerega, L. Lapinski, M.J. Nowak, H. Rostkowska, *J. Phys. Chem. A* **110** (2006) 10236.

[198]. A.T. Balaban, D.C. Oniciu, A.R. Katritzky, *Chem. Rev.* **104** (2004) 2777.

[199]. P. Prusiner, M. Sundaralingam, *Acta Crystallogr. B* **28** (1972) 2148.

[200]. A. Torreggiani, M. Tamba, A. Trinchero, G. Fini, *J. Mol. Struct.* **651−653** (2003) 91.

[201]. M.K. Shukla, P.C. Mishra, *Spectrochim. Acta A* **52** (1996) 1547.

[202]. M.T. Chenon, R.J. Pugmire, D.M. Grant, R.P. Panzica, L.B. Townsend, *J. Heterocycl. Chem.* **10** (1973) 431.

[203]. M.E. Costas, R. Acevedo-Chavez, *J. Comput. Chem.* **20** (1999) 200.

[204]. B. Hernandez, F.J. Luque, M. Orozco, *J. Org. Chem.* **61** (1996) 5964.

[205]. S. Breda, I. Reva, L. Lapinski, R. Fausto, *Phys. Chem. Chem. Phys*. **6** (2004) 929.

[206]. R.H. Fish, G. Jaouen*, Organometallics* **22** (2003) 2166.

[207]. E. Freisinger, I.B. Rother, M.S. Lüth, B. Lippert, *PNAS* **100** (2003) 3748.

[208]. J. Lin, C. Yu, S. Peng, I. Akiyama, K. Li, Li Kao Lee, P.R. LeBreton, *J. Phys. Chem.* **84** (1980) 1006.

[209]. A.R.I. Munns, P. Tollin, *Acta Crystallogr. B* **26** (1970) 1101.

[210]. M.E. Costas, R. Acevedo-Chávez, *J. Phys. Chem. A* **101** (1997) 8309.

[211]. R. Ramaekers, G. Maes, L. Adamowicz, A. Dkhissi, *J. Mol. Struct.* **560** (2001) 205.

[212]. M.K. Shukla, J. Leszczynski, *THEOCHEM* **529** (2000) 99.

[213]. M.L. San Roman-Zimbron, M.E. Costas, R. Acevedo-Chavez, *THEOCHEM* **711** (2004) 83.

[214]. D. Lichtenberg, F. Bergmann, Z. Neiman, *Isr. J. Chem.* **10** (1972) 805.

[215]. G.G. Sheina, S.G. Stephanian, E.D. Radchenko, Y.P. Blagoi, *J. Mol. Struct.* **158** (1987) 275.

[216]. H.W. Schmalle, G. Hänggi, E. Dubler, *Acta Crystallogr. C* **44** (1988) 732.

[217]. J. Sponer, J. Leszczynski, *Struct. Chem.* **6** (1995) 281.

[218]. M.K. Shukla, P.C. Mishra, *J. Mol. Struct.* **324** (1994) 241.

[219]. M.T. Chenon, R.J. Pugmire, D.M. Grant, R.P. Panzica, L.B. Townsend, *J. Am. Chem. Soc.* **97** (1975) 4636.

[220]. B. Pullman, A. Pullman, *Adv. Heterocycl. Chem.* 13 (1971) 77.

[221]. R. Ramaekers, A. Dkhissi, L. Adamowicz, G. Maes, *J. Phys.Chem. A* **106** (2002) 4502.

[222]. J.G. Contreras, J.B. Alderete, *Mol. Engng*. **2** (1992) 29.

[223]. M. Nonella, G. Hänggi, E. Dubler, *J. Mol. Struct. (THEOCHEM)* **279** (1993) 173.

[224]. A. Bond, W. Jones, *Acta Cryst. C* **55** (1999) 1536.

[225]. H. Rostkowska, M.J. Nowak, L. Lapinski, L. Adamowicz, *Phys.Chem. Chem. Phys.* **3** (2001) 3012.

[226]. L. Khriachtchev, M. Pettersson, S. Tuominen, M. Rasanen, *J.Chem. Phys.* **107** (1997) 7252.

[227]. A. Engdahl, G. Karlstrom, B.Nelander, *J. Chem. Phys.* **118** (2003) 7797.

[228]. Z.Mielke, A.Olbert-Majkut, K.G. Tokhadze, *J. Chem. Phys.* **118** (2003) 1364.

[229]. A. Olbert-Majkut, Z.Mielke, K.G. Tokhadze,. *J. Mol. Struct.* **665** (2003) 321.

[230]. B.-M. Cheng, Y.-P.Lee, J.F. Ogilvie, *Chem. Phys. Lett.* **151** (1988) 109.

[231]. L. Lapinski, A. Gerega, A.L. Sobolewski and M.J. Nowak, *J. Phys. Chem. A* **112** (2008) 238.

[232]. T.M. Krygowski, M.K. Cyrañski, Z. Czarnocki, G. Häfelinger and A.R. Katritzky, *Tetrahedron* ***56*** (2000) 1783.

[233]. K. Jug, D.C. Oniciu, A.R. Katritzky, *Chem. Rev.* **101 (**2001) 1421.

[234]. A.R. Katritzky, MJ. Karelson, P.A. Harris; *Heterocycles* **32** (1991) 329.

[235]. A.R. Katritzky, M. Karelson, S. Sild, T.M. Krygowski, and K. Jug, *J. Org. Chem*. **63** (1998) 5228.

[236]. A.R. Katritzky, M. Karelson, and N. Malhotra, *Heterocycles* **32** (1991) 127.

[237]. A.R. Katritzky, *Handbook of Heterocyclic Chemistry*; Pergamon Press: Oxford, 1985.

[238]. T. Eicher, S. Hauptmann, *The Chemistry of Heterocycles. Structure, Reactions, Syntheses, and Applications*; Georg Thieme Verlag: Stuttgart, 1995.

[239]. A.R Katritzky, A.F.Pozharskii, *Handbook of Heterocyclic Chemistry*, 2nd ed.; Pergamon Press: Oxford, 2000.

[240]. K.B. Wiberg, Aromaticity and its Chemical Manifestations. In *Pauling's Legacy: Modern Modeling of the Chemical Bond*; Z.B.Macsić, W.J. Orville-Thomas, Eds.; Elsevier: Amsterdam, 1999; p 519.

[241]. V.I. Minkin, M.N. Glukhovtsev, B.Ya. Simkin, *Aromaticity and Antiaromaticity. Electronic and Structural Aspects*; Wiley-Interscience: New York, 1994.

[242]. M.J. Nowak, L. Lapinski, J.S. Kwiatkowski, J. Leszczyński, *Spectrochem. Acta A* **47** (1991) 1006.

[243]. M.J. Nowak, H. Rostkowska, L. Lapinski, J.S. Kwiatkowski, J. Leszczyński, *Spectrochem. Acta A* **50** (1994) 1081.

[244]. M.J. Nowak, H. Rostkowska, L. Lapinski, J.S. Kwiatkowski, J. Leszczyński, *J. Phys. Chem.* **98** (1994) 2813.

Appendix

This Section contains:

- Schemes of molecular structures with atom numbering for the studied compounds: 2-pyridinone, 4-pyrimidinone and 2-pyrazinone (Appendix A), 2-quinoxalinone, 2-quinolinone, 1-isoquinolinone, 4-quinazolinone and 3-hydroxyisoquinoline (Appendix B), allopurinol, 9-methylhypoxanthine and hypoxanthine (Appendix C), and *N*-hydroxypyridine-2(1*H*)-thione (Appendix D).

- The tables are presented providing definitions of the internal coordinates used in the normal mode analysis carried out for the tautomers of these compounds. In these tables $r_{i,j}$ is the distance between atoms A_i and A_j; $\beta_{i,j,k}$ is the angle between vectors A_kA_i and A_kA_j; $\tau_{i,j,k,l}$ is the dihedral angle between the plane defined by A_i, A_j, A_k and the plane defined by A_j, A_k, A_l atoms; $\gamma_{i,j,k,l}$ is the angle between the vector A_kA_i and the plane defined by atoms A_j, A_k, A_l. a = cos 144º= -0.8090; b = cos 72º = 0.3090.

- The tables providing wavenumbers and relative intensities of observed absorption bands compared with theoretical predictions of the infrared spectra (including the PED analysis of the normal modes) of the oxo and hydroxy tautomers of the compounds are also presented. In these tables, integral intensities of the observed spectral bands are given in arbitrary units. Theoretical calculations carried out at DFT(B3LYP) level, using different basis sets: cc-pVTZ for compounds in Appendices A and B, 6-31++(d,p) for the compounds in Appendices C and D. The theoretical positions of absorption bands were scaled down by a factor of 0.98. PED's lower than 10% are not included. Wavenumbers of the strongest components of split bands are bold.

Appendix A

Spectroscopic data of systems with one heterocyclic ring

2(1H)-pyridinone

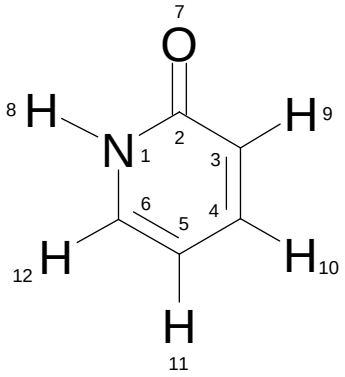

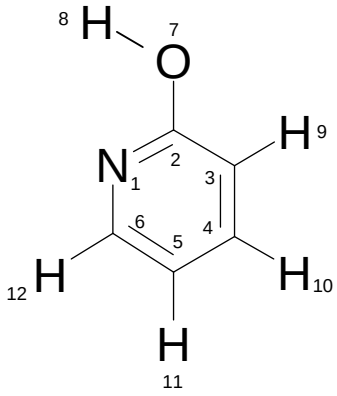

2(1H)-pyridinone

2PDo

2-hydroxypyridine

2PDh

Scheme A1*. Atom numbering for tautomers of 2-pyridinone.*

Table A1. *Internal coordinates used in the normal mode analysis for* ***2-pyridinone*** *and* ***2-hydroxypyridine*** *(atom numbering as in Scheme A1).*

In-plane		
Ring stretching		
$S_1 = r_{1,2}$		νN1C2
$S_2 = r_{2,3}$		νC2C3
$S_3 = r_{3,4}$		νC3C4
$S_4 = r_{4,5}$		νC4C5
$S_5 = r_{5,6}$		νC5C6
$S_6 = r_{6,1}$		νC6C1
Stretching NH, CO, CH		
$S_7 = r_{2,7}$		νCO
$S_8 = r_{1,8}$	oxo	νN1H
$S'_8 = r_{7,8}$	hydroxy	νOH
$S_9 = r_{3,9}$		νC3H
$S_{10} = r_{4,10}$		νC4H
$S_{11} = r_{5,11}$		νC5H
$S_{12} = r_{6,12}$		νC6H
Ring in-plane deformation		
$S_{13} = (6^{-1/2})(\beta_{6,2,1} - \beta_{1,3,2} + \beta_{2,4,3} - \beta_{3,5,4} + \beta_{4,6,5} - \beta_{5,1,6})$		βR1
$S_{14} = (12^{-1/2})(2\beta_{6,2,1} - \beta_{1,3,2} - \beta_{2,4,3} + 2\beta_{3,5,4} - \beta_{4,6,5} - \beta_{5,1,6})$		βR2
$S_{15} = (1/2)(\beta_{1,3,2} - \beta_{2,4,3} + \beta_{4,6,5} - \beta_{5,1,6})$		βR3
Bending CO, CH, NH, OH		
$S_{16} = (2^{-1/2})(\beta_{2,8,1} - \beta_{6,8,1})$	oxo	βN1H
$S'_{16} = \beta_{8,2,7}$	hydroxy	βOH
$S_{17} = (2^{-1/2})(\beta_{3,7,2} - \beta_{1,7,2})$		βCO
$S_{18} = (2^{-1/2})(\beta_{4,9,3} - \beta_{2,9,3})$		βC3H
$S_{19} = (2^{-1/2})(\beta_{5,10,4} - \beta_{3,10,4})$		βC4H
$S_{20} = (2^{-1/2})(\beta_{6,11,5} - \beta_{4,11,5})$		βC5H
$S_{21} = (2^{-1/2})(\beta_{1,12,6} - \beta_{5,12,6})$		βC6H
Out-of-plane		
Wagging CO, NH, CH		
$S_{22} = \gamma_{7,1,2,3}$		γCO
$S_{23} = \gamma_{9,2,3,4}$		γC3H
$S_{24} = \gamma_{10,3,4,5}$		γC4H
$S_{25} = \gamma_{11,4,5,6}$		γC5H
$S_{26} = \gamma_{12,5,6,1}$		γC6H
$S_{27} = \gamma_{8,6,1,2}$	oxo	γN1H
Torsion OH		
$S'_{27} = (2^{-1/2})(\tau_{8,7,2,3} + \tau_{8,7,2,1})$	hydroxy	τOH
Ring torsion		
$S_{28} = (6^{-1/2})(\tau_{2,1,6,5} - \tau_{1,6,5,4} + \tau_{6,5,4,3} - \tau_{5,4,3,2} + \tau_{4,3,2,1} - \tau_{3,2,1,6})$		τR1
$S_{29} = (12^{-1/2})(2\tau_{1,6,5,4} - \tau_{2,1,6,5} - \tau_{6,5,4,3} + 2\tau_{4,3,2,1} - \tau_{5,4,3,2} - \tau_{3,2,1,6})$		τR2
$S_{30} = (1/2)(\tau_{2,1,6,5} - \tau_{6,5,4,3} + \tau_{5,4,3,2} - \tau_{3,2,1,6})$		τR3

Table A2. *Experimental wavenumbers ($\tilde{\nu}$ /cm^{-1}) and relative integral intensities (I) of the absorption bands in the spectrum of* ***2-pyridinone*** *isolated in an Ar matrix, compared with wavenumbers ($\tilde{\nu}$ /cm^{-1}), absolute intensities (Ath / km mol^{-1}) and potential energy distribution (PED / %) calculated for the* ***2-pyridinone.***

Observed Ar matrix, T = 10 K		**Calculated B3LYP/cc-pVTZ**		
$\tilde{\nu}$	**I**	$\tilde{\nu}$	**Ath**	**PED (%)**
3438, 3434, 3431	80	3522	57	νN1H (100)
		3160	4	νC5H (87), νC6H (10)
		3146	2	νC3H (95)
		3134	2	νC6H (89), νC5H (10)
		3104	11	νC4H (95)
1704, 1702	430	1722	583	νCO (65)
1693, **1689**	42			
1629, **1623**	67	1631	42	νC5C6 (36), νC3C4 (21), β C6H (11)
1551	26	1551	52	νC3C4 (29), νC4C5 (17), νC5C6 (15)
		1465	1	νC6C1 (22), β C6H (22), β C5H (21), νC3C4 (11)
1399	6	1428	7	β N1H (28), β C4H (18), νCO (12), νC4C5 (10), β C3H (10)
1348, 1344	7	1364	3	β C4H (22), β N1H (18), β C3H (17), β C5H (15), β C6H (11)
1237, 1233	15	1214	23	β C6H (20), νC6C1 (18), νN1C2 (15), νC5C6 (11), β N1H (11)
1203	16	1199	5	β C3H (33), β C6H (20), νC2C3 (15)
1152, 1149	22	1144	19	β C4H (32), β C5H (27), νN1C2 (10)
1087, 1084	15	1090	17	νC6C1 (24), νC5C6 (20), β C5H (16), β N1H (11)
1001	2	999	5	νC4C5 (57)
		997	0	γC4H (78), γC3H (37)
991	15	984	12	β R1 (80)
		936	0	γC6H (77), γC5H (36)
840	17	847	18	γC3H (52), γCO (26), γC4H (15)
814	8	802	9	νN1C2 (41), νC2C3 (34)
761	63	761	62	γC5H (39), γCO (36), γC6H (14)
722	11	730	4	τR1 (28), γC5H (21), γN1H (16), γCO (13), γC3H (11), γC4H (10)
683, **680**	43	691	39	γN1H (66), τR1 (42)
		607	1	β R2 (49), β R3 (24), νC2C3 (11)
542, 540	13	538	7	β R3 (59), β R2 (21)
485	34	483	38	τR2 (28), τR1 (26), γCO (19), γN1H (16)
453	10	449	7	β CO (69), β R2 (17)
		385	1	τR3 (86), τR2 (27)
		171	3	τR2 (53), τR3 (25), τR1 (23)

Table A3. *Experimental wavenumbers ($\tilde{\nu}$ /cm^{-1}) and relative integral intensities (I) of the absorption bands in the spectrum of* ***2(1H)-pyridone*** *isolated in an Ar matrix, compared with wavenumbers ($\tilde{\nu}$ /cm^{-1}), absolute intensities (Ath / km mol^{-1}) and potential energy distribution (PED / %) calculated for the* ***2-hydroxypyridine.***

Observed Ar matrix, T = 10 K		**Calculated B3LYP/CC-pVTZ**		
$\tilde{\nu}$	**I**	$\tilde{\nu}$	**Ath**	**PED (%)**
3577, **3574**	111	3683	76	νOH (100)
		3144	2	νC3H (78), νC4H (11), νC5H (10)
3105	3	3137	14	νC5H (78), νC3H (15)
		3112	8	νC4H (85)
3038	7	3092	16	νC6H (95)
1610, 1608	59	1617	85	νC2C3 (24), νC5C6 (20), νC3C4 (11)
1586, 1583	74	1594	86	νC4C5 (23), νC3C4 (22), νN1C2 (18), β C4H (12)
1481, 1479	144	1484	113	β C6H (29), β C3H (18), νN1C2 (15)
1464, 1461, 1455, 1453	53	1464	54	β C5H (28), νC5C6 (12), β C4H (12), νC6C1 (11), νC2C3 (10)
1346, 1343	23	1346	24	β C6H (32), β OH (25), β C4H (19), β C3H (11)
1314	11			
1300	66	1301	88	νCO (40), νC3C4 (14), β R1 (13)
1261, 1259	14	1285	10	νC6C1 (42), νN1C2 (13), νC5C6 (12)
1209, 1207	12			
1189	23			
1180	5			
1173, 1170	89	1176	135	β OH (41), β C5H (16), νN1C2 (11), νC2C3 (10), β C6H (10)
1141, 1140	48	1144	37	β C4H (30), β C3H (28), β C5H (13)
1095, 1090	22	1088	27	β C5H (23), νC5C6 (22), νC3C4 (12)
1065	8			
1041	5	1043	4	νC4C5 (41), νC5C6 (17), β C3H (14)
993, 992	10	989	7	β R1 (57), νN1C2 (12), νC6C1 (11)
		988	0	γC4H (67), γC5H (26), γC3H (18), γC6H (10)
		965	0	γC6H (78), γC4H (15), γC5H (11)
863	2	867	2	γC3H (61), γC5H (25), γC6H (10)
846, 844	15	846	13	νCO (26), νC2C3 (22), β R1 (17), β R3 (14), νN1C2 (12)
779	59	783	54	γC5H (34), γCO (33), τR1 (18)
738	6	745	7	τR1 (64), γC3H (13), γC4H (10), γC5H (10)
626	2	630	3	β R2 (62), β R3 (21)
		557	1	β R3 (55), β R2 (19), νCO (14)
535, 534	5	552	24	τOH (43), γCO (22), τR1 (20), τR2 (14)
470, 468	102	491	88	τOH (56), γCO (21), τR2 (13)
		417	0	τR3 (96), τR2 (15)
418, 415	19	412	16	β CO (78), β R2 (10)
		212	1	τR2 (69), γCO (15), τR3 (11)

4-pyrimidinone

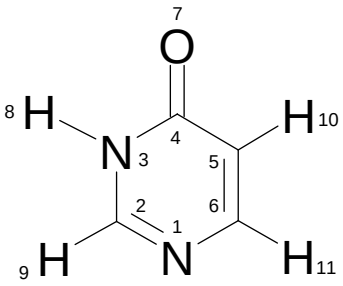

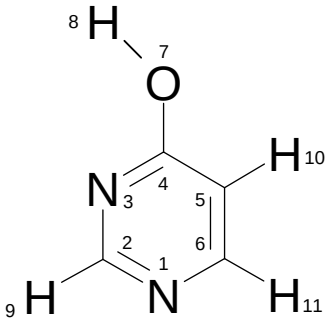

4-pyrimidinone

4PMo

4-hydroxypyrimidine

4PMh

***Scheme A2**. Atom numbering for tautomers of 4-pyrimidinone.*

Table A4. *Internal coordinates used in the normal mode analysis for* ***4-pyrimidinone*** *and* ***4-hydroxypyrimidine*** *(atom numbering as in Scheme A2).*

In-plane		
Ring stretchings		
$S_1 = r_{1,2}$		ν N1C2
$S_2 = r_{2,3}$		ν C2N3
$S_3 = r_{3,4}$		ν N3C4
$S_4 = r_{4,5}$		ν C4C5
$S_5 = r_{5,6}$		ν C5C6
$S_6 = r_{6,1}$		ν C6C1
Stretching NH, CO, CH		
$S_7 = r_{4,7}$		ν CO
$S_8 = r_{3,8}$	oxo	ν N3H
$S'_8 = r_{7,8}$	hydroxy	ν OH
$S_9 = r_{2,9}$		ν C2H
$S_{10} = r_{5,10}$		ν C5H
$S_{11} = r_{6,11}$		ν C6H
Ring in-plane deformation		
$S_{12} = (6^{-1/2})(\beta_{6,2,1} - \beta_{1,3,2} + \beta_{2,4,3} - \beta_{3,5,4} + \beta_{4,6,5} - \beta_{5,1,6})$		β R1
$S_{13} = (12^{-1/2})(2\beta_{6,2,1} - \beta_{1,3,2} - \beta_{2,4,3} + 2\beta_{3,5,4} - \beta_{4,6,5} - \beta_{5,1,6})$		β R2
$S_{14} = (1/2)(\beta_{1,3,2} - \beta_{2,4,3} + \beta_{4,6,5} - \beta_{5,1,6})$		β R3
Bending CO, CH, NH,		
$S_{15} = (2^{-1/2})(\beta_{2,8,3} - \beta_{4,8,3})$	oxo	β N3H
$S'_{15} = \beta_{8,4,7}$	hydroxy	β OH
$S_{16} = (2^{-1/2})(\beta_{3,7,4} - \beta_{5,7,4})$		β CO
$S_{17} = (2^{-1/2})(\beta_{1,9,2} - \beta_{3,9,2})$		β C2H
$S_{18} = (2^{-1/2})(\beta_{4,10,5} - \beta_{6,10,5})$		β C5H
$S_{19} = (2^{-1/2})(\beta_{5,11,6} - \beta_{1,11,6})$		β C6H
Out-of-plane		
Wagging CO, NH, CH		
$S_{20} = \gamma_{7,3,4,5}$		γ CO
$S_{21} = \gamma_{9,1,2,3}$		γ C2H
$S_{22} = \gamma_{10,4,5,6}$		γ C5H
$S_{23} = \gamma_{11,5,6,1}$		γ C6H
$S_{24} = \gamma_{8,2,3,4}$	oxo	γ N3H
Torsion OH		
$S'_{24} = (2^{-1/2})(\tau_{8,7,4,3} + \tau_{8,7,4,5})$	hydroxy	τ OH
Ring torsion		
$S_{25} = (6^{-1/2})(\tau_{2,1,6,5} - \tau_{1,6,5,4} + \tau_{6,5,4,3} - \tau_{5,4,3,2} + \tau_{4,3,2,1} - \tau_{3,2,1,6})$		τ R1
$S_{26} = (12^{-1/2})(2\tau_{1,6,5,4} - \tau_{2,1,6,5} - \tau_{6,5,4,3} + 2\tau_{4,3,2,1} - \tau_{5,4,3,2} - \tau_{3,2,1,6})$		τ R2
$S_{27} = (1/2)(\tau_{2,1,6,5} - \tau_{6,5,4,3} + \tau_{5,4,3,2} - \tau_{3,2,1,6})$		τ R3

Table A5. *Experimental wavenumbers ($\tilde{\nu}$ /cm^{-1}) and relative integral intensities (I) of the absorption bands in the spectrum of* ***4-pyrimidinone*** *isolated in an Ar matrix, compared with wavenumbers ($\tilde{\nu}$ /cm^{-1}), absolute intensities (Ath / km mol^{-1}) and potential energy distribution (PED / %) calculated for the* ***4-pyrimidinone.***

Observed Ar matrix, T = 10 K		**Calculated B3LYP/CC-pVTZ**		
$\tilde{\nu}$	**I**	$\tilde{\nu}$	**Ath**	**PED (%)**
3441, **3428,** 3421	106	3506	50	νN3H (100)
		3152	2	νC5H (97)
		3104	11	νC6H (92)
		3096	14	νC2H (94)
1767	9			
1754	9			
1726	530	1744	588	νCO (72)
1690	4			
1681	9			
1651	7			
1648	3			
1622	2			
1611	68	1616	74	νN1C2 (39), νC5C6 (23), β C2H (11)
1546, 1544, 1540, 1538	72	1543	99	νC5C6 (34), νN1C2 (19)
1434	7	1434	8	β N3H (39), νC2N3 (28)
1414	14	1419	21	β C5H (24), β C6H (24), β C2H (16), νC6C1 (13)
1397	3			
1394	1			
1366, 1360	22	1370	14	β C2H (44), β C6H (18), νN1C2 (16)
1226	67	1224	45	β C6H (26), νC6C1 (16), νC2N3 (13), β C2H (11)
1206, 1203	3	1187	7	β C5H (32), νC4C5 (21), νN3C4 (19)
1116, 1103	8 6	1114	11	νC2N3 (31), β N3H (25), νN1C2 (10)
1025	12	1019	11	β R1 (35), νC6C1 (23), β C5H (16), νN3C4 (10)
		1004	0	γC6H (85), γC5H (25)
972	43	973	39	β R1 (45), νC6C1 (33)
		945	0	γC2H (100)
838, 833	39	846	35	γC5H (62), γCO (27), γC6H (16)
827	5	813	4	νN3C4 (46), νC4C5 (32)
754	13	760	16	γCO (46), τR1 (42), γN3H (12)
709, **705**	33	718	33	γN3H (76), τR1 (28)
651	1	650	1	β R3 (73), νC4C5 (12)
535	1	531	1	β R2 (81)
502	43	501	48	τR3 (33), τR1 (21), γCO (19), γN3H (17)
455	10	451	10	β CO (71), β R3 (10)
		358	0	τR2 (111)
		171	10	τR3 (74), τR1 (25)

Table A6. *Experimental wavenumbers ($\tilde{\nu}$ /cm^{-1}) and relative integral intensities (I) of the absorption bands in the spectrum of* ***4-pyrimidinone*** *isolated in an Ar matrix, compared with wavenumbers ($\tilde{\nu}$ /cm^{-1}), absolute intensities (Ath / km mol^{-1}) and potential energy distribution (PED / %) calculated for the* ***4-hydroxypyrimidine.***

Observed Ar matrix, T = 10 K		**Calculated B3LYP/CC-pVTZ**		
$\tilde{\nu}$	**I**	$\tilde{\nu}$	**Ath**	**PED (%)**
3562	117	3671	83	νOH (100)
		3151	2	νC5H (98)
3047	10	3100	14	νC2H (93)
		3094	21	νC6H (91)
1607	122	1609	145	νC4C5 (34), νN1C2(15)
1596	6			
1589	26			
1580, 1578, 1575	161	1583	219	νC5C6 (30), νN3C4 (19), νC6C1 (14), β C6H (14)
1565	3			
1559	3			
1544	12			
1522	5			
1479	136	1480	116	β C2H (27), νN3C4 (15), β C5H (14), β C6H (12), νCO (11)
1398, 1395	55	1404	52	β C2H (18), β C6H (15), νC2N3 (13), νC6C1 (11), νN1C2 (10), νC5C6 (10)
1358	11	1356	5	β C2H (32), β OH (21), β C6H (18), β C5H (15)
1311	25	1318	35	νCO (36), νC2N3 (20), β C6H (15), β R1 (12)
1277, 1275	15			
1246 1244	73	1263	84	νN1C2 (35), νC2N3 (20), β OH (15)
1210	7			
1177	7			
1168	6			
1160	42	1180	35	νC6C1 (26), β C6H (15), β C5H (12), νC5C6 (10), β R1 (10)
1145	63	1142	120	β OH (40), νC4C5 (17), νN1C2 (15), νN3C4 (11)
1116	23			
1046, 1042	9	1063	1	β C5H (42), νC6C1 (21), νC5C6 (17)
		1005	0	γC6H (64), γC2H (35), γC5H (10)
992	16	986	16	β R1 (46), νC6C1 (13), νN1C2 (10), νC2N3 (10)
		969	0	γC2H (70), γC5H (16), γC6H (26)
867	34	867	31	νCO (27), νC4C5 (22), β R1 (16), νN3C4 (14), β R2 (13)
837, **835**	29	840	31	γC5H (70), γCO (23), γC6H (14)
776	10	785	10	τR1 (81), γCO (21)
679	7	680	6	β R3 (82)
564	3	580	20	τOH (44), γCO (21), τR1 (17), τR3 (16)
554	3	551	3	β R2 (75), νCO (12)
498, 496	102	518	94	τOH (54), γCO (21), τR3 (13)
419	16	415	14	β CO (79)
		383	0	τR2 (106)
		207	0	τR3 (74), γCO (15), τR1 (11)

2-pyrazinone

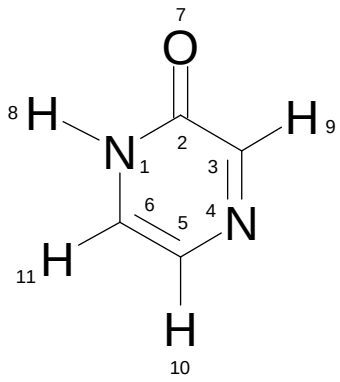

2-pyrazinone

2PZo

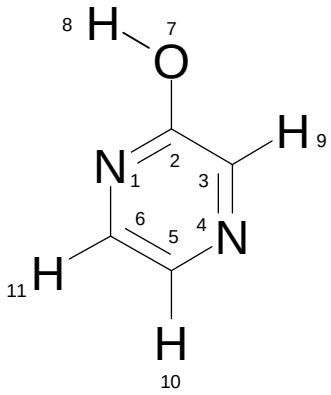

2-hydroxypyrazine

2PZh

Scheme A3. *Atom numbering for tautomers of 2-pyrazinone*

Table A7. *Internal coordinates used in the normal mode analysis for* ***2-pyrazinone*** *and* ***2-hydroxypyrazine*** *(atom numbering as in Scheme A3).*

In-plane		
Ring stretching		
$S_1 = r_{1,2}$		ν N1C2
$S_2 = r_{2,3}$		ν C2C3
$S_3 = r_{3,4}$		ν C3N4
$S_4 = r_{4,5}$		ν N4C5
$S_5 = r_{5,6}$		ν C5C6
$S_6 = r_{6,1}$		ν C6C1
Stretching NH, CO, CH		
$S_7 = r_{2,7}$		ν CO
$S_8 = r_{1,8}$	oxo	ν N1H
$S'_8 = r_{7,8}$	hydroxy	ν OH
$S_9 = r_{3,9}$		ν C3H
$S_{10} = r_{5,10}$		ν C5H
$S_{11} = r_{6,11}$		ν C6H
Ring in-plane deformation		
$S_{12} = (6^{-1/2})(\beta_{2,4,3} - \beta_{3,5,4} + \beta_{4,6,5} - \beta_{5,1,6} + \beta_{6,2,1} - \beta_{1,3,2})$		β R1
$S_{13} = (12^{-1/2})(2\beta_{2,4,3} - \beta_{3,5,4} - \beta_{4,6,5} + 2\beta_{5,1,6} - \beta_{6,2,1} - \beta_{1,3,2})$		β R2
$S_{14} = (1/2)(\beta_{3,5,4} - \beta_{4,6,5} + \beta_{6,2,1} - \beta_{1,3,2})$		β R3
Bending CO, CH, NH,		
$S_{15} = (2^{-1/2})(\beta_{2,8,1} - \beta_{6,8,1})$	oxo	β N1H
$S'_{15} = \beta_{8,2,7}$	hydroxy	β OH
$S_{16} = (2^{-1/2})(\beta_{3,7,2} - \beta_{1,7,2})$		β CO
$S_{17} = (2^{-1/2})(\beta_{4,9,3} - \beta_{2,9,3})$		β C3H
$S_{18} = (2^{-1/2})(\beta_{4,10,5} - \beta_{6,10,5})$		β C5H
$S_{19} = (2^{-1/2})(\beta_{5,11,6} - \beta_{1,11,6})$		β C6H
Out-of-plane		
Wagging CO, NH, CH		
$S_{20} = \gamma_{7,1,2,3}$		γ CO
$S_{21} = \gamma_{9,2,3,4}$		γ C3H
$S_{22} = \gamma_{10,4,5,6}$		γ C5H
$S_{23} = \gamma_{11,5,6,1}$		γ C6H
$S_{24} = \gamma_{8,6,1,2}$	oxo	γ N1H
Torsion OH		
$S'_{24} = (2^{-1/2})(\tau_{8,7,2,3} + \tau_{8,7,2,1})$	hydroxy	τ OH
Ring torsion		
$S_{25} = (6^{-1/2})(\tau_{5,4,3,2} - \tau_{4,3,2,1} + \tau_{3,2,1,6} - \tau_{2,1,6,5} + \tau_{1,6,5,4} - \tau_{6,5,4,3})$		τ R1
$S_{26} = (12^{-1/2})(2\tau_{6,5,4,3} - \tau_{5,4,3,2} - \tau_{4,3,2,1} + 2\tau_{3,2,1,6} - \tau_{2,1,6,5} - \tau_{1,6,5,4})$		τ R2
$S_{27} = (1/2)(\tau_{5,4,3,2} - \tau_{4,3,2,1} + \tau_{2,1,6,5} - \tau_{1,6,5,4})$		τ R3

Table A8. *Experimental wavenumbers ($\tilde{\nu}$ /cm^{-1}) and relative integral intensities (I) of the absorption bands in the spectrum of* ***2-pyrazinone*** *isolated in an Ar matrix, compared with wavenumbers ($\tilde{\nu}$ /cm^{-1}), absolute intensities (Ath / km mol^{-1}) and potential energy distribution (PED / %) calculated for the* ***2-pyrazinone.***

Observed Ar matrix, T = 10 K		**Calculated B3LYP/cc-pVTZ**		
$\tilde{\nu}$	**I**	$\tilde{\nu}$	**Ath**	**PED (%)**
3430	62	3514	60	νN1H (100)
		3152	11	νC5H (63), νC6H (36)
		3134	0	νC6H (63), νC5H (37)
		3095	8	νC3H (99)
1723, **1711,** 1700, 1673	444	1727	493	νCO (74)
1615	32	1616	39	νC5C6 (41), νC3N4 (21), β C6H (13)
1549, 1545, **1539**	145	1526	23	νC3N4 (45), β N1H (12), νC5C6 (10)
		1463	6	νC6C1 (25), β C5H (25), β C6H (15), β N1H (14)
		1385	6	β N1H (32), νN4C5 (15), β C5H (11), β C6H (10)
		1338	2	β C3H (63), β C5H (20)
		1213	22	νN1C2 (30), νC2C3 (22), νC5C6 (11)
		1208	4	β C6H (40), β C5H (24)
1144, 1122	67	1121	23	νC6C1 (29), β N1H (17), νC5C6 (12), β C5H (12), νN4C5 (10)
		1035	4	νN4C5 (34), β R1 (29), νC6C1 (11), νC5C6 (10)
		973	9	β R1 (55), νN4C5 (19)
		930	0	γC3H (50), γC5H (35), γC6H (20)
		925	4	γC6H (48), γC3H (47), γC5H (18)
835, 820	62	809	18	νN1C2 (41), νC2C3 (30)
792	27	800	35	γC5H (47), γC6H (31), γCO (16)
		753	5	γCO (39), γN1H (28), τR1 (28)
688	54	704	73	γN1H (58), τR1 (46)
		606	3	β R2 (71), νC2C3 (18)
		550	13	β R3 (71)
		485	7	γCO (30), τR2 (21), γN1H (19), τR1 (18)
		435	10	β CO (68), β R3 (16)
		401	11	τR3 (87), τR2 (23)
		163	4	τR2 (67), τR1 (21), τR3 (14)

Table A9. *Experimental wavenumbers ($\tilde{\nu}$ /cm^{-1}) and relative integral intensities (I) of the absorption bands in the spectrum of* ***2-hydroxypyrazine*** *isolated in an Ar matrix, compared with wavenumbers ($\tilde{\nu}$ /cm^{-1}), absolute intensities (Ath / km mol^{-1}) and potential energy distribution (PED / %) calculated for the* ***2-hydroxypyrazine.***

Observed Ar matrix, T = 10 K		**Calculated B3LYP/cc-pVTZ**		
$\tilde{\nu}$	**I**	$\tilde{\nu}$	**Ath**	**PED (%)**
3575	78	3679	78	νOH (100)
		3118	20	νC5H (71), νC6H (23)
		3107	19	νC3H (94)
		3096	5	νC6H (75), νC5H (25)
1607	18	1600	15	νC2C3 (23), νC5C6 (21)
1546	110	1560	100	νN1C2 (31), νC3N4 (25), νN4C5 (13), νC6C1 (13)
1475	49	1479	49	β C6H (26), β C3H (16), β C5H (15), νN4C5 (13), νC6C1 (13)
1459, **1442,** 1439, 1431	105	1445	89	β C5H (26), νC5C6 (14), νCO (12), νC2C3 (11), νC3N4 (11), β OH (10)
1382	2			
1340	3			
1324	16	1328	10	β C3H (32), β C6H (26), β OH (17), β C5H (12)
1305, 1293	61	1306	92	νCO (35), β C3H (14), β C6H (12), νC3N4 (10)
1262	4			
1219	39	1230	22	νC6C1 (33), νC3N4 (15), νN4C5 (15), β OH (14), νC5C6 (11)
1200, 1191	27	1195	43	β C5H (24), νC3N4 (18), β C3H (16), β OH (13)
1173	20			
1133, **1119**	141	1128	167	β OH (32), νN4C5 (20), νC2C3 (14), νN1C2 (13)
1184	6	1063	8	νC5C6 (38), νN4C5 (24), β C6H (14)
1061	7			
1010	30	1006	29	β R1 (57), νN1C2 (13), νC2C3 (13), νC6C1 (10)
988	5			
		968	0	γC6H (71), γC5H (42)
917	2	925	1	γC3H (85), γC5H (10)
856	5	860	2	νCO (22), νC2C3 (18), β R1 (17), β R2 (16), νN1C2 (12)
840	29	848	28	γC5H (51), γC6H (23), γCO (14), γC3H (11)
754	1	765	1	τR1 (86), γCO (10)
		635	0	β R2 (71)
574	2	573	1	β R3 (69), νCO (14)
542	26	559	46	γCO (41), τOH (27), τR2 (16), τR1 (13)
454	111	484	69	τOH (71), γCO (19)
421	3	429	6	τR3 (70), τR2 (36)
408	17	405	15	β CO (79)
		204	0	τR2 (51), τR3 (32), γCO (13)

Appendix B

Spectroscopic data of systems with heterocyclic ring and fused benzene ring

2-quinoxalinone

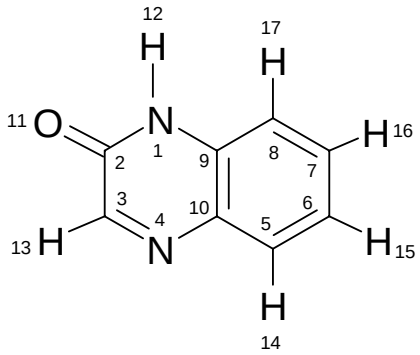

2QXo

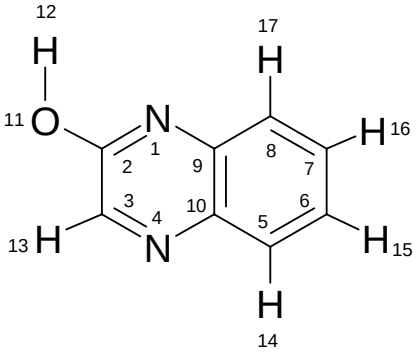

2QXh

Scheme B1. *Atom numbering for tautomers of 2-quinoxalinone.*

Table B1. *Internal coordinates used in the normal mode analysis for* ***2-quinoxalinone*** *forms* ***oxo*** *and* ***hydroxy*** *(atom numbering as in Scheme B1).*

In-plane		
Ring stretchings		
$S_1 = r_{1,2}$		ν N1C2
$S_2 = r_{2,3}$		ν C2C3
$S_3 = r_{3,4}$		ν C3N4
$S_4 = r_{4,10}$		ν N4C10
$S_5 = r_{10,9}$		ν C10C9
$S_6 = r_{9,1}$		ν C9N1
$S_7 = r_{10,5}$		ν C10C5
$S_8 = r_{5,6}$		ν C5C6
$S_9 = r_{6,7}$		ν C6C7
$S_{10} = r_{7,8}$		ν C7C8
$S_{11} = r_{8,9}$		ν C8C9
Stretching NH, CO, CH		
$S_{12} = r_{1,12}$	oxo	ν N1H
$S'_{12} = r_{11,12}$	hydroxy	ν OH
$S_{13} = r_{2,11}$		ν CO
$S_{14} = r_{3,13}$		ν C3H
$S_{15} = r_{5,14}$		ν C5H
$S_{16} = r_{6,15}$		ν C6H
$S_{17} = r_{7,16}$		ν C7H
$S_{18} = r_{8,17}$		ν C8H
Ring in-plane deformation		
$S_{19} = (6^{-1/2})(\beta_{9,2,1} - \beta_{1,3,2} + \beta_{2,4,3} - \beta_{3,10,4} + \beta_{4,9,10} - \beta_{10,1,9})$		β R1
$S_{20} = (12^{-1/2})(2\beta_{9,2,1} - \beta_{1,3,2} - \beta_{2,4,3} + 2\beta_{3,10,4} - \beta_{4,9,10} - \beta_{10,1,9})$		β R2
$S_{21} = (1/2)(\beta_{1,3,2} - \beta_{2,4,3} + \beta_{4,9,10} - \beta_{10,1,9})$		β R3
$S_{22} = (6^{-1/2})(\beta_{7,9,8} - \beta_{8,10,9} + \beta_{9,5,10} - \beta_{10,6,5} + \beta_{5,7,6} - \beta_{6,8,7})$		β R4
$S_{23} = (12^{-1/2})(2\beta_{7,9,8} - \beta_{8,10,9} - \beta_{9,5,10} + 2\beta_{10,6,5} - \beta_{5,7,6} - \beta_{6,8,7})$		β R5
$S_{24} = (1/2)(\beta_{8,10,9} - \beta_{9,5,10} + \beta_{5,7,6} - \beta_{6,8,7})$		β R6
Bendings CO, CH, NH,		
$S_{25} = (2^{-1/2})(\beta_{2,12,1} - \beta_{9,12,1})$	oxo	β N1H
$S'_{25} = \beta_{12,2,11}$	hydroxy	β OH
$S_{26} = (2^{-1/2})(\beta_{3,11,2} - \beta_{1,11,2})$		β CO
$S_{27} = (2^{-1/2})(\beta_{4,13,3} - \beta_{2,13,3})$		β C3H
$S_{28} = (2^{-1/2})(\beta_{6,14,5} - \beta_{10,14,5})$		β C5H
$S_{29} = (2^{-1/2})(\beta_{7,15,6} - \beta_{5,15,6})$		β C6H
$S_{30} = (2^{-1/2})(\beta_{8,16,7} - \beta_{6,16,7})$		β C7H
$S_{31} = (2^{-1/2})(\beta_{9,17,8} - \beta_{7,17,8})$		β C8H
Out-of-plane		
Wagging CO, NH, CH		
$S_{32} = \gamma_{11,3,2,1}$		γ CO
$S_{33} = \gamma_{13,4,3,2}$		γ C3H
$S_{34} = \gamma_{14,10,5,6}$		γ C5H
$S_{35} = \gamma_{15,5,6,7}$		γ C6H
$S_{36} = \gamma_{16,6,7,8}$		γ C7H
$S_{37} = \gamma_{17,7,8,9}$		γ C8H
$S_{38} = \gamma_{12,9,1,2}$	oxo	γ N1H
Torsion OH		
$S'_{38} = (2^{-1/2})(\tau_{12,11,2,3} + \tau_{12,11,2,1})$	hydroxy	τ OH
Ring torsions		
$S_{39} = (6^{-1/2})(\tau_{2,1,9,10} - \tau_{1,9,10,4} + \tau_{9,10,4,3} - \tau_{10,4,3,2} + \tau_{4,3,2,1} - \tau_{3,2,1,9})$		τ R1
$S_{40} = (12^{-1/2})(2\tau_{1,9,10,4} - \tau_{2,1,9,10} - \tau_{9,10,4,3} + 2\tau_{4,3,2,1} - \tau_{10,4,3,2} - \tau_{3,2,1,9})$		τ R2
$S_{41} = (1/2)(\tau_{2,1,9,10} - \tau_{9,10,4,3} + \tau_{10,4,3,2} - \tau_{3,2,1,9})$		τ R3
$S_{42} = (6^{-1/2})(\tau_{9,8,7,6} - \tau_{8,7,6,5} + \tau_{7,6,5,10} - \tau_{6,5,10,9} + \tau_{5,10,9,8} - \tau_{10,9,8,7})$		τ R4
$S_{43} = (12^{-1/2})(2\tau_{8,7,6,5} - \tau_{9,8,7,6} - \tau_{7,6,5,10} + 2\tau_{5,10,9,8} - \tau_{6,5,10,9} - \tau_{10,9,8,7})$		τ R5
$S_{44} = (1/2)(\tau_{9,8,7,6} - \tau_{7,6,5,10} + \tau_{6,5,10,9} - \tau_{10,9,8,7})$		τ R6
Two rings relative torsion		
$S_{45} = (2^{-1/2})(\tau_{5,10,9,1} - \tau_{4,10,9,8})$		τ RR

Table B2. *Experimental wavenumbers ($\tilde{\nu}$ /cm^{-1}) and relative integral intensities (I) of the absorption bands in the spectrum of* ***2-quinoxalinone*** *isolated in an Ar matrix, compared with wavenumbers ($\tilde{\nu}$ /cm^{-1}), absolute intensities (Ath / km mol^{-1}) and potential energy distribution (PED / %) calculated for the* ***oxo*** *form of* ***2-quinoxalinone.***

Observed Ar matrix, T = 10 K		**Calculated B3LYP/cc-pVTZ**		
$\tilde{\nu}$	**I**	$\tilde{\nu}$	**Ath**	**PED (%)**
3419	65	3505	36	νN1H (100)
		3140	9	νC5H (54), νC6H (37)
		3128	8	νC7H (41), νC5H (37), νC6H (18)
		3118	6	νC6H (43), νC7H (33), νC8H (15)
		3103	4	νC8H (80), νC7H (18)
		3091	8	νC3H (100)
1784	13			
1747	7			
1724, **1710,** 1698, 1678	623	1724	621	νCO (76)
1617, 1599	59	1620	53	νC5C6 (21), νC8C9 (16), νC10C5 (13), νC7C8 (13)
		1600	0	νC3N4 (41), νC10C9 (14)
1565	7	1574	20	νC3N4 (30), νC6C7 (11)
1493	3	1494	2	βC6H (21), νC10C5 (13), βC8H (12), βC5H (10)
1479, **1477**	25	1475	20	βC7H (17), νC5C6 (13), νC10C9 (11), βC8H (11), νC9N1 (10)
1439	2			
		1403	1	βN1H (34), βC7H (15), νC9N1 (11)
1365, **1357**	10	1356	7	βC3H (57), νN4C10 (14)
1335, 1331	25	1332	16	νC10C9 (16), νC7C8 (16), νC5C6 (10), νC8C9 (10)
1320, 1318	4			
1312, 1310	2			
1306, 1303	8	1290	12	βC5H (24), νN1C2 (16), νC2C3 (10)
1266	2	1251	5	νN1C2 (22), βC8H (21)
1249, 1245, 1241, 1237, **1235**	9	1242	11	βN1H (29), νC9N1 (20), νC8C9 (13)
		1196	1	νN4C10 (27), βC6H (17)
1155, **1151**	6	1154	5	βC7H (36), βC8H (18), νC7C8 (10)
1121	4	1121	5	βC6H (20), βC5H (18), νC5C6 (14), νC7C8 (12), βR4 (11)
1033, **1031**	5	1031	5	νC6C7 (46), νC5C6 (13), νC7C8 (13), βC5H (12)
		982	0	γC6H (51), γC5H (33), γC7H (33)
945	12	955	6	γC5H (39), γC7H (39), γC8H (21)
940	21	932	28	νN1C2 (26), βR1 (26), νC2C3 (24)
923	7	931	8	γC3H (89), γCO (11)
917, 914, 912	3	912	5	βR4 (50), βR1 (11)
		863	0	γC8H (45), γC6H (19), γC5H (17)
775	8	784	4	τR1 (33), τR4 (28), γC8H (15), γCO (14)
771	2	772	2	νC10C9 (21), νN4C10 (18), νC10C5 (18), βR1 (12)
758, **752,** 751	64	758	77	γC6H (35), γC7H (21), γC5H (14), γC8H (11)
716	1			
705	27	717	32	γCO (44), γN1H (36), τR4 (22)
		714	0	νC2C3 (22), βR1 (18), βR5 (12), νC10C9 (10)
626	35	640	29	γN1H (57), τR4 (27), τR1 (13)
604, **602**	13	605	12	βR5 (42), βR2 (27), νC2C3 (14)
		550	0	τR5 (42), τR4 (23), τR2 (14)
530	2	529	3	βR6 (34), βR5 (17), βR3 (13), νN4C10 (11)
515	2			
486, **481**	15	479	18	βCO (38), βR3 (30), βR2 (19)
467, **462**	6	466	6	τR6 (41), τRR (33), τR3 (18)
459	7	457	7	βR2 (32), βR3 (24), νC9N1 (10)
		396	2	τR3 (39), τR6 (39), τR5 (11)
		306	2	βR6 (29), βCO (22), βR3 (11)
		265	6	τR1 (30), τR6 (25), τRR (23), τR5 (18)
		173	0	τR2 (32), τR5 (26), τRR (18), τR3 (15)
		100	1	τR2 (39), τR3 (36), τRR (10)

Table B3. *Experimental wavenumbers ($\tilde{\nu}$ /cm^{-1}) and relative integral intensities (I) of the absorption bands in the spectrum of* ***2-quinoxalinone*** *isolated in an Ar matrix, compared with wavenumbers ($\tilde{\nu}$ /cm^{-1}), absolute intensities (Ath / km mol^{-1}) and potential energy distribution (PED / %) calculated for the* ***hydroxy*** *form of* ***2-quinoxalinone.***

Observed Ar matrix, T = 10 K		**Calculated B3LYP/cc-pVTZ**		
$\tilde{\nu}$	**I**	$\tilde{\nu}$	**Ath**	**PED (%)**
3581, **3568**	127	3675	77	νOH (100)
		3136	12	νC5H (44), νC6H (26), νC8H (16), νC7H (13)
		3130	12	νC8H (57), νC5H (29), νC7H (12)
		3119	6	νC6H (40), νC5H (23), νC7H (20), νC8H (17)
		3107	2	νC7H (55), νC6H (32)
		3097	11	νC3H (100)
1828	4			
1818	12			
1644	17			
1618	7	1626	13	νC7C8 (21), νC5C6 (19)
1593, **1591,** 1588	135	1594	159	νN1C2 (36), νC3N4 (21)
1581	20	1580	4	νC10C9 (16), νC3N4 (14), νC6C7 (10)
1544	15			
1519, 1510, **1507**	52	1516	34	νC6C7 (17), νC8C9 (10)
1480, 1473	16	1479	15	β C7H (17), β C6H (16), νC8C9 (10)
1448, 1435, **1433,** 1420	77	1439	72	νCO (12), νC3N4 (11), νC2C3 (10), β C5H (10)
1384	10	1380	40	νC3N4 (22), νC10C9 (17), β C8H (14), νN1C2 (12)
		1361	0	β C3H (31), νC9N1 (14), β OH (12), νN4C10 (10)
1357	5			
1347, 1341	60	1342	53	νC10C9 (21), νC7C8 (16), νC5C6 (13), νCO (10)
		1279	1	β C5H (17), β C3H (15), β R1 (14), β C7H (10), β C8H (10)
1237	6	1236	4	νC9N1 (24), νC10C5 (20)
		1209	5	νN4C10 (24), β C3H (18), νC8C9 (12), β R4 (11), β C6H (11)
1192, 1191 1166	101 140	1172	317	β OH (51), νCO (14), νN1C2 (10)
1139, 1134	87	1142	29	β C7H (26), β C6H (14), β C8H (11)
1124	8	1124	6	β C5H (15), β C6H (15), νC5C6 (14), νC7C8 (12), β R4 (11), β C7H (10)
1020, 1013	8	1018	10	νC6C7 (50), β C5H (11), β C8H (11), νC5C6 (10), νC7C8 (10)
		992	0	γC7H (45), γC6H (41), γC8H (19), γC5H (18)
989, 983	25	981	25	νC2C3 (36), β R1 (19)
954	4	968	3	γC5H (42), γC8H (31), γC7H (20), γC6H (17)
923	4	917	11	γC3H (93)
912	8	908	7	β R4 (54), β R1(10)
		884	1	γC8H (28), γC5H (21), τR1 (17), γC6H (11)
805	1	802	1	τR1 (39), τR4 (29), γC8H (13)
775	5	773	1	νC10C9 (28), νC10C5 (18), νN4C10 (15)
769, 763, **762**	60	770	60	γC6H (34), γC7H (23), γC5H (19), γC8H (10)
741	5			
718	5	717	6	β R1 (23), νC2C3 (15), νCO (15)
682	8	692	11	τR4 (38), τR1 (15), γCO (33), τR2 (11)
614	5	617	5	β R5 (46), β R2 (33)
556, **553**	20	566	41	τR4 (30), τR5 (24), τOH (23), γCO (16)
		532	1	β R6 (26), β R3 (23), β R5 (17), νC8C9 (12)
501	30	523	40	τOH (47), τR5 (11), τR3 (12), τRR (12)
475	9	480	25	τRR (25), τOH (24), τR6 (21), τR3 (17)
465, 464	55	474	18	β CO (36), β R3 (23), β R6 (13)
		464	5	β R2 (30), β R3 (19), β R5 (11)
		418	1	τR6 (48), τR3 (36)
		308	0	τR5 (27), γCO (19), τR1 (20), τR6 (20)
		296	5	β CO (38), β R6 (26)
		177	1	τRR (30), τR2 (21), τR5 (19), τR3 (14), τR6 (12)
		117	1	τR2 (45), τR3 (17), τRR (15), τR5 (11)

2-quinolinone

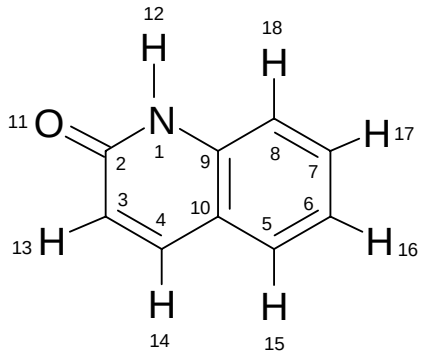

2QLo

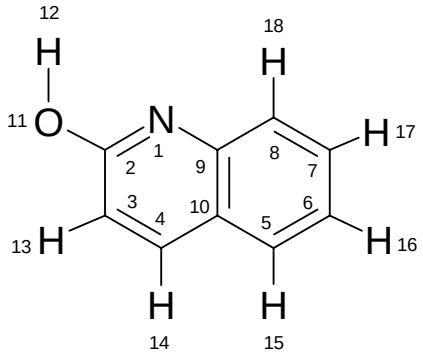

2QLh

Scheme B2. *Atom numbering for tautomers of 2-quinolinone.*

Table B4. *Internal coordinates used in the normal mode analysis for* ***2-quinolinone*** *forms* ***oxo*** *and* ***hydroxy*** *(atom numbering as in Scheme B2).*

In-plane		
Ring stretchings		
$S_1 = r_{1,2}$		ν N1C2
$S_2 = r_{2,3}$		ν C2C3
$S_3 = r_{3,4}$		ν C3C4
$S_4 = r_{4,10}$		ν C4C10
$S_5 = r_{10,9}$		ν C10C9
$S_6 = r_{9,1}$		ν C9N1
$S_7 = r_{10,5}$		ν C10C5
$S_8 = r_{5,6}$		ν C5C6
$S_9 = r_{6,7}$		ν C6C7
$S_{10} = r_{7,8}$		ν C7C8
$S_{11} = r_{8,9}$		ν C8C9
Stretching NH, CO, CH		
$S_{12} = r_{1,12}$	oxo	ν N1H
$S'_{12} = r_{11,12}$	hydroxy	ν OH
$S_{13} = r_{2,11}$		ν CO
$S_{14} = r_{3,13}$		ν C3H
$S_{15} = r_{4,14}$		ν C4H
$S_{16} = r_{5,15}$		ν C5H
$S_{17} = r_{6,16}$		ν C6H
$S_{18} = r_{7,17}$		ν C7H
$S_{19} = r_{8,18}$		ν C8H
Ring in-plane deformation		
$S_{20} = (6^{-1/2})(\beta_{9,2,1} - \beta_{1,3,2} + \beta_{2,4,3} - \beta_{3,10,4} + \beta_{4,9,10} - \beta_{10,1,9})$		β R1
$S_{21} = (12^{-1/2})(2\beta_{9,2,1} - \beta_{1,3,2} - \beta_{2,4,3} + 2\beta_{3,10,4} - \beta_{4,9,10} - \beta_{10,1,9})$		β R2
$S_{22} = (1/2)(\beta_{1,3,2} - \beta_{2,4,3} + \beta_{4,9,10} - \beta_{10,1,9})$		β R3
$S_{23} = (6^{-1/2})(\beta_{7,9,8} - \beta_{8,10,9} + \beta_{9,5,10} - \beta_{10,6,5} + \beta_{5,7,6} - \beta_{6,8,7})$		β R4
$S_{24} = (12^{-1/2})(2\beta_{7,9,8} - \beta_{8,10,9} - \beta_{9,5,10} + 2\beta_{10,6,5} - \beta_{5,7,6} - \beta_{6,8,7})$		β R5
$S_{25} = (1/2)(\beta_{8,10,9} - \beta_{9,5,10} + \beta_{5,7,6} - \beta_{6,8,7})$		β R6
Bendings CO, CH, NH,		
$S_{26} = (2^{-1/2})(\beta_{2,12,1} - \beta_{9,12,1})$	oxo	β N1H
$S'_{26} = \beta_{12,2,11}$	hydroxy	β OH
$S_{27} = (2^{-1/2})(\beta_{3,11,2} - \beta_{1,11,2})$		β CO
$S_{28} = (2^{-1/2})(\beta_{4,13,3} - \beta_{2,13,3})$		β C3H
$S_{29} = (2^{-1/2})(\beta_{10,14,4} - \beta_{3,14,4})$		β C4H
$S_{30} = (2^{-1/2})(\beta_{6,15,5} - \beta_{10,15,5})$		β C5H
$S_{31} = (2^{-1/2})(\beta_{7,16,6} - \beta_{5,16,6})$		β C6H
$S_{32} = (2^{-1/2})(\beta_{8,17,7} - \beta_{6,17,7})$		β C7H
$S_{33} = (2^{-1/2})(\beta_{9,18,8} - \beta_{7,18,8})$		β C8H
Out-of-plane		
Wagging CO, NH, CH		
$S_{34} = \gamma_{11,3,2,1}$		γ CO
$S_{35} = \gamma_{13,4,3,2}$		γ C3H
$S_{36} = \gamma_{14,10,4,3}$		γ C4H
$S_{37} = \gamma_{15,10,5,6}$		γ C5H
$S_{38} = \gamma_{16,5,6,7}$		γ C6H
$S_{39} = \gamma_{17,6,7,8}$		γ C7H
$S_{40} = \gamma_{18,7,8,9}$		γ C8H
$S_{41} = \gamma_{12,9,1,2}$	oxo	γ N1H
Torsion OH		
$S'_{41} = (2^{-1/2})(\tau_{12,11,2,3} + \tau_{12,11,2,1})$	hydroxy	τ OH
Ring torsions		
$S_{42} = (6^{-1/2})(\tau_{2,1,9,10} - \tau_{1,9,10,4} + \tau_{9,10,4,3} - \tau_{10,4,3,2} + \tau_{4,3,2,1} - \tau_{3,2,1,9})$		τ R1
$S_{43} = (12^{-1/2})(2\tau_{1,9,10,4} - \tau_{2,1,9,10} - \tau_{9,10,4,3} + 2\tau_{4,3,2,1} - \tau_{10,4,3,2} - \tau_{3,2,1,9})$		τ R2
$S_{44} = (1/2)(\tau_{2,1,9,10} - \tau_{9,10,4,3} + \tau_{10,4,3,2} - \tau_{3,2,1,9})$		τ R3
$S_{45} = (6^{-1/2})(\tau_{9,8,7,6} - \tau_{8,7,6,5} + \tau_{7,6,5,10} - \tau_{6,5,10,9} + \tau_{5,10,9,8} - \tau_{10,9,8,7})$		τ R4
$S_{46} = (12^{-1/2})(2\tau_{8,7,6,5} - \tau_{9,8,7,6} - \tau_{7,6,5,10} + 2\tau_{5,10,9,8} - \tau_{6,5,10,9} - \tau_{10,9,8,7})$		τ R5
$S_{47} = (1/2)(\tau_{9,8,7,6} - \tau_{7,6,5,10} + \tau_{6,5,10,9} - \tau_{10,9,8,7})$		τ R6
Two rings relative torsion		
$S_{48} = (2^{-1/2})(\tau_{5,10,9,1} - \tau_{4,10,9,8})$		τ RR

Table B5. *Experimental wavenumbers ($\tilde{\nu}$ /cm^{-1}) and relative integral intensities (I) of the absorption bands in the spectrum of* ***2-quinolinone*** *isolated in an Ar matrix, compared with wavenumbers ($\tilde{\nu}$ /cm^{-1}), absolute intensities (Ath / km mol^{-1}) and potential energy distribution (PED / %) calculated for the* ***oxo*** *form of* ***2-quinolinone.***

Observed Ar matrix, T = 10 K		**Calculated B3LYP/cc-pVTZ**		
$\tilde{\nu}$	**I**	$\tilde{\nu}$	**Ath**	**PED (%)**
3427	62	3515	37	νN1H (100)
3088 3073 3068 3060 3055 3042	20	3148	2	νC3H (97)
		3134	14	νC6H (64), νC7H (26)
		3119	15	νC7H (51), νC6H (20), νC8H (20)
		3106	2	νC5H (66), νC8H (22)
		3102	7	νC8H (56), νC7H (21), νC5H (15)
		3096	7	νC4H (94)
1752	20			
1702, 1693	728	1716	720	νCO (69)
1628	14	1631	38	νC3C4 (21), νC10C5 (12), νC7C8 (11)
1611	35	1612	23	νC3C4 (22), νC5C6(20), νC8C9 (11), νC10C9 (10)
1572	5	1573	16	νC7C8 (16), νC3C4 (14), νC6C7 (13), νC10C9 (11), β C7H (11)
1500	0.2	1503	2	β C8H (17), β C5H (14), β C6H (14), νC6C7 (11), νC10C5 (10)
1469	21	1466	21	νC9N1 (13), β C6H (13), β C7H (12), νC3C4 (11), νC5C6 (11)
1419	9	1425	7	β N1H (23), β C4H (17), νCO (10), β CO (10)
1399, **1392**	12	1392	5	β CO (16), β N1H (13), β C4H (13), β C5H (11), β C7H (11)
1339	15	1341	12	νC7C8 (19), νC10C9 (18), νC5C6 (17)
1311	7			
1297, 1295	7			
		1287	0	β C5H (18), νC9N1 (12), νC10C5 (12), β CO (10)
1267	30	1254	12	β N1H (18), β C8H (18), νC8C9 (10), β C5H (13)
1254, **1249**	22	1246	49	νN1C2 (29), νC2C3 (13), β CO (13), νC9N1 (11)
1221, **1216**	8	1218	8	νC4C10 (20), νC8C9 (17), β C4H (15), νC10C5 (11), β C6H (10)
1155, 1149	8	1161	5	β C7H (26), β C6H (23), β C8H (12), β C5H (11)
1440, **1135**	13	1138	18	νC5C6 (15), β C7H (14), νC7C8 (12), β C6H (10)
1120, 1119	14	1119	16	β CO (28), β C4H (14), β R4 (11)
1035	2	1036	2	νC6C7 (48), νC5C6 (13), νC7C8 (13)
		998	0	γC4H (72), γC3H (43)
		973	0	γC7H (51), γC6H (43), γC5H (15), γC8H (12)
937	2	942	3	γC5H (51), γC7H (24), γC8H (21), γC6H (13)
926, 922	10	921	4	β R1 (35), β R4(28)
		915	9	β R4 (26), νN1C2 (19), νC2C3 (19)
857	6	865	7	γC8H (34), γC3H (15), γC6H (14), γC5H (13)
830	44	835	47	γC3H (31), γCO (27), γC4H (17), γC8H (15)
		774	0	τR4 (39), τR1 (35), γCO (18)
769	4	765	4	νC10C9 (27), νC4C10 (18), νC10C5 (14)
757, **751**	58	754	59	γC6H (36), γC7H (22), γC5H (15), γC8H (12)
729	1	725	1	β R1 (25), νC2C3 (19), β R6(10)
693	14	702	15	γCO (29), γN1H (29), τR4 (24), γC3H (11)
620	23	632	30	γN1H (69), τR4 (17), τR1 (13)
619	23	621	7	β R5 (49), β R2 (26)
541	1	546	1	τR5 (43), τR4 (23), τR2 (13)
526	5	526	6	β R6 (34), β CO (16), β R5 (15), νC4C10 (11), β R3 (10)
484	8	484	9	β R2 (40), β CO (26), β R3 (13)
461, **456**	13	459	17	τR6 (45), τRR (30), τR3 (20)
444	5	442	5	β R3 (43), νC9N1 (12)
		379	1	τR3 (47), τR6 (38)
		301	2	β R6 (29), β CO (18), β R3 (15)
		259	2	τR1 (34), τR5 (22), τR6 (22), τRR (20)
		168	1	τR2 (38), τR5 (22), τRR (20), τR3 (12)
		104	2	τR3 (38), τR2 (34), τRR (12)

1-isoquinolinone

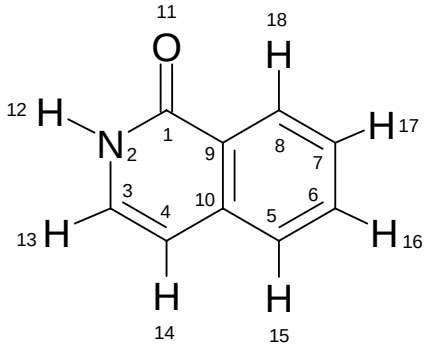

1IQo

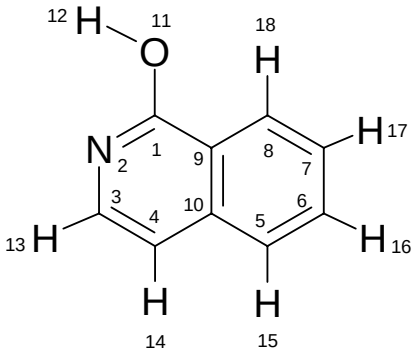

1IQh

Scheme B3. *Atom numbering for tautomers of 1-isoquinolinone.*

Table B7. *Internal coordinates used in the normal mode analysis for* ***1-isoquinolinone*** *forms* ***oxo*** *and* ***hydroxy*** *(atom numbering as in Scheme B3).*

In-plane		
Ring stretchings		
$S_1 = r_{1,2}$		νC1N2
$S_2 = r_{2,3}$		νN2C3
$S_3 = r_{3,4}$		νC3C4
$S_4 = r_{4,10}$		νC4C10
$S_5 = r_{10,9}$		νC10C9
$S_6 = r_{9,1}$		νC9C1
$S_7 = r_{10,5}$		νC10C5
$S_8 = r_{5,6}$		νC5C6
$S_9 = r_{6,7}$		νC6C7
$S_{10} = r_{7,8}$		νC7C8
$S_{11} = r_{8,9}$		νC8C9
Stretching NH, CO, CH		
$S_{12} = r_{1,11}$		νCO
$S_{13} = r_{2,12}$	oxo	νN2H
$S'_{13} = r_{11,12}$	hydroxy	νOH
$S_{14} = r_{3,13}$		νC3H
$S_{15} = r_{4,14}$		νC4H
$S_{16} = r_{5,15}$		νC5H
$S_{17} = r_{6,16}$		νC6H
$S_{18} = r_{7,17}$		νC7H
$S_{19} = r_{8,18}$		νC8H
Ring in-plane deformation		
$S_{20} = (6^{-1/2})(\beta_{9,2,1} - \beta_{1,3,2} + \beta_{2,4,3} - \beta_{3,10,4} + \beta_{4,9,10} - \beta_{10,1,9})$		βR1
$S_{21} = (12^{-1/2})(2\beta_{9,2,1} - \beta_{1,3,2} - \beta_{2,4,3} + 2\beta_{3,10,4} - \beta_{4,9,10} - \beta_{10,1,9})$		βR2
$S_{22} = (1/2)(\beta_{1,3,2} - \beta_{2,4,3} + \beta_{4,9,10} - \beta_{10,1,9})$		βR3
$S_{23} = (6^{-1/2})(\beta_{7,9,8} - \beta_{8,10,9} + \beta_{9,5,10} - \beta_{10,6,5} + \beta_{5,7,6} - \beta_{6,8,7})$		βR4
$S_{24} = (12^{-1/2})(2\beta_{7,9,8} - \beta_{8,10,9} - \beta_{9,5,10} + 2\beta_{10,6,5} - \beta_{5,7,6} - \beta_{6,8,7})$		βR5
$S_{25} = (1/2)(\beta_{8,10,9} - \beta_{9,5,10} + \beta_{5,7,6} - \beta_{6,8,7})$		βR6
Bendings CO, CH, NH,		
$S_{26} = (2^{-1/2})(\beta_{3,12,2} - \beta_{1,12,2})$	oxo	βN2H
$S'_{26} = \beta_{12,1,11}$	hydroxy	βOH
$S_{27} = (2^{-1/2})(\beta_{2,11,1} - \beta_{9,11,1})$		βCO
$S_{28} = (2^{-1/2})(\beta_{4,13,3} - \beta_{2,13,3})$		βC3H
$S_{29} = (2^{-1/2})(\beta_{10,14,4} - \beta_{3,14,4})$		βC4H
$S_{30} = (2^{-1/2})(\beta_{6,15,5} - \beta_{10,15,5})$		βC5H
$S_{31} = (2^{-1/2})(\beta_{7,16,6} - \beta_{5,16,6})$		βC6H
$S_{32} = (2^{-1/2})(\beta_{8,17,7} - \beta_{6,17,7})$		βC7H
$S_{33} = (2^{-1/2})(\beta_{9,18,8} - \beta_{7,18,8})$		βC8H
Out-of-plane		
Wagging CO, NH, CH		
$S_{34} = \gamma_{11,9,1,2}$		γCO
$S_{35} = \gamma_{13,2,3,4}$		γC3H
$S_{36} = \gamma_{14,3,4,10}$		γC4H
$S_{37} = \gamma_{15,10,5,6}$		γC5H
$S_{38} = \gamma_{16,5,6,7}$		γC6H
$S_{39} = \gamma_{17,6,7,8}$		γC7H
$S_{40} = \gamma_{18,7,8,9}$		γC8H
$S_{41} = \gamma_{12,1,2,3}$	oxo	γN2H
Torsion OH		
$S'_{41} = (2^{-1/2})(\tau_{12,11,1,2} + \tau_{12,11,1,9})$	hydroxy	τOH
Ring torsions		
$S_{42} = (6^{-1/2})(\tau_{2,1,9,10} - \tau_{1,9,10,4} + \tau_{9,10,4,3} - \tau_{10,4,3,2} + \tau_{4,3,2,1} - \tau_{3,2,1,9})$		τR1
$S_{43} = (12^{-1/2})(2\tau_{1,9,10,4} - \tau_{2,1,9,10} - \tau_{9,10,4,3} + 2\tau_{4,3,2,1} - \tau_{10,4,3,2} - \tau_{3,2,1,9})$		τR2
$S_{44} = (1/2)(\tau_{2,1,9,10} - \tau_{9,10,4,3} + \tau_{10,4,3,2} - \tau_{3,2,1,9})$		τR3
$S_{45} = (6^{-1/2})(\tau_{9,8,7,6} - \tau_{8,7,6,5} + \tau_{7,6,5,10} - \tau_{6,5,10,9} + \tau_{5,10,9,8} - \tau_{10,9,8,7})$		τR4
$S_{46} = (12^{-1/2})(2\tau_{8,7,6,5} - \tau_{9,8,7,6} - \tau_{7,6,5,10} + 2\tau_{5,10,9,8} - \tau_{6,5,10,9} - \tau_{10,9,8,7})$		τR5
$S_{47} = (1/2)(\tau_{9,8,7,6} - \tau_{7,6,5,10} + \tau_{6,5,10,9} - \tau_{10,9,8,7})$		τR6
Two rings relative torsion		
$S_{48} = (2^{-1/2})(\tau_{5,10,9,1} - \tau_{4,10,9,8})$		τRR

Table B8. *Experimental wavenumbers ($\tilde{\nu}$ /cm^{-1}) and relative integral intensities (I) of the absorption bands in the spectrum of* ***1-isoquinolinone*** *isolated in an Ar matrix, compared with wavenumbers ($\tilde{\nu}$ /cm^{-1}), absolute intensities (Ath / km mol^{-1}) and potential energy distribution (PED / %) calculated for the* ***oxo*** *form of* ***1-isoquinolinone.***

Observed Ar matrix, T = 10 K		**Calculated B3LYP/CC-pVTZ**		
$\tilde{\nu}$	**I**	$\tilde{\nu}$	**Ath**	**PED (%)**
3449, **3444**	106	3534	70	νN2H (100)
		3150	9	νC4H (52), νC3H (47)
		3139	7	νC8H (83), νC7H (15)
		3133	0	νC3H (52), νC4H (47)
		3125	14	νC6H (42), νC7H (34), νC8H (13), νC5H (11)
		3114	14	νC7H (43), νC5H (39), νC6H (14)
		3101	2	νC5H (49), νC6H (42)
1702, **1696,** 1684, 1681	521	1708	492	νCO (74)
1641	59	1642	72	νC3C4 (53), β C3H (10)
1623	4			
1615, 1608	15	1616	25	νC5C6 (23), νC7C8 (16), νC8C9 (13), νC10C5 (10), β R6 (10)
1563	5	1558	6	νC6C7 (23), νC10C9 (15), νC7C8 (10), β C7H (10)
1504	2			
1493, **1490**	25	1495	26	νC4C10 (13), β C5H (12)
1460	1			
		1463	0	β C7H (23), β C6H (12), νC8C9 (11), νC5C6 (10)
1447, 1440, 1434	9	1446	19	β N2H (18), νN2C3 (17), β C4H (12), β C5H (12)
1423	2			
1397, 1392	7	1398	2	β N2H (26), β C3H (20), β C4H (11)
1338	22	1329	23	νC10C9 (22), νC7C8 (17), νC5C6 (15), νC10C5 (10), νC8C9 (10)
1319	18			
1306	9	1290	16	β C5H (17), νC9C1 (14), νC1N2 (13), β C7H (10)
1271	3			
1251, 1242	5	1249	8	β C8H (25), νC8C9 (13), νC1N2 (10), β C5H (10)
1219, 1217	9	1209	9	νC4C10 (17), β C3H (16), νC10C5 (14), νC9C1 (13)
1203	21	1201	27	β C4H (31), β C3H (19), β N2H (14), νN2C3 (11)
1188	8			
1155	4	1159	4	β C6H (32), β C5H (17), β C7H (15)
1135, 1132, 1127	20	1129	17	β C7H (21), νC7C8 (17), νC5C6 (12), νC1N2 (11)
1096	7	1095	9	β R4 (22), νN2C3 (17), β C4H (14), νC3C4 (12)
1063, 1058	17	1061	15	νN2C3 (22), β R4 (15)
1026	11	1027	15	νC6C7 (44), νC5C6 (13), νC7C8 (13)
1013	2			
		995	0	γC7H (47), γC8H (42), γC6H (27)
963	2	972	1	γC6H (45), γC8H (35), γC5H (30)
		929	0	γC3H (73), γC4H (43)
905	4	901	3	β R1 (39), β R4 (16)
877	2	885	2	γC5H (44), γC7H (23), γC8H (15)
		804	0	γCO (40), τR4 (23), τR1 (13), γC5H (12)
789	15	789	7	β R4 (21), β R1 (18), β R6 (17), νC4C10 (10), νC10C5 (10)
784	62	787	69	γC7H (25), γC4H (22), γC3H (12), γC6H (10)
		738	0	γC4H (38), γC3H (20), γC7H (11)
		717	0	β R5 (27), νC10C9 (20), νC1N2 (12), νC9C1 (12)
705	77	713	80	γCO (38), τR4 (33), γN2H (30)
625	27	634	21	γN2H (51), τR4 (31), τR1 (17)
589	2	588	2	β R5 (45), β R2 (18), νC1N2 (10), β CO (10)
565	2	570	2	τR1 (24), γN2H (21), τR3 (21), τRR (14), τR4 (10)
530	5	529	5	β CO (33), β R2 (24), β R6 (22)
487	5	484	4	β R2 (32), β R3 (18), β R6 (18)
466	3	463	2	β R3 (29), νC9C1 (16), νC10C5 (11), β R5 (11)
452	2	460	1	τR5 (54), τR2 (38)

Table B8. *(Continuating).*

Observed Ar matrix, T = 10 K		**Calculated B3LYP/CC-pVTZ**		
$\tilde{\nu}$	**I**	$\tilde{\nu}$	**Ath**	**PED (%)**
409	6	414	10	τR6 (82)
		289	6	βR6 (27), βR3 (24), βCO (20), νC9C1 (10)
		225	2	τR2 (27), τRR (27), τR3 (16), τR6 (11), τR5 (10)
		164	2	τRR (34), τR2 (23), τR3 (15), τR5 (14), τR6 (10)
		120	5	τR3 (53), τR1 (24), τR5 (13)

Table B9. *Experimental wavenumbers ($\tilde{\nu}$ /cm^{-1}) and relative integral intensities (I) of the absorption bands in the spectrum of* ***1-isoquinolinone*** *isolated in an Ar matrix, compared with wavenumbers ($\tilde{\nu}$ /cm^{-1}), absolute intensities (Ath / km mol^{-1}) and potential energy distribution (PED / %) calculated for the* ***hydroxy*** *form of* ***1-isoquinolinone.***

Observed Ar matrix, T = 10 K		**Calculated B3LYP/CC-pVTZ**		
$\tilde{\nu}$	**I**	$\tilde{\nu}$	**Ath**	**PED (%)**
3572	117	3679	93	νOH (100)
		3142	6	νC8H (87), νC7H (12)
		3126	19	νC4H (55), νC6H (15), νC3H (10)
		3124	21	νC6H (31), νC4H (28), νC7H (22)
		3114	10	νC7H (48), νC5H (41)
		3102	1	νC6H (38), νC5H (32), νC3H (17), νC7H (10)
		3101	11	νC3H (66), νC4H (15), νC5H (10)
1643, **1638**	100	1638	50	νC5C6 (10)
1601	47	1603	20	νC3C4 (23), νC5C6 (20)
1583	57	1581	88	νC10C9 (19), νC7C8 (18), νC1N2 (16), νC6C7 (11)
1506	48	1512	53	νC6C7 (14), β C6H (11), β C5H (10)
1460	17	1464	7	β C3H (19), β C7H (17), β C4H (10)
1442	39	1442	43	νC9C1 (15), β C6H (13), νC3C4 (10)
1413	30	1417	66	β C3H (14), νCO (13), β C6H (11)
1391	48	1386	76	νC1N2 (24), νC3C4 (16), νC10C9 (14), β C5H (10)
		1357	1	νC10C9 (18), νC5C6 (16), νC7C8 (14)
1280	13	1287	31	β R1 (17), β C8H (17), νN2C3 (13), νCO (13), β C3H (12)
1268	36	1256	24	β C5H (20), β C3H (16), β C8H (10)
1254, 1251	23	1221	22	β C4H (21), β OH (14), νC4C10 (12), β R4 (10)
1224	56	1200	66	β OH (24), β C7H (17), β C6H (13), νC9C1 (10)
1210	32			
1201	18			
1151	30	1154	43	β C7H (29), β C8H (20), νC7C8 (14)
1146	14	1149	5	β C6H (25), β C5H (24), νC5C6 (16)
1097	4	1092	4	β R4 (21), β C4H (17), νC3C4 (11), νCO (10)
1049	82	1049	90	νN2C3 (24), β R4 (12)
1026, 1018	27	1023	13	νC6C7 (53), νC5C6 (11), νC7C8 (10)
		991	0	γC6H (45), γC7H (40), γC8H (20), γC5H (17)
		968	0	γC8H (30), γC3H (26), γC5H (18), γC4H (14), γC6H (14), γC7H (11)
		962	1	γC3H (56), γC4H (19), γC8H (15), γC5H (10), γC6H (10)
898	6	894	7	β R1 (32), β R4 (21)
871	4	880	5	γC5H (34), γC8H (19), γC7H (13)
814	53	818	51	γC4H (55), γC3H (18), γC7H (13)
		802	0	τR1 (31), τR4 (26), γCO (20), γC5H (12)
789	24	793	6	β R4 (21), β R1 (20), β R6 (13), β R3 (12)
775	24			
769	16			
748	12	753	17	γC7H (24), γC6H (16), γC4H (14), γC8H (13), γC5H (11)
		722	1	β R5 (24), νC10C9 (20), νC9C1 (10)
683 676	26 20	685	36	τR4 (53), γCO (32)
588	2	588	3	β R5 (40), β R2 (26)
580	5	587	10	τR1 (35), τR4 (17), τR3 (16), γCO (15), τRR (10)
505	52	535	64	τOH (86)
517	8	516	9	β R2 (27), β R6 (21), β CO (21)
		496	0	β R6 (24), β R2 (20), β R3 (20)
		468	0	τR5 (48), τR2 (47)
		467	1	β R3 (27), β CO (25), νC10C5 (12), R5 (10)
413	11	418	16	τR6 (80), τRR (10)
		277	5	β CO (28), β R6 (26), β R3 (21)
		264	5	τR3 (39), τR5 (16), γCO (14), τR2 (13)
		170	1	τRR (48), τR6 (19), τR3 (14)
		131	0	τR3 (34), τR2 (23), τR5 (22), τR1 (12)

4-quinazolinone

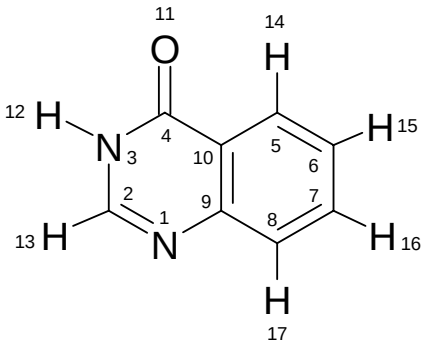

4QZo

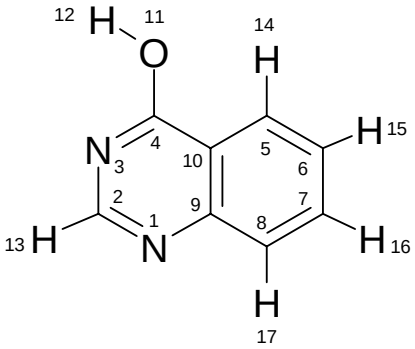

4QZh

Scheme B4. *Atom numbering for tautomers of 4-quinazolinone.*

Table B10. *Internal coordinates used in the normal mode analysis for* ***4-hydroxyquinazoline*** *forms* ***oxo*** *and* ***hydroxy*** *(atom numbering as in Scheme B4).*

In-plane		
Ring stretchings		
$S_1 = r_{1,2}$		ν N1C2
$S_2 = r_{2,3}$		ν C2N3
$S_3 = r_{3,4}$		ν N3C4
$S_4 = r_{4,10}$		ν C4C10
$S_5 = r_{10,9}$		ν C10C9
$S_6 = r_{9,1}$		ν C9N1
$S_7 = r_{10,5}$		ν C10C5
$S_8 = r_{5,6}$		ν C5C6
$S_9 = r_{6,7}$		ν C6C7
$S_{10} = r_{7,8}$		ν C7C8
$S_{11} = r_{8,9}$		ν C8C9
Stretching NH, CO, CH		
$S_{12} = r_{4,11}$		ν CO
$S_{13} = r_{3,12}$	oxo	ν N3H
$S'_{13} = r_{11,12}$	hydroxy	ν OH
$S_{14} = r_{2,13}$		ν C2H
$S_{15} = r_{5,14}$		ν C5H
$S_{16} = r_{6,15}$		ν C6H
$S_{17} = r_{7,16}$		ν C7H
$S_{18} = r_{8,17}$		ν C8H
Ring in-plane deformation		
$S_{19} = (6^{-1/2})(\beta_{9,2,1} - \beta_{1,3,2} + \beta_{2,4,3} - \beta_{3,10,4} + \beta_{4,9,10} - \beta_{10,1,9})$		β R1
$S_{20} = (12^{-1/2})(2\beta_{9,2,1} - \beta_{1,3,2} - \beta_{2,4,3} + 2\beta_{3,10,4} - \beta_{4,9,10} - \beta_{10,1,9})$		β R2
$S_{21} = (1/2)(\beta_{1,3,2} - \beta_{2,4,3} + \beta_{4,9,10} - \beta_{10,1,9})$		β R3
$S_{22} = (6^{-1/2})(\beta_{7,9,8} - \beta_{8,10,9} + \beta_{9,5,10} - \beta_{10,6,5} + \beta_{5,7,6} - \beta_{6,8,7})$		β R4
$S_{23} = (12^{-1/2})(2\beta_{7,9,8} - \beta_{8,10,9} - \beta_{9,5,10} + 2\beta_{10,6,5} - \beta_{5,7,6} - \beta_{6,8,7})$		β R5
$S_{24} = (1/2)(\beta_{8,10,9} - \beta_{9,5,10} + \beta_{5,7,6} - \beta_{6,8,7})$		β R6
Bendings CO, CH, NH,		
$S_{25} = (2^{-1/2})(\beta_{2,12,3} - \beta_{4,12,3})$	oxo	β N3H
$S'_{25} = \beta_{12,4,11}$	hydroxy	β OH
$S_{26} = (2^{-1/2})(\beta_{3,11,4} - \beta_{10,11,4})$		β CO
$S_{27} = (2^{-1/2})(\beta_{1,13,2} - \beta_{3,13,2})$		β C2H
$S_{28} = (2^{-1/2})(\beta_{10,14,5} - \beta_{6,14,5})$		β C5H
$S_{29} = (2^{-1/2})(\beta_{5,15,6} - \beta_{7,15,6})$		β C6H
$S_{30} = (2^{-1/2})(\beta_{6,16,7} - \beta_{8,16,7})$		β C7H
$S_{31} = (2^{-1/2})(\beta_{7,17,8} - \beta_{9,17,8})$		β C8H
Out-of-plane		
Wagging CO, NH, CH		
$S_{32} = \gamma_{11,3,4,10}$		γ CO
$S_{33} = \gamma_{13,1,2,3}$		γ C2H
$S_{34} = \gamma_{14,10,5,6}$		γ C5H
$S_{35} = \gamma_{15,5,6,7}$		γ C6H
$S_{36} = \gamma_{16,6,7,8}$		γ C7H
$S_{37} = \gamma_{17,7,8,9}$		γ C8H
$S_{38} = \gamma_{12,2,3,4}$	oxo	γ N3H
Torsion OH		
$S'_{38} = (2^{-1/2})(\tau_{12,11,4,3} + \tau_{12,11,14,10})$	hydroxy	τ OH
Ring torsions		
$S_{39} = (6^{-1/2})(\tau_{2,1,9,10} - \tau_{1,9,10,4} + \tau_{9,10,4,3} - \tau_{10,4,3,2} + \tau_{4,3,2,1} - \tau_{3,2,1,9})$		τ R1
$S_{40} = (12^{-1/2})(2\tau_{1,9,10,4} - \tau_{2,1,9,10} - \tau_{9,10,4,3} + 2\tau_{4,3,2,1} - \tau_{10,4,3,2} - \tau_{3,2,1,9})$		τ R2
$S_{41} = (1/2)(\tau_{2,1,9,10} - \tau_{9,10,4,3} + \tau_{10,4,3,2} - \tau_{3,2,1,9})$		τ R3
$S_{42} = (6^{-1/2})(\tau_{9,8,7,6} - \tau_{8,7,6,5} + \tau_{7,6,5,10} - \tau_{6,5,10,9} + \tau_{5,10,9,8} - \tau_{10,9,8,7})$		τ R4
$S_{43} = (12^{-1/2})(2\tau_{8,7,6,5} - \tau_{9,8,7,6} - \tau_{7,6,5,10} + 2\tau_{5,10,9,8} - \tau_{6,5,10,9} - \tau_{10,9,8,7})$		τ R5
$S_{44} = (1/2)(\tau_{9,8,7,6} - \tau_{7,6,5,10} + \tau_{6,5,10,9} - \tau_{10,9,8,7})$		τ R6
Two rings relative torsion		
$S_{45} = (2^{-1/2})(\tau_{5,10,9,1} - \tau_{4,10,9,8})$		τ RR

Table B11. *Experimental wavenumbers ($\tilde{\nu}$ /cm^{-1}) and relative integral intensities (I) of the absorption bands in the spectrum of* ***4-hydroxyquinazoline*** *isolated in an Ar matrix, compared with wavenumbers ($\tilde{\nu}$ /cm^{-1}), absolute intensities (Ath/km mol^{-1}) and potential energy distribution (PED/%) calculated for the* ***oxo*** *form of* ***4-hydroxyquinazoline.***

Observed Ar matrix, T = 10 K		**Calculated B3LYP/CC-pVTZ**		
$\tilde{\nu}$	**I**	$\tilde{\nu}$	**Ath**	**PED (%)**
3432	105	3519	63	νN3H (100)
		3139	9	νC5H (57), νC6H (19), νC8H (16)
		3135	5	νC8H (67), νC5H (23)
		3123	8	νC6H (53), νC7H (20), νC5H (17), νC8H (10)
		3108	4	νC7H (65), νC6H (26)
		3093	12	νC2H (100)
1738, 1731, **1722,** 1714, 1704	489	1730	496	νCO (78)
1681	24			
1625	100	1632	96	νN1C2 (58), β C2H (10)
1618	80	1616	108	νC5C6 (20), νC10C5 (13), νC7C8 (13), νC8C9 (12)
1571	4	1566	6	νC6C7 (24), νC10C9 (17), β R5 (10)
1478	51	1479	49	β C8H (17), β C5H (16), νC10C9 (12)
1468	16	1470	19	β C7H (23), β C6H (21), νC10C5 (10)
1429	13	1426	23	β N3H (41), νC2N3 (21)
1414, 1411	9			
1390	12			
		1393	8	β C2H (64), νN1C2 (11), νC9N1 (10)
1351	7			
1319, 1318	40	1320	23	νC10C9 (24), νC5C6 (16), νC10C5 (13), νC7C8 (11), ν C8C9 (11)
1307, 1303 1292, 1286	5 12	1295	20	β C8H (18), β C6H (12), νC4C10 (10), β C5H (10)
1250, **1243**	19	1238	25	β C5H (23), νN3C4 (11), β C8H (11)
1225, 1222	13	1215	5	νC9N1 (23), νC4C10 (14), νC8C9 (10), β C2H (10), β C7H (10)
1153	6	1155	8	β C7H (27), β C6H (20), β C8H (15), νC6C7 (10)
1133	41	1129	38	νC5C6 (15), β C6H (15), νN3C4 (14)
1103	6	1103	9	β R4 (26), νC2N3 (22), β N3H (12)
1071, 1068	11	1066	10	νC2N3 (18), β R4 (16), νN3C4 (13), β CO (11)
1021	10	1025	11	νC6C7 (45), νC7C8 (14), νC5C6 (13)
		1001	0	γC7H (46), γC6H (38), γC5H (20), γC8H (19)
965	2	981	2	γC5H (49), γC8H (29), γC7H (20), γC6H (13)
931	5	935	5	γC2H (100)
911, 908	13	901	11	β R1 (47), νN3C4 (10)
		896	1	γC8H (36), γC5H (19), γC6H (17)
811	5	811	6	β R4 (29), β R6 (16), νC9N1 (13), νC8C9 (10), β R1 (10)
		806	1	γCO (37), τR4 (24), τR1 (18), γC8H (10)
781, **776**	47	784	42	γC6H (36), γC7H (18), γC5H (13), τRR (10)
709	74	719	80	γCO (37), γN3H (36), τR4 (22)
		718	1	β R5 (26), νC10C9 (20), νC4C10 (13), νN3C4 (12)
652, **646**	18	656	14	γN3H (44), τR4 (36), τR1 (15)
582, 580	11	586	7	γN3H (21), τR1 (18), τR3 (18), τR4 (15), τRR (13)
		581	2	β R5 (45), β R2 (13), νN3C4 (12), β CO (12)
528	9	527	9	β CO (31), β R2 (25), β R6 (23)
		492	1	β R3 (40), β R6 (16), β R2 (10)
488	4	485	4	β R2 (36), β R5 (16)
		467	4	τR5 (57), τR2 (38)
416	9	422	10	τR6 (85)
		290	4	β R6 (27), β CO (24), β R3 (19), νC4C10 (12)
		229	0	τRR (32), τR2 (24), τR6 (13), τR5 (11), τR3 (10)
		158	6	τRR (31), τR2 (27), τR3 (21), τR5 (11), τR6 (10)
		123	7	τR3 (48), τR1 (26), τR5 (16)

Table B12. *Experimental wavenumbers ($\tilde{\nu}$ /cm^{-1}) and relative integral intensities (I) of the absorption bands in the spectrum of* ***4-hydroxyquinazoline*** *isolated in an Ar matrix, compared with wavenumbers ($\tilde{\nu}$ /cm^{-1}), absolute intensities (Ath/km mol^{-1}) and potential energy distribution (PED / %) calculated for the* ***hydroxy*** *form of* ***4-hydroxyquinazoline.***

Observed Ar matrix, T = 10 K		**Calculated B3LYP/CC-pVTZ**		
$\tilde{\nu}$	**I**	$\tilde{\nu}$	**Ath**	**PED (%)**
3561	146	3669	103	νOH (100)
		3140	7	νC5H (65), νC6H (17), νC8H (12)
		3136	6	νC8H (74), νC5H (17)
		3122	9	νC6H (55), νC7H (22), νC5H (15)
		3107	4	νC7H (65), νC6H (28)
		3097	25	νC2H (100)
1641, 1636	52			
		1632	85	νC7C8 (15), νC10C5 (11), νC5C6 (11), νC4C10 (10)
1596, 1592	93	1600	78	νN3C4 (21), νN1C2 (18), νC5C6 (13)
1576, **1572**	101	1572	114	νC10C9 (21), νC6C7 (14), νC5C6 (10), β R5 (10)
1500, 1496	127	1505	139	νC6C7 (13), νN3C4 (10), νC8C9 (10), β C5H (10), β C7H (10), β C8H (10)
1457	9	1465	10	β C6H (18), β C2H (15), β C7H (13)
1436	67	1436	103	νCO (21), β C5H (12), νC4C10 (11)
1419	2	1405	8	β C2H (47), νC9N1 (12)
1376	67	1370	62	νC10C9 (23), νN1C2 (18), νN3C4 (16)
1322	35	1330	60	β OH (19), νN1C2 (17)
		1297	3	νC2N3 (21), β C2H (16), νCO (15)
1267, 1263	25	1272	15	β C5H (21), β C8H (17), β R1 (10)
1216	19			
1206	84	1202	43	β OH (20), β C6H (17), β C7H (16), νC9N1 (12)
1196	15			
1183	23	1188	15	νC2N3 (13), β C8H (12), β R4 (11)
1148	32	1148	45	β C6H (23), β C5H (14), β OH (11)
		1117	1	β R4 (16), β C7H (15), β C8H (13), νC7C8 (11), νC2N3 (10)
1064, 1061, **1058**	88	1060	111	νC2N3 (19), β R4 (16), νCO (13)
1028	6	1020	7	νC6C7 (54), νC7C8 (12), νC5C6 (10)
		1001	0	γC7H (58), γC8H (32), γC6H (25)
965	11	976	5	γC2H (34), γC5H (34), γC6H (24), γC8H (16)
		969	1	γC2H (72), γC5H (18), γC6H (10)
903	30	899	32	β R1 (40), β R4 (12), νCO (11)
890	7	891	3	γC8H (29), γC5H (22), τR1 (15), γC7H (13), γC6H (10)
820	4	819	4	β R4 (31), β R6 (13), β R3 (12), νC8C9 (11), β R1 (11)
800	19	813	3	τR1 (34), τR4 (24), γCO (18), γC8H (12)
771	80	779	47	γC6H (35), γC7H (19), γC5H (18), τRR (11)
712	16	726	2	β R5 (22), νC10C9 (21), νC4C10 (12), νC10C5 (11)
686, 676	31 33	696	43	τR4 (51), γCO (31)
		606	3	τR1 (27), τR4 (24), τR3 (16), γCO (13)
583	5	583	8	β R5 (41), β R2 (23)
530, 527	54	558	70	τOH (85)
		517	2	β R2 (29), β R6 (20), β CO (15)
		504	0	β R3 (26), β R2 (22), β R6 (18)
		491	3	β CO (28), β R3 (14), β R5 (13), νC8C9 (12)
482	5	469	1	τR5 (49), τR2 (44)
419	15	425	12	τR6 (78)
		279	5	β CO (32), β R6 (26), β R3 (16)
		263	0	τR3 (34), τR5 (15), τR2 (14), γCO (14), τRR (11)
		170	2	τRR (48), τR3 (21), τR6 (19)
		128	0	τR3 (29), τR2 (27), τR5 (24), τR1 (13)

3-hydroxyisoquinoline

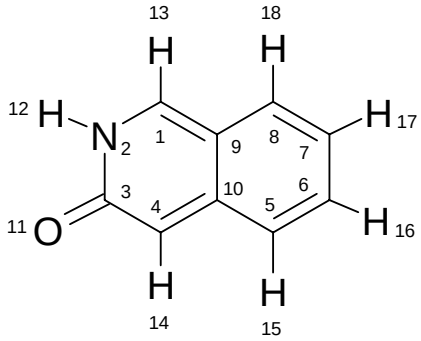

3IQo

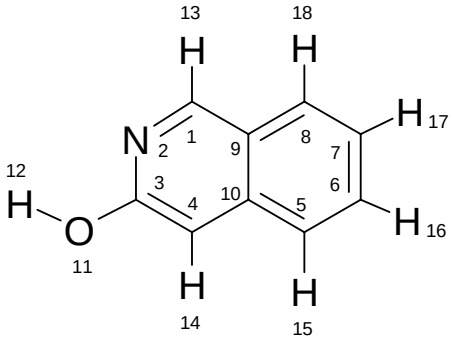

3IQh

Scheme B5. *Atom numbering for tautomers of 3-hydroxyquinoline.*

Table B13. *Internal coordinates used in the normal mode analysis for* ***3-hydroxyisoquinoline*** *(atom numbering as in Scheme B5).*

In-plane	
Ring stretchings	
$S_1 = r_{1,2}$	νC1N2
$S_2 = r_{2,3}$	νN2C3
$S_3 = r_{3,4}$	νC3C4
$S_4 = r_{4,10}$	νC4C10
$S_5 = r_{10,9}$	νC10C9
$S_6 = r_{9,1}$	νC9C1
$S_7 = r_{10,5}$	νC10C5
$S_8 = r_{5,6}$	νC5C6
$S_9 = r_{6,7}$	νC6C7
$S_{10} = r_{7,8}$	νC7C8
$S_{11} = r_{8,9}$	νC8C9
Stretching NH, CO, CH, OH	
$S_{12} = r_{1,13}$	νC1H
$S_{13} = r_{11,12}$	νOH
$S_{14} = r_{3,11}$	νCO
$S_{15} = r_{4,14}$	νC4H
$S_{16} = r_{5,15}$	νC5H
$S_{17} = r_{6,16}$	νC6H
$S_{18} = r_{7,17}$	νC7H
$S_{19} = r_{8,18}$	νC8H
Ring in-plane deformation	
$S_{20} = (6^{-1/2})(\beta_{9,2,1} - \beta_{1,3,2} + \beta_{2,4,3} - \beta_{3,10,4} + \beta_{4,9,10} - \beta_{10,1,9})$	β R1
$S_{21} = (12^{-1/2})(2\beta_{9,2,1} - \beta_{1,3,2} - \beta_{2,4,3} + 2\beta_{3,10,4} - \beta_{4,9,10} - \beta_{10,1,9})$	β R2
$S_{22} = (1/2)(\beta_{1,3,2} - \beta_{2,4,3} + \beta_{4,9,10} - \beta_{10,1,9})$	β R3
$S_{23} = (6^{-1/2})(\beta_{7,9,8} - \beta_{8,10,9} + \beta_{9,5,10} - \beta_{10,6,5} + \beta_{5,7,6} - \beta_{6,8,7})$	β R4
$S_{24} = (12^{-1/2})(2\beta_{7,9,8} - \beta_{8,10,9} - \beta_{9,5,10} + 2\beta_{10,6,5} - \beta_{5,7,6} - \beta_{6,8,7})$	β R5
$S_{25} = (1/2)(\beta_{8,10,9} - \beta_{9,5,10} + \beta_{5,7,6} - \beta_{6,8,7})$	β R6
Bendings CO, CH, NH, OH	
$S_{26} = (2^{-1/2})(\beta_{2,13,1} - \beta_{9,13,1})$	β C1H
$S_{27} = \beta_{12,3,11}$	β OH
$S_{28} = (2^{-1/2})(\beta_{4,11,3} - \beta_{2,11,3})$	β CO
$S_{29} = (2^{-1/2})(\beta_{10,14,4} - \beta_{3,14,4})$	β C4H
$S_{30} = (2^{-1/2})(\beta_{6,15,5} - \beta_{10,15,5})$	β C5H
$S_{31} = (2^{-1/2})(\beta_{7,16,6} - \beta_{5,16,6})$	β C6H
$S_{32} = (2^{-1/2})(\beta_{8,17,7} - \beta_{6,17,7})$	β C7H
$S_{33} = (2^{-1/2})(\beta_{9,18,8} - \beta_{7,18,8})$	β C8H
Out-of-plane	
Wagging CO, NH, CH	
$S_{34} = \gamma_{11,2,3,4}$	γCO
$S_{35} = \gamma_{13,9,1,2}$	γC1H
$S_{36} = \gamma_{14,3,4,10}$	γC4H
$S_{37} = \gamma_{15,10,5,6}$	γC5H
$S_{38} = \gamma_{16,5,6,7}$	γC6H
$S_{39} = \gamma_{17,6,7,8}$	γC7H
$S_{40} = \gamma_{18,7,8,9}$	γC8H
Torsion OH	
$S_{41} = (2^{-1/2})(\tau_{12,11,3,4} + \tau_{12,11,3,2})$	τOH
Ring torsions	
$S_{42} = (6^{-1/2})(\tau_{2,1,9,10} - \tau_{1,9,10,4} + \tau_{9,10,4,3} - \tau_{10,4,3,2} + \tau_{4,3,2,1} - \tau_{3,2,1,9})$	τR1
$S_{43} = (12^{-1/2})(2\tau_{1,9,10,4} - \tau_{2,1,9,10} - \tau_{9,10,4,3} + 2\tau_{4,3,2,1} - \tau_{10,4,3,2} - \tau_{3,2,1,9})$	τR2
$S_{44} = (1/2)(\tau_{2,1,9,10} - \tau_{9,10,4,3} + \tau_{10,4,3,2} - \tau_{3,2,1,9})$	τR3
$S_{45} = (6^{-1/2})(\tau_{9,8,7,6} - \tau_{8,7,6,5} + \tau_{7,6,5,10} - \tau_{6,5,10,9} + \tau_{5,10,9,8} - \tau_{10,9,8,7})$	τR4
$S_{46} = (12^{-1/2})(2\tau_{8,7,6,5} - \tau_{9,8,7,6} - \tau_{7,6,5,10} + 2\tau_{5,10,9,8} - \tau_{6,5,10,9} - \tau_{10,9,8,7})$	τR5
$S_{47} = (1/2)(\tau_{9,8,7,6} - \tau_{7,6,5,10} + \tau_{6,5,10,9} - \tau_{10,9,8,7})$	τR6
Two rings relative torsion	
$S_{48} = (2^{-1/2})(\tau_{5,10,9,1} - \tau_{4,10,9,8})$	τRR

Table B14. *Experimental wavenumbers ($\tilde{\nu}$ /cm^{-1}) and relative integral intensities (I) of the absorption bands in the spectrum of carbostyril isolated in an Ar matrix, compared with wavenumbers ($\tilde{\nu}$ /cm^{-1}), absolute intensities (Ath / km mol^{-1}) and potential energy distribution (PED / %) calculated for* ***3-hydroxyisoquinoline.***

Observed Ar matrix, T = 10 K		**Calculated B3LYP/CC-pVTZ**		
$\tilde{\nu}$	**I**	$\tilde{\nu}$	**Ath**	**PED (%)**
3585, 3582	153	3689	103	νOH (100)
		3131	4	νC4H (96)
3074	17	3128	19	νC7H (58), νC6H (25)
3044	4	3116	22	νC5H (41), νC6H (29), νC7H (21)
		3104	2	νC8H (42), νC5H (35), νC6H (21)
		3099	3	νC8H (41), νC6H (23), νC7H (18), νC5H (17)
2997	4	3071	17	νC1H (99)
1656, 1652, **1644,** 1641, 1632	157	1642	188	νC3C4 (16)
1625	7			
1611	37	1618	41	νC5C6 (23), νC3C4 (19), νC7C8 (11)
1586, **1581**	33	1576	33	νC10C9 (18), νC7C8 (18), νC1N2 (16)
1566, 1561	10			
1515, **1505,** 1498	69	1513	69	νC4C10 (13), νC6C7 (13), νC10C5 (10), β C6H (10)
1482	6			
1465, **1464,** 1461	62	1465	49	β C6H (15), β C7H (13), νC8C9 (10)
1453, **1451**	69	1458	84	β C1H (15), β C4H (13), νN2C3 (10)
1393	6	1383	3	νC10C9 (22), νC9C1 (11), β C5H (10)
1368	4	1379	3	νC5C6 (16), β C1H (16), νC7C8 (14), β C5H (11)
1333	29	1348	15	νC1N2 (41), β C8H (10)
1298, **1296**	108	1302	130	β C1H (21), νCO (19), νC4C10 (12)
1273, **1269**	14	1265	17	νC9C1 (14), β C4H (14), β R1 (12), β R4 (12), νC10C5 (10), β C5H (10), β C8H (10)
1228, **1224,** 1219	113	1227	95	νC8C9 (22), νC9C1 (14), β C1H (10)
1201	12	1195	19	β OH (33), β C5H (12)
1171, 1163	81	1167	91	β C7H (27), β C4H (17), β C8H (14), β C6H (12), β OH (10)
1139, 1128	10	1142	24	β C6H (24), β C5H (18), νC5C6 (17)
1118, 1111, 1108	62	1129	38	νC7C8 (15), β C4H (15), β C7H (13), β C8H (12), νC10C5 (10)
1075	0.5			
1014	3	1018	3	νC6C7 (57)
		985	0	γC6H (56), γC7H (31), γC5H (25), γC8H (11)
956	6	962	5	γC8H (42), γC1H (23), γC7H (18), γC5H (17), γC6H (11)
959	22	958	25	νN2C3 (30), β R1 (19), νC3C4 (13), β R4 (10)
927	5	936	3	γC1H (77), γC7H (12)
911, **910**	21	909	16	β R4 (50)
870, 867	27	875	24	γC4H (43), γC5H (17), γC8H (12), γC6H (11)
839	13	844	13	γC4H (49), γC5H (19), γC8H (17), γC7H (13)
		781	0	τR1 (49), τR4 (35)
		780	0	νC10C9 (40), β R2 (19)
754, 748	40	752	35	γC7H (31), γC8H (19), γC6H (17), γC5H (11)
		739	1	β R1 (29), νCO (14), νC8C9 (13)
691	12	700	14	τR4 (38), γCO (31), τR1 (15)
628	10	632	9	β R5 (57), β R2 (26)
535, 532	5	543	7	τR5 (34), τR4 (29), γCO (17), τR1 (13)
		532	2	β R6 (44), β CO (20), β R3 (14)
		495	33	τOH (66), τR3 (11), τRR (11)
471	1	471	1	β R2 (34), β R5 (16), β CO (10)
446, 441	107	462	71	τOH (30), τR3 (25), τR6 (21), τRR (18)
423	5	422	7	β R3 (56), β CO (24)
		421	1	τR6 (41), τR3 (30), τR5 (13), τR2 (11)
		290	4	β R6 (29), β CO (28)
		286	0	τR6 (26), τR5 (20), τR1 (18), γCO (12), τR3 (12), τRR (12)
		180	0	τR2 (35), τR5 (28), τRR (19)
		116	0	τR3 (29), τR2 (28), τRR (24)

Appendix C

Spectroscopic data of systems with heterocyclic ring and fused five-membered ring

allopurinol

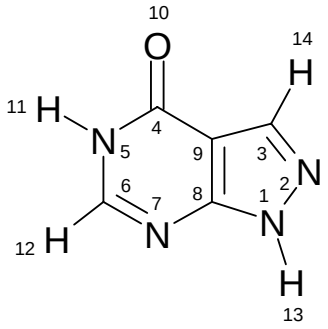

AI

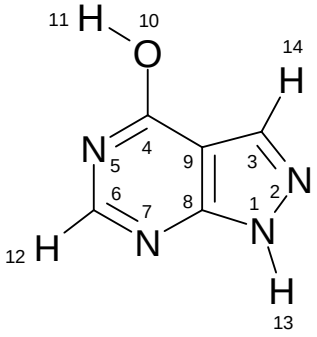

AIII

Scheme C1. *Atom numbering for tautomers of allopurinol.*

Table C1. *Internal coordinates used in the normal mode analysis for allopurinol forms oxo* ***AI*** *and hydroxy* ***AIII*** *(atom numbering as in Scheme C1).*

In-plane		
Ring stretchings		
$S_1 = r_{1,2}$		νN1N2
$S_2 = r_{2,3}$		νN2C3
$S_3 = r_{3,9}$		νC3C9
$S_4 = r_{8,9}$		νC8C9
$S_5 = r_{1,8}$		νN1C8
$S_6 = r_{4,9}$		νC4C9
$S_7 = r_{4,5}$		νC4N5
$S_8 = r_{5,6}$		νN5C6
$S_9 = r_{6,7}$		νC6N7
$S_{10} = r_{7,8}$		νN7C8
Stretchings CO, OH, NH, CH		
$S_{11} = r_{4,10}$		νCO
$S_{12} = r_{11,5}$	**AI**	νN5H
$S'_{12} = r_{11,10}$	**AIII**	νOH
$S_{13} = r_{12,6}$		νC6H
$S_{14} = r_{13,1}$		νN1H
$S_{15} = r_{14,3}$		νC3H
Ring in-plane deformation		
$S_{16} = (6^{-1/2})(\beta_{5,7,6} - \beta_{6,8,7} + \beta_{7,9,8} - \beta_{8,4,9} + \beta_{9,5,4} - \beta_{4,6,5})$		βR1
$S_{17} = (12^{-1/2})(2\beta_{5,7,6} - \beta_{6,8,7} - \beta_{7,9,8} + 2\beta_{8,4,9} - \beta_{9,5,4} - \beta_{4,6,5})$		βR2
$S_{18} = (1/2)(\beta_{6,8,7} - \beta_{7,9,8} + \beta_{9,5,4} - \beta_{4,6,5})$		βR3
$S_{19} = ((1+ 2a^2 + 2b^2)^{-1/2})(\beta_{3,1,2} + a(\beta_{9,2,3} + \beta_{2,8,1}) + b(\beta_{8,3,9} + \beta_{1,9,8}))$		βR4
$S_{20} = (2(a - b)^2 + 2(1 - a)^2)^{-1/2})((a - b)(\beta_{9,2,3} - \beta_{2,8,1}) + (1 - a)(\beta_{8,3,9} - \beta_{1,9,8}))$		βR5
Bendings CO, OH, NH, CH		
$S_{21} = (2^{-1/2})(\beta_{5,10,4} - \beta_{9,10,4})$		βCO
$S_{22} = (2^{-1/2})(\beta_{6,11,5} - \beta_{4,11,5})$	**AI**	βN5H
$S'_{22} = \beta_{11,4,10}$	**AIII**	βOH
$S_{23} = (2^{-1/2})(\beta_{7,12,6} - \beta_{5,12,6})$		βC6H
$S_{24} = (2^{-1/2})(\beta_{2,13,1} - \beta_{8,13,1})$		βN1H
$S_{25} = (2^{-1/2})(\beta_{9,14,3} - \beta_{2,14,3})$		βC3H
Out-of-plane		
Torsion OH		
$S'_{26} = (2^{-1/2})(\tau_{11,10,4,5} + \tau_{11,10,4,9})$	**AIII**	τOH
Wagging CO, NH, CH		
$S_{26} = \gamma_{11,4,5,6}$	**AI**	γN5H
$S_{27} = \gamma_{10,9,4,5}$		γCO
$S_{28} = \gamma_{12,5,6,7}$		γC6H
$S_{29} = \gamma_{13,2,1,8}$		γN1H
$S_{30} = \gamma_{14,9,3,2}$		γC3H
Ring torsions		
$S_{31} = (6^{-1/2})(\tau_{5,6,7,8} - \tau_{6,7,8,9} + \tau_{7,8,9,4} - \tau_{8,9,4,5} + \tau_{9,4,5,6} - \tau_{4,5,6,7})$		τR1
$S_{32} = (12^{-1/2})(2\tau_{5,6,7,8} - \tau_{6,7,8,9} - \tau_{7,8,9,4} + 2\tau_{8,9,4,5} - \tau_{9,4,5,6} - \tau_{4,5,6,7})$		τR2
$S_{33} = (1/2)(\tau_{6,7,8,9} - \tau_{7,8,9,4} + \tau_{9,4,5,6} - \tau_{4,5,6,7})$		τR3
$S_{34} = ((1 + 2a^2 + 2b^2)^{-1/2})(\tau_{8,9,3,2} + b(\tau_{3,4,1,8} + \tau_{2,1,8,9}) + a(\tau_{9,3,2,1} + \tau_{1,8,9,3}))$		τR4
$S_{35} = (2(a - b)^2 + 2(1 - a)^2)^{-1/2})((a - b)(\tau_{1,8,9,3} - \tau_{9,3,2,1}) + (1 - a)(\tau_{2,1,8,9} - \tau_{3,2,1,8}))$		τR5
Two rings relative torsion		
$S_{36} = (2^{-1/2})(\tau_{4,9,8,1} - \tau_{3,9,8,7})$		τRR

Table C2. *Experimental wavenumbers ($\tilde{\nu}$ /cm^{-1}) and relative integral intensities (I) of the absorption bands in the spectrum of* ***allopurinol*** *isolated in an Ar matrix, compared with wavenumbers ($\tilde{\nu}$ /cm^{-1}), absolute intensities (Ath / km mol^{-1}) and potential energy distribution (PED / %) calculated for the* ***oxo*** *form* ***AI***.

Observed Ar matrix, T = 10 K		**Calculated B3LYP/6-31++G(d, p)**		
$\tilde{\nu}$	**I**	$\tilde{\nu}$	**Ath**	**PED (%)**
3491, 3488	163	3594	113	νN1H (100)
3432, 3430	113	3531	75	νN5H (100)
		3209	0	νC3H (99)
		3135	4	νC6H (100)
1747, 1744, 1730, 1725	607	1753	710	νCO (72), νC4C9 (13)
1695	33			
1644	3			
1610, **1603**, 1597	110	1608	156	νC6N7 (53), βC6H (13)
1558, 1550	115	1561	91	νN7C8 (26), νC8C9 (22), βN1H (18), νN1C8 (13)
1517	16	1515	20	νN1C8 (18), νC3C9 (16), βC3H (11)
1502	4			
1450	4			
1434	7	1443	12	νN2C3 (21), βN5H (16), βN1H (11), νN5C6 (10)
1412	1	1408	1	βN5H (24), νC8C9 (20), νN1C8 (16), νN5C6 (10)
1391	21	1397	25	νN2C3 (28), νC3C9 (20), νC4C9 (13), βN5H (10)
1382	7			
1363, 1360, **1355**	21	1368	10	βC6H (57), νC6N7 (11), νN2C3 (10)
1303	7	1298	2	βN1H (45), νN1C8 (10)
1269	3			
1230, 1222	28	1222	25	βC3H (26), βR5 (24), νC4C9 (16)
1202, 1196	27	1205	33	βC3H (33), νC3C9 (12)
1169	1			
1151	2			
1118, 1112	15	1116	10	νN5C6 (43), βN5H (22)
1098	4			
1077	10	1075	31	νN1N2 (59)
1066	1			
1047	43	1039	36	νC4N5 (32), βCO (16), νN1N2 (12)
1017, 1013	16			
942	25	934	39	βR4 (61), νC8C9 (13)
935	22	926	3	γC6H (107)
897	10	887	13	βR1 (51), βR2 (12)
870	13	871	18	γC3H (103)
783, **781**	31	765	20	γCO (37), τR1 (37), τR4 (19)
725, **723**	28	715	47	γCO (42), γN5H (34), τR5 (14)
691	8	685	10	νN7C8 (22), νC4N5 (19), νN1C8 (10)
662	3	661	2	τR5 (54), τR4 (25), γN5H (19)
656	3			
643, **637**	57	636	61	γN5H (42), τR4 (30), τR3 (15), γCO (11)
598	12	594	11	βR5 (28), νC4C9 (19), βR2 (12), βCO (11)
549	70	550	88	γN1H (54), τR2 (17), τR4 (16), τR1 (15)
534, 532	4	526	4	βR2 (37), βCO (23), νC4N5 (10), βR1 (10)
509, 507	3	506	2	γN1H (42), τR2 (25), τR5 (15), τR1 (13)
504	3	498	2	βR3 (68)
		307	3	βCO (34), βR2 (18), νC4C9 (13)
		261	0	τR3 (57), τRR (19), τR5 (14), τR4 (10)
		192	2	τRR (63), τR3 (25)
		154	6	τR2 (59), τR1 (28), τR3 (10)

Table C3. *Experimental wavenumbers ($\tilde{\nu}$ /cm^{-1}) and relative integral intensities (I) of the absorption bands in the spectrum of the form photoproduced upon UV irradiation of* ***allopurinol*** *isolated in an Ar matrix, compared with wavenumbers ($\tilde{\nu}$ /cm^{-1}), absolute intensities (Ath / km mol^{-1}) and potential energy distribution (PED / %) calculated for the* ***hydroxy*** *form* ***AIIIa***.

Observed Ar matrix, T = 10 K		**Calculated B3LYP/6-31++G(d, p)**		
$\tilde{\nu}$	**I**	$\tilde{\nu}$	**Ath**	**PED (%)**
3559, 3555	189	3676	108	νOH (100)
3498, 3495	180	3601	117	νN1H (100)
3479	60			
		3206	1	νC3H (99)
		3137	13	νC6H (100)
1646, 1642, **1634**	193	1637	211	νC4C9 (34), νN7C8 (11), νC3C9 (10)
1588, 1585, 1580	160	1589	260	νC8C9 (21), νN7C8 (17), βN1H (10)
1518, 1513	45			
1493	11			
1483	43	1492	48	νC4N5 (17), βC6H (17), νN2C3 (14), νN1C8 (13)
1465, 1462, 1459, 1455	108	1472	137	νN2C3 (30), νCO (16), νC4N5 (11)
1437	15	1433	11	νN1C8 (27), βN1H (17), βC6H (14), νC8C9 (12)
1369	19	1375	47	βC6H (24), νC8C9 (16), νN2C3 (14), νCO (11)
1358	6			
1351, 1346	57	1359	94	νC6N7 (29), νC3C9 (21), νN7C9 (12)
1335	49	1325	53	νC6N7 (20), βOH (17), νC4N5 (12), νC3C9 (12), νN2C3 (11)
1315, 1307	43	1313	33	νN5C6 (22), βC6H (21), βOH (14), βN1H (11), νCO (10)
1300	9			
1271	9	1276	10	βN1H (29), νN5C6 (12), βOH (11)
1262	3			
1249	5			
1234	3			
1207	4			
1201, 1199	8	1211	12	βC3H (49), βOH (15)
1152	19	1152	9	βR5 (22), νN5C6 (17)
1087, **1081**	104	1084	164	βOH (17), νC4N5 (16), νN1N2 (14), νN5C6 (13)
1059	10	1065	3	νN1N2 (61)
981, 976	26	957	4	γC6H (108)
936	53	931	57	βR4 (60), νC8C9 (16)
926	5			
887	21	882	32	βR1 (49), βR2 (19)
857, **856**	10	856	17	γC3H (101)
798	27	788	23	τR1 (56), γCO (19), τR4 (16)
		706	3	νN7C8 (21), βR5 (10)
692	10	683	18	γCO (47), τR5 (24), τRR (14), τR3 (10)
656	19	656	8	τR4 (55), τR5 (37)
		603	1	βR5 (30), νC4C9 (20), βR2 (14)
559	38	560	115	τ OH (22), τR2 (21), τR1 (17), γN1H (15)
527, 526, 523	79	552	51	τ OH (70), τR1 (10)
		521	0	βR3 (51), βR2 (23)
		519	4	βCO (32), βR2 (16), νN1C8 (13), βR3 (13)
489 485	21	494	31	γN1H (81)
		293	5	βCO (44), βR2 (12), νC4C9 (10)
		292	1	τR3 (56), τR5 (15), τR4 (10)
		203	1	τRR (71), τR3 (20)
		166	0	τR2 (67), τR1 (16), γCO (11)

9-methylhypoxanthine

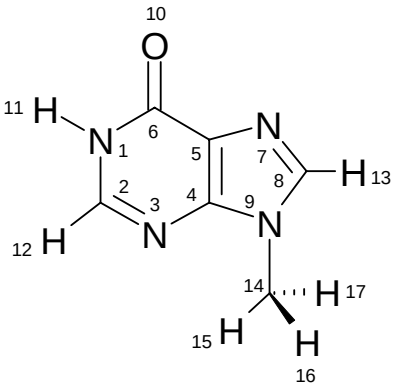

mHxI

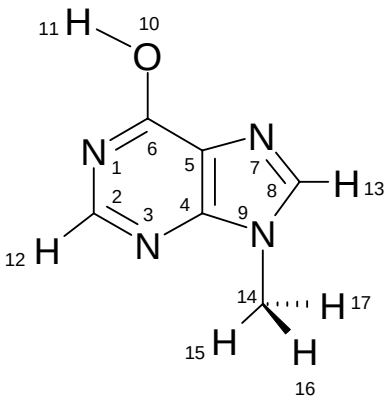

mHxII

Scheme C2. *Atom numbering for tautomers of 9-methylhypoxanthine.*

Table C4. *Internal coordinates used in the normal mode analysis for 9-methylhypoxanthine forms* ***mHxI*** *and* ***mHxII*** *(atom numbering as in Scheme C2).*

In-plane		
Ring stretchings		
$S_1 = r_{1,2}$		νN1C2
$S_2 = r_{2,3}$		νC2N3
$S_3 = r_{3,4}$		νN3C4
$S_4 = r_{4,5}$		νC4C5
$S_5 = r_{5,6}$		νC5C6
$S_6 = r_{6,1}$		νC6N1
$S_7 = r_{5,7}$		νC5N7
$S_8 = r_{7,8}$		νN7C8
$S_9 = r_{8,9}$		νC8N9
$S_{10} = r_{9,4}$		νN9C4
Stretchings CO, OH (for hydroxy form), NH, CH		
$S_{11} = r_{10,6}$		νCO
$S'_{12} = r_{11,10}$	**mHxII**	νOH
$S_{12} = r_{11,1}$	**mHxI**	νN1H
$S_{13} = r_{12,2}$		νC2H
$S_{14} = r_{13,8}$		νC8H
$S_{15} = r_{14,9}$		νN9C14
Stretchings of methyl-group		
$S_{16} = (3^{-1/2})(r_{14,15} + r_{14,16} + r_{14,17})$		νMe1
$S_{17} = (6^{-1/2})(2r_{14,15} - r_{14,16} - r_{14,17})$		νMe2
$S_{18} = (2^{-1/2})(r_{14,16} - r_{14,17})$		νMe3
Ring in-plane deformation		
$S_{19} = (6^{-1/2})(\beta_{1,3,2} - \beta_{2,4,3} + \beta_{3,5,4} - \beta_{4,6,5} + \beta_{5,1,6} - \beta_{6,2,1})$		βR1
$S_{20} = (12^{-1/2})(2\beta_{1,3,2} - \beta_{2,4,3} - \beta_{3,5,4} + 2\beta_{4,6,5} - \beta_{5,1,6} - \beta_{6,2,1})$		βR2
$S_{21} = (1/2)(\beta_{2,4,3} - \beta_{3,5,4} + \beta_{5,1,6} - \beta_{6,2,1})$		βR3
$S_{22} = ((1+ 2a^2 + 2b^2)^{-1/2})(\beta_{7,9,8} + a(\beta_{5,8,7} + \beta_{8,4,9}) + b(\beta_{4,7,5} + \beta_{9,5,4}))$		βR4
$S_{23} = (2(a - b)^2 + 2(1 - a)^2)^{-1/2})((a - b)(\beta_{5,8,7} - \beta_{8,4,9}) + (1 - a)(\beta_{4,7,5} - \beta_{9,5,4}))$		βR5
Bendings CO, OH, NH, CH		
$S_{24} = (2^{-1/2})(\beta_{1,10,6} - \beta_{5,10,6})$		βCO
$S'_{25} = \beta_{11,6,10}$	**mHxII**	βOH
$S_{25} = (2^{-1/2})(\beta_{2,11,1} - \beta_{6,11,1})$	**mHxI**	βN1H
$S_{26} = (2^{-1/2})(\beta_{3,12,2} - \beta_{1,12,2})$		βC2H
$S_{27} = (2^{-1/2})(\beta_{7,13,8} - \beta_{9,13,8})$		βC8H
$S_{28} = (2^{-1/2})(\beta_{8,14,9} - \beta_{4,14,9})$		βN9C14
Bendings of methyl-group		
$S_{29} = (6^{-1/2})(\beta_{15,17,14} + \beta_{15,16,14} + \beta_{17,16,14} - \beta_{9,15,14} - \beta_{9,16,14} - \beta_{9,17,14})$		βMe1
$S_{30} = (6^{-1/2})(2\beta_{17,16,14} - \beta_{15,17,14} - \beta_{15,16,14})$		βMe2
$S_{31} = (6^{-1/2})(2\beta_{9,15,14} - \beta_{9,17,14} - \beta_{9,16,14})$		βMe3
$S_{32} = (2^{-1/2})(\beta_{15,17,14} - \beta_{15,16,14})$		βMe4
$S_{33} = (2^{-1/2})(\beta_{9,17,14} - \beta_{9,16,14})$		βMe5
Out-of-plane		
Torsion OH		
$S'_{34} = (2^{-1/2})(\tau_{11,10,6,1} + \tau_{11,10,6,5})$	**mHxII**	τOH
Wagging CO, NH, CH		
$S_{34} = \gamma_{11,6,1,2}$	**mHxI**	γN1H
$S_{35} = \gamma_{10,5,6,1}$		γCO
$S_{36} = \gamma_{12,1,2,3}$		γC2H
$S_{37} = \gamma_{13,7,8,9}$		γC8H
$S_{38} = \gamma_{14,8,9,4}$		γN9C14
Ring torsions		
$S_{39} = (6^{-1/2})(\tau_{1,2,3,4} - \tau_{2,3,4,5} + \tau_{3,4,5,6} - \tau_{4,5,6,1} + \tau_{5,6,1,2} - \tau_{6,1,2,3})$		τR1
$S_{40} = (12^{-1/2})(2\tau_{1,2,3,4} - \tau_{2,3,4,5} - \tau_{3,4,5,6} + 2\tau_{4,5,6,1} - \tau_{5,6,1,2} - \tau_{6,1,2,3})$		τR2
$S_{41} = (1/2)(\tau_{2,3,4,5} - \tau_{3,4,5,6} + \tau_{5,6,1,2} - \tau_{6,1,2,3})$		τR3
$S_{42} = ((1 + 2a^2 + 2b^2)^{-1/2})(\tau_{4,5,7,8} + b(\tau_{7,8,9,4} + \tau_{8,9,4,5}) + a(\tau_{5,7,8,9} + \tau_{9,4,5,7}))$		τR4
$S_{43} = (2(a - b)^2 + 2(1 - a)^2)^{-1/2})((a - b)(\tau_{9,4,5,7} - \tau_{5,7,8,9}) + (1 - a)(\tau_{8,9,4,5} - \tau_{7,8,9,4}))$		τR5
Two rings relative torsion		
$S_{44} = (2^{-1/2})(\tau_{6,5,4,9} - \tau_{7,5,4,3})$		τRR
Torsion of methyl-group		
$S_{45} = (6^{-1/2})(\tau_{15,14,9,8} + \tau_{15,14,9,4} + \tau_{17,14,9,8} + \tau_{17,14,9,4} + \tau_{16,14,9,8} + \tau_{16,14,9,4})$		τMe

***Table C5**. Experimental wavenumbers ($\tilde{\nu}$ /cm^{-1}) and relative integral intensities (I) of the absorption bands in the spectrum of the oxo form of **9-methylhypoxanthine** isolated in an Ar matrix, compared with wavenumbers ($\tilde{\nu}$ /cm^{-1}), absolute intensities (Ath / km mol^{-1}) and potential energy distribution (PED / %) calculated for the oxo form **mHxI**.*

Observed Ar matrix, T = 10 K		**Calculated B3LYP/6-31++G(d, p)**		
$\tilde{\nu}$	**I**	$\tilde{\nu}$	**Ath**	**PED (%)**
3433, 3430, 3424, 3422	100	3527	68	νN1H (100)
		3190	0	νC8H (99)
3115	1	3136	4	νC2H (100)
2998	3	3095	6	νMe2 (93)
2961	9	3073	9	νMe3 (93)
2930, 2922, 2888	11	3002	37	νMe1 (98)
1775	8			
1764, 1760, **1750,** 1744	583	1761	764	νCO (72), νC5C6 (13)
1738, **1732,** 1725	178			
1702	35			
1658	12			
1594	79	1597	126	νC2N3 (54), βC2H (15)
1579, 1576	8			
1547	51	1547	40	νN3C4 (23), νN9C4 (18), νN7C8 (15), νC4C5 (14)
1522	46	1516	57	νC4C5 (26)
1506	2			
1475	9	1486	14	βMe2 (76), βMe3 (11)
1450, 1447	6	1456	11	βMe4 (89)
		1447	1	βN1H (26), νN7C8 (20)
1440	1	1434	4	βMe1 (72), νN7C8 (11)
1408, **1404**	19	1409	15	νN7C8 (16), βMe1 (15), βN1H (13), νN9C4 (12), νN1C2 (10), νC4C5 (10)
1377	25	1373	20	βC2H (26), νC5C6 (14), νN9C14 (10)
1353	40	1356	34	βC2H (33), νC2N3 (18), νC5N7 (16)
1343	19	1342	18	νC8N9 (25), νC5N7 (16)
1290	1			
1272, 1268, **1264**	10	1271	5	βC8H (28), νC8N9 (12), βMe3 (11)
1215	43	1214	41	βC8H (36), νN9C14 (15)
1141, 1139	61	1133	40	νN1C2 (33), βN1H (19), νC6N1 (12)
1127	0	1126	1	βMe5 (87)
1101	17	1098	28	νN1C2 (17), βR1 (16)
1084, **1081**	1			
1051, 1045, 1040	34	1043	34	βMe3 (45), νC8N9 (26), βR4 (13)
		1008	15	νC6N1 (25), βR4 (17), βCO (12), βR5 (11)
924, 921	3	910	4	γC2H (107)
899	4	892	5	βR1 (47), βR2 (10), νC5N7 (10)
839, **832**	6	819	11	γC8H (100)
784	12	758	8	γCO (33), τR1 (32), τR4 (26)
725	8	721	14	νN9C14 (31), βR4 (28), βR2 (13), νC8N9 (10)
721	11	713	37	γN1H (47), γCO (40)
713	1			
704, 702	13	697	14	νN3C4 (24), νC6N1 (14), νN9C4 (12), βR4 (10)
660, **654**	56	650	61	τR5 (45), γN1H (30), τRR (12), τR4 (10)
640	1	636	0	τR4 (51), γN1H (17), γCO (14), τR3 (11)
599, 595	13	587	11	βCO (25), νC6N1 (23), βR5 (18)
545, **542**	12	536	18	τR2 (39), τR1 (27), τR5 (26), γN1H (10)

Table C5. *(Continuating).*

Observed Ar matrix, T = 10 K		**Calculated B3LYP/6-31++G(d, p)**		
$\tilde{\nu}$	**I**	$\tilde{\nu}$	**Ath**	**PED (%)**
522	1	518	3	βR2 (35), βR5 (14), νN9C14 (11), βN9C14 (10)
		504	2	βR3 (69), βR2 (11)
		352	4	βCO (41), βN9C14 (19), νC5C6 (16)
		267	0	τR3 (62), γN9C14 (22)
		246	1	τRR (55), γN9C14 (24)
		224	1	βN9C14 (51), βR2 (11)
		170	12	τR2 (35), τR3 (30), γN9C14 (18), τRR (14)
		109	0	γN9C14 (29), τR2 (24), τR1 (21)
		50	0	τMe (95)

***Table C6**. Experimental wavenumbers ($\tilde{\nu}$ /cm^{-1}) and relative integral intensities (I) of the absorption bands in the spectrum of the hydroxy form **of 9-methylhypoxanthine** isolated in an Ar matrix, compared with wavenumbers ($\tilde{\nu}$ /cm^{-1}), absolute intensities (Ath / km mol^{-1}) and potential energy distribution (PED / %) calculated for the oxo form **mHxIIa**.*

Observed Ar matrix, T = 10 K		**Calculated B3LYP/6-31++G(d, p)**		
$\tilde{\nu}$	**I**	$\tilde{\nu}$	**Ath**	**PED (%)**
3577, 3563, **3557**	100	3682	106	νOH (100)
		3185	0	νC8H (99)
2995	6	3137	14	νC2H (100)
2963	11	3093	7	νMe2 (99)
2924	13	3072	9	νMe3 (99)
2801	15	3001	38	νMe1 (99)
1639, **1636**	98	1633	224	νC5C6 (39)
1585	120	1586	180	νN3C4 (26), νC4C5 (22), νN1C2 (10)
1520	69	1517	57	νN7C8 (21), βC8H (17) , βR5 (11)
1490	6			
1478	26	1489	36	βMe2 (74), βMe3 (13)
1471, **1468**, 1467	100	1472	132	βC2H (31), νC6N1 (23), νCO (12), νC2N3 (11)
1447	19	1454	11	βMe4 (90)
1430	18	1441	15	βMe1 (42), νN7C8 (31)
1413	26	1417	26	βMe1 (46), νN9C14 (15), νN7C8 (10)
1361	31	1363	37	βC2H (41), νC6N1 (11)
1347	34	1345	55	νC5N7 (15), νN7C8 (13), νC4C5 (12), νC2N3 (10), νC8N9 (10)
1327, **1318**, 1313	147	1330	169	νC2N3 (19), νC8N9 (14), νCO (12)
1307	19	1323	10	νN1C2 (26), νC2N3 (16), νCO (14), βC2H (10)
1282, 1272	11	1289	15	βOH (33), νC5N7 (23), νN1C2 (15)
1236, 1235	31	1243	27	βC8H (41), νN7C8 (11), βMe3 (10)
1213, 1207	43	1204	55	νN9C14 (17), βC8H (17)
1192	6			
1126	7	1127	1	βMe5 (89), βMe4 (10)
1111, 1109, 1107	58	1111	98	βOH (27), νN1C2 (20), νC6N1 (20)
1052, **1050**	12	1045	8	βMe3 (50),νC8N9 (28)
1023, **1022**	86	1019	99	βR4 (25), νCO (16), νN9C14 (10), βR5 (10)
952	4	946	5	γC2H (108)
894, 889	9	887	8	βR1 (43), βR2 (15)
855	2	845	7	γC8H (100)
809, 803, 802	24	786	12	τR1 (52), τR4 (22), γCO (18)
735	6	731	5	νN9C14 (21), βR2 (17), νC8N9 (10), βR4 (10)
727	5			
718	12	714	11	βR4 (29), νN3C4 (13), νC5C6 (12)
686	2	677	7	γCO (49), τR3 (14), τR5 (11), τRR (11), τR4 (10)
647, **646**	33	644	40	τR4 (52), τR5 (32)
		592	2	βR5 (25), βCO (25)
535	4	560	2	τR2 (32), τR5 (28), τR1 (24)
515, 512	45	540	89	τOH (88)
		529	4	βR3 (35), νN9C14 (12), βR2 (11), βN9C14 (10)
		520	1	βR3 (35), βR2 (34)
		331	10	βCO (49), βN9C14 (22)
		298	0	τR3 (63), τR5 (11)
		253	1	τRR (48), γN9C14 (32)
		220	5	βN9C14 (49), βR2 (10)
		190	1	τR2 (47), γN9C14 (24), τRR (17)
		110	5	γN9C14 (34), τR2(23), τR1 (10)
		13	0	τMe (96)

hypoxanthine

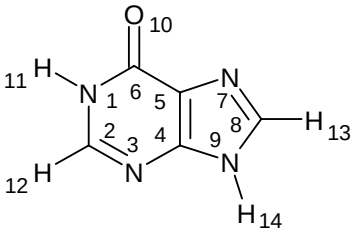

oxo-N(9)-H
HxI

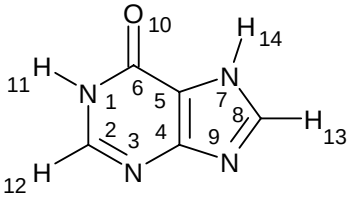

oxo-N(7)-H
HxII

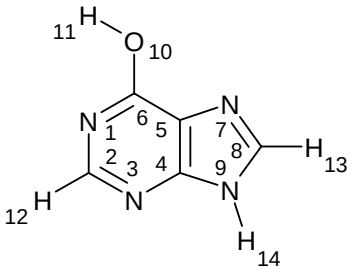

hydroxy-N(9)-H
HxIII

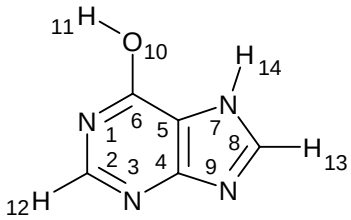

hydroxy-N(7)-H
HxIV

Scheme C3*. Atom numbering for tautomers of hypoxanthine.*

Table C7. *Internal coordinates used in the normal mode analysis for* ***hypoxanthine*** *forms* ***HxI*** *and* ***HxII*** *(atom numbering as in Scheme C3).*

In-plane		
Ring stretchings		
$S_1 = r_{1,2}$		νN1C2
$S_2 = r_{2,3}$		νC2N3
$S_3 = r_{3,4}$		νN3C4
$S_4 = r_{4,5}$		νC4C5
$S_5 = r_{5,6}$		νC5C6
$S_6 = r_{6,1}$		νC6N1
$S_7 = r_{5,7}$		νC5N7
$S_8 = r_{7,8}$		νN7C8
$S_9 = r_{8,9}$		νC8N9
$S_{10} = r_{9,4}$		νN9C4
Stretching CO		
$S_{11} = r_{10,6}$		νC=O
Stretching CH, NH		
$S_{12} = r_{11,1}$		νN1H
$S_{13} = r_{12,2}$		νC2H
$S_{14} = r_{13,8}$		νC8H
$S_{15} = r_{14,9}$	**HxI**	νN9H
$S'_{15} = r_{14,7}$	**HxII**	νN7H
Ring in-plane deformation		
$S_{16} = (6^{-1/2})(\beta_{1,3,2} - \beta_{2,4,3} + \beta_{3,5,4} - \beta_{4,6,5} + \beta_{5,1,6} - \beta_{6,2,1})$		β R1
$S_{17} = (12^{-1/2})(2\beta_{1,3,2} - \beta_{2,4,3} - \beta_{3,5,4} + 2\beta_{4,6,5} - \beta_{5,1,6} - \beta_{6,2,1})$		β R2
$S_{18} = (1/2)(\beta_{2,4,3} - \beta_{3,5,4} + \beta_{5,1,6} - \beta_{6,2,1})$		β R3
$S_{19} = ((1+ 2a^2 + 2b^2)^{-1/2})(\beta_{7,9,8} + a(\beta_{5,8,7} + \beta_{8,4,9}) + b(\beta_{4,7,5} + \beta_{9,5,4}))$		β R4
$S_{20} = ((2(a - b)^2 + 2(1 - a)^2)^{-1/2})((a - b)(\beta_{5,8,7} - \beta_{8,4,9}) + (1 - a)(\beta_{4,7,5} - \beta_{9,5,4}))$		β R5
Bendings CO, CH, NH,		
$S_{21} = (2^{-1/2})(\beta_{1,10,6} - \beta_{5,10,6})$		β C=O
$S_{22} = (2^{-1/2})(\beta_{2,11,1} - \beta_{6,11,1})$		β N1H
$S_{23} = (2^{-1/2})(\beta_{3,12,2} - \beta_{1,12,2})$		β C2H
$S_{24} = (2^{-1/2})(\beta_{7,13,8} - \beta_{9,13,8})$		β C8H
$S_{25} = (2^{-1/2})(\beta_{8,14,9} - \beta_{4,14,9})$	**HxI**	β N9H
$S'_{25} = (2^{-1/2})(\beta_{5,14,7} - \beta_{8,14,7})$	**HxII**	β N7H
Out-of-plane		
Wagging CO, NH, CH		
$S_{26} = \gamma_{10,5,6,1}$		γC=O
$S_{27} = \gamma_{11,6,1,2}$		γN1H
$S_{28} = \gamma_{12,1,2,3}$		γC2H
$S_{29} = \gamma_{13,7,8,9}$		γC8H
$S_{30} = \gamma_{14,8,9,4}$	**HxI**	γN9H
$S'_{30} = \gamma_{14,5,7,8}$	**HxII**	γN7H
Ring torsions		
$S_{31} = (6^{-1/2})(\tau_{1,2,3,4} - \tau_{2,3,4,5} + \tau_{3,4,5,6} - \tau_{4,5,6,1} + \tau_{5,6,1,2} - \tau_{6,1,2,3})$		τ R1
$S_{32} = (12^{-1/2})(2\tau_{1,2,3,4} - \tau_{2,3,4,5} - \tau_{3,4,5,6} + 2\tau_{4,5,6,1} - \tau_{5,6,1,2} - \tau_{6,1,2,3})$		τ R2
$S_{33} = (1/2)(\tau_{2,3,4,5} - \tau_{3,4,5,6} + \tau_{5,6,1,2} - \tau_{6,1,2,3})$		τ R3
$S_{34} = ((1+ 2a^2 + 2b^2)^{-1/2})(\tau_{4,5,7,8} + b(\tau_{7,8,9,4} + \tau_{8,9,4,5}) + a(\tau_{5,7,8,9} + \tau_{9,4,5,7}))$		τ R4
$S_{35} = ((2(a - b)^2 + 2(1 - a)^2)^{-1/2})((a - b)(\tau_{9,4,5,7} - \tau_{5,7,8,9}) + (1 - a)(\tau_{8,9,4,5} - \tau_{7,8,9,4}))$		τ R5
Two rings relative torsion		
$S_{36} = (2^{-1/2})(\tau_{6,5,4,9} - \tau_{7,5,4,3})$		τ RR

Table C8. *Internal coordinates used in the normal mode analysis for hypoxanthine forms* ***HxIII*** *and* ***HxIV*** *(atom numbering as in Chart S1)*

In-plane		
Ring stretchings		
$S_1 = r_{1,2}$		νN1C2
$S_2 = r_{2,3}$		νC2N3
$S_3 = r_{3,4}$		νN3C4
$S_4 = r_{4,5}$		νC4C5
$S_5 = r_{5,6}$		νC5C6
$S_6 = r_{6,1}$		νC6N1
$S_7 = r_{5,7}$		νC5N7
$S_8 = r_{7,8}$		νN7C8
$S_9 = r_{8,9}$		νC8N9
$S_{10} = r_{9,4}$		νN9C4
Stretching CO		
$S_{11} = r_{10,6}$		νCO
Stretching OH, CH, NH		
$S_{12} = r_{11,10}$		νOH
$S_{13} = r_{12,2}$		νC2H
$S_{14} = r_{13,8}$		νC8H
$S_{15} = r_{14,9}$	**HxIII**	νN9H
$S'_{15} = r_{14,7}$	**HxIV**	νN7H
Ring in-plane deformation		
$S_{16} = (6^{-1/2})(\beta_{1,3,2} - \beta_{2,4,3} + \beta_{3,5,4} - \beta_{4,6,5} + \beta_{5,1,6} - \beta_{6,2,1})$		β R1
$S_{17} = (12^{-1/2})(2\beta_{1,3,2} - \beta_{2,4,3} - \beta_{3,5,4} + 2\beta_{4,6,5} - \beta_{5,1,6} - \beta_{6,2,1})$		β R2
$S_{18} = (1/2)(\beta_{2,4,3} - \beta_{3,5,4} + \beta_{5,1,6} - \beta_{6,2,1})$		β R3
$S_{19} = ((1+ 2a^2 + 2b^2)^{-1/2})(\beta_{7,9,8} + a(\beta_{5,8,7} + \beta_{8,4,9}) + b(\beta_{4,7,5} + \beta_{9,5,4}))$		β R4
$S_{20} = ((2(a - b)^2 + 2(1 - a)^2)^{-1/2})((a - b)(\beta_{5,8,7} - \beta_{8,4,9}) + (1 - a)(\beta_{4,7,5} - \beta_{9,5,4}))$		β R5
Bendings CO, CH, NH, OH		
$S_{21} = (2^{-1/2})(\beta_{1,10,6} - \beta_{5,10,6})$		β C-O
$S_{22} = \beta_{11,6,10}$		β OH
$S_{23} = (2^{-1/2})(\beta_{3,12,2} - \beta_{1,12,2})$		β C2H
$S_{24} = (2^{-1/2})(\beta_{7,13,8} - \beta_{9,13,8})$		β C8H
$S_{25} = (2^{-1/2})(\beta_{8,14,9} - \beta_{4,14,9})$	**HxIII**	β N9H
$S'_{25} = (2^{-1/2})(\beta_{5,14,7} - \beta_{8,14,7})$	**HxIV**	β N7H
Out-of-plane		
Torsion OH		
$S_{26} = (2^{-1/2})(\tau_{11,10,6,1} + \tau_{11,10,6,5})$		τ OH
Wagging CO, NH, CH		
$S_{27} = \gamma_{10,5,6,1}$		γCO
$S_{28} = \gamma_{12,1,2,3}$		γC2H
$S_{29} = \gamma_{13,7,8,9}$		γC8H
$S_{30} = \gamma_{14,8,9,4}$	**HxIII**	γN9H
$S'_{30} = \gamma_{14,5,7,8}$	**HxIV**	γN7H
Ring torsions		
$S_{31} = (6^{-1/2})(\tau_{1,2,3,4} - \tau_{2,3,4,5} + \tau_{3,4,5,6} - \tau_{4,5,6,1} + \tau_{5,6,1,2} - \tau_{6,1,2,3})$		τR1
$S_{32} = (12^{-1/2})(2\tau_{1,2,3,4} - \tau_{2,3,4,5} - \tau_{3,4,5,6} + 2\tau_{4,5,6,1} - \tau_{5,6,1,2} - \tau_{6,1,2,3})$		τR2
$S_{33} = (1/2)(\tau_{2,3,4,5} - \tau_{3,4,5,6} + \tau_{5,6,1,2} - \tau_{6,1,2,3})$		τR3
$S_{34} = ((1+ 2a^2 + 2b^2)^{-1/2})(\tau_{4,5,7,8} + b(\tau_{7,8,9,4} + \tau_{8,9,4,5}) + a(\tau_{5,7,8,9} + \tau_{9,4,5,7}))$		τR4
$S_{35} = ((2(a - b)^2 + 2(1 - a)^2)^{-1/2})((a - b)(\tau_{9,4,5,7} - \tau_{5,7,8,9}) + (1 - a)(\tau_{8,9,4,5} - \tau_{7,8,9,4}))$		τR5
Two rings relative torsion		
$S_{36} = (2^{-1/2})(\tau_{6,5,4,9} - \tau_{7,5,4,3})$		τRR

Table C9. *Spectral positions (wavenumbers $\tilde{\nu}$ /cm^{-1}) and relative intensities (I) of the absorption bands found in the IR spectrum of* ***hypoxanthine*** *isolated in an Ar matrix (10K).*

$\tilde{\nu}$	I	form	normal mode number	description of the mode
3566, 3561	0.5	**HxIII**		
3490, 3484, **3482**	18.3	**HxI**	Q1	νN9H
3478	18.5	**HxII**	Q1	νN7H
3431	15.9	**HxII**	Q2	νN1H
3428	11.4	**HxI+HxII**	Q2	νN1H
1772	1.5	**HxI**		
1753, 1751, 1742	50.9	**HxI**	Q5	νC=O
1735, 1733, 1727	106.3	**HxII**	Q5	νC=O
1712	5.9	**HxII**		
1642, 1635	0.4	**HxIII**		
1600, **1596**	9.7[a]	**HxII**	Q6	νring
1597, 1593	overlap[a]	**HxI**	Q6	νring
1582	0.4	**HxI**		
1560, **1555**	7.1	**HxI**	Q7	νring
1534, 1531	4.8	**HxII**	Q7	νring
1522, 1519, 1515, 1512	0.9	**HxII**		
1510	0.3	**HxI**		
1500	1.2	**HxI**	Q8	νring
1471	0.7	**III**		
1450	0.3	**HxI**	Q9	νring, β N1H
1437	4.2	**HxII**	Q9	νring, β CH, β ring
1415, 1412, **1409**	2.4	**HxII**	Q10	β N1H, β N7H, νring
1407	0.5	**HxI**	Q10	β N1H, νring, β CH
1400	0.8	**HxII**		
1388, 1387, **1381**	11.9	**HxII**	Q11	β CH, νring
1373	0.4	**HxI**	Q11	β N9H, β CH, νring
1371	9.9	**HxII**	Q12	νring, β N7H
1351	0.7	**HxII**		
1350, **1349**	1.3	**HxI**	Q12	νring, β CH
1342	1.6	**HxI**	Q13	νring, β CH
1330	0.1	**HxIII**		
1326, 1325	3.3	**HxII**	Q13	β CH, νring
1319, 1318	0.2	**HxIII**		
1315	0.5	**HxII**		
1281, 1278	0.5	**HxII**		
1269	0.4	**HxIII**		
1267	0.3	**HxI**	Q14	β CH, νring
1239, 1237	0.2	**HxIII**		
1190, **1185**	12.7	**HxII**	Q15	β CH, β ring, νring
1173, 1172	5.7	**HxI**	Q15	β CH, β ring
1112, 1111	1.3	**HxII**	Q16	νring, β N1H
1101, **1100**	1.7	**HxI**	Q16	νring, β N1H
1087	0.4	**HxI**		
1089, **1084**, 1081	7.0	**HxII**	Q17	νring, β N7H, β CH
1074	0.1	**HxIII**		
1062, 1055	5.5	**HxII**	Q18	νring, β ring, β C=O
1059, 1058	1.1	**HxI**	Q17	νring, β N9H
1048	0.5	**HxI**	Q18	νring, β C=O
931	0.3	**HxI**	Q19	β ring
925	0.1	**HxIII**		
924	0.2	**HxI**	Q20	γCH
919	0.8	**HxII**	Q20	γCH
892	0.6	**HxI**	Q21	β ring

Table C9. *(Continuating).*

$\tilde{\nu}$	I	form	normal mode number	description of the mode
891	0.5	**HxII**	Q21	β ring
886	0.1	**HxIII**		
859, 858	1.7	**HxII**	Q22	γ CH
837	0.5	**HxI**	Q22	γ CH
811	0.4	**HxII**		
788, **787**, 785	2.7[a]	**HxII**	Q23	τ ring
787, 785	overlap[a]	**HxI**	Q23	γ C=O, τ ring
729, **728**	4.1	**HxII**	Q24	γ C=O, γ N1H
720	2.4	**HxI**	Q24	γ N1H, γ C=O
701	0.4	**HxII**	Q25	ν ring
693	0.6	**HxI**	Q25	ν ring
659	4.4[a]	**HxII**	Q26	γ N1H, τ ring
659	overlap[a]	**HxI**	Q26	τ ring
641	0.8	**HxI**	Q27	τ ring, γ N1H
628, **624**	4.7	**HxII**	Q27	τ ring, γ N1H
605	1.2	**HxII**	Q28	β ring, ν ring, β C=O
600	0.6	**HxI**	Q28	β ring, ν ring, β C=O
563, **560**, 558	7.0	**HxI**	Q29	γ N9H, τ ring
555, **554**	3.9	**HxII**	Q29	τ ring
535, 533	0.8	**HxI**	Q30	β ring, β C=O
526, 523	11.9	**HxII**	Q31	γ N7H
510	0.7	**HxII**	Q32	β ring

[a] Summaric intensity of overlapping bands.

Table C10. *Spectral positions (wavenumbers $\tilde{\nu}$ /cm^{-1})) and relative intensities (I) of the absorption bands attributed to the* ***hydroxy*** *tautomers of* ***hypoxanthin****e. The bands were found in the IR spectra obtained after UV irradiations of hypoxanthine isolated in an Ar matrix.*

$\tilde{\nu}$	I	Mode number	Description of the mode
Form **HxIII** hydroxy-N(9)-H			
3566, 3561	7.3	Q1	νOH
3496	4.4	Q2	νN9H
1642, 1635	3.9	Q5	νring
1624	4.8	Q6	νring
1471	4.8	Q8	νring, βCH
1421	0.8	Q9	νring
1338	2.7	Q11/Q12	νring, βCH / νC-O, νring
1330	1.6	Q11/Q12	νring, βCH / νC-O, νring
1319, 1318	2.0	Q11/Q12	νring, βCH / νC-O, νring
1291	0.7	Q13	νring, βCH
1269	1.5	Q14	βOH, νring
1239, 1237	1.2	Q15	βCH, νring
1083, 1074	4.6	Q17	νring, βOH
925	0.4	Q20	βring, νring
886	0.4	Q21	βring
570	1.2	Q28	τring, γN9H
523, 521	4.0	Q29	τOH
Form **HxIV** hydroxy-N(7)-H			
3568, 3563	12.9	Q1	νOH
3490	7.8	Q2	νN7H
1662	7.2	Q5	νring
1566	14.4	Q6	νring
1492	2.1	Q7	νring, βCH
1480	1.7	Q8	βCH, νring
1398	7.6	Q9	βN7H, νring
1385, **1381**	10.4	Q10	νring
1354	5.6	Q11	νring
1332	2.6	Q12	βCH, νring
1304	0.9	Q13	νring, βOH
1236	2.1	Q15	βCH, βOH, νring
1054	7.3	Q18	νC-O, βring, βN7H
956, 951	1.1	Q19	γCH
878, **875**	1.2	Q21/Q22	βring, γCH
490	8.2	Q31	τOH

Table C11. *Calculated vibrational frequencies, intensities and potential energy distributions for* ***hypoxanthine*** *form* ***HxI (oxo-N9)*** *(frequencies (ṽ) in cm^{-1}, intensities (A^{th}) in km mol^{-1}, PED's in %). Definition of internal coordinates is given in Table C7.*

Normal vibrations calculated at the DFT(B3LYP)/6-31++G(d, p) level			
Nr	**ṽ**	**A^{th}**	**PED**
Q1	3582	89	νN9H (100)
Q2	3528	66	νN1H (100)
Q3	3202	0	νC8H (99)
Q4	3137	4	νC2H (100)
Q5	1764	723	νC=O (73), νC5C6 (13)
Q6	1598	102	νC2N3 (55), β C2H (15)
Q7	1564	66	νN3C4 (25), νC4C5 (18), νN9C4 (14), β N9H (14), νN7C8 (14)
Q8	1499	33	νN7C8 (21), νC4C5 (20), β C8H (12)
Q9	1454	4	νN7C8 (24), β N1H (23)
Q10	1407	5	β N1H (18), νC4C5 (17), β C2H (17), νN1C2 (16)
Q11	1379	23	β N9H (24), β C2H (18), νC8N9 (16)
Q12	1352	35	νC5N7 (30), β C2H (21), νC2N3 (14)
Q13	1332	4	νC5C6 (15), νN9C4 (14), β C8H (14), β C2H (12)
Q14	1274	5	β C8H (31), νN7C8 (14), β N9H (10), νN3C4 (10)
Q15	1170	80	β C8H (18), β R1 (14), νN1C2 (11)
Q16	1115	11	νN1C2 (41), β N1H (21)
Q17	1061	18	νC8N9 (53), β N9H (31)
Q18	1045	41	νC6N1 (34), β C=O (21)
Q19	926	5	β R4 (76), νC4C5 (11)
Q20	914	3	γC2H (107)
Q21	884	9	β R1(52), β R2 (13)
Q22	821	15	γC8H (100)
Q23	759	8	γC=O (34), τR1 (32), τR4 (27)
Q24	713	46	γN1H (48), γC=O (38)
Q25	688	10	νN3C4 (22), νC6N1 (19), νN9C4 (12)
Q26	656	18	τ R5 (56), τR4 (23), γN1H (14)
Q27	638	15	τR4 (32), γN1H (32), γC=O (17), τR3 (15)
Q28	595	8	β R5 (31), νC5C6 (20), β C=O (12)
Q29	557	121	γN9H (53), τR2 (19), τR1 (17)
Q30	526	11	β R2 (41), β C=O (19), νC6N1 (11), β R1 (10)
Q31	516	13	γN9H (48), τR2 (22), τR5 (16), τR1 (12)
Q32	498	2	β R3 (69)
Q33	315	1	β C=O (38), β R2 (17), νC5C6 (12)
Q34	263	0	τR3 (58), τRR (20), τR5 (15)
Q35	203	17	τRR (63), τR3 (28)
Q36	149	1	τR2 (59), τR1 (31)

***Table C12**. Calculated vibrational frequencies, intensities and potential energy distributions for **hypoxanthine** form **HxII (oxo-N7)** (frequencies ($\tilde{\nu}$) in cm^{-1}, intensities (A^{th}) in km mol^{-1}, PED's in %). Definition of internal coordinates is given in Table C7.*

Normal vibrations calculated at the DFT(B3LYP)/6-31++G(d, p) level			
Nr	**$\tilde{\nu}$**	**A^{th}**	**PED**
Q1	3582	102	νN7H (100)
Q2	3531	70	νN1H (100)
Q3	3203	1	νC8H (99)
Q4	3134	6	νC2H (100)
Q5	1739	796	νC=O (64), νC5C6 (16)
Q6	1608	75	νC2N3 (52), β C2H (10)
Q7	1526	30	νC4C5 (18), β N7H (14), νC2N3 (12), νC8N9 (11), νC5N7 (10)
Q8	1515	9	νC4C5 (27), νN3C4 (25)
Q9	1441	36	νC8N9 (32), β C8H (15), β R5 (13), νC5N7 (11)
Q10	1410	25	β N1H (39), β N7H (16), νN1C2 (16), νN7C8 (11)
Q11	1387	33	β C2H (45), νC5N7 (11), νC2N3 (10), νC4C5 (10), νN3C4 (10)
Q12	1378	90	νN7C8 (16), νN9C4 (13), β N7H (13), νC8N9 (11)
Q13	1325	28	β C2H (29), νN9C4 (22), νC5N7 (13), νN3C4 (12)
Q14	1273	0	β C8H (31), νC8N9 (24), νC5C6 (11), νN9C4 (10)
Q15	1184	75	β C8H (18), β R1 (18), νC6N1 (15), νC5N7 (10)
Q16	1101	8	νN1C2 (43), β N1H (20)
Q17	1080	43	νN7C8 (48), β N7H (23), β C8H (10)
Q18	1060	14	νC6N1 (21), β R5 (14), β C=O (13)
Q19	938	1	β R4 (73), νC4C5 (13)
Q20	910	6	γC2H (107)
Q21	882	3	β R1 (53), β R2 (15)
Q22	845	13	γC8H (103)
Q23	757	5	τR1 (43), τR5 (27), τR4 (13), γC=O (12)
Q24	716	32	γC=O (69), γN1H (25), τR5 (10)
Q25	697	3	νN3C4 (25), νC6N1 (16), νN9C4 (10)
Q26	658	28	γN1H (46), τR5 (32), τR4 (13)
Q27	620	41	τR4 (41), γN1H (21), γN7H (12), τR3 (11), γC=O (11)
Q28	600	6	β R5 (33), νC5C6 (17), β C=O (13)
Q29	547	20	τR2 (39), τR1 (29), τR4 (12), τR5 (12), γN1H (11)
Q30	538	3	β R2 (35), β C=O (22), νC6N1 (11)
Q31	516	84	γN7H (86)
Q32	504	3	β R3 (68), β R2 (11)
Q33	300	17	β C=O (39), β R2 (17), νC5C6 (12)
Q34	270	5	τR3 (54), τRR (25), τR4 (12)
Q35	191	12	τRR (54), τR3 (37), τR2 (10)
Q36	156	15	τR2 (52), τR1 (36)

Table C13. *Calculated vibrational frequencies, intensities and potential energy distributions for* ***hypoxanthine*** *form* ***HxIII (hydroxy-N9)*** *(frequencies (ṽ) in cm^{-1}, intensities (A^{th}) in km mol^{-1}, PED's in %). Definition of internal coordinates is given in Table C8.*

Normal vibrations calculated at the DFT(B3LYP)/6-31++G(d, p) level			
Nr	**ṽ**	**A^{th}**	**PED**
Q1	3681	104	νOH (100)
Q2	3587	94	νN9H (100)
Q3	3198	0	νC8H (99)
Q4	3138	13	νC2H (100)
Q5	1638	168	νC5C6 (35), νN3C4 (11)
Q6	1597	238	νC4C5 (23), νN3C4 (20), νN1C2 (11)
Q7	1499	26	νN7C8 (49), β C8H (21)
Q8	1477	158	νC6N1 (29), β C2H (26), νC-O (14), νC2N3 (13)
Q9	1415	29	νN9C4 (28), νC4C5 (20), νN7C8 (11)
Q10	1393	8	β C2H (33), β N9H (31), νC8N9 (17)
Q11	1340	90	νC4C5 (16), β C8H (16), νC6N1 (11), νC5N7 (10)
Q12	1335	150	νC-O (17), νC5N7 (15), νC2N3 (15), β R1 (14)
Q13	1311	7	νC2N3 (35), νN1C2 (28), β C2H (17)
Q14	1275	23	β OH (42), νC5N7 (25)
Q15	1249	23	β C8H (38), νN7C8 (17), β N9H (10)
Q16	1131	2	β R5 (14), νN1C2 (13), νC2N3 (10)
Q17	1081	185	νC6N1 (21), β OH (18), νC-O (13), β R5 (10)
Q18	1061	11	νC8N9 (56), β N9H (32)
Q19	948	5	γC2H (108)
Q20	921	14	β R4 (73), νC4C5 (13)
Q21	880	15	β R1 (49), β R2 (20)
Q22	847	10	γC8H (100)
Q23	785	11	τR1 (52), τR4 (22), γC-O (18)
Q24	712	2	νN3C4 (19), νN9C4 (11)
Q25	676	13	γC-O (49), τR3 (14), τR5 (13), τR4 (11), τRR (10)
Q26	652	11	τR4 (48), τR5 (40)
Q27	607	1	β R5 (36), νC5C6 (19), β R2 (10)
Q28	567	37	τR2 (29), τR1 (23), τR5 (18), γN9H (16)
Q29	545	135	τOH (88)
Q30	525	8	β C-O (28), β R2 (22), νN9C4 (13), β R3 (11)
Q31	520	0	β R3 (54), β R2 (21)
Q32	508	40	γN9H (79)
Q33	297	13	β C-O (48), β R2 (12)
Q34	296	0	τR3 (59), τR5 (16)
Q35	216	12	τRR (70), τR3 (17)
Q36	162	3	τR2 (64), τR1 (17), γC-O (12)

***Table C14**. Calculated vibrational frequencies, intensities and potential energy distributions for **hypoxanthine** form **HxIV (hydroxy-N7)** (frequencies ($\tilde{\nu}$) in cm^{-1}, intensities (A^{th}) in km mol^{-1}, PED's in %). Definition of internal coordinates is given in Table C8.*

Normal vibrations calculated at the DFT(B3LYP)/6-31++G(d, p) level			
Nr	$\tilde{\nu}$	A^{th}	**PED**
Q1	3683	104	νOH (100)
Q2	3593	95	νN7H (100)
Q3	3196	1	νC8H (99)
Q4	3137	15	νC2H (100)
Q5	1662	167	νC5C6 (43), νC5N7 (13)
Q6	1566	260	νN3C4 (24), νC6N1 (23), νC4C5 (22)
Q7	1504	50	νC8N9 (52), β C8H (19)
Q8	1485	24	β C2H (35), νC2N3 (17), νC6N1 (15)
Q9	1399	136	β N7H (40), νN7C8 (24)
Q10	1380	128	νC4C5 (20), νC2N3 (19), νC5N7 (18), νN3C4 (13), β C2H (10)
Q11	1362	53	νN9C4 (18), νC4C5 (13), β R1 (11), νC2N3 (11), νC8N9 (10)
Q12	1337	47	β C2H (45), νN9C4 (13), β OH (11), νN3C4 (10)
Q13	1303	5	νC2N3 (29), νC5N7 (14), β OH (13), νC8N9 (12)
Q14	1266	22	νN1C2 (40), β OH (13)
Q15	1239	49	β C8H (35), β OH (15), νC8N9 (13), β N7H (10)
Q16	1130	21	νN1C2 (20), β OH (16), β R5 (11)
Q17	1084	46	νN7C8 (48), β N7H (17)
Q18	1055	146	νC-O (15), β R5 (14), β N7H (13)
Q19	949	6	γC2H (108)
Q20	929	3	β R4 (70), νC4C5 (17)
Q21	872	20	β R1 (47), β R2 (19)
Q22	865	14	γC8H (103)
Q23	781	12	τR1 (56), τR5 (21), τR4 (11)
Q24	713	2	νN3C4 (22), νN9C4 (11), β R5 (10)
Q25	684	5	γC-O (48), τR5 (31), τRR (12)
Q26	623	3	τR4 (58), τR5 (17)
Q27	606	1	β R5 (36), νC5C6 (19)
Q28	572	0	τR2 (35), τR1 (25), γC-O (15), τR5 (14)
Q29	536	0	β C-O (26), β R3 (23), β R2 (16), νN9C4 (15)
Q30	518	1	β R3 (42), β R2 (30)
Q31	512	138	τOH (93)
Q32	449	83	γN7H (93)
Q33	299	4	τR3 (54), τR4 (15), τRR (14)
Q34	287	13	β C-O (49), β R2 (11)
Q35	212	7	τRR (62), τR3 (19), τR2 (15)
Q36	165	4	τR2 (57), τR1 (20), γC-O (12)

Appendix D

Spectroscopic data of *N*-hydroxypyridine-2(1*H*)-thione

N-hydroxypyridine-2(1H)-thione

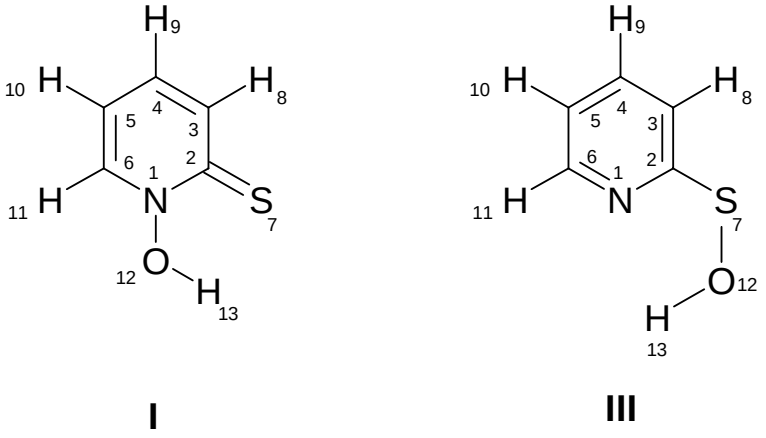

Scheme D1. *Atom numbering for isomers of* N-*hydroxypyridine-2(1*H*)-thione.*

Table D1. *Internal coordinates (S_i) used in the normal mode analysis for* ***N-hydroxypyridine-2(1H)-thione*** *(**NpI**) and* ***2-hydroxysulfanyl-pyridine*** *(**NpIII**) (atom numbering as in Chart D1).*

Ring stretching		
$S_1 = r_{1,2}$		ν N1C2
$S_2 = r_{2,3}$		ν C2C3
$S_3 = r_{3,4}$		ν C3C4
$S_4 = r_{4,5}$		ν C4C5
$S_5 = r_{5,6}$		ν C5C6
$S_6 = r_{6,1}$		ν C6N1
Stretching CS, CH		
$S_7 = r_{2,7}$		ν CS
$S_8 = r_{3,8}$		ν C3H
$S_9 = r_{4,9}$		ν C4H
$S_{10} = r_{5,10}$		ν C5H
$S_{11} = r_{6,11}$		ν C6H
Ring in-plane deformation		
$S_{12} = (6^{-1/2})(\beta_{1,3,2} - \beta_{2,4,3} + \beta_{3,5,4} - \beta_{4,6,5} + \beta_{5,1,6} - \beta_{6,2,1})$		β R1
$S_{13} = (12^{-1/2})(2\beta_{6,2,1} - \beta_{1,3,2} - \beta_{2,4,3} + 2\beta_{3,5,4} - \beta_{4,6,5} - \beta_{5,1,6})$		β R2
$S_{14} = (1/2)(\beta_{1,3,2} - \beta_{2,4,3} + \beta_{4,6,5} - \beta_{5,1,6})$		β R3
Bending CS, CH		
$S_{15} = (2^{-1/2})(\beta_{3,7,2} - \beta_{1,7,2})$		β CS
$S_{16} = (2^{-1/2})(\beta_{4,8,3} - \beta_{2,8,3})$		β C3H
$S_{17} = (2^{-1/2})(\beta_{5,9,4} - \beta_{3,9,4})$		β C4H
$S_{18} = (2^{-1/2})(\beta_{6,10,5} - \beta_{4,10,5})$		β C5H
$S_{19} = (2^{-1/2})(\beta_{1,11,6} - \beta_{5,11,6})$		β C6H
Wagging CS, CH		
$S_{20} = \gamma_{7,1,2,3}$		γ CS
$S_{21} = \gamma_{8,2,3,4}$		γ C3H
$S_{22} = \gamma_{9,3,4,5}$		γ C4H
$S_{23} = \gamma_{10,4,5,6}$		γ C5H
$S_{24} = \gamma_{11,5,6,1}$		γ C6H
Ring torsion		
$S_{25} = (6^{-1/2})(\tau_{1,2,3,4} - \tau_{2,3,4,5} + \tau_{3,4,5,6} - \tau_{4,5,6,1} + \tau_{5,6,1,2} - \tau_{6,1,2,3})$		τ R1
$S_{26} = (12^{-1/2})(2\tau_{2,3,4,5} - \tau_{3,4,5,6} - \tau_{4,5,6,1} + 2\tau_{5,6,1,2} - \tau_{6,1,2,3} - \tau_{1,2,3,4})$		τ R2
$S_{27} = (1/2)(\tau_{3,4,5,6} - \tau_{4,5,6,1} + \tau_{6,1,2,3} - \tau_{1,2,3,4})$		τ R3
Stretching NO, SO, OH		
$S_{28} = r_{1,12}$	**NpI**	ν NO
$S'_{28} = r_{7,12}$	**NpIII**	ν SO
$S_{29} = r_{12,13}$		ν OH
Bending NO, SO, OH		
$S_{30} = (2^{-1/2})(\beta_{2,12,1} - \beta_{6,12,1})$	**NpI**	β NO
$S'_{30} = \beta_{12,2,7}$	**NpIII**	β SO
$S_{31} = \beta_{13,1,12}$	**NpI**	β OH
$S'_{31} = \beta_{13,7,12}$	**NpIII**	β OH
Out-of-plane NO, SO, OH		
$S_{32} = \gamma_{12,6,1,2}$	**NpI**	γ NO
$S'_{32} = (2^{-1/2})(\tau_{12,7,2,1} + \tau_{12,7,2,3})$	**NpIII**	τ SO
$S_{33} = (2^{-1/2})(\tau_{13,12,1,2} + \tau_{13,12,1,6})$	**NpI**	τ OH
$S'_{33} = \tau_{13,12,7,2}$	**NpIII**	τ OH

Table D2. *Experimental wavenumbers ($\tilde{\nu}$ /cm^{-1}) and relative integral intensities (I) of the absorption bands in the spectrum of* ***N-hydroxypyridine-2(1H)-thione*** *isolated in low-temperature matrixes, compared with wavenumbers ($\tilde{\nu}$ /cm^{-1}), absolute intensities (A^{th} / km mol^{-1}) and potential energy distribution (PED / %) calculated for form* ***NpI****.*

Experimental				**Calculated B3LYP/6-311++G(d, p)**		
Ar matrix		**N_2 matrix**				
$\tilde{\nu}$	**I**	$\tilde{\nu}$	**I**	$\tilde{\nu}$	**A^{th}**	**PED (%)**
				3170	1	νC6H (80), νC5H (18)
				3154	0.2	νC3H (59), νC5H (24)
				3152	1	νC5H (54), νC3H (36), νC6H (10)
				3121	6	νC4H (91)
				3018	258	νOH (98)
1620, 1611, 1605, 1590	78	1620, 1610	56	1616	75	νC5C6 (27), νC3C4 (24), νC6N1 (11)
1570, **1566**	112	1579, **1569**, 1557	128	1577	92	βNO (48)
1497, 1491, 1489	143	1499, **1489**	118	1501	98	βNO (28), νC4C5 (21), νC3C4 (18), βC4H (13)
1475, 1474	5	1477	8			
1461	138	1461	170	1459	87	βC3H (25), βC6H (23)
1420, **1419**, 1413	174	**1421**, 1417	199	1415	108	βC5H (25), βC4H (19), νC2C3 (12), βNO (11), νC6N1 (10)
1269	41	1272, 1263	49	1263	43	βC6H (28), βC3H (20), νC6N1 (17)
1217, 1212	15	1215	17	1209	2	νC2C3 (31), βC3H (19), νN1C2 (18), νC6N1 (13)
1195	36	1197	35	1191	41	νNO (37), νC5C6 (20), βC5H (13), βR1 (12)
1179	58	1182, 1180, 1177	57	1166	25	βC4H (43), νC3C4 (16), νCS (11)
1157, 1154, 1150	14	1163	11			
1141, 1140	92	1144	90	1133	96	βC5H (29), νN1C2 (20), βC6H (18)
1117	7	1112	6			
1104	6					
1079	27	1080	30	1079	42	βR1 (46), νCS (12)
1016	7	1019	9	1019	5	νC4C5 (56)
				969	0.2	γC4H (75), γC3H (39)
927, 925	1	934	2	917	1	γC6H (65), γC5H (47)

Table D2. *(Continuating).*

Experimental				Calculated B3LYP/6-311++G(d, p)		
Ar matrix		N_2 matrix				
$\tilde{\nu}$	**I**	$\tilde{\nu}$	**I**	$\tilde{\nu}$	**A^{th}**	**PED (%)**
832	1	848	1	830	1	γC3H (55), γC6H (22), γC4H (16)
816	22	815	21	811	19	βR1 (30), νNO (26), βR2 (10)
743, 742, 740	83	**752**, 748	86	735	70	γC5H (46), γC6H (21), γC4H (17), γC3H (10)
717	14	716	16	710	8	βR3 (37), νN1C2 (26), νCS (18)
				645	3	τR1 (72), γCS (37)
613, 609	40	618	29	585	46	τOH (91), τR1 (13)
567, 566	2	566	3	564	2	βR2 (51), βR3 (14), νC2C3 (11), νNO (10)
531	18	533, 534	22	526	14	βOH (52), νCS (12)
515, **513**	9	514	8	494	18	τR3 (38), γCS (30), γNO (19), τR1 (13)
421, 415	12	423	11	407	8	τR2 (71), γNO (31)
397, 396	8			398	7	βR3 (27), βOH (22), νCS (19), βR2 (18)
302	7			299	5	βCS (81)
				240	0.01	γNO (56), τR2 (33), γCS (16)
				141	0.2	τR3 (71), τR1 (25), γCS (10)

Table D3. *Experimental wavenumbers ($\tilde{\nu}$ /cm^{-1}) and relative integral intensities (I) of the absorption bands in the spectrum of deuterated* ***N-hydroxypyridine-2(1H)-thione*** *isolated in low-temperature matrixes, compared with wavenumbers ($\tilde{\nu}$ /cm^{-1}), absolute intensities (Ath / km mol^{-1}) and potential energy distribution (PED / %) calculated for* ***NpDI***.

Experimental				**Calculated**		
Ar matrix		**N_2 matrix**		**B3LYP/6-311++G(d, p)**		
$\tilde{\nu}$	**I**	$\tilde{\nu}$	**I**	$\tilde{\nu}$	**Ath**	**PED (%)**
				3170	1	νC6H (80), νC5H (18)
				3154	0.3	νC3H (59), νC5H (24)
				3152	1	νC5H (54), νC3H (35), νC6H (10)
				3121	6	νC4H (92)
				2197	147	νOD (98)
1632, 1621, **1610**	54	1630, 1620, **1608**	60	1616	64	νC5C6 (29), νC3C4 (23), νC6N1 (10)
1543, **1541**	87	1544, 1542	86	1538	86	νC4C5 (27), νC5C6 (16), νC3C4 (14)
1492	9					
1461	130	1461	158	1459	84	βC3H (25), βC6H (23), νC3C4 (10)
1447, **1439**, 1432	52	1449, 1445, **1437**	63	1440	40	βC4H (26), νC6N1 (21), βC5H (14), νC2C3 (10)
1308	36	1306	39	1311	26	βC6H (23), νC6N1 (17), βNO (14), βC5H (13)
1242, **1237**, **1228**	65	1239, 1235, 1228, 1225	72	1230	48	νC2C3 (34), βC3H (27), νN1C2 (12)
1204, **1193**	52	1206, 1204, **1194**, 1191	51	1192	42	νNO (40), νC5C6 (15), βR1 (13), βC5H (11)
1178, **1176**	46	1174	36	1168	23	βC4H (41), νC3C4 (19), νCS (11), βC3H (11)
1146, **1141**, 1139	102	1157, **1144**	89	1140	65	βC6H (28), βC5H (24), νNO (10)
1115	80	1116, **1115**	85	1103	115	βR1 (23), νN1C2 (19), βNO (19), νCS (13), βC4H (10)
1054	30	1054	27	1050	15	βNO (28), βR1 (20), νC4C5 (11), νC6N1 (11), νC3C4 (10), βC5H (10)
1010, 1006	14	1013, **1008**	22	1007	13	νC4C5 (42), βNO (18)
				969	0.2	γC4H (75), γC3H (39)
				917	1	γC6H (65), γC5H (47)
850, 846	6			830	1	γC3H (55), γC6H (22), γC4H (16)
810	16	811	14	807	16	βR1 (29), νNO (26), νC6N1 (11), βR2 (11)
743, 740	71	751, **747**	84	735	70	γC5H (46), γC6H (21), γC4H (17), γC3H (10)
717	11	715	15	710	8	βR3 (37), νN1C2 (26), νCS (18)

Table D3. *(Continuating).*

Experimental				**Calculated**		
Ar matrix		**N_2 matrix**		**B3LYP/6-311++G(d, p)**		
$\tilde{\nu}$	**I**	$\tilde{\nu}$	**I**	$\tilde{\nu}$	**A^{th}**	**PED (%)**
				644	1	τR1 (78), γCS (33)
565, 563	4	563	4	562	3	βR2 (48), βR3 (15), νC2C3 (10)
516, 513	19	518, **514**	18	511	14	βOD (44), νCS (13), βCS (11)
				502	3	γCS (43), τR3 (30), γNO (19), τR1 (19)
457, 454	10	463	3	429	15	τOD (64), τR2 (32)
408, 405, **403**	26	410	24	398	27	τR2 (42), τOD (37), γNO (23), τR3 (11)
393, **392**	9			394	7	βR3 (25), βOD (23), νCS (17), βR2 (17)
296	11			292	6	βCS (77), βOD (13)
				238	0.1	γNO (57), τR2 (32), γCS (15)
				141	0.1	τR3 (71), τR1 (25), γCS (10), τR2 (10)

Table D4. *Experimental wavenumbers ($\tilde{\nu}$ /cm^{-1}) and relative integral intensities (I) of the absorption bands in the spectrum of the photoproduct generated upon UV (λ > 345 nm) irradiation of* ***N-hydroxypyridine-2(1H)-thione*** *and its deuterated isotopomer isolated in Ar matrices, compared with wavenumbers ($\tilde{\nu}$ /cm^{-1}), absolute intensities (Ath / km mol^{-1}) and potential energy distribution (PED / %) calculated for the form* ***NpIIIb*** *and* ***NpDIIIb****.*

Experimental, Ar matrix				**Calculated, B3LYP/6-311++G(d,p)**					
not deuterated NpIIIb		**deuterated NpDIIIb**		**not deuterated NpIIIb**			**deuterated NpDIIIb**		
$\tilde{\nu}$	**I**	**$\tilde{\nu}$**	**I**	**$\tilde{\nu}$**	**Ath**	**PED (%)**	**$\tilde{\nu}$**	**Ath**	**PED (%)**
3588, **3577**	118			3711	83	νOH (100)			
3091	3			3149	2	νC3H (95)	3149	2	νC3H (95)
3061	21	3062	37	3134	11	νC5H (85)	3134	11	νC5H (85)
				3110	9	νC4H (86)	3110	9	νC4H (86)
3000	4	2984	35	3094	16	νC6H (93)	3094	16	νC6H (93)
		2650, **2643**	55				2703	48	νOD (100)
1603	3	1603	3						
1577	78	1588, **1577**	80	1581	105	νC3C4 (28), νC5C6 (16), νC6N1 (14)	1581	105	νC3C4 (28), νC5C6 (16), νC6N1 (14)
1565	33	1565	30	1572	35	νC4C5 (32), νN1C2 (16), νC2C3 (12), νC5C6 (10)	1572	35	νC4C5 (32), νN1C2 (15), νC2C3 (12), νC5C6 (10)
1465	8	1463	7						
1452, **1450**	44	1452, **1450**	40	1450	48	βC6H (37), βC3H (18), νN1C2 (17)	1450	49	βC6H (37), βC3H (18), νN1C2 (17)
1422, 1421	92	1421	88	1420	71	βC4H (28), βC5H (26), νC2C3 (14), νC6N1 (13)	1420	71	βC4H (28), βC5H (26), νC2C3 (14), νC6N1 (13)
1280	5	1279	4	1281	4	βC6H (42), νC6N1 (19), βC3H (18)	1281	3	βC6H (42), νC6N1 (19), βC3H (18)
				1268	2	νN1C2 (27), νC6N1 (24), νC2C3 (12), νC5C6 (10)	1268	2	νN1C2 (27), νC6N1 (24), νC2C3 (12), νC5C6 (10)
1153, 1150	17	**1153**, 1149	20	1150	3	βC4H (41), νC3C4 (18), βC3H (14), βC5H (14)	1149	2	βC4H (41), νC3C4 (18), βC3H (14), βC5H (14)
1169	60			1131	66	βOH (68)			
1142, **1140**, 1133	35	1141, **1139**, 1136, 1132	37	1125	29	βOH (32), βR1 (12), βC5H (12), νC2C3 (11)	1127	54	βR1 (18), βC5H (16), νC2C3 (15), νCS (13)
1095	1	1095	3	1085	6	βC5H (21), βR1 (18), βC3H (16), νC5C6 (13)	1085	6	βC5H (22), βR1 (18), βC3H (16), νC5C6 (13)
1042	5	1042	3	1039	5	νC4C5 (36), νC5C6 (24)	1039	6	νC4C5 (36), νC5C6 (24)
				987	0.02	γC4H (59), γC5H (29), γC3H (20), γC6H (13)	987	0.02	γC4H (59), γC5H (29), γC3H (20), γC6H (13)

Table D4. *(Continuating).*

Experimental, Ar matrix				**Calculated, B3LYP/6-311++G(d,p)**					
not deuterated NpIIIb		**deuterated NpDIIIb**		**not deuterated NpIIIb**			**deuterated NpDIIIb**		
$\tilde{\nu}$	**I**	**$\tilde{\nu}$**	**I**	**$\tilde{\nu}$**	**A [th]**	**PED (%)**	**$\tilde{\nu}$**	**A [th]**	**PED (%)**
986	5	986	4	983	4	βR1 (46), νN1C2 (16), νC2C3 (12), νC6N1 (12)	983	4	βR1 (46), νN1C2 (16), νC2C3 (12), νC6N1 (12)
				961	1	γC6H (74), γC4H (18)	961	0.5	γC6H (74), γC4H (18)
				877	0.5	γC3H (59), γC5H (30), γC6H (11)	877	0.5	γC3H (59), γC5H (30), γC6H (11)
		863	26				827	26	βOD (101)
782, 777, 773	76	781, 775, 772	65	756	61	γC5H (40), γC4H (24), γC3H (19)	756	61	γC5H (40), γC4H (24), γC3H (19)
762, **758**	57	**757**, 756	62	732	5	τR1 (95)	732	0.3	τR1 (102)
735	5	735	2	732	8	βR3 (38), νSO (25), νCS (16)	731	9	βR3 (41), νSO (25), νCS (17)
729	39	729	26	707	84	νSO (69), βR3 (16)	704	76	νSO (74), βR3 (14)
616	3	616	3	616	4	βR2 (76), βR3 (12)	616	4	βR2 (76), βR3 (12)
480	6	477	4	476	6	τR3 (47), γCS (42)	475	4	τR3 (49), γCS (43)
454	6	453	6	442	6	βSO (30), νCS (27), βR3 (14)	441	4	βSO (30), νCS (27), βR3 (14)
396	6	396	2	399	4	τR2 (110)	399	4	τR2 (111)
372	81			353	111	τOH (90)			
344	5			331	16	νCS (30), βSO (27), βCS (23)	331	4	νCS (30), βSO (28), βCS (25)
		282	55				261	69	τOD (94)
				181	5	βCS (54), βSO (38)	179	4	βCS (50), βSO (35)
				164	3	τR3 (50), γCS (38)	161	4	τR3 (43), γCS (35)
				82	3	τSO (100)	79	2	τSO (100)

Table D5. *Experimental wavenumbers ($\tilde{\nu}$ /cm^{-1}) and relative integral intensities (I) of the absorption bands in the spectrum of the photoproduct generated upon UV (λ > 295 nm) irradiation of* ***N-hydroxypyridine-2(1H)-thione*** *and its deuterated isotopomer isolated in N_2 matrixes, compared with wavenumbers ($\tilde{\nu}$ /cm^{-1}), absolute intensities (A^{th} / km mol^{-1}) and potential energy distribution (PED / %) calculated for the form* ***NpIIIb*** *and* ***NpDIIIb****.*

Experimental, N_2 matrix				**Calculated, B3LYP/6-311++G(d,p)**					
not deuterated NpIIIb		**deuterated NpDIIIb**		**not deuterated NpIIIb**			**deuterated NpDIIIb**		
$\tilde{\nu}$	**I**	**$\tilde{\nu}$**	**I**	**$\tilde{\nu}$**	**A^{th}**	**PED (%)**	**$\tilde{\nu}$**	**A^{th}**	**PED (%)**
3566	163			3711	83	νOH (100)			
3091	2	3091	1	3149	2	νC3H (95)	3149	2	νC3H (95)
3070	4	3070	6	3134	11	νC5H (85)	3134	11	νC5H (85)
3061	14	3061	13	3110	9	νC4H (86)	3110	9	νC4H (86)
3000	1	3000	2	3094	16	νC6H (93)	3094	16	νC6H (93)
		2643, **2636, 2634**	115				2703	48	νOD (100)
1603	3	1603	4						
1589, **1576**	91	1589, 1577, **1576**	90	1581	105	νC3C4 (28), νC5C6 (16), νC6N1 (14)	1581	105	νC3C4 (28), νC5C6 (16), νC6N1 (14)
1564	35	1564	30	1572	35	νC4C5 (32), νN1C2 (16), νC2C3 (12), νC5C6 (10)	1572	35	νC4C5 (32), νN1C2 (15), νC2C3 (12), νC5C6 (10)
1452	52	1451	44	1450	48	βC6H (37), βC3H (18), νN1C2 (17)	1450	49	βC6H (37), βC3H (18), νN1C2 (17)
1422	96	1422	83	1420	71	βC4H (28), βC5H (26), νC2C3 (14), νC6N1 (13)	1420	71	βC4H (28), βC5H (26), νC2C3 (14), νC6N1 (13)
1280	6	1280	6	1281	4	βC6H (42), νC6N1 (19), βC3H (18)	1281	3	βC6H (42), νC6N1 (19), βC3H (18)
				1268	2	νN1C2 (27), νC6N1 (24), νC2C3 (12), νC5C6 (10)	1268	2	νN1C2 (27), νC6N1 (24), νC2C3 (12), νC5C6 (10)
		1184	5						
1151	12	1151	16	1150	3	βC4H (41), νC3C4 (18), βC3H (14), βC5H (14)	1149	2	βC4H (41), νC3C4 (18), βC3H (14), βC5H (14)
1198	54			1131	66	βOH (68)			
1143, 1133	37	1144, 1142, 1134	33	1125	29	βOH (32), βR1 (12), βC5H (12), νC2C3 (11)	1127	54	βR1 (18), βC5H (16), νC2C3 (15), νCS (13)
1092	3	1093	1	1085	6	βC5H (21), βR1 (18), βC3H (16), νC5C6 (13)	1085	6	βC5H (22), βR1 (18), βC3H (16), νC5C6 (13)
1069, 1061	3	1067	3						
1042	6	1041	7	1039	5	νC4C5 (36), νC5C6 (24)	1039	6	νC4C5 (36), νC5C6 (24)
				987	0.02	γC4H (59), γC5H (29), γC3H (20), γC6H (13)	987	0.02	γC4H (59), γC5H (29), γC3H (20), γC6H (13)

Table D5. *(Continuating).*

Experimental, N_2 matrix				**Calculated, B3LYP/6-311++G(d,p)**					
not deuterated NpIIIb		**deuterated NpDIIIb**		**not deuterated NpIIIb**			**deuterated NpDIIIb**		
$\tilde{\nu}$	**I**	**$\tilde{\nu}$**	**I**	**$\tilde{\nu}$**	**A^{th}**	**PED (%)**	**$\tilde{\nu}$**	**A^{th}**	**PED (%)**
992, **987**	7	986	4	983	4	βR1 (46), νN1C2 (16), νC2C3 (12), νC6N1 (12)	983	4	βR1 (46), νN1C2 (16), νC2C3 (12), νC6N1 (12)
				961	1	γC6H (74), γC4H (18)	961	0.5	γC6H (74), γC4H (18)
				877	0.5	γC3H (59), γC5H (30), γC6H (11)	877	0.5	γC3H (59), γC5H (30), γC6H (11)
		886, 879	50				827	26	βOD (101)
783	87	**782**, 779	65	756	61	γC5H (40), γC4H (24), γC3H (19)	756	61	γC5H (40), γC4H (24), γC3H (19)
763	68	765, 761	63	732	5	τR1 (95)	732	0.3	τR1 (102)
736	2	736	1	732	8	βR3 (38), νSO (25), νCS (16)	731	9	βR3 (41), νSO (25), νCS (17)
728	24	728	24	707	84	νSO (69), βR3 (16)	704	76	νSO (74), βR3 (14)
616	3	616	4	616	4	βR2 (76), βR3 (12)	616	4	βR2 (76), βR3 (12)
487	29	479	5	476	6	τR3 (47), γCS (42)	475	4	τR3 (49), γCS (43)
457	14	455	6	442	6	βSO (30), νCS (27), βR3 (14)	441	4	βSO (30), νCS (27), βR3 (14)
				399	4	τR2 (110)	399	4	τR2 (111)
				353	111	τOH (90)			
				331	16	νCS (30), βSO (27), βCS (23)	331	4	νCS (30), βSO (28), βCS (25)
							261	69	τOD (94)
				181	5	βCS (54), βSO (38)	179	4	βCS (50), βSO (35)
				164	3	τR3 (50), γCS (38)	161	4	τR3 (43), γCS (35)
				82	3	τSO (100)	79	2	τSO (100)

Table D6. *Experimental wavenumbers ($\tilde{\nu}$ /cm^{-1}) and relative integral intensities (I) of the absorption bands in the spectrum of the photoproduct generated upon UV (λ > 385 nm) irradiation of* ***N-hydroxypyridine-2(1H)-thione*** *and its deuterated isotopomer isolated in Ar matrixes, compared with wavenumbers ($\tilde{\nu}$ /cm^{-1}), absolute intensities (Ath / km mol^{-1}) and potential energy distribution (PED / %) calculated for forms* ***NpIIIa*** *and* ***NpDIIIa****.*

Experimental, Ar matrix				**Calculated, B3LYP/6-311++G(d,p)**					
not deuterated NpIIIa		**deuterated NpDIIIa**		**not deuterated NpIIIa**			**deuterated NpDIIIa**		
$\tilde{\nu}$	**I**	**$\tilde{\nu}$**	**I [a]**	**$\tilde{\nu}$**	**Ath**	**PED [c] (%)**	**$\tilde{\nu}$**	**Ath**	**PED [c] (%)**
				3347	153	νOH (100)			
				3140	8	νC5H (80), νC4H (13)	3140	7	νC5H (81), νC4H (12)
				3125	8	νC3H (56), νC4H (33), νC5H (10)	3125	8	νC3H (56), νC4H (32), νC5H (10)
				3111	3	νC4H (50), νC3H (40)	3111	3	νC4H (50), νC3H (39)
				3104	13	νC6H (85)	3104	12	νC6H (85)
							2435	85	νOD (100)
1593, 1589	111	1592, 1589	106	1591	107	νC3C4 (27), νC5C6 (20), νC6N1 (11), νC2C3 (10)	1591	107	νC3C4 (27), νC5C6 (20), νC6N1 (11), νC2C3 (10)
1560	46	1559	69	1564	45	νC4C5 (31), νN1C2 (17)	1564	45	νC4C5 (31), νN1C2 (16)
1490	8	1467	12						
1456, 1453	82	**1455**, 1453	40	1454	51	βC6H (36), βC3H (21), νN1C2 (15)	1454	49	βC6H (36), βC3H (22), νN1C2 (15)
1427, **1423**, 1420	133	1423, **1422**	93	1421	70	βC5H (27), βC4H (26), νC2C3 (14), νC6N1 (14)	1421	73	βC5H (27), βC4H (26), νC2C3 (14), νC6N1 (13)
1314, 1308	108			1293	27	βOH (47), νC6N1 (20), βC6H (14)			
1264, 1244, 1241	54			1263	99	βOH (47), νC6N1 (22)			
1285, 1283	20	1285	12	1284	10	βC6H (25), νN1C2 (24), νC2C3 (20)	1285	7	βC6H (40), νN1C2 (25), νC2C3 (15)
		1270	3				1276	8	νC6N1 (32), νN1C2 (25), νC5C6 (12)
1196	3								
1169	5	1177, **1175**	5						
1161, 1159, **1157**	8	1162, 1159,11**57**	14	1155	4	βC4H (42), νC3C4 (17), βC3H (15), βC5H (14)	1155	3	βC4H (42), νC3C4 (17), βC3H (16), βC5H (15)
1146, **1142**	78	1146, **1143**, 1138, 1136	92	1131	67	βR1 (19), βC5H (17), νC2C3 (15), νC5C6 (11), νCS (11)	1131	73	βR1 (19), βC5H (17), νC2C3 (15), νC5C6 (11), νCS (11)
1095	5	1094	3	1091	13	βR1 (22), βC5H (20), βC3H (13), νC5C6 (12), νC6N1 (11)	1091	15	βR1 (22), βC5H (21), νC5C6 (13), βC3H (13)νC6N1 (10)
1038	2	1038	7	1037	3	νC4C5 (43), νC5C6 (17)	1038	8	νC4C5 (43), νC5C6 (17)
988, 987	14	990	20	983	11	βR1 (44), νN1C2 (17), νC2C3 (14), νC6N1 (12)	983	11	βR1 (44), νN1C2 (17), νC2C3 (14), νC6N1 (12)
				981	0.04	γC4H (68), γC5H (26), γC3H (19)	981	0.03	γC4H (68), γC5H (26), γC3H (19)

Table D6. *(Continuating).*

Experimental, N_2 matrix				**Calculated, B3LYP/6-311++G(d,p)**					
not deuterated NpIIIa		**deuterated NpDIIIa**		**not deuterated NpIIIa**			**deuterated NpDIIIa**		
$\tilde{\nu}$	**I [a]**	**$\tilde{\nu}$**	**I [a]**	**$\tilde{\nu}$ [b]**	**A [th]**	**PED [c] (%)**	**$\tilde{\nu}$ [b]**	**A [th]**	**PED [c] (%)**
				957	0.2	γC6H (79), γC4H (14), γC5H (13)	957	0.2	γC6H (79), γC4H (14), γC5H (13)
		970, **966**	71				944	50	βOD (98)
				856	0.03	γC3H (56), γC5H (35), γC6H (12)	856	0.04	γC3H (56), γC5H (35), γC6H (12)
783, 776	88	786, **782**	75	748	64	γC5H (36), γC3H (27), γC4H (23)	748	62	γC5H (36), γC3H (27), γC4H (23)
753	79	755, 752	73	732	15	νSO (51), βR3 (22), νCS (14)	731	12	νSO (48), βR3 (24), νCS (14)
744	9			720	3	τR1 (100), γCS (15)	718	2	τR1 (100), γCS (14)
729, 728	32	**730**, 728	32	717	64	νSO (47), βR3 (33), νCS (10)	717	64	νSO (51), βR3 (31)
627, **626**	6	627, **626**	8	625	5	βR2 (78)	625	5	βR2 (78)
480, **478**	13	473	7	461	10	βSO (33), νCS (27), βCS (15), βR3 (14)	455	10	νCS (30), βSO (28), βR3 (15), βCS (15)
439	19			515	26	τOH (46), τR3 (23), γCS (19), τR1 (11)			
430	25			428	59	τOH (37), τR3 (24), γCS (23), τR2 (16)			
							479	0.03	τR3 (47), γCS (40), τR1 (10)
		408, **403**	18				406	15	τR2 (100)
374	5			394	4	τR2 (92), τOH (17)			
				355	4	νCS (32), βSO (27), βR3 (12), βCS (11)	350	5	νCS (29), βSO (27), βCS (15), βR3 (11)
		372	19				322	4	τOD (93)
				209	4	βCS (63), βSO (32)	202	4	βCS (60), βSO (35)
				162	1	τR3 (55), γCS (40)	162	1	τR3 (56), γCS (40)
				80	2	τSO (101)	80	2	τSO (101)

***Table D7**. Experimental wavenumbers ($\tilde{\nu}$ /cm^{-1}) and relative integral intensities (I) of the absorption bands in the spectrum of the photoproduct generated upon UV (λ > 345 nm) irradiation of **N-hydroxypyridine-2(1H)-thione** and its deuterated isotopomer isolated in N_2 matrices, compared with wavenumbers ($\tilde{\nu}$ /cm^{-1}), absolute intensities (A^{th} / km mol^{-1}) and potential energy distribution (PED / %) calculated for forms **NpIIIa** and **NpDIIIa**.*

Experimental, N_2 matrix				**Calculated, B3LYP/6-311++G(d,p)**					
not deuterated NpIIIa		**deuterated NpDIIIa**		**not deuterated NpIIIa**			**deuterated NpDIIIa**		
$\tilde{\nu}$	**I**	**$\tilde{\nu}$**	**I**	**$\tilde{\nu}$**	**A^{th}**	**PED (%)**	**$\tilde{\nu}$**	**A^{th}**	**PED (%)**
3050	205			3347	153	νOH (100)			
				3140	8	νC5H (80), νC4H (13)	3140	7	νC5H (81), νC4H (12)
				3125	8	νC3H (56), νC4H (33), νC5H (10)	3125	8	νC3H (56), νC4H (32), νC5H (10)
				3111	3	νC4H (50), νC3H (40)	3111	3	νC4H (50), νC3H (39)
				3104	13	νC6H (85)	3104	12	νC6H (85)
		2245	110				2435	85	νOD (100)
1590	120	1589	110	1591	107	νC3C4 (27), νC5C6 (20), νC6N1 (11), νC2C3 (10)	1591	107	νC3C4 (27), νC5C6 (20), νC6N1 (11), νC2C3 (10)
1559	50	1559	49	1564	45	νC4C5 (31), νN1C2 (17)	1564	45	νC4C5 (31), νN1C2 (16)
1465, **1456**	87	1456	62	1454	51	βC6H (36), βC3H (21), νN1C2 (15)	1454	49	βC6H (36), βC3H (22), νN1C2 (15)
1422	113	1423	117	1421	70	βC5H (27), βC4H (26), νC2C3 (14), νC6N1 (14)	1421	73	βC5H (27), βC4H (26), νC2C3 (14), νC6N1 (13)
1311	83			1293	27	βOH (47), νC6N1 (20), βC6H (14)			
1269, 1245	67			1263	99	βOH (47), νC6N1 (22)			
1285	22	1287	12	1284	10	βC6H (25), νN1C2 (24), νC2C3 (20)	1285	7	βC6H (40), νN1C2 (25), νC2C3 (15)
		1257, 1245	7				1276	8	νC6N1 (32), νN1C2 (25), νC5C6 (12)
1158	13	1162, **1157**	7	1155	4	βC4H (42), νC3C4 (17), βC3H (15), βC5H (14)	1155	3	βC4H (42), νC3C4 (17), βC3H (16), βC5H (15)
1144, 1133	88	1146, 1138	98	1131	67	βR1 (19), βC5H (17), νC2C3 (15), νC5C6 (11), νCS (11)	1131	73	βR1 (19), βC5H (17), νC2C3 (15), νC5C6 (11), νCS (11)
1094	5	1095	4	1091	13	βR1 (22), βC5H (20), βC3H (13), νC5C6 (12), νC6N1 (11)	1091	15	βR1 (22), βC5H (21), νC5C6 (13), βC3H (13)νC6N1 (10)
1039	2	1039	9	1037	3	νC4C5 (43), νC5C6 (17)	1038	8	νC4C5 (43), νC5C6 (17)
987	16	990	16	983	11	βR1 (44), νN1C2 (17), νC2C3 (14), νC6N1 (12)	983	11	βR1 (44), νN1C2 (17), νC2C3 (14), νC6N1 (12)
				981	0.04	γC4H (68), γC5H (26), γC3H (19)	981	0.03	γC4H (68), γC5H (26), γC3H (19)
				957	0.2	γC6H (79), γC4H (14), γC5H (13)	957	0.2	γC6H (79), γC4H (14), γC5H (13)
		965	68				944	50	βOD (98)

Table D7. *Continuating).*

Experimental, N_2 matrix				**Calculated, B3LYP/6-311++G(d,p)**					
not deuterated NpIIIa		**deuterated NpDIIIa**		**not deuterated NpIIIa**			**deuterated NpDIIIa**		
$\tilde{\nu}$	**I**	**$\tilde{\nu}$**	**I**	**$\tilde{\nu}$**	**A^{th}**	**PED (%)**	**$\tilde{\nu}^{b}$**	**A^{th}**	**PED^{c} (%)**
				856	0.03	γC3H (56), γC5H (35), γC6H (12)	856	0.04	γC3H (56), γC5H (35), γC6H (12)
781	97	779	78	748	64	γC5H (36), γC3H (27), γC4H (23)	748	62	γC5H (36), γC3H (27), γC4H (23)
761	99	759	85	732	15	νSO (51), βR3 (22), νCS (14)	731	12	νSO (48), βR3 (24), νCS (14)
				720	3	τR1 (100), γCS (15)	718	2	τR1 (100), γCS (14)
731, **726**	40	730	37	717	64	νSO (47), βR3 (33), νCS (10)	717	64	νSO (51), βR3 (31)
626	7	626	8	625	5	βR2 (78)	625	5	βR2 (78)
477	10	471	4	461	10	βSO (33), νCS (27), βCS (15), βR3 (14)	455	10	νCS (30), βSO (28), βR3 (15), βCS (15)
528	8			515	26	τOH (46), τR3 (23), γCS (19), τR1 (11)			
448	27			428	59	τOH (37), τR3 (24), γCS (23), τR2 (16)			
							479	0.03	τR3 (47), γCS (40), τR1 (10)
		405	17				406	15	τR2 (100)
				394	4	τR2 (92), τOH (17)			
				355	4	νCS (32), βSO (27), βR3 (12), βCS (11)	350	5	νCS (29), βSO (27), βCS (15), βR3 (11)
							322	4	τOD (93)
				209	4	βCS (63), βSO (32)	202	4	βCS (60), βSO (35)
				162	1	τR3 (55), γCS (40)	162	1	τR3 (56), γCS (40)
				80	2	τSO (101)	80	2	τSO (101)